Non-covalent Intermolecular Interactions in Polymer Design: Segmented Copolymers to Non-viral Gene Delivery Vectors

Daniel James Buckwalter

Dissertation submitted to the faculty of Virginia Polytechnic Institute and State University in partial fulfillment of the requirements for the degree of

Doctor of Philosophy In
Chemistry

Timothy E. Long, Chair
James M. Tanko
Robert B. Moore
John B. Matson

May 3, 2013
Blacksburg, VA

Keywords: poly(amide), oxamide, segmented copolymer, trioxamide, poly(urea), poly(urea oxamide), non-viral gene delivery, click cluster, AD-PEG, AD-MAG

Non-covalent Intermolecular Interactions in Polymer Design: Segmented Copolymers to Non-viral Gene Delivery Vectors

Daniel J. Buckwalter

ABSTRACT

Non-covalent intermolecular interactions play a large role in determining the properties of a given system, from segmented copolymers to interactions of functionalized polymers with non-viral nucleic acids delivery vehicles. The ability to control the intermolecular interactions of a given system allow for tailoring of that system to yield a desired outcome, whether it is a copolymers mechanical properties or the colloidal stability of a pDNA-delivery vector complex. Each chemical system relies on one or more types of intermolecular interaction such as hydrogen bonding, cooperative π-π stacking, electrostatic interactions, van der waals forces, metal-ligand coordination, or hydrophobic/solvophobic effects. The following research describes the tailoring of specific intermolecular interactions aimed at altering the physical properties of segmented copolymers and non-viral gene delivery vectors.

Amide containing segmented copolymers relies heavily on hydrogen bonding intermolecular interactions for physical crosslinking to impart the necessary microphase separated morphology responsible for a copolymers physical properties. Amide containing hard segments are composed of various chemical structures from crystalline aramids to amorphous alkyl amides with each structure possessing unique intermolecular interactions. Variations to either of the copolymer segments alters the copolymers physical properties allowing for tuning of a copolymers properties for a particular application. The synthetic strategies, structure-property relationships, and physical properties of amide containing segmented copolymers are

thoroughly reported in the literature. Each class of segmented copolymer that contain amide hydrogen bonding groups exhibits a wide range of tunable properties desirable for many applications. The segmented copolymers discussed here include poly(ether-*block*-amide)s, poly(ether ester amide)s, poly(ester amide)s, poly(oxamide)s, PDMS polyamides, and polyamides containing urethane, urea, or imide groups.

The structure-property relationships (SPR) of poly(oxamide) segmented copolymers is not well understood with only one report currently found in literature. The effects of oxamide spacing in the hard segment and molecular weight of the soft segments in PDMS poly(oxamide) segmented copolymers demonstrated the changes in physical properties associated with minor structural variations. The optically clear PDMS poly(oxamide) copolymers possessed good mechanical properties after bulk polymerization of ethyl oxalate terminated PDMS oligomers with alkyl diamines or varied length. FTIR spectroscopy experiments revealed an ordered hydrogen bonding carbonyl stretching band for each copolymer and as the spacing between oxamide groups increased, the temperature at which the hard segment order was disrupted decreased. The increased spacing between oxamide groups also led to a decrease in the flow temperature observed with dynamic mechanical analysis. Copolymer tensile properties decrease with increased oxamide spacing as well as the hysteresis. The structure-property investigations of PDMS poly(oxamide) segmented copolymers showed that the shortest oxamide spacing resulted in materials with optimal mechanical properties.

A new class of non-chain extended segmented copolymers that contained both urea and oxamide hydrogen bonding groups in the hard segment were synthesized. PDMS poly(urea oxamide) (PDMS-UOx) copolymers displayed thermoplastic elastomer behavior with enhanced physical properties compared to PDMS polyurea (PDMS-U) controls. Synthesis of a difunctional

oxamic hydrazide terminated PDMS oligomer through a two-step end capping procedure with diethyl oxalate and hydrazine proved highly efficient. Solution polymerization of the oxamic hydrazide PDMS oligomers with HMDI afforded the desired PDMS-UOx segmented copolymer, which yielded optically clear, tough elastomeric films. Dynamic mechanical analysis showed a large temperature insensitive rubbery plateau that extended up to 186 ˚C for PDMS-UOx copolymers and demonstrated increased rubbery plateau ranges of up to 120 ˚C when compared to the respective PDMS-U control. The increase in thermomechanical properties with the presence of oxamide groups in the hard segment was due to the increased hydrogen bonding, which resulted in a higher degree of microphase separation. DMA, SAXS, and AFM confirmed better phase separation of the PDMS-UOx copolymers compared to PDMS-U controls and DSC and WAXD verified the amorphous character of PDMS-UOx. Oxamide incorporation showed a profound effect on the physical properties of PDMS-UOx copolymers compared to the controls and demonstrated promise for potential commercial applications.

Two novel segmented copolymers based on a poly(propylene glycol) (PPG) that contained two or three oxamide groups in the hard segment were synthesized. Synthesis of non-chain extended PPG poly(trioxamide) (PPG-TriOx) and PPG poly(urea oxamide) (PPG-UOx) segmented copolymers utilized the two-step end-capping procedure with diethyl oxalate and hydrazine then subsequent polymerization with oxalyl chloride or HMDI, respectively. The physical properties of the PPG-TriOx and PPG-UOx copolymers were compared to those of PPG poly(urea) (PPG-U) and poly(oxamide) (PPG-Ox) copolymers. FTIR studies suggested the presence of an ordered hydrogen bonded hard segment for PGG-TriOx and PPG-Ox copolymers with PPG-TriOx possessing a lower energy ordered hydrogen bonding structure. PPG-UOx copolymers exhibited a larger rubbery plateau and higher moduli compared to PPG-U

copolymers and also a dramatic increase in the tensile properties with the increased hydrogen bonding. The described copolymers provided a good example of the utility of this new step-growth polymerization chemistry for producing segmented copolymers with strong hydrogen bonding capabilities.

Non-viral nucleic acid delivery has become a hot field in the past 15 years due to increased safety, compared to viral vectors, and ability to synthetically alter the material properties. Altering a synthetic non-viral delivery vector allows for custom tailoring of a delivery vector for various therapeutic applications depending on the target disease. The types of non-viral delivery vectors are diverse, however the lack of understanding of the endocytic mechanisms, endosomal escape, and nucleic acid trafficking is not well understood. This lack of understanding into these complex processes limits the effective design of non-viral nucleic acid delivery vehicles to take advantage of the cellular machinery, as in the case of viral vectors.

Mechanisms for cellular internalization of polymer-nucleic acid complexes are important for the future design of nucleic acid delivery vehicles. It is well known that the mammalian cell surface is covered with glycosaminoglycans (GAG) that carry a negative charge. In an effort to probe the effect of GAG charge density on the affinity of cationic poly(glcoamidoamine) (PGAA)-pDNA complexes, quartz crystal microbalance was employed to measure the mass of GAGs that associated with a polyplex monolayer. Affinity of six different GAGs that varied in the charge density were measured for polyplexes formed with poly(galactaramidopentaethylenetetramine) (G4) cationic polymers and pDNA. Results showed that the affinity of GAGs for G4 polyplexes was not completely dependent on the electrostatic interactions indicating that other factors contribute to the GAG-polyplex interactions. The results

provided some insight into the interactions of polyplexes with cell surface GAGs and the role they play in cellular internalization.

Two adamantane terminated polymers were investigated to study the non-covalent inclusion complexation with click cluster non-viral nucleic acid delivery vehicles for passive targeting of the click cluster-pDNA complexes (polyplex). Incorporation of adamantyl terminated poly(ethylene glycol) (Ad-PEG) and poly(2-deoxy-2-methacrylamido glucopyranose) (Ad-pMAG) polymers into the polyplex formulation revealed increased colloidal stability under physiological salt concentrations. Ad-pMAG polyplexes resulted in lower cellular uptake for HeLa cells and not two glioblastoma cell lines indicating the pMAG corona imparts some cell line specificity to the polyplexes. Ad-pMAG provided favorable biological properties when incorporated into the polyplexes as well as increased polyplex physical properties.

ACKNOWLEDGEMENTS

I would like to extend my sincerest thanks firstly to my advisor, Dr. Timothy Long who not only adopted me into his academic family, but provided me with an exciting project to round out my graduate career. Tim has been there for me in my research and also in all the big decisions that has led me to where I am today. The polymer synthesis and characterization skills I acquired working in the Long group will greatly benefit me in all my future endeavors. I would also like to thank my PhD committee members: Dr. Jim Tanko, Dr. Robert Moore, and Dr. John Matsen. Their advice and direction was very helpful, especially through the big changes to my committee and research. I would like to thank Charlie Leir for his discussions and guidance when starting on my new research project in the Long group, which was key to getting my projects off the ground. A very sincere thank you goes out to the Virginia Tech chemistry department and faculty for the support over the past 4 years through academic fellowships and countless other forms of support that were invaluable to my success in graduate school. I found a wealth of wisdom and outpouring from the chemistry faculty when making the decision stay here at Virginia Tech, in particular Dr. Harry Dorn, Dr. Paul Deck, and Dr. Tim Long. I cannot fully express the gratitude I feel toward the chemistry department in words and hope to continue a productive relationship for many years to come.

The help of many others proved invaluable as I worked my way through graduate school. A big thanks to Valerie Owens, Naya Sou, Brent Bowden, Tammy Jo Hiner, Teresa Dickerson, Angie Miller, Joli Huynh, and EMille Shepherd for everything. I know I would not have been able to get my committee all together without their help. Everyday life would not have gone so smoothly without the paperwork, ordering, and scheduling help they provided.

girls have been the light of my life and continually keep me motivated to work hard and excel in my career. My parents Denny and Diane Buckwalter supported me for so many years and always encouraged me to do my best and work hard in everything I do. My success in life up to this point is a direct consequence of their love, guidance, and support. Thanks to my sisters Susan and Melinda as well as all my grandparents, in-laws, uncles, aunts, and cousins for their support through the years, especially Nana. I also must thank all the great friends I have made over the past 5 years here in Blacksburg and they are friendships I will cherish for years to come.

ATTRIBUTION

Prof. Timothy E. Long
PhD advisor, Professor of Chemistry, Associate Dean to the College of Science, Virginia Tech

Prof. Robert B. Moore
Professor of Chemistry, Associate Director for Research and Scholarship (ICTAS), Virginia Tech

Dr. Charles M. Leir
Former corporate scientist from 3M, collaborated on the activated TMS ester project

Mingqiang Zhang
Current graduate student in Dr. Robert Moore's research group, collaborated on the small angle x-ray scattering analysis of PDMS poly(oxamide) segmented copolymers

Amanda Hudson
Current graduate student in Dr. Robert Moore's research group, collaborated on variable temperature FT-IR analysis of PDMS and PPG poly(urea), poly(urea oxamide), and poly(trioxamide) segmented copolymers

David Inglefield
Current graduate student in Dr. Timothy Long's research group, collaborated on the atomic force microscopy imaging of PDMS poly(urea) and poly(urea oxamide) segmented copolymers

Josh S. Enokida
Current undergraduate student working on research in Dr. Timothy Long's lab, collaborated with the synthesis of PDMS poly(oxamide) segmented copolymers.

Dr. Anton Sizovs
Former graduate student in Dr. Teresa Reineke's research group, synthesized the Ad-pMAG polymers

Dr. Nilesh P. Ingle
Current postdoctoral researcher in Dr. Reineke's research group, collaborated on the cell culture work for the biological evaluation of targeted click cluster/pDNA polyplexes

Table of Contents

List of Figures

List of Tables

List of Schemes

Chapter 1: Introduction

1.1 Dissertation Overview

The overarching theme of this dissertation is the tailoring of macromolecular intermolecular interactions focused on hydrogen bonding, electrostatic interactions, and non-covalent inclusion complexation. The following dissertation is split into two parts focused on two very different fields of polymer chemistry. Part I of this document describes the manipulation of hydrogen bonding in oxamide containing segmented copolymers and the development of a new step-growth polymerization strategy for novel segmented copolymers. Part II focuses on the interactions of negatively charged cell membrane components and positively charged polymer-pDNA complexes. In addition the investigation into the complexation of functionalized polymers with a non-viral nucleic acid delivery vector and its effect on complexation and biological activity is reported.

Chapter two reviews the synthesis, application, and physical properties of amide containing segmented copolymers including poly(ether-*block*-amide)s, poly(ether ester amide)s, poly(ester amide)s, poly(oxamide)s, PDMS poly(amide)s, and poly(amide)s containing urethanes, ureas, and imide groups. The third chapter provides insight into the structure-property relationships of poly(dimethyl siloxane) (PDMS) poly(oxamide) segmented copolymers with a focus on the effects of spacing between oxamide groups in the hard segment and PDMS molecular weight. PDMS poly(oxamide) copolymers were synthesized with the methylene spacing between oxamide groups varied from 2 to 8 methylene groups and PDMS molecular weight of 2, 5, and 12 kg/mol. The increase in oxamide spacing decreased the thermal stability of hard segment order and resulted in reduced mechanical properties. The fourth chapter details the development of a new step-growth polymerization strategy based on oxamic hydrazide

terminated PDMS oligomers for the formation of PDMS poly(urea oxamide) segmented copolymers. Comparisons were made between poly(urea oxamide) and poly(urea) controls focused on the changes in physical properties associated with the presence of the oxamide groups in the hard segment. Thermal, thermomechanical, tensile, and X-ray scattering analysis revealed the major differences in the morphology and mechanical properties when comparing copolymers. A significantly longer workable window and better tensile properties were realized with poly(urea oxamide) segmented copolymers.

Chapter five describes the synthesis and characterization of two new segmented copolymers based on poly(propylene glycol) (PPG) soft segments. Synthesis of PPG poly(trioxamide) and PPG poly(urea oxamide) relied on the use of oxamic hydrazide terminated PPG oligomers. Both copolymers were compared to previously reported copolymers and demonstrated the utility of the oxamic hydrazide polymerization strategy to yield novel, strong hydrogen bonding hard segment chemical structures. The sixth chapter summarizes the accomplishments and findings of Part I of this dissertation. Chapter seven introduces the potential research projects that could stem from the research presented in Part I of this dissertation.

The eighth chapter begins Part II of the dissertation and reviews the field of non-viral delivery of nucleic acids for therapeutic applications. The process and various mechanisms for non-viral gene delivery are discussed as well as the types of nucleic acids used. An in-depth description is provided on the various types and targeting of delivery vectors including cationic polymers, dendrimers, and theranostics. The ninth chapter describes a series of quartz crystal microbalance experiments aimed at probing the interactions of negatively charged glycosaminoglycans and positively charged poly(glycoamidoamine)-pDNA polyplexes. The

relative affinity of each glycosaminoglycan studied revealed a trend of glycosaminoglycan-polyplex association that is independent of the charge density associated with each glycosaminoglycan providing insight into the interactions that lead to cellular endocytosis of polyplexes.

Chapter ten details the initial studies into the development of a non-covalent targeting platform for *in vivo* passive targeting of click cluster non-viral delivery vectors. The synthesis of two adamantane terminated polymers were described and subsequently utilized on the formulation of click cluster-pDNA polyplexes to investigate the effects on polyplex and biological properties. NMR titration studies revealed the formation of a strong inclusion complex between the terminal adamantane of Ad-PEG and the β-cyclodextrin core of the click cluster delivery vector. Dynamic light scattering analysis showed that Ad-p(MAG) polymers imparted increased colloidal stability to polyplexes and various biological assays revealed significant changes to the cellular uptake, toxicity, and transfection when Ad-p(MAG) was incorporated into the polyplex formulation. The eleventh chapter summarizes the accomplishment and discoveries reported in Part II of this dissertation and chapter twelve describes the possible future work stemming from the research projects described in Part II.

Part I

Chapter 2: Polyamide Containing Segmented Copolymers

2.1 Abstract

This review highlights the synthesis, physical properties, and applications of common segmented copolymers containing amide hydrogen bonding groups. Amide hydrogen bonding plays a crucial role in the physical properties associated with amide-containing segmented copolymers. Amide hard segments are accessible in many different forms from amorphous alkyl amides to crystalline aramids and greatly influence copolymer morphology and mechanical properties. Variations in copolymer structure allows for the fine tuning of physical properties and the ability to predict changes in mechanical performance based upon structural modifications. Topics this review include are the various synthetic methods for producing well-defined amide-containing segmented copolymers as well as common applications. Also, the morphological and mechanical properties associated with changes in copolymer structure are discussed.

2.2 List of Abbreviations Used

HS- hard segment
SS- soft segment
TPE- thermoplastic elastomer
PTMO- poly(tetramethylene oxide)
PEG - poly(ethylene glycol)
PPG- poly(propylene glycol)
PPE- poly(2,6-dimethyl-1,4-phenylene ether)
PDMS- poly(dimethyl siloxane)
PEBA- poly(ether-*b*-amide)
PA- poly(amide)
ABS- poly(acrylonitrile butadiene styrene)
PEEA- poly(ether ester amide)
PLLA- poly($_{L,L}$-lactide)

PEA- poly(ester amide)
ROP- ring opening polymerization
CLA- ε-caprolactam
CLO- ε-caprolactone
PBA- poly(butylene adipate)
HMDI- 4,4′-methylenebis(cyclohexyl isocyanate)
PDMS-PA- poly(dimethyl siloxane) poly(amide)
PDMS-PAr- poly(dimethyl siloxane) poly(aramide)
PAEI- poly(amide ester imide)
PAIU- poly(amide imide urethane)
PAU- poly(amide urethane)
PEUA- poly(ester urethane amide)
PUUA- poly(urethane urea amide)

2.3 Introduction

Segmented copolymers typically consist of two covalently linked oligomeric segments with very different physical characteristics termed the hard segment (HS) and soft segment (SS). Generally, the HS and SS are incompatible with each other due to differences in the hydrophobic/hydrophilic nature of each segment. Also, strong intermolecular interactions between the HS structures, such as hydrogen bonding, lead to physical crosslinking between polymer chains.[1-3] The inherent incompatibility of the two copolymer segments in concert with the physical crosslinking intermolecular interactions results in the formation of a microphase separated morphology.[4] Factors necessary to generate a microphase separated system include the overall degree of polymerization (N), volume fraction of the segment (f), and Flory-Huggins interaction parameter (χ).[5] Microphase separated morphologies consist of amorphous, semi-crystalline, or combination of both HS microdomains dispersed throughout the soft polymer matrix (Figure 2.1). The extent and nature of the microphase separated morphology, controlled through copolymer composition, significantly affects the mechanical properties of a copolymer.[6]
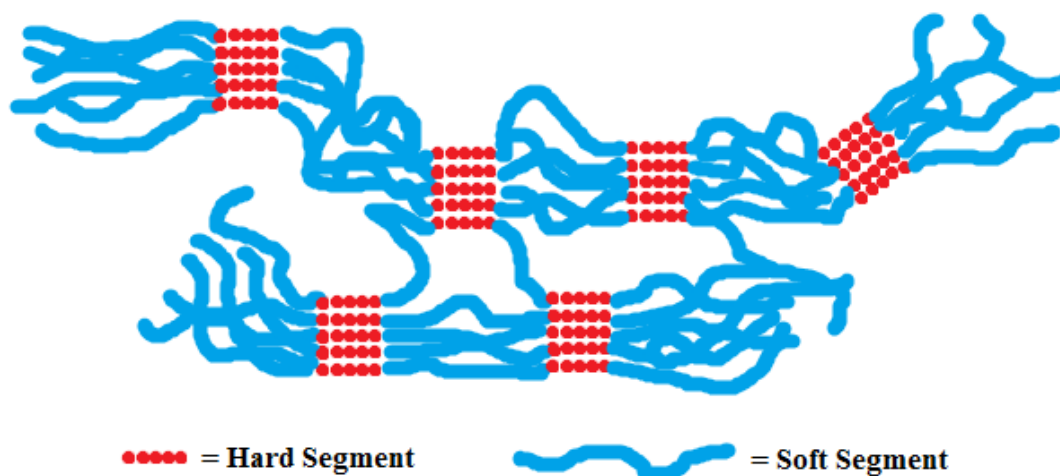
Figure 2.1. Conceptual drawing of a microphase separated segmented copolymer

Soft segment compositions typically include a low T_g oligomeric sequence such as poly(tetramethylene oxide) (PTMO), poly(ethylene glycol) (PEG), poly(propylene glycol) (PPG), poly(dimethyl siloxane) (PDMS), or a polyester, which impart flexibility and incompatibility with the polar HS.[7-10] Incorporation of polyethers into segmented copolymers serve as the soft, flexible low T_g segment, which promotes microphase separation. Polyether SS oligomers are commercially available with varied functionality, composition, and molecular weight. These SS provide alkali and solvent resistance, varying hydrophilicity, and hydrolytic stability. However, limitations exist for polyether SS in some applications due to UV radiation sensitivity.[11] PDMS is often employed in polyamide (PA) segmented copolymers, and offers UV, thermal, and oxidative stability as well as high gas permeability, hydrophobicity, and physiological inertness.[12] PDMS is one of the most flexible polymer chains known to exist and combined with unique physical properties provided an excellent SS for segmented copolymers.[13] Most HS include highly polar groups, which form physical crosslinks necessary to impart microphase separated morphologies and subsequent copolymer physical properties through intermolecular interactions such as hydrogen bonding.[14] Examples of common polar HS

structures include amides,[15] urethanes,[16,17] ureas,[18,19] imides,[20,21] esters,[22,23] or a combination of two or more of these functionalities.[24-26] HS structure (aromaticity, symmetry, and number of hydrogen bonding groups) and size (molecular weight, number of repeat units) play an important role in determining the physical properties of a copolymer.[27,28] Through variations in the HS architecture and subsequent intermolecular interactions, researchers effectively tuned the physical properties of many different amide containing segmented copolymers.

The amide functionality possess strong hydrogen bonding characteristics that are well-suited for the formation of strong physical crosslinks necessary for good physical properties of a segmented copolymer. When compared to other hydrogen bonding groups commonly found in segmented copolymers, amide groups exhibit one of the strongest intermolecular interactions. Using group contribution method calculations, the cohesive energy density of hydrogen bonding for urea, amide, urethane, and imide was 2079, 1862, 1385, and 980 J/cm^3, respectively, and the hydrogen bonding energy of amide groups was 32.5 kJ/mol.[29] Amides play one of the most important roles of any hydrogen bonding group and provide a fundamental intermolecular interaction in polypeptides, essential to every living organism.[30] Hydrogen bonding interactions and the hydrophobicity of polypeptides determine protein structure and motions essential to the proper function of every protein.[31] Similarly, the role of amide hydrogen bonding in segmented copolymers is crucial for the morphology and physical properties. Formation of PA segmented copolymers involves many different polymerization chemistries. Polymerization between amines and acid chlorides or carboxylic acids proved very efficient, often utilizing a catalyst in the case of low temperature carboxylic acid/amine polymerization.[32-34] The use of diesters and diamines was also useful for PA synthesis, but the polymerization is often inefficient for polymerization due to the ester reactivity and required use of a catalyst such as an enzyme.[35] Other PA

polymerization strategies include ring opening polymerization of caprolactam or polymerization between a dicarboxylic acid and diisocyanate.[36] Efforts of many researchers throughout the world yielded a large amount of research into the synthesis, morphology, and physical properties of amide-containing segmented copolymers. This review discusses the various types of amide-containing segmented copolymers as well as the synthesis, applications, and properties associated with each type of copolymer.

2.4 Poly(ether-block-amide) Segmented Copolymers

2.4.1 Background

Poly(ether-*block*-amide) (PEBA) segmented copolymers are high performance block copolymers consisting of soft polyether blocks and hard PA blocks commercialized under the trademark Pebax®. Arkema Inc. first commercialized Pebax® thermoplastic elastomers in 1981 as part of an initiative to develop "soft" nylon materials. Development of Pebax® copolymers provided high performance materials with tunable properties. Altering the composition and length of the soft and hard blocks provides a high level of variability in copolymer properties.[37]

Commercial applications for PEBA segmented copolymers, in particular Pebax®, includes advanced separation membranes, biomedical devices, food packaging, various textile modifiers, mechanical parts, construction materials, electron equipment, aviation industry, and automotive applications.[38-42] Pebax® possesses the ability to act as efficient gas separation membranes and the ability to alter the selectivity for a particular gas, leading to a recent increased interest in PEBA copolymers for gas separation membranes. For example, the separation of polar and nonpolar gas mixtures relied on altering the copolymers chemical composition to obtain optimal separation for a given mixture.[43] PEBA block copolymers with a low PA content exhibited the highest levels of gas permeation. Armstrong et al. also

demonstrated the dramatic effect polyether mechanical orientation had on gas diffusion through PEBA membranes. Uniaxial orientation of the SS occurred after applying 400% strain to a PEBA composed of PTMO/nylon-12 and an observed decrease in the gas diffusion up to 3.5x resulted. Strain-induced crystallization of PTMO severely restricts diffusion of gas through the SS leading to a decrease in gas permeation.[44] Another application for PEBA block copolymers receiving attention recently is for use as antistatic agents. Wang et al. recently published a report on the blending of acrylonitrile butadiene styrene (ABS) resin with a PEBA composed of PTMO/nylon-6 to impart antistatic properties to the blended material. Through variations in the ratio of PEBA and ABS in the blends, they were able to reduce the surface resistivity 4 orders of magnitude and retain persistent antistatic abilities.[45]

2.4.2 Synthesis

Synthesis of PEBA segmented copolymers relies on the covalent attachment of two oligomeric sequences to form the desired block copolymers. The most common PEBA precursors include nylon 6 and nylon 12 as the hard amide block and PEG or PTMO as the soft flexible segment. One method for preparation of PEBA block copolymers required the melt polycondensation of carboxylic acid terminated nylon oligomers with alcohol terminated PEs at high temperatures (~250 °C). A catalysis, such as $Ti(OR)_4$, are often necessary to drive the formation of ester linkages between the two different blocks.[39] The polyether selection for copolymerization with PA oligomers affects the rate of esterification, primarily due to the moisture content in polyether oligomers with the reported observed reactivity as follows: PEG < PPG < PTMO.[46] Peyravi et al. described a slightly different synthetic strategy for producing PEBA copolymers through a three step route (Scheme 2.1). First, end-capping of nylon 6 with an excess of adipic acid at high temperature yielded a carboxylic acid terminated oligomer. Chain

extension with hexamethylenediamine and copolymerization with PEG, Ti(OBu)$_4$, and Irganox 1010 in the melt provided the desired PEG/nylon-6 segmented block copolymer.[47] The stepwise method established an easy route for varying copolymer composition and reliable thermoplastic elastomers (TPE) with crystalline micro-domains. Preparation of PEBA films relies on melt pressing or a solution casting procedure. Both methods proved useful for film formation, but the thickness of films had a significant effect on the morphology displayed, particularly with solution casting methods.[48]

Scheme 2.1. Synthesis of PEO-nylon-6 poly(ether-block-amide) segmented copolymer through a three-step melt polycondensation method[47]
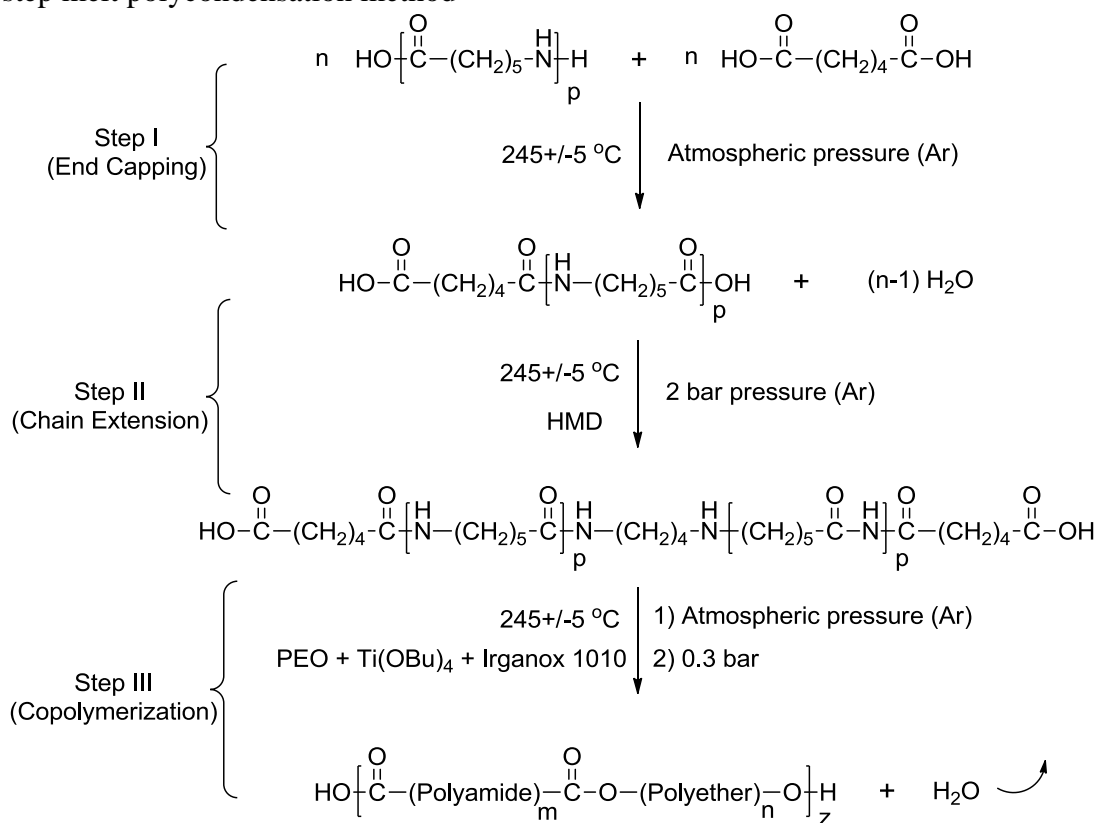
2.4.3 Properties

PEBA segmented copolymers exhibit a high degree of microphase separation, elucidated through various morphological studies. X-ray diffraction (XRD), differential scanning calorimetry (DSC), and nuclear magnetic resonance (NMR) spectroscopy have elucidated the

10

finely microphase separated morphology, which revealed well defined PA crystals spread throughout amorphous and semi-crystalline PE/PA phases in PEG/nylon-12 containing PEBA block copolymers.[49] The crystallization behavior of Pebax® suggested the block copolymer microphase separation occured through HS crystallization into amorphous and crystalline regions instead of the formation of hard and soft domains commonly observed in segmented copolymers.[50] The long ribbon-like PA crystalline regions provide copolymer strength upon mechanical deformation. Atomic force microscopy (AFM) and small angle X-ray scattering (SAXS) analysis revealed the formation of nanofibrils oriented in the direction of an applied strain, which acted as the load-bearing nanostructures that dominated the mechanical properties (Figure 2.2).[51] Strain induced fibrillation occurs in a three stage molecular orientation that started with alignment of the PTMO soft block. Further strain caused a rotation of the PA lamellae and eventual plastic deformation, which ultimately led to fibril formation.[52] Uniaxial deformation of PEBA copolymers also affected the T_m of the polyether soft segment. DSC studies showed the appearance of a higher polyether T_m, which increased in intensity with the increase in strain without changes in the PA T_m.[53]

The stability and nature of PA hard segments greatly determine the effects of thermal energy on PEBA block copolymers. Loss of PA hydrogen bonding at high temperatures coincides with melting of the crystalline PA domains and leads to the T_f of PEBA block copolymers. Linear viscoelasticity studies revealed that as the temperature of the melt increases, the well-defined microphase separated structure transitioned from a weak back to a stiff structure after a large-amplitude oscillation shear. AFM also indicated a change in the microphase separated morphology of the PEBA melt with increased temperature.[54]
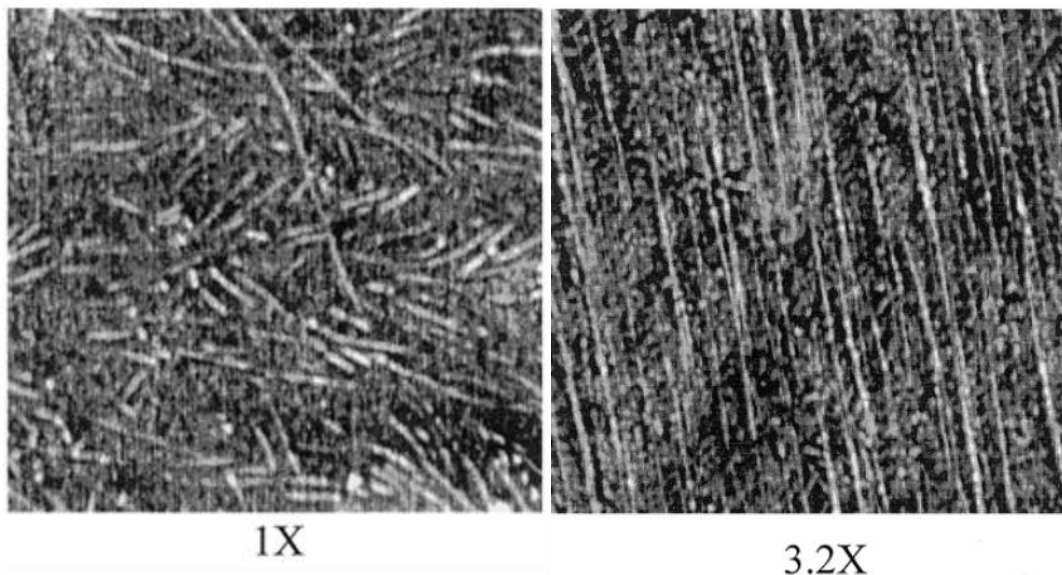
Figure 2.2. AFM phase images of Pebax® 3533 film under a 1x and 3.2x elongation with the stress direction close to vertical and images are 1μm x 1 μm[51]

PEBA segmented block copolymers demonstrated thermal degradation temperatures under non-oxidative conditions from $380 - 415$ ˚C ($T_{d\ 10\%}$), similar to the nylon-12 oligomers. Besides the polyether T_g, DSC revealed a nylon-12 T_m between $161 - 165$ ˚C.[46] Dynamic mechanical analysis often showed a large rubbery plateau, indicative of microphase separated morphologies with a drop in storage modulus that corresponded to a PA T_g.[46] Figure 2.3 depicts the DMA storage modulus and tan δ curves for a PTMO/nylon-12 containing PEBA and reveals the evidence of multiple transitions. Transition 1 included transitions that occured in the amorphous polyether and PA regions. Transition 2 corresponded to the T_g of the PTMO soft segment, and transition 3 to the crystallization and melting of PTMO. The region labeled as transition 4 arose from the PA T_g and increased with increased PA content, which overlapped to some degree with polyether melting. The sudden increase in tan δ in the transition 5 region corresponded to melting of the PEBA copolymer.[55] The DMA polyether T_g often resided at slightly higher temperatures than those observed with DSC due to some degree of phase mixing

with the amorphous HS domains.[56,57] The storage modulus of the rubbery plateau scaled with the

PA HS mol%, similar to poly(urea) and poly(urethane) segmented copolymers.[58]
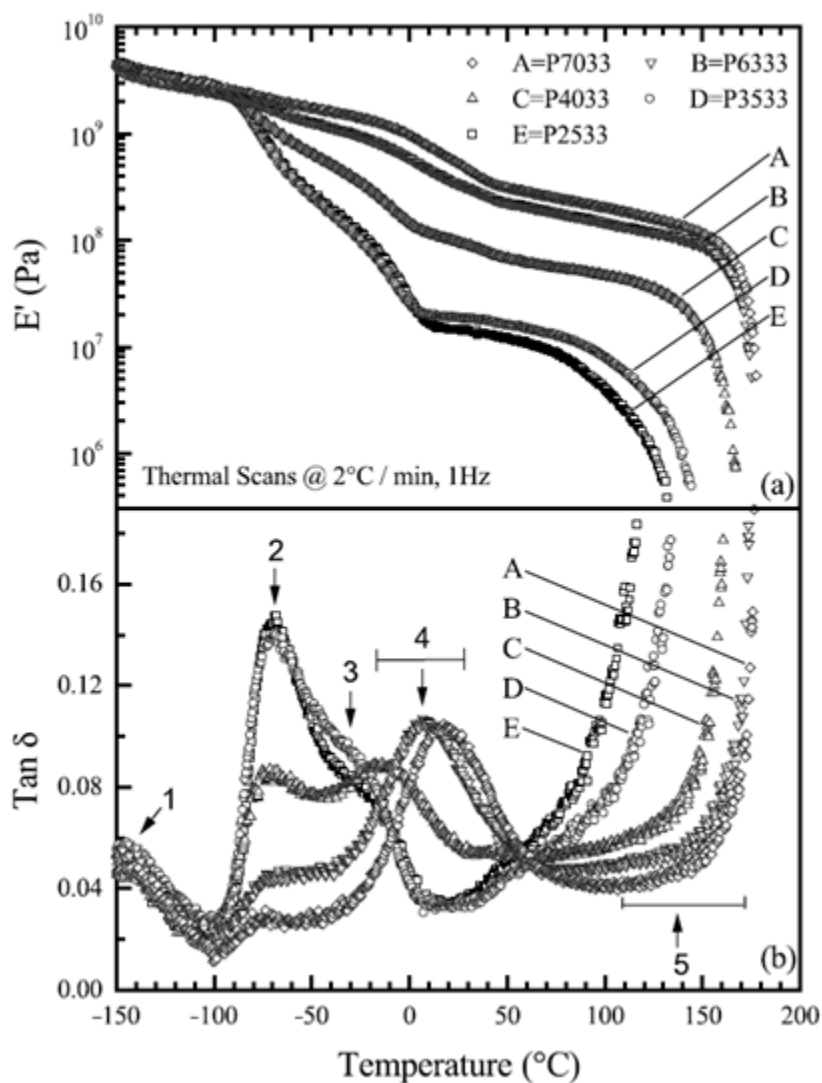
Figure 2.3. DMA traces of the (a) storage modulus and (b) tan δ of Pebax® films composed of nylon 12 and PTMO with transitions 4 and 5 indicating a general temperature range[55]

Tensile properties of PEBA segmented block copolymers demonstrated a dependence on

copolymer composition and often exhibited high elongation values (Figure 2.4). An increased

mol% PA in Pebax® films from 12 to 73% revealed an increase in the stress at break and

Young's modulus. Furthermore, a decrease in strain at break occured with each increase in the

mol% PA.[55] The decrease in strain at break with an increased HS wt% content was common for

many segmented copolymers such as poly(urea)s and poly(urethane)s.[59-61] Overall, PEBA segmented block copolymers provide high performance TPE materials with tunable physical properties for a wide range of applications.
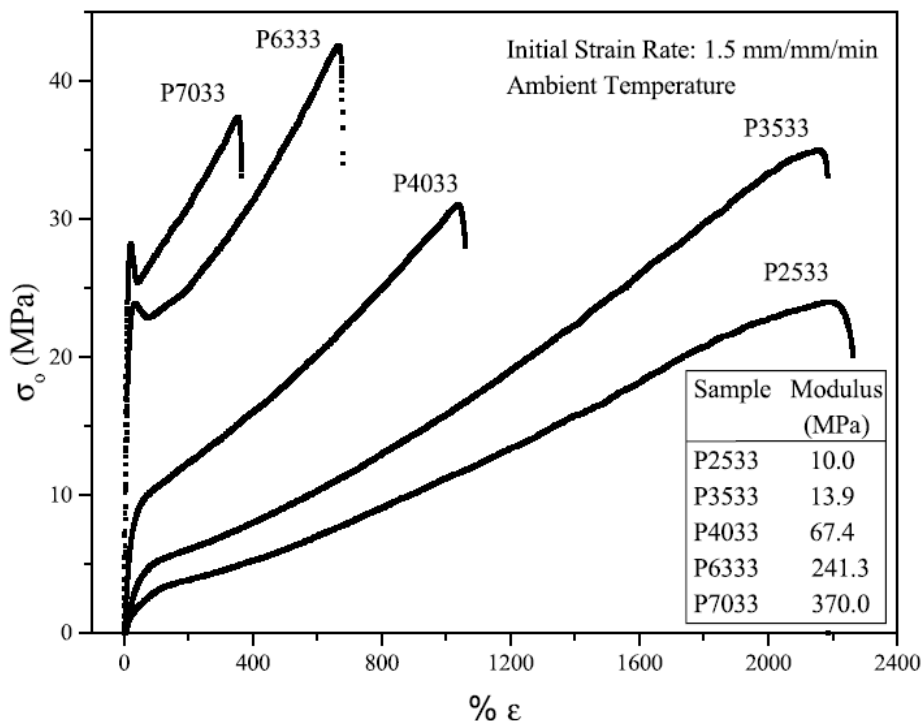
Figure 2.4. Stress vs. strain curve for Pebax® films increasing in mol% PA content with P2533 containing 12 mol% and P7033 containing 73 mol%[55]

2.5 Poly(ether ester amide) Segmented Copolymers

2.5.1 Background

Poly(ether ester amide) (PEEA) segmented copolymers are composed of a polyether oligomeric soft segment covalently linked to a short oligoamide HS through an ester linkage, which yields a flexible, elastic copolymer. The oligoamide HS is responsible for forming the often semi-crystalline physical crosslinks in PEEA copolymers. PEEA copolymers exhibit good mechanical properties, high T_m's, fast HS crystallization, solvent resistance, and low moisture absorbance. Applications for PEEA segmented copolymers include engineered plastics,

thermoplastic elastomers, and elastic textile fibers.[62,63] Also, investigations into the use of PEEA segmented copolymers for drug delivery applications as biocompatible and enzymatically degradable systems proved successful.[64] Hydrophilic PEEA copolymers contained poly($_{L,L}$-lactide) (PLLA), PLLA-PEG-PLLA macromonomers,[65] or poly(ϵ-caprolactone) and sebacoyl chloride,[64] for example, with various hydrophilic diamines. Characterization demonstrated a highly microphase separated PEEA copolymer with promising properties for oral drug delivery applications.[65] Other similar copolymers that contained PEG and a diamide containing HS also demonstrated good properties for use in biomedical devices.[66]

2.5.2 Synthesis

PEEA segmented copolymers are commonly synthesized through melt polycondensation of a soft hydroxy terminated polyether oligomer, such as PTMO, with a short methyl ester terminated oligoamide monomer and diol chain extender. Other commonly utilized PEs include PEG and poly(2,6-dimethyl-1,4-phenylene ether) (PPE) oligomers, which have a high T_g around 200 ˚C.[67,68] PPE also possess good flame retardation, low moisture uptake, and high toughness, but exhibits poor processability and low solvent resistance.[15] Amide ester monomers are usually comprised of aramids, containing multiple terephthalamide groups, or oligolactam containing monomers.[69,70] The aramid monomers are typically composed of 2 or 3 terephthalamide units separated with a short alkyl or aromatic spacer (Figure 2.5). Aramid crystallization imparts an increase in the dimensional stability, mechanical properties, and solvent resistance of PEEA copolymers.[71] Melt polymerization conducted under inert atmosphere at high temperature and low pressure proved successful. For example, a one-pot polymerization strategy began with a reaction vessel loaded with the polyether oligomer, diol chain extender, oligoamide-dimethyl, and catalyst solution. The polymerization proceeds through slowly increasing the temperature in

-T6T6T-

-T6T-

-TΦT-

R = poly(ether)
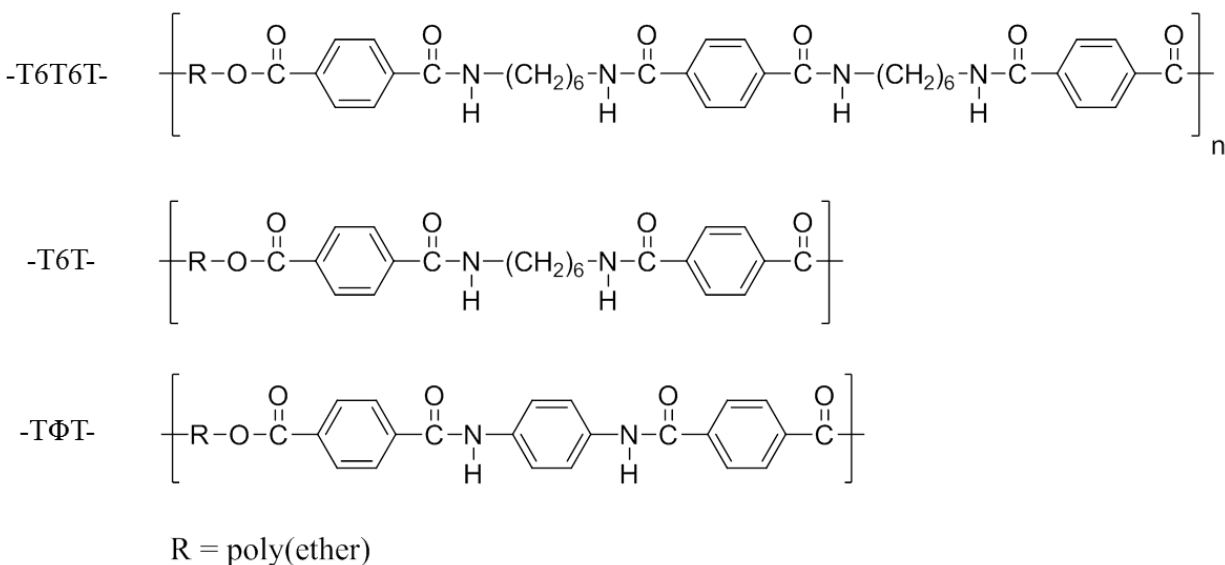
Figure 2.5. Aramid hard segment structures commonly found in PEEA segmented copolymers

a stepwise fashion up to 250 – 280 ˚C with the addition of reduced pressure to achieve high

monomer conversion through removal of the condensate (Scheme 2.2).[72,73] Utilizing an aramid

with a high melting point, such as TΦT-dimethyl (371 ˚C m.p.) required the use of solvent, such

as NMP, for polymerization in some cases.[74] A similar synthetic method for producing PEEA tri-

block copolymers utilized a uniform monomethyl aramid to end-cap a PTMO middle block,

Scheme 2.2. Melt polymerization of a PPE-2T/C12/T6T6T PEEA segmented copolymer[73]

1) 180 °C, 30 min
2) 220 °C, 30 min
3) 250 °C, 1 h
4) 280 °C, 1 h
5) P < 1 mbar, 1 h

T6T6T-dimethyl

Ti(i-OC$_3$H$_7$)$_4$

16
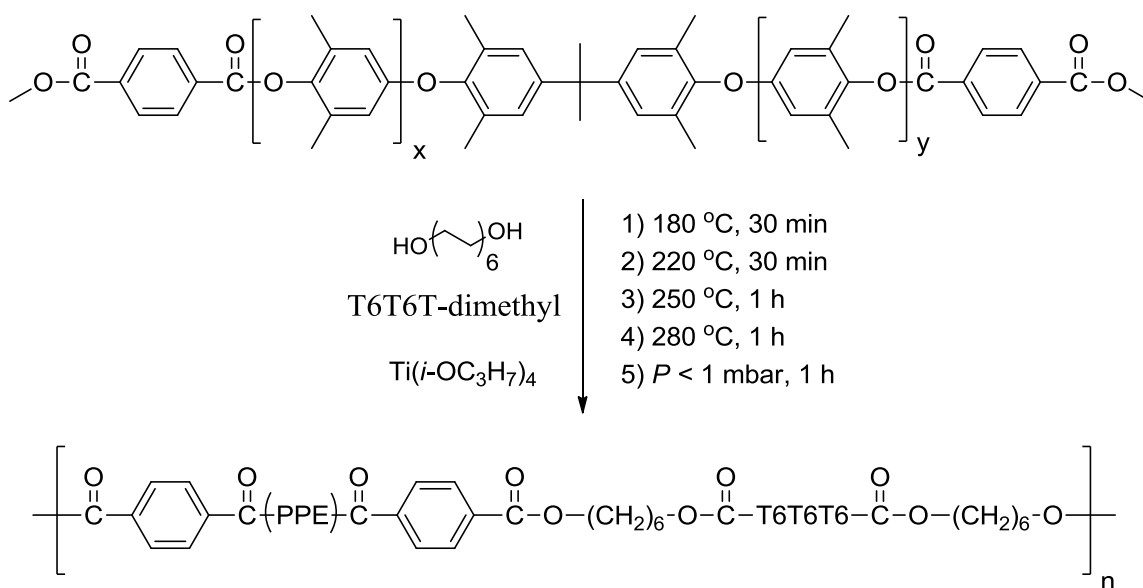
with variations of PTMO molecular weight occurred through extension with terephthalate. This synthetic method yielded ductile PEEA tri-block copolymers that exhibited elastic behavior, even at low molecular weights (>6000 g/mol).[75]

2.5.3 Structure Property Relationships

The role of hydrogen bonding plays an important role in determining copolymer bulk morphologies and physical properties as in other segmented copolymers. PEEA segmented copolymers demonstrated high levels of microphase separation and crystallinity, which depended on the amide containing HS structure.[76,77] Comparisons of hydrogen bonding PTMO-T6T6T and non-hydrogen bonding PTMO-TPTPT (tetraamidepiperazine terephthalamide) segmented copolymers revealed the important role of hydrogen bonding in poly(ether ester amide) segmented copolymers. Tensile analysis of PTMO-TPTPT demonstrated lower storage moduli and lower yield stresses due to the lack of hydrogen bonding (Figure 2.6). The reduced
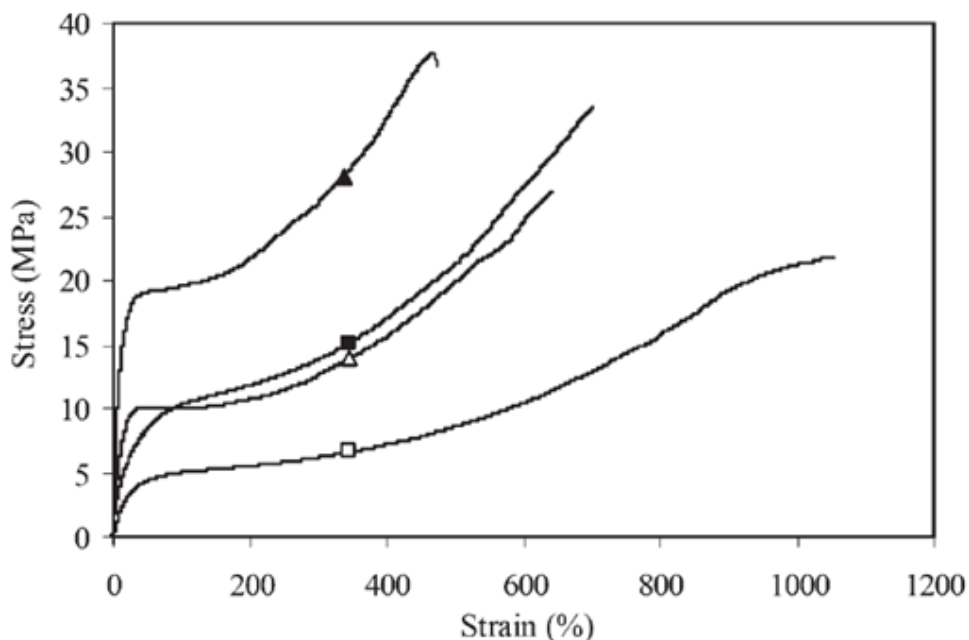
Figure 2.6. Stress-strain curves for hydrogen bonding $PTMO_{1000}$-T6T6T (▲), $PTMO_{2000}$-T6T6T (■) copolymers and non-hydrogen bonding $PTMO_{1000}$-TPTPT (Δ), $PTMO_{2000}$-TPTPT (□) segmented copolymers[72]

reinforcing effect of HS crystallites and poor crystalline packing caused significant reduction in mechanical properties.[72] Van der Schuur et al. showed that increasing the number of amide hydrogen bonding groups in the HS from 2 (T6T) to 6 (T6T6T6T) led to an increase in storage modulus, T_m, and T_f of the PEEA segmented copolymers. The increased amide length also resulted in improved elastic properties partly due to increased thickness of the crystallites.[78] The presence of a uniform, monodisperse crystallizable HS yielded more complete crystallization within the copolymer and improved mechanical properties when compared to PEEA copolymers containing polydisperse HSs (Figure 2.7). Polydisperse HSs produced lower moduli, yield
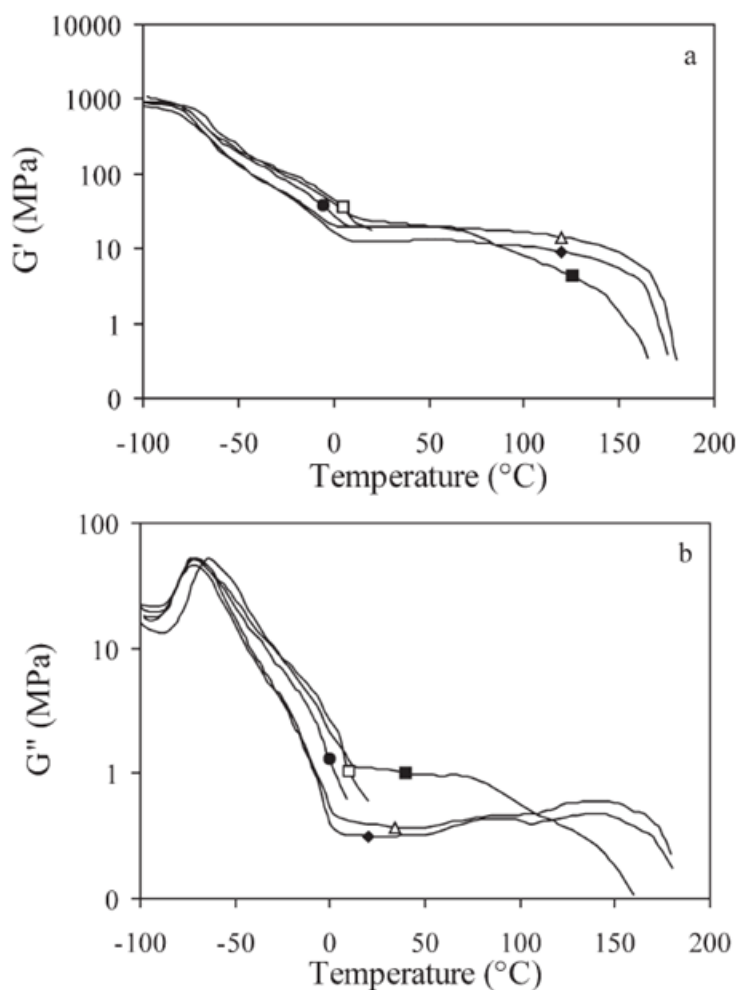
Figure 2.7. Storage (a) and loss modulus (b) as a function of temperature for PTMO$_{2000}$-T6A6T segmented copolymers with increasing HS PDI: monodisperse (Δ), 1.03 ($\blacklozenge$), 1.07 ($\bullet$), 1.09 ($\square$), and 1.20 ($\blacksquare$)[80]

strength, DMA T_f, and elastic properties as well as an increased temperature dependence on the DMA rubbery plateau. The reduced mechanical properties of PEEAs with non-uniform HS occured due to the presence of liquid-liquid demixed phase content and reduced crystallinity.[79,80] Husken et al. investigated how changes in the T6T6T semi-crystalline HS composition in PEG-T6T6T segmented copolymers altered the hydrophobicity of the PEEAs surface. The contact angle decreased as the concentration of T6T6T HS decreased, which indicated an increase in the hydrophilicity of the PEEA surface.[81] HS content not only affected copolymer bulk morphologies and mechanical properties, but also the surface properties of PEEA segmented copolymers.

The ability of the HS to crystallize also had a dramatic effect on morphology and the subsequent physical properties of PEEA segmented copolymers. DSC and WAXD techniques revealed that the amide containing HS of PEEA copolymers rapidly crystallize due to the nature and uniformity of the oligoamides used for polymerization.[82] Copolymers composed of a crystalline HS showed lower polyether T_g values than amorphous HSs, which indicated an increased phase separated morphology with the presence of crystalline HS. HS crystallinity also imparted increased moduli and elasticity in PEEA copolymers.[4] The temperature where polyether T_g appeared in PEEA copolymers, with changes in copolymer composition, provided insight into the level of crystallinity that a particular oligoamide HS possessed.[83] For example, PEEA copolymers containing the same PTMO molecular weight demonstrated SS T_gs of -70 and -55 °C, the copolymer with a T_g of -70 °C would have a higher degree of HS crystallinity resulting in greater microphase separation. The copolymer that exhibited a T_g of -55 ° would inherently include amorphous hard domains mixed with the soft matrix thereby increasing the PTMO T_g. Despite the highly crystalline nature of many PEEA HSs, the elastomers often appear

transparent due to the inability of the small amide nanoribbons to scatter light, as in the case of PTMO-TΦT PEEA copolymers.[76] PEEA segmented copolymers composed of non-crystallizable oligoamide HS, such as *m*-xylene isophthalamide, showed segmental demixing leading to microphase separation. The bulk morphology of non-crystalline PEEA copolymers exhibited spherical HS domains of varied size spread throughout the polyether matrix (Figure 2.8). PEEA copolymers containing 2 *m*-xylene isophthalamide units revealed minimal phase separation, resulting in poor mechanical properties.[84] Incorporation of chemical crosslinks through trifunctional polyether oligomers into to the non-crystalline PEEA copolymers demonstrated no effect on the polyether T_g or storage modulus. However, a large decrease in tensile properties and compression set resulted due to the decrease in physical crosslinks.[85]
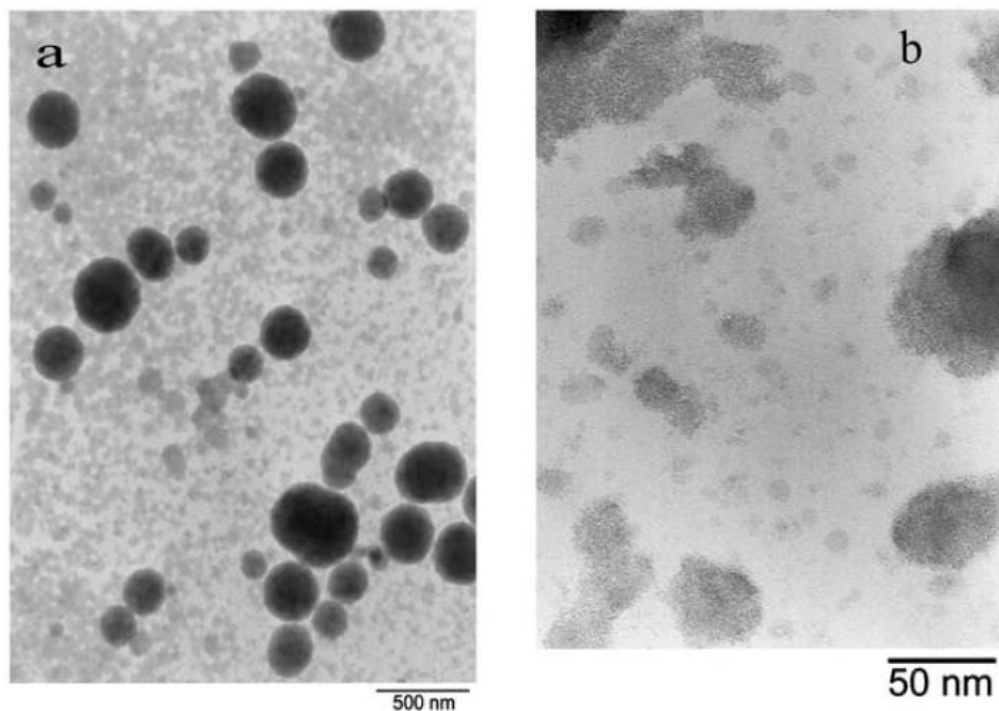
Figure 2.8. TEM images of PEEA copolymers comprised of uniform *m*-xylylene isophthalamide non-crystallisable HS and poly(propylene oxide) SS: 52,000x (a) and 120,000x (b)[84]

Dynamic mechanical behavior of PEEA segmented copolymers revealed large temperature insensitive rubbery plateaus typical of highly microphase-separated segmented copolymers. The plateau region and storage moduli are highly dependent on copolymer composition, which allows for the tuning of mechanical properties through altering copolymer structure.[24,26,29] Increasing polyether SS length resulted in a systematic decrease in the observed T_f and storage moduli of PEEA copolymers due to a decreased wt% HS composition.[83,86,87] Husken et al. studied the effect of alkyl spacing between terephthalamide groups in a crystalline tetra-amide HS (TxTxT, x = alkyl spacer) on the dynamic mechanical behavior of PEEA segmented copolymers (Figure 2.9). The T_f temperature decreased linearly with no significant
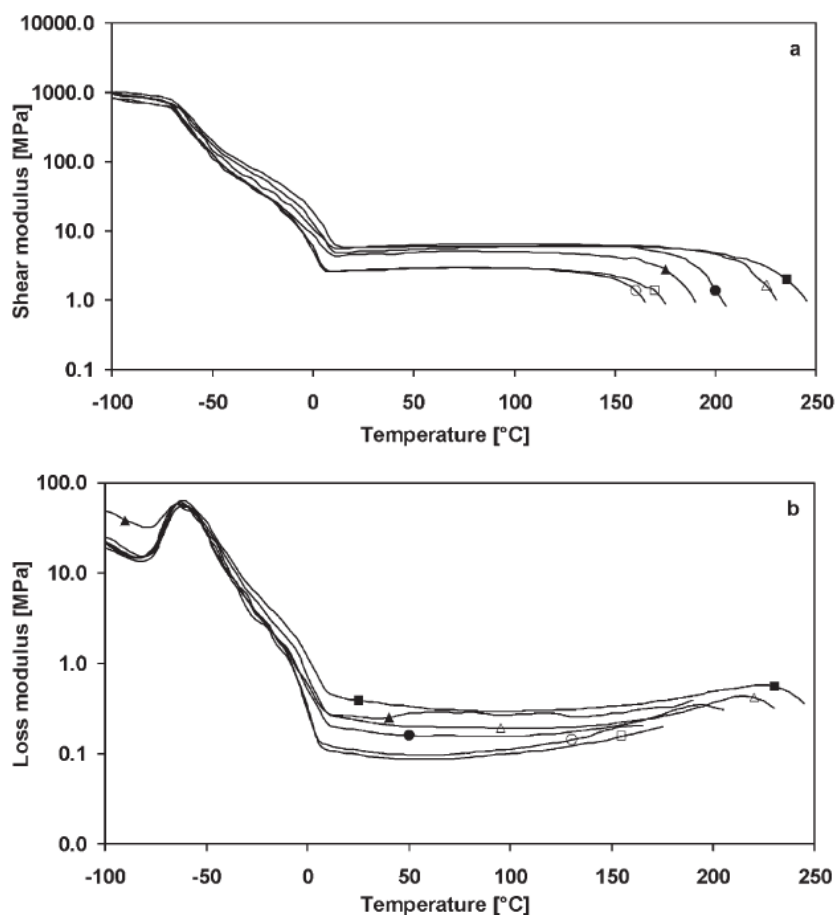
Figure 2.9. Effect of alkyl spacing between terephthalamide groups in the HS on the shear modulus (a) and loss modulus (b) of (PTMO$_{1000}$-T)$_{6000}$-TxTxT segmented copolymers with increasing even and odd spacing: T2T2T (■), T4T4T (Δ), T6T6T (●), T8T8T (▲), T3T3T (□), T7T7T (○)[88]

change in the rubbery plateau storage moduli as the alkyl spacing between terephthalamide groups increased from 2 to 8 methylene groups. Presence of an odd spacer revealed an odd-even effect that resulted in lower T_f values and storage moduli primarily due to lower crystallinity.[88]

Niesten et al. investigated the tensile and elastic properties of a series of PEEA segmented copolymers, and found that varying the aramid (TΦT) content in PTMO based PEEA segmented copolymers yielded a linear increase in Young's modulus typical of segmented copolymers. However, strain at break proved independent of TΦT content and there was also little effect on the stress at break. Elasticity of the copolymers appeared to increase with the decrease in TΦT content, but poor mechanical properties occurred at very low concentrations.[89] Biemond et al. investigated the effects of temperature on the tensile properties for a PTMO-T6A6T PEEA segmented copolymer. No significant change in the modulus is observed as the temperature increased from 20 to 110 ˚C, which indicated no changes in the polyether matrix. However, yield stress and yield strain systematically decreased with increasing temperature and the strain at break also showed a decrease over this temperature range (Figure 2.10).[90] Krijgsman et al. demonstrated the tensile properties of PTMO-T6T6T extruded threads containing various PTMO SS lengths. All the tested threads exhibited a strain at break >1000% with little strain hardening and the modulus and stress at break increased with the increase in T6T6T wt% content.[91] Niesten et al. also proposed that during mechanical deformation, disruption of the crystalline network occured when large lamellae were deformed into smaller lamellae structures and became oriented perpendicular to the polymer chains. The oriented lamellae then broke down further into square crystallites which orient parallel to the chain direction and eventually film fracture occured (Figure 2.11).[92]
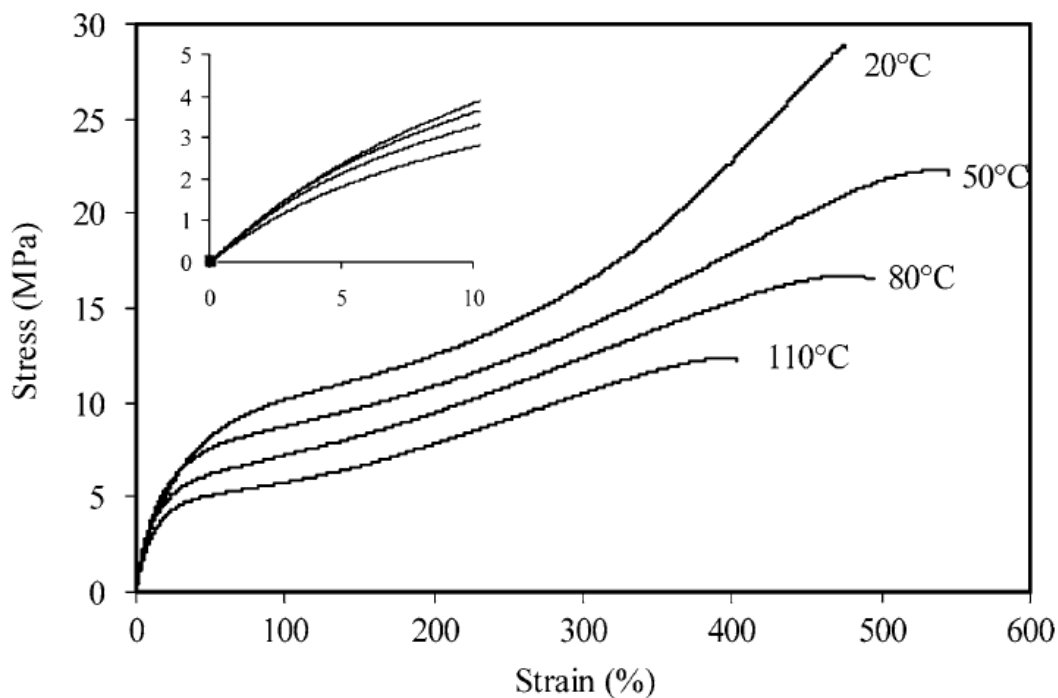
Figure 2.10. Effect of temperature on the stress-strain curves of PTMO2000-T6A6T segmented copolymers[90]

λ = 1   λ = 3   λ > 8
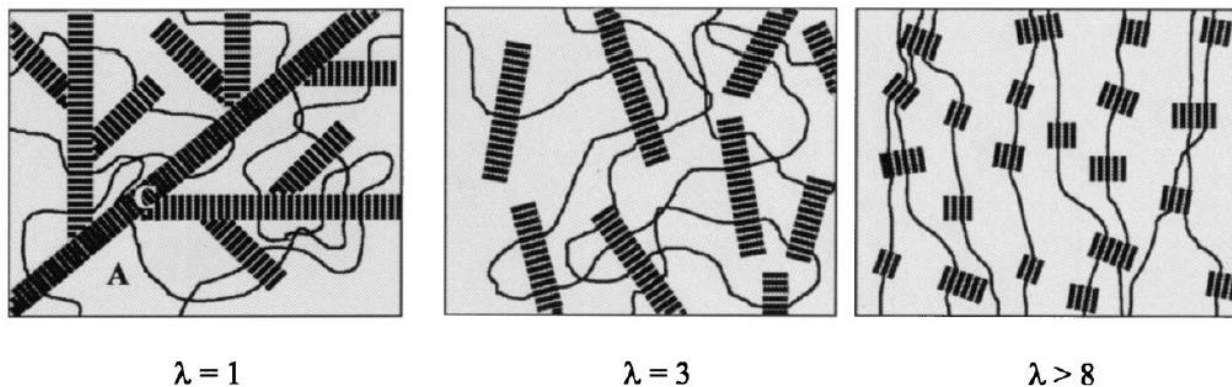
Figure 2.11. Schematic representation of the microstructural changes upon mechanical deformation for PTMO-TΦT segmented copolymers[92]

2.6 Poly(ester amide) Segmented Copolymers

2.6.1 Background

Poly(ester amide) (PEA) segmented copolymers are another class of segmented copolymers containing ester groups, except that PEAs utilize long polyester segments that function as the copolymer SS. Aliphatic polyesters typically demonstrate poor physical and

mechanical properties, but incorporation of amide segments into the polyester backbone, as with PEA copolymers, provides a useful microphase separated segmented copolymer. PEA copolymers exhibit TPE behavior and tunable properties through changes in copolymer composition.[93] PEAs also demonstrate favorable properties of both polyesters and PA including degradability, excellent toughness, and good processing properties. The biodegradation aspect of PEA segmented copolymers provided a driving force for the development and understanding of more environmentally friendly plastics due to the growing issue of plastic waste in the environment.[94] Besides PEA TPE applications, copolymers also showed promise for biomedical applications due to the biocompatible and biodegradable nature of the copolymers along with the ability to tune physical properties.[95] Lips et al. reported the *in vivo* use of aliphatic PEA copolymers as biodegradable implants, which slowly degraded over time through ester bond cleavage and showed that PEAs were suitable for biomedical implant applications.[96] Pang et al. developed functionalized, water soluble PEA copolymers based on L-arginine, DL-2-allylglycine, oligoethylene glycol, and an aliphatic diacid. *In vitro* toxicity studies revealed the lack of toxicity after exposure to the PEA segmented copolymers, which supported the potential biomedical use of the copolymers and their derivatives.[97]

2.6.2 Synthetic Strategies

Synthesis of poly(ester amide) segmented copolymers included melt polymerization of a small diester, aliphatic diol, and oligoamide monomers such as dimethyl terephthalate, hexanediol, and T6T6T-dimethyl for example (Scheme 2.3). Melt polymerization proceeded with all the monomers being loaded into a reaction flask under inert atmosphere with a catalyst, such as $Ti(i-OCH_3)_4$, and heated to ~180 ˚C. Increasing the polymerization temperature to ~ 250 ˚C and applying a low vacuum removed the excess hexanediol to achieve high molecular weight

macromolecules. Lastly, increasing the temperature again 10 to 20 ˚C and placing the

polymerization under a high vacuum further drove the polymerization to completion.[98] The use

of diisocyanates were also useful for synthesis of PEA segmented copolymers. Jeong et al.

demonstrated the polycondensation of 4,4'-methylenediphenyl diisocyanate, diacid poly(ester)

oligomers, and aliphatic dicarboxylic acids in solution at 200 ˚C, which yielded elastomeric films

with good tensile properties.[99] Another route for polycondensation of PEA segmented

copolymers included the use of biocatalytic methods for polymerization. Synthesizing

poly(dimethyl siloxane) based PEAs through a bulk polymerization strategy with an immobilized

Candida antartica Lipase B (Novozym 435), which catalyzes the polymerization of a diester,

diamine, and aliphatic diol afforded a useful PEA segmented copolymer. However, amide

formation occurred faster with this polymerization strategy, and led to a block like sequence

distribution within the copolymers.[100,101]

Scheme 2.3. Melt polymerization of PEA segmented copolymer composed of poly(hexamethylene terephthalate) and T6T6T[98]
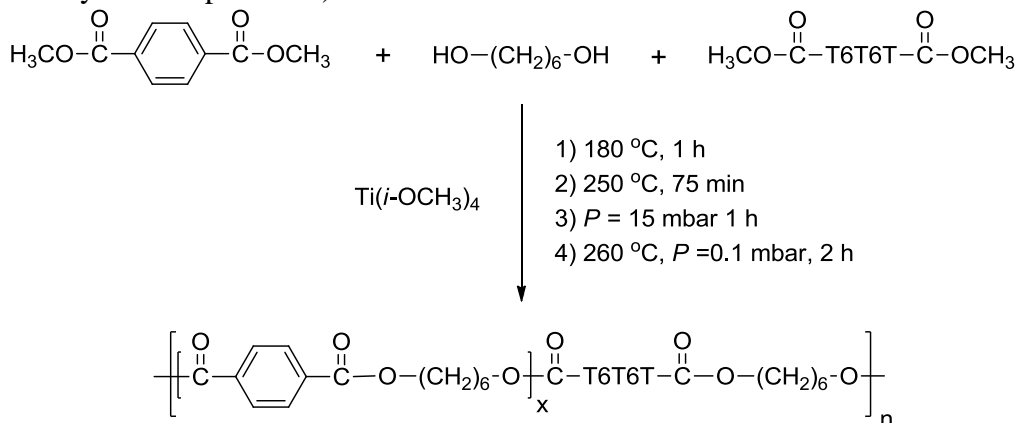
Anionic ring-opening polymerization (ROP) strategies utilizing ε-caprolactone (CLO)

and ε-caprolactam (CLA) also provided excellent PEA segmented copolymers. Chromcová et al.

reported the anionic ROP of CLO and CLA using a polymerization casting technique at 150 ˚C

with 1 mol% CLA-MgBr initiator that provided very tough PEA copolymers.[102] Similarly,

Bernášková et al. demonstrated the preparation of PEA copolymers through anionic ring-opening polymerization of CLA in the presence of poly(ϵ-caprolactone) (PCLO) at temperatures ranging from 90 to 180 ˚C. Anionic ring-opening polymerization of CLA and PCLO initiated with solid CLA-MgBr yielded ductile films with reduced tensile properties compared to PEA copolymers produced from CLA and CLO alone.[103]

2.6.3 Properties

DSC and DMA of PEA segmented copolymers often suggested a microphase separated three-phase structure that possessed a poly(ester) T_g and two T_ms corresponding to the melting of the polyester and crystalline amide containing HS, depending on PEA composition.[98] However, some PEA copolymers that contain non-uniform HS lengths displayed two melting transitions attributed to crystals containing a single ester amide group and those containing 2 or more ester amide groups.[104] The T_g of the poly(ester) SS in PEA copolymers often depended on the copolymer wt% HS content. For example, a PEA segmented copolymer composed of a poly(butylene adipate) (PBA) SS and bisamide HS exhibited an increase in the PBA T_g from -52 ˚C for the homopolymer to -5 ˚C for the PEA containing 85 mol% HS (Figure 2.12). This change in T_g indicated an increase in phase mixing of the soft polyester segments with the amide HS at higher mol% HS content. The increase in mol% HS also revealed an increase in the HS T_m and DMA T_f.[93] The trend of increased T_g and T_m of PEA copolymers with the increase in mol% HS was typically observed for PEA segmented copolymers.[104-106]
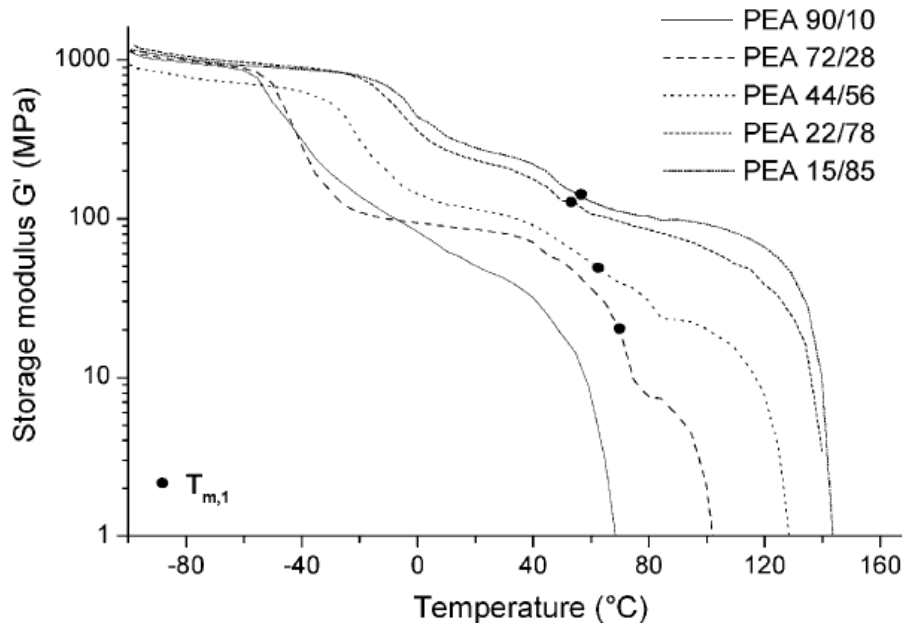
Figure 2.12. Dynamic mechanical behavior of PEA segmented copolymers with increasing mol% HS (10 – 85%)[93]

PEA segmented copolymers demonstrated tensile properties typically observed for TPEs with high stress and strain at break. Varying the amide HS content of PEA copolymers allowed for the fine tuning of the tensile properties that a PEA copolymer containing a crystallisable bisamide HS exhibited. For example, varying the molar ratios of bisamide-diol, 1,4-butanediol, and dimethyl adipate resulted in a systematic increase in tensile properties when the HS increased from 10 to 85 mol% (Figure 2.13). The PBA-bisamide copolymer showed an increase in modulus from 70 to 524 MPa and stress at break from 8 to 28 MPa with a corresponding decrease in the strain at break.[93]

PEA segmented copolymers with various ratios of CLA and CLO exhibited systematically decreased T_g values with the decrease in lactam units from 48 °C for PCLA to -57 °C for PCLO. A decrease in copolymer T_f occurred with increasing molar ratios of the SS lactone units and copolymers containing 30 to 90% lactone units yielded tough materials.[102] Hydrolytic degradation studies of PEA copolymers comprised of CLA and CLO units showed
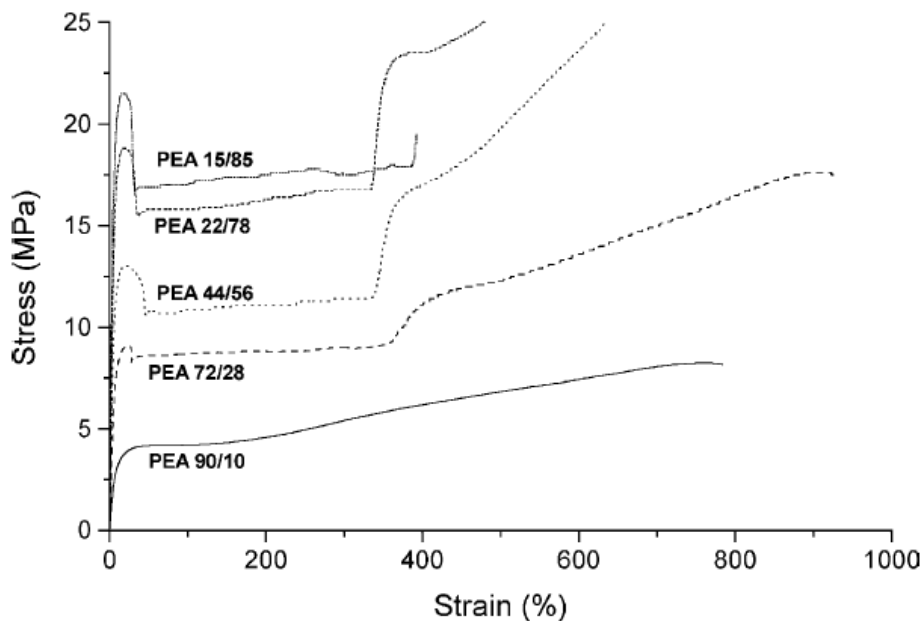
Figure 2.13. Effect of HS mol% (10 − 85%) on the tensile properties of PBA-bisamide PEA segmented copolymers[93]

degradation in phosphate buffer occurred through ester bond cleavage. When compared to CLO homopolymers, PEA copolymers composed of CLA and CLO demonstrated increased degradation rates of hydrolysis due to the presence of hydrophilic CLA units.[107] Overall, the structure property relationships of PEA copolymers were similar to other segmented copolymers with respect to variations in the copolymer HS wt%, and possessed tunable properties for a wide range of applications.

2.7 Poly(oxamide) Segmented Copolymers

2.7.1 Background

Oxamide groups are a special type of hydrogen bonding moiety that contain two amide groups covalently linked together at their carbonyls. Studies have shown that oxamide groups exhibit strong hydrogen bonding interactions and form semi-crystalline nanostructures in some cases.[108,109] The oxalate precursors provide increased reactivity toward amines compared to traditional esters and the oxamide functionality allows for development of unique hydrogen

28

bonding structures for segmented copolymers (Figure 2.14). Few examples currently exist in literature that describe the synthesis and properties of oxamide containing segmented copolymers. Schulze first reported the synthesis of poly(oxamide) segmented copolymers in a 1978 patent that described the methods for synthesis of PPG poly(oxamide) segmented copolymers.[110] Leir et al. published patents in 2007 that detailed the synthesis and film forming methods for PDMS poly(oxamide) segmented copolymers, which yielded optically clear TPEs with shore A hardness values from 14 to 88 depending on copolymer composition..[111-114] More recently, Sajbrandi et al. published a report for the synthesis and characterization of PTMO poly(oxamide) segmented copolymers, which provided insight into the structure property relationships of poly(oxamide) segmented copolymers.[115,116] Our recent research has focuses on the development and understanding of poly(oxamide) segmented copolymers through detailed structure-property relationship studies, and synthesis of novel oxamide containing segmented copolymers.[117-119]
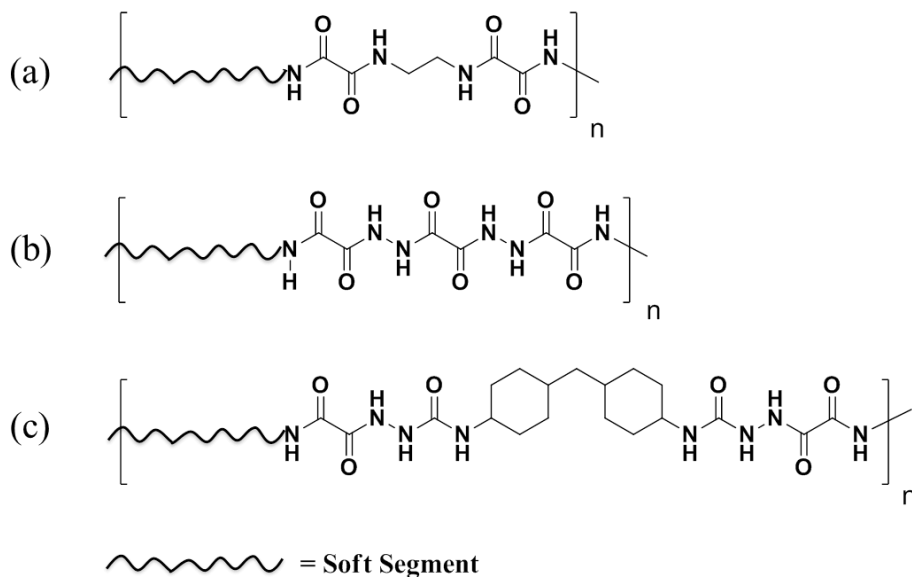
Figure 2.14. HS structures of (a) poly(oxamide), (b) poly(trioxamide), and (c) poly(urea oxamide) segmented copolymers

2.7.2 Synthesis

29

The most common source of oxamide groups for the synthesis of poly(oxamide) segmented copolymers is diethyl oxalate. All the published poly(oxamide) copolymers are comprised of an oligomeric SS and oxamide containing HS of uniform length. Preparation of poly(oxamide) copolymers began with the end-capping of amine terminated polyethers or PDMS oligomers with an excess of diethyl oxalate in the bulk from 0 to 23 ˚C or solution at 23 ˚C, which yielded difunctional ethyl oxalate terminated oligomers. After removal of excess diethyl oxalate, step-growth polymerization with a 1:1 stoichiometric amount of diamine provided the desired poly(oxamide) segmented copolymer (Scheme 2.4).[115,117] Depending on the nature of the reactants, polymerization of ethyl oxalate terminated oligomers with diamines required various polymerization temperatures. Ethyl oxalate terminated PDMS oligomers efficiently polymerized

Scheme 2.4. Synthesis of PTMO polyoxamide segmented copolymers[115]
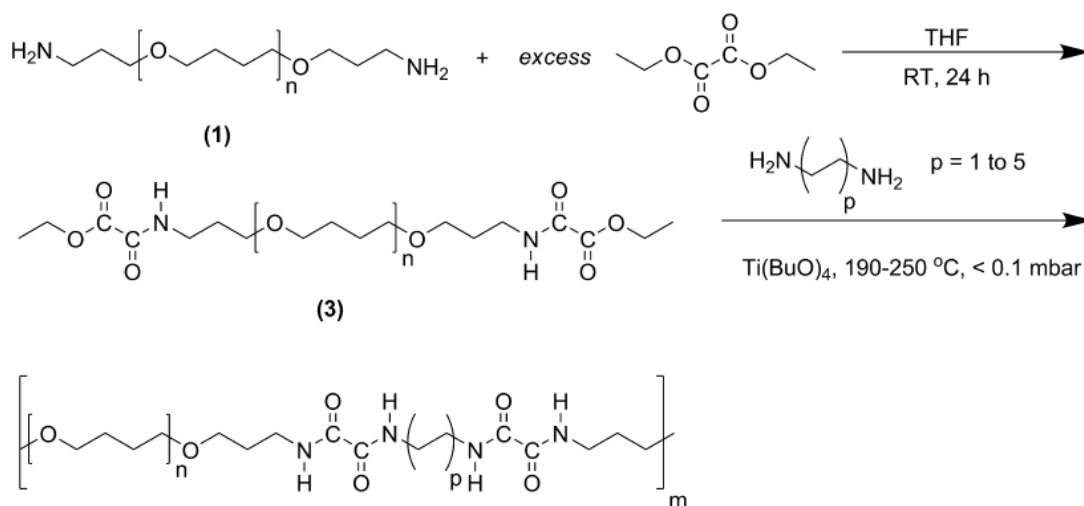
with diamines from 23 to 120 ˚C without catalyst and afforded optically clear, elastic films.[118] PTMO based poly(oxamide) copolymers were melt polymerized at 190 to 250 ˚C with a Ti(BuO)$_4$ catalyst and resulted in yellow transparent films.[115] Other oxamide containing segmented copolymers recently developed included PDMS poly(urea oxamide) and PPG poly(trioxamide). These novel copolymers were obtained through solution polymerization of

oxamic hydrazide terminated oligomers with 4,4′-methylenebis(cyclohexyl isocyanate) (HMDI) or oxalyl chloride.[117,119]

2.7.3 Properties

Poly(oxamide) segmented copolymers exhibited highly microphase separated bulk morphologies. The bisoxamide HS formed strong hydrogen bonding physical crosslinks and possessed a semi-crystalline nanostructure observed with DSC, WAXD, and AFM (Figure 2.15).
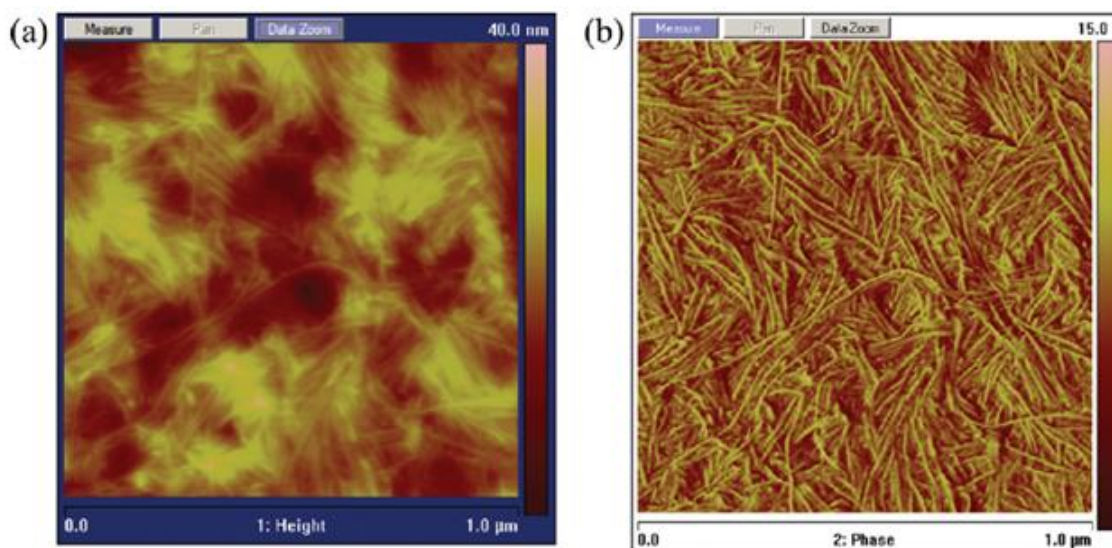
Figure 2.15. AFM (a) height and (b) phase image of PTMO poly(oxamide) segmented copolymer containing two oxamide groups in the HS[115]

Melting of the crystalline bisoxamide HS domains resulted in the onset of flow for each copolymer. PTMO based poly(oxamide)s also showed a high moduli >120 MPa with stress and strain at break up to 27 MPa and 900%, respectively.[115] Poly(oxamide) copolymers based on PDMS demonstrated a Young's modulus, stress at break, and strain at break of 96 MPa, 8 MPa, and 940%, respectively. However, copolymer composition and level of crystallinity greatly affected the mechanical properties.[118] DMA revealed long temperature insensitive service windows up to 180 ˚C for PDMS poly(oxamide) copolymers, and the rubbery plateau length and storage moduli varied with copolymer composition (Figure 2.16).[115,117,118]

31
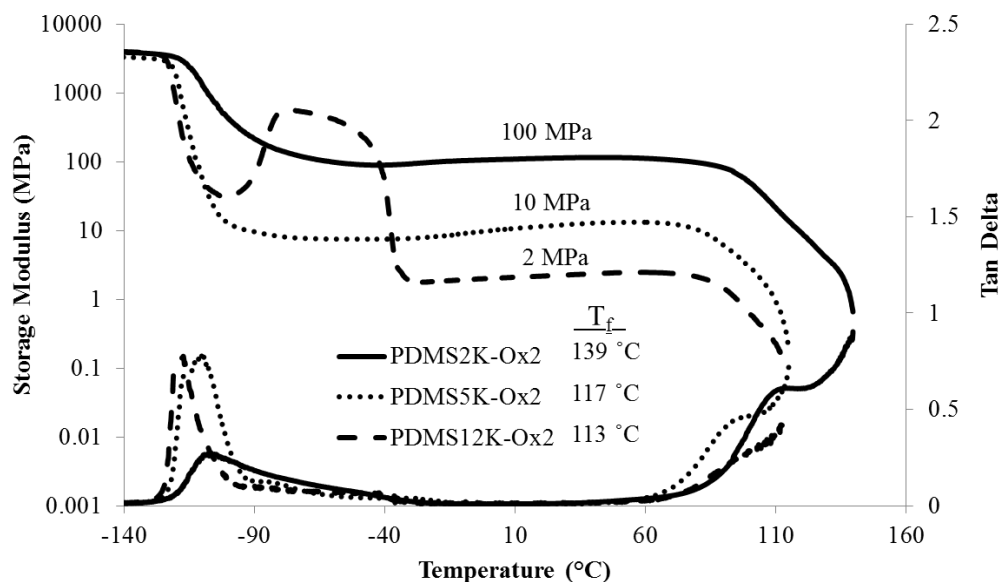
Figure 2.16. DMA traces of PDMS poly(oxamide) copolymers with PDMS$_{2000}$, PDMS$_{5000}$, and PDMS$_{12000}$ SS[118]

Recent reports include the structure-property relationships of poly(oxamide) copolymers for both PTMO and PDMS based copolymers. The distance between oxamide groups and number of oxamides in the HS resulted in large differences in the mechanical properties of the copolymers. Sijbrandi et al. demonstrated that two oxamide groups in the HS provided sufficient physical crosslinking to impart microphase separation and copolymers that contain a single oxamide group exhibited poor mechanical properties due to insufficient physical crosslinking. Increasing from two to three oxamide groups in the HS caused an increased T_f and storage modulus, but reduced the tensile properties.[115] Spacing between oxamide groups also proved important with the most significant effects observed with PDMS-based copolymers. As oxamide spacing increased, the T_m and T_f decreased due to a reduction in the cooperative effects of neighboring hydrogen bonds, and resulted in decreased thermal stability of the HS order.[115,118] Variable temperature FTIR spectroscopy revealed the effect of oxamide spacing on the thermal stability of poly(oxamide) HS order and the ordered, hydrogen bonding disruption occurred at

32

lower temperatures with an increase in oxamide spacing (Figure 2.17). A reduction in tensile properties and hysteresis also occurred as a result of the increase in distance between oxamide groups.[118] The structure-property relationship studies of poly(oxamide) segmented copolymers suggested the shortest, even spaced oxamide linkers provided optimal physical properties.
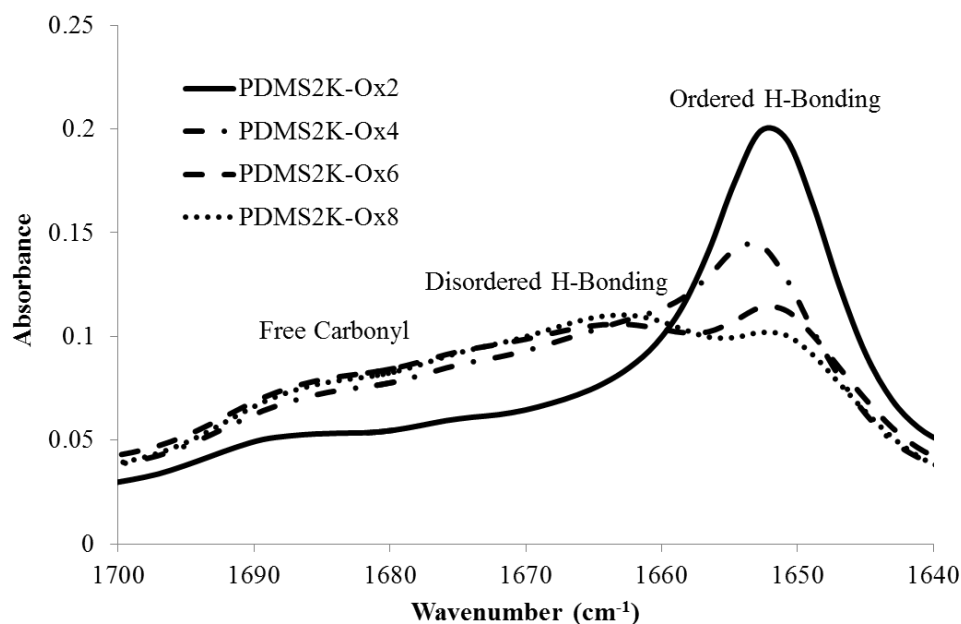
Figure 2.17. FTIR spectra at 100 ˚C of PDMS$_{2000}$ poly(oxamide) segmented copolymers with 2, 4, 6, and 8 methylene groups between oxamides in the HS[118]

The recent development of poly(urea oxamide) copolymers represented a new family of segmented copolymers containing both oxamide and urea hydrogen bonding groups covalently linked in the uniform HS structure. Poly(urea oxamide) segmented copolymers yielded excellent tough, elastic films with superior physical properties compared to traditional poly(urea) analogs. The enhanced hydrogen bonding of the urea oxamide HS led to increased microphase separated morphologies and service windows compared to polyurea analogs. Poly(urea oxamide) copolymers also demonstrated a higher Young's moduli and stress at break, but a decrease in the strain at break resulted.[117,119] Oxamide containing segmented copolymers is an important class of TPEs, which possess unique, tunable physical properties and mild polymerization conditions.

33

2.8 Poly(dimethyl siloxane) Poly(amide) Segmented Copolymers

2.8.1 Background

Segmented copolymers comprised of a PDMS SS and amide containing HS stand in a class of their own when compared to other amide containing segmented copolymers due to the nature of the PDMS SS. A high degree of incompatibility between PDMS and polar amide containing HSs exist and lead to highly microphase separated morphologies with a wide range of physical properties. Applications of PDMS poly(amide) (PDMS-PA) segmented copolymers include thermoplastic adhesives, cosmetics, fabric finishing agents, anti-cloud coatings, and production of organic-inorganic hybrid composites.[114,120-122] PDMS-PA copolymers also provide efficient gas permeable membranes for applications with a membrane-liquid interface due to the high tensile strength and low interface resistance that yields highly oxygen permeable membranes.[123] Studies into the biomedical applicability of PDMS-PA copolymers demonstrated the effects of copolymer composition on surface interactions of various biomolecules as well as compatibility with blood, and showed PDMS-PA copolymers were inert *in vivo*.[124,125] A number of PDMS-PA segmented copolymers were reported that included organometallic structural features. For example, two PDMS-PA copolymers containing pendent trichlorogermyl or ferrocene groups both exhibited good thermal and mechanical properties for use as protective coatings.[126,127] However, a majority of the research conducted on PDMS-PA copolymers included PDMS poly(aramid) (PDMS-PAr) segmented copolymers that Imai et al. introduced in 1989.[128]

2.8.2 Synthesis and Properties

McGrath et al. first introduced the synthesis of PDMS-PA segmented copolymers that typically required step-growth polymerization of an amino-alkyl terminated PDMS oligomer

with a di-functional monomer.[129] Policastro et al. reported the step-growth polymerization of aminopropyl terminated PDMS with 2,2'-*p*-phenylenebis(4,4-dimethyl-5-oxazolone) in CHCl$_3$, which yielded transparent, elastic films.[130] Another synthetic route to PDMS-PA copolymers involved polycondensation of diester monomers with diamino PDMS oligomers. The polarity differences of PDMS and the polar diester monomer resulted in heterogeneous reactions, often leading to poor polymerization. The most common synthetic route for polymerization included polar diacid chloride monomers with diamino PDMS oligomers.[120,128] For example, aminophenyl aniline, isophthaloyl chloride, triethylamine, and aminopropyl terminated PDMS successfully polymerized at 0 °C in CHCl$_3$ for 1 h and then at 23 °C for 5 h under nitrogen atmosphere (Scheme 2.5). A one or two-step solution polymerization strategy provided the desired PDMS-

Scheme 2.5. Synthesis of PDMS-PAr segmented copolymers through a one or two-step polymerization scheme[128]
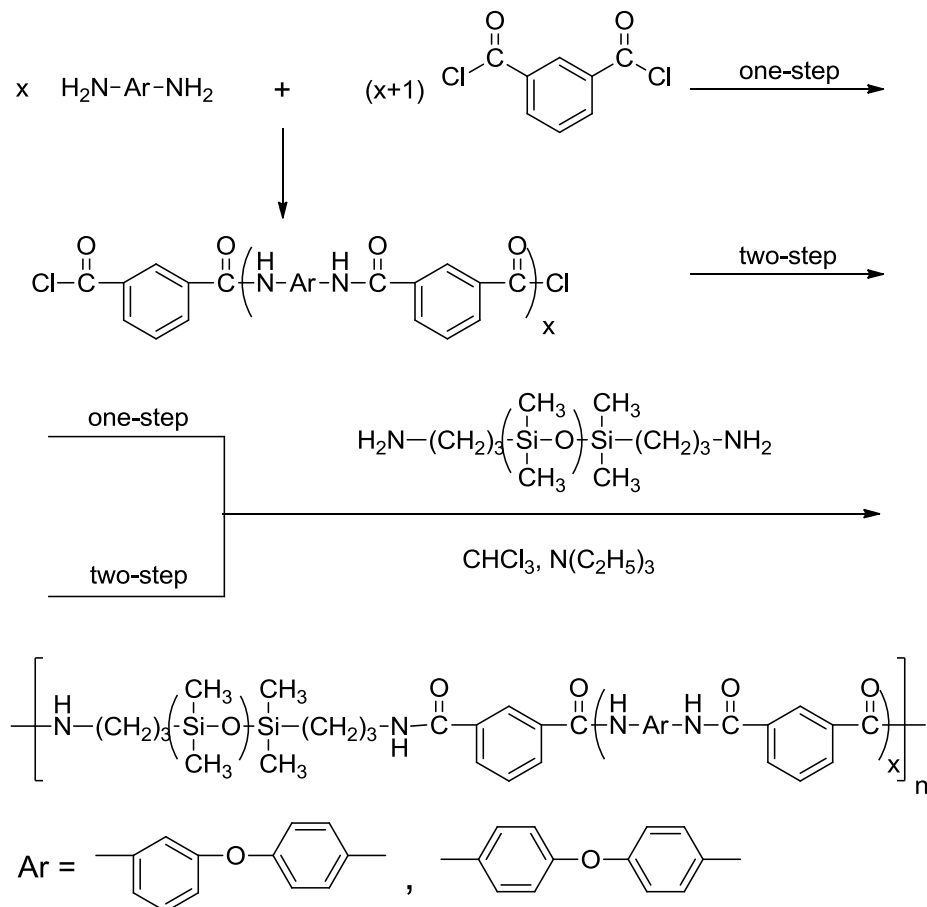
PAr copolymers, but the two-step strategy yielded copolymers with better defined microphase separated morphologies and tensile properties.[128] A similar polymerization strategy utilized 1,3-bis(3-aminopropyl)-l,l,3,3-tetramethyldisiloxane (BATS) for the polymerization of PDMS-PAr, which provided transparent plastic films useful for surface coatings and biomaterial applications.[131] Copolymers containing random sequences of diamino disiloxane and aramid segments yielded tough, single phase materials with poor tensile properties.[132]

The microphase separated bulk morphologies of PDMS-PA segmented copolymers change with variations in copolymer composition.[133,134] The surface of PDMS-PA segmented copolymers contained primarily only PDMS SS, even at lower PDMS wt% composition due to the low PDMS surface energy. The phase separated bulk morphology resided deeper in the films, which resulted in the observed mechanical properties.[135] Randomly sequenced aramid HS of PDMS-PAr copolymers exhibited high T_g values ranging from 150 to 240 ˚C, but depended on wt% HS content and length of aramid HS. Copolymers with alternating hard and soft segments showed only a PDMS T_g (-123 ˚C) and the lack of aramid T_g is attributed to the semi-crystalline nature of the uniform aramid HS.[136] The dynamic mechanical behavior of PDMS-PAr revealed a relatively temperature insensitive rubbery plateau with storage moduli that decreased with an increase in the PDMS wt% content (Figure 2.18). Molecular weight of the aramid HS sequence, or PDMS wt%, ultimately determined the temperature for the onset of flow of each PDMS-PAr copolymer. The highest T_f results with the lowest PDMS wt% copolymer composition and gradually decreases as the PDMS content increases.[137]
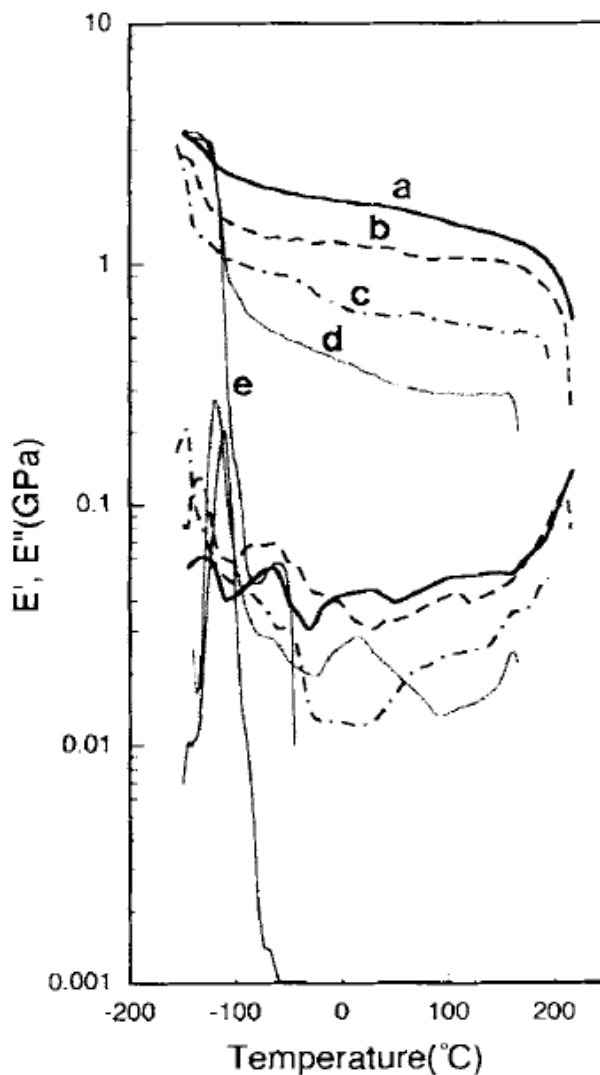
Figure 2.18. DMA of PDMS-PAr segmented copolymers at a PDMS wt% content of (a) 26 wt%, (b) 35 wt%, (c) 46 wt%, (d) 53 wt%, and (e) 75 wt%[137]

Regularity of aramid HSs in PDMS-PAr copolymers also had a significant impact on tensile properties. Copolymers composed of random HS sequences demonstrated an increase in stress at break with the decrease in copolymer PDMS content with values ranging from 54 to 6 MPa for PDMS-PAr copolymers containing 20 to 73 wt% PDMS (1680 g/mol), respectively. Copolymer moduli increased while strain at break decreased with the decrease in copolymer PDMS content. Copolymers that possessed a uniform aramid HS exhibited lower moduli and stress at break than the randomly sequenced HS counterparts, but show a large increase in the

strain at break.[136] An aramid homopolymer, composed of 3,4'-diaminodiphenyl ether and isophthaloyl chloride, demonstrated a very high stress at break of ~100 MPa and an elongation similar to a PDMS-PAr containing 55 wt% SS.[123] Generally for PDMS-PA segmented copolymers, lower PDMS wt% content leads to increased stress at break and moduli.

2.9 Poly(amide) Segmented Copolymers Containing Urethane, Urea, and Imide Groups

2.9.1 Background and Synthesis

Many examples of segmented PA copolymers containing multiple hydrogen bonding groups exist in literature such as poly(amide ester imide) (PAEI), poly(amide imide urethane) (PAIU), poly(amide urethane) (PAU), poly(ester urethane amide) (PEUA) and poly(urethane urea amide) (PUUA) segmented copolymers. Applications for these types of PA segmented copolymers include electrical insulating materials, circuit board materials, chiral phases for enantiomeric separations, protective coatings, and slowly biodegrading materials.[138-141] Some of these segmented copolymers also find applications for biomedical devices. For example, PUUA segmented copolymers composed of a polyether SS showed promising properties for antithrombogenic applications due to favorable surface properties of the copolymer and tuning of the surface properties through structural variation.[142]

A wide range of synthetic strategies enabled the production of these segmented copolymers. Synthesis of PEG containing PAEI segmented copolymers with a carboxylic acid terminated imide-PEG-imide oligomer and various aromatic diamines occured through solution polymerization in a mixture of pyridine, NMP, TPP, and CaCl$_2$ as a condensing agent.[143] Mallakpour et al. reported the two-step synthesis of PAIU segmented copolymers that contained a PEG SS through a pre-polymerization method in NMP with no catalyst.[144] Novel amide imide

diacid monomers containing various chiral amino acids and excess MDI, afforded a pre-polymer that were subsequently polymerized with a PEG diol to yield a ductile, free-standing film.[145] Baez et al. formed a prepolymer with PCL diol and 1,6-hexanediisocyanate in DMAc at 80 ˚C to synthesize PEUA copolymers. Chain extension in DMAc with a diamide-diol monomer provided the final PEUA copolymer and a ductile film is obtained after solution casting.[140] Using a amide-diamine chain extender instead of amide-diol, and the same prepolymer method for the preparation of PUUA segmented copolymers resulted in an excellent TPE with a service window exceeding 250 ˚C.[146]

2.9.2 Properties

PAEI segmented copolymers containing a PEG SS were highly soluble copolymers with good thermal stability. DSC and XRD of the PAEI copolymers revealed a single T_g and semi-crystalline HS domains.[143] Optically active PAIU segmented copolymers containing a polyether SS demonstrated higher thermal stability compared to poly(ether urethane) copolymers with 10% weight loss observed at ~300 ˚C. PAIU copolymers also revealed two T_gs, one for both the SS and HS, as well as evidence of a slightly phase-mixed morphology despite the semi-crystalline nature of the HS.[139] The amide-imide diacid structure greatly affected the thermal stability of PAIU copolymers and copolymers that contained 4,4'-(Hexafluoroisopropylidene)-*N*,*N*-bis(phthaloyll-leucine-*p*-amidobenzoic acid) HS content showed the poorest thermal stability.[147] Even though polyether based PAIU segmented copolymers exhibited microphase-separated morphologies, the films lacked a temperature insensitive rubbery plateau region in the DMA. The thermomechanical behavior and T_f of PAIU copolymers are highly dependent on the type of polyether SS used as well as the HS wt% content.[139]

PEUA segmented copolymers based on PCL were elastic, microphase separated copolymers with biodegradable amide linkages. Copolymers exhibited a T_m for both segments and the HS T_m increases with the increase in HS wt%. The PCL based PEUA copolymers showed good tensile properties with elongation values at lower wt% HS content, up to 1500%. Stress at break did not significantly change with HS wt% unlike the moduli, which increased with higher HS wt% from 37 to 210 MPa.[140] Van der Schuur et al. investigated the structure property relationships of PUUA segmented copolymers that particularly focused on the length of the amide HS (hexamethylenediamine, 6T6, and 6T6T6). PUUA copolymers containing 6T6 HS exhibited microphase-separation through crystallization, similar to the PEEA segmented copolymers previously discussed. DMA showed an increase in T_f and service window storage moduli for PUUA copolymers with increased HS length (Figure 2.19). Copolymers that
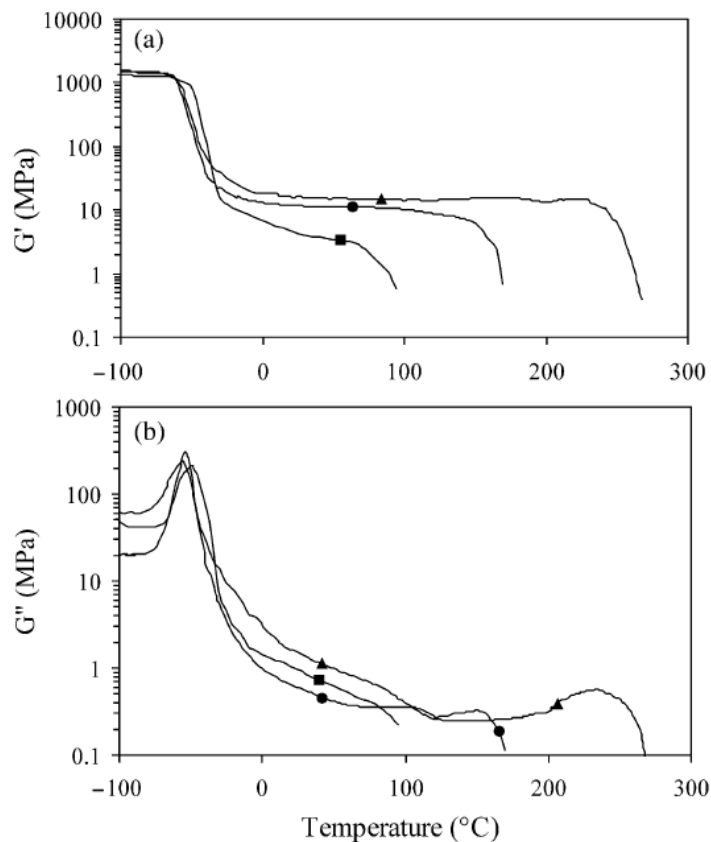
Figure 2.19. Effect of amide HS length on the (a) storage modulus and (b) loss modulus of PUUA segmented copolymers: HMDA (■), 6T6 (●), 6T6T6 (▲)[146]

40

contained 6T6 HS exhibited enhanced tensile properties over the hexamethylenediamine HS and superior thermomechanical behaviors compared to a commercial thermoplastic urethane.[146] The presence of amide groups in the hard segment of PUUA copolymers imparted improved mechanical strength and energy dissipation due to higher amounts of HS interconnectivity when compared to poly(urethane urea) analogs.[148]

2.10 Conclusions and Outlook

Amide hydrogen bonding groups in segmented copolymers play an important role in determining the thermal and mechanical properties of PA segmented copolymers. The strong hydrogen bonding intermolecular interactions of amide groups provide the physical crosslinks necessary for imparting microphase separated morphologies. The ability and strength of amide HS hydrogen bonding relies primarily on the structure of the HS and number of amide groups present. The extent of crystallinity that an amide HS possesses also significantly affects the microphase separation, mechanical properties, thermal stability, and appearance of the segmented copolymer. Multiple researchers demonstrated a wide range of copolymer physical properties and potential applications through changes in copolymer composition. Variations in the soft segment structure (PEG, PPG, PTMO, PDMS, polyester, PPE) as well as the molecular weight greatly influenced copolymer performance. The literature contains reports of a wide variety of segmented copolymers with various amide HS architectures, ranging from aramids to oxamides and exemplifies the potential for tuning segmented copolymers through structural modifications.

Poly(ether-*block*-amide) (PEBA) segmented copolymers are high performance thermoplastic elastomers with excellent physical properties such as high tensile strength, large workable temperature windows, chemical resistance, and good processability. Synthesis of

PEBA segmented copolymer is well developed and provides a method for synthesis of a wide variety of PEBA structures. A large and diverse number of applications for PEBA copolymers exist with many more to come as new structures and physical properties are realized. New copolymer architectures and the use of organic and inorganic modifying agents will open new horizons for PEBA segmented copolymers. Poly(ether ester amide) (PEEA) copolymers possess many options for new structural copolymers building off the current understanding of the structure property relationships of PEEA segmented copolymers. PEEA copolymers have excellent, tunable physical properties aligned with many commercial applications. The ability to alter surface chemistry and subsequent properties showed promise for biomedical applications. Poly(ester amide) (PEA) copolymer also exhibited physical properties desirable for various biomedical applications, and the degradation abilities in conjunction with good physical properties provide a large opportunity for further studies into the properties and applications of novel PEA copolymers.

Poly(oxamide) segmented copolymers demonstrate excellent physical properties and unique polymerization chemistry. Recent studies into the structure property relationship of poly(oxamide) copolymers reported excellent thermoplastic elastomer behavior with the ability to tune physical properties through polymer structural modifications. Examples of current applications are limited, but there are many opportunities to exploit using the unique oxamide chemistry. Poly(oxamide) segmented copolymers are highly processable and detailed research into the processability of poly(oxamide)s is needed. Poly(dimethyl siloxane) (PDMS) segmented copolymers have excellent properties with well understood polymerization chemistry. The unique properties of PDMS imparts enhanced physical properties including flexibility, gas permeation, chemical resistance, etc., which are useful for many commercial applications

including thermoplastic adhesives, textiles, separation membranes, and coatings. New HS structures are needed for PDMS segmented copolymers to develop the next generation of PDMS-based high performance materials. Amide-containing segmented copolymers composed of multiple hydrogen bonding groups in conjunction with amides proved useful in developing novel segmented copolymers with unique and tunable physical properties. Many of these copolymers, which include esters, urethanes, ureas, and imides, exemplify the copolymer structural possibilities. Many of these copolymers exhibited enhanced physical properties and showed how combinations of polymerization chemistries can result in unique, useful materials. Despite the extensive research reported on amide containing segmented copolymers, there exists multiple future research avenues. Current understanding of the structure-property relations for amide-containing segmented copolymers provides a large toolbox for future development of new segmented copolymers with excellent, application specific properties and ability to accurately predict the properties a new segmented copolymer composition will exhibit.

2.11 References

(1)   Castagna, A. M.; Pangon, A.; Choi, T.; Dillon, G. P.; Runt, J. *Macromolecules* **2012**, *45*, 8438.
(2)   Chakrabarty, S.; Nisenholt, M.; Wynne, K. J. *Macromolecules* **2012**, *45*, 7900.
(3)   ten Cate, A. T.; Sijbesma, R. P. *Macromolecular Rapid Communications* **2002**, *23*, 1094.
(4)   van der Schuur, M. J.; Gaymans, R. J. *Polymer* **2007**, *48*, 1998.
(5)   Camberlin, Y.; Pascault, J. P. *Journal of Polymer Science Part B-Polymer Physics* **1984**, *22*, 1835.
(6)   Versteegen, R. M.; Sijbesma, R. P.; Meijer, E. W. *Macromolecules* **2005**, *38*, 3176.
(7)   Fang, J.; Tanaka, K.; Kita, H.; Okamoto, K.-I.; Ito, Y. *Journal of Polymer Science Part B: Polymer Physics* **2000**, *38*, 1123.
(8)   Mallakpour, S.; Rafiemanzelat, F. *Polymer Bulletin (Heidelberg, Ger.)* **2006**, *56*, 9.
(9)   Okoroafor, E.; Rault, J. *Journal of Polymer Science Part B: Polymer Physics* **1991**, *29*, 1427.
(10)   Tavernier, B.; Mewis, J.; Van Puyvelde, P.; Takenaka, M.; Ernst, B.; Hashimoto, T. *Polymer Engineering & Science* **2008**, *48*, 2418.
(11)   Dodge, J.; John Wiley & Sons, Inc.: 2003, p 197.
(12)   Yilgor, I.; Eynur, T.; Bilgin, S.; Yilgor, E.; Wilkes, G. L. *Polymer* **2011**, *52*, 266.
(13)   Mark, J. E. *Accounts of Chemical Research* **2004**, *37*, 946.

(14) Das, S.; Yilgor, I.; Yilgor, E.; Wilkes, G. L. *Polymer* **2008**, *49*, 174.

(15) Krijgsman, J.; Feijen, J.; Gaymans, R. J. *Polymer* **2004**, *45*, 8523.

(16) Korley, L. T. J.; Pate, B. D.; Thomas, E. L.; Hammond, P. T. *Polymer* **2006**, *47*, 3073.

(17) Pukánszky Jr, B.; Bagdi, K.; Tóvölgyi, Z.; Varga, J.; Botz, L.; Hudak, S.; Dóczi, T.; Pukánszky, B. *European Polymer Journal* **2008**, *44*, 2431.

(18) Jewrajka, S. K.; Yilgor, E.; Yilgor, I.; Kennedy, J. P. *Journal Polymer Science Part A: Polymer Chemistry* **2008**, *47*, 38.

(19) Tang, D.; Mulder, D.-J.; Noordover, B. A. J.; Koning, C. E. *Macromolecular Rapid Communications* **2011**, *32*, 1379.

(20) June, S. M.; Suga, T.; Heath, W. H.; Long, T. E.; Lin, Q.; Puligadda, R. *Journal of Adhesion* **2010**, *86*, 1012.

(21) Xi, K.; Meng, Z.; Heng, L.; Ge, R.; He, H.; Yu, X.; Jia, X. *Journal of Applied Polymer Science* **2009**, *113*, 1633.

(22) June, S. M.; Bissel, P.; Long, T. E. *Journal of Polymer Science Part A: Polymer Chemistry* **2012**, *50*, 3797.

(23) Zhang, M.; Moore, R. B.; Long, T. E. *Journal Polymer Science Part A: Polymer Chemistry* **2012**, *50*, 3710.

(24) Oprea, S.; Potolinca, V. O. *Designed Monomers and Polymers* **2013**, *16*, 47.

(25) Niesten, M.; Gaymans, R. J. *Journal of Applied Polymer Science* **2001**, *81*, 1372.

(26) Strawhecker, K. E.; Hsieh, A. J.; Chantawansri, T. L.; Kalcioglu, Z. I.; Van, V. K. J. *Polymer* **2013**, *54*, 901.

(27) Sheth, J. P.; Klinedinst, D. B.; Wilkes, G. L.; Iskender, Y.; Yilgor, I. *Polymer* **2005**, *46*, 7317.

(28) Sheth, J. P.; Yilgor, E.; Erenturk, B.; Ozhalici, H.; Yilgor, I.; Wilkes, G. L. *Polymer* **2005**, *46*, 8185.

(29) Yilgor, I.; Yilgor, E. *Polymer Reviews* **2007**, *47*, 487.

(30) Baldwin, R. L. *Journal of Biological Chemistry* **2003**, *278*, 17581.

(31) Sheu, S.-Y.; Yang, D.-Y.; Selzle, H. L.; Schlag, E. W. *Proceedings of the National Academy of Sciences* **2003**, *100*, 12683.

(32) Mallakpour, S.; Kowsari, E. *Journal of Applied Polymer Science* **2006**, *99*, 1038.

(33) Pattabiraman, V. R. B. J. W. *Nature* **2011**, *480*, 471.

(34) Shabbir, S.; Zulfiqar, S.; Ahmad, Z.; Sarwar, M. I. *Tetrahedron* **2010**, *66*, 7204.

(35) Poulhès, F.; Mouysset, D.; Gil, G.; Bertrand, M. P.; Gastaldi, S. *Polymer* **2012**, *53*, 1172.

(36) Yi, C.; Peng, Z.; Wang, H.; Li, M.; Wang, C. *Polymer International* **2011**, *60*, 1728.

(37) Arsenault, S. *Annual Technical Conference - Society of Plastic Engineering* **2008**, *66th*, 775.

(38) Choi, M.-C.; Jung, J.-Y.; Yeom, H.-S.; Chang, Y.-W. *Polymer Engineering & Science* **2012**, n/a.

(39) Gugliuzza, A.; John Wiley & Sons, Inc.: 2012; Vol. 4, p 111.

(40) Wang, Y.; Alhassan, S. M.; Yang, V. H.; Schiraldi, D. A. *Composites Part B: Engineering* **2013**, *45*, 625.

(41) Huoli; Lihua *Advanced Material Research (Durnten-Zurich, Switz.)* **2012**, *512-515*, 2185.

(42) Yoshino, M.; Ito, K.; Kita, H.; Okamoto, K.-I. *Journal of Polymer Science Part B: Polymer Physics* **2000**, *38*, 1707.

(43) Kim, J. H.; Ha, S. Y.; Lee, Y. M. *Journal of Membrane Science* **2001**, *190*, 179.

(44) Armstrong, S.; Freeman, B.; Hiltner, A.; Baer, E. *Polymer* **2012**, *53*, 1383.

(45)   Wang, G.; Xue, B. *Journal of Applied Polymer Science* **2010**, *118*, 2448.

(46)   Boulares, A.; Tessier, M.; Maréchal, E. *Polymer* **2000**, *41*, 3561.

(47)   Peyravi, M.; Babaluo, A. A.; Ardestani, M. A.; Aghjeh, M. K. R.; Pishghadam, S. R.; Hadi, P. *Journal of Applied Polymer Science* **2010**, *118*, 1211.

(48)   Sauer, B. B.; McLean, R. S.; Thomas, R. R. *Polymer International* **2000**, *49*, 449.

(49)   Hatfield, G. R.; Guo, Y.; Killinger, W. E.; Andrejak, R. A.; Roubicek, P. M. *Macromolecules* **1993**, *26*, 6350.

(50)   Begenir, A.; Michielsen, S.; Pourdeyhimi, B. *Journal of Applied Polymer Science* **2009**, *111*, 1246.

(51)   Sauer, B. B.; McLean, R. S.; Brill, D. J.; Londono, D. J. *Journal of Polymer Science Part B: Polymer Physics* **2002**, *40*, 1727.

(52)   Song, Y.; Yamamoto, H.; Nemoto, N. *Macromolecules* **2004**, *37*, 6219.

(53)   Konyukhova, E. V.; Buzin, A. I.; Godovsky, Y. K. *Thermochimica Acta* **2002**, *391*, 271.

(54)   Yang, I. K.; Tsai, P. H. *Journal of Polymer Science Part B-Polymer Physics* **2005**, *43*, 2557.

(55)   Sheth, J. P.; Xu, J.; Wilkes, G. L. *Polymer* **2003**, *44*, 743.

(56)   Alberola, N.; Vassel, A.; Christophe Helluin, J. *Makromolekulare Chemie. Macromolecular Symposia* **1989**, *23*, 219.

(57)   Hucher, C.; Eustache, R. P.; Beaume, F.; Tekely, P. *Macromolecules* **2005**, *38*, 9200.

(58)   Sheth, J. P.; Aneja, A.; Wilkes, G. L.; Yilgor, E.; Atilla, G. E.; Yilgor, I.; Beyer, F. L. *Polymer* **2004**, *45*, 6919.

(59)   Klinedinst, D. B.; Yilgör, E.; Yilgör, I.; Beyer, F. L.; Wilkes, G. L. *Polymer* **2005**, *46*, 10191.

(60)   Versteegen, R. M.; Kleppinger, R.; Sijbesma, R. P.; Meijer, E. W. *Macromolecules* **2006**, *39*, 772.

(61)   Wisse, E.; Spiering, A. J. H.; van Leeuwen, E. N. M.; Renken, R. A. E.; Dankers, P. Y. W.; Brouwer, L. A.; van Luyn, M. J. A.; Harmsen, M. C.; Sommerdijk, N.; Meijer, E. W. *Biomacromolecules* **2006**, *7*, 3385.

(62)   Guang, L.; Gaymans, R. J. *Polymer* **1997**, *38*, 4891.

(63)   Niesten, M. C. E. J.; Tol, R.; Gaymans, R. J. *Polymer* **2001**, *42*, 931.

(64)   Quaglia, F.; Vignola, M. C.; De Rosa, G.; La Rotonda, M. I.; Maglio, G.; Palumbo, R. *Journal of Controlled Release* **2002**, *83*, 263.

(65)   D'Angelo, S.; Galletti, P.; Maglio, G.; Malinconico, M.; Morelli, P.; Palumbo, R.; Vignola, M. C. *Polymer* **2001**, *42*, 3383.

(66)   Deschamps, A. A.; Grijpma, D. W.; Feijen, J. *Journal of Biomaterials Science, Polymer Edition* **2002**, *13*, 1337.

(67)   Krijgsman, J.; Feijen, J.; Gaymans, R. J. *Macromolecular Symposia* **2003**, *199*, 135.

(68)   Krijgsman, J.; Biemond, G. J. E.; Gaymans, R. J. *Journal of Applied Polymer Science* **2007**, *103*, 512.

(69)   Ghosh, S.; Bhattacharyya, A. K.; Khastgir, D.; Bhowmick, A. K. *Journal of Applied Polymer Science* **1999**, *71*, 1739.

(70)   van Hutten, P. F.; Mangnus, R. M.; Gaymans, R. J. *Polymer* **1993**, *34*, 4193.

(71)   Krijgsman, J.; Biemond, G. J. E.; Gaymans, R. J. *Polymer* **2005**, *46*, 8250.

(72)   Biemond, G. J. E.; Feijen, J.; Gaymans, R. J. *Macromolecular Materials and Engineering* **2009**, *294*, 492.

(73)   Krijgsman, J.; Feijen, J.; Gaymans, R. J. *Polymer* **2004**, *45*, 4677.

(74)   Niesten, M. C. E. J.; Feijen, J.; Gaymans, R. J. *Polymer* **2000**, *41*, 8487.

(75)   Arun, A.; Gaymans, R. J. *Journal of Applied Polymer Science* **2009**, *111*, 1780.

(76)   Sauer, B. B.; McLean, R. S.; Gaymans, R. J.; Niesten, M. C. J. E. *Journal of Polymer Science, Part B: Polymer Physics* **2004**, *42*, 1783.

(77)   Biemond, G. J. E.; Feijen, J.; Gaymans, R. J. *Journal of Applied Polymer Science* **2007**, *105*, 951.

(78)   van der Schuur, M.; Gaymans, R. J. *Journal of Polymer Science Part A: Polymer Chemistry* **2006**, *44*, 4769.

(79)   van der Schuur, M.; Boer, J. d.; Gaymans, R. J. *Polymer* **2005**, *46*, 9243.

(80)   Biemond, G. J. E.; Feijen, J.; Gaymans, R. J. *Polymer Engineering & Science* **2008**, *48*, 1389.

(81)   Husken, D.; Feijen, J.; Gaymans, R. J. *Journal of Applied Polymer Science* **2009**, *114*, 1264.

(82)   Krijgsman, J.; Feijen, J.; Gaymans, R. J. *Polymer* **2004**, *45*, 4685.

(83)   Bouma, K.; Wester, G. A.; Gaymans, R. J. *Journal of Applied Polymer Science* **2001**, *80*, 1173.

(84)   van der Schuur, M.; van der Heide, E.; Feijen, J.; Gaymans, R. J. *Polymer* **2005**, *46*, 3616.

(85)   van der Schuur, M.; Gaymans, R. J. *Polymer* **2005**, *46*, 6862.

(86)   Krijgsman, J.; Husken, D.; Gaymans, R. J. *Polymer* **2003**, *44*, 7573.

(87)   Niesten, M.; ten Brinke, J. W.; Gaymans, R. J. *Polymer* **2001**, *42*, 1461.

(88)   Husken, D.; Krijgsman, J.; Gaymans, R. J. *Polymer* **2004**, *45*, 4837.

(89)   Niesten, M. C. E. J.; Gaymans, R. J. *Polymer* **2001**, *42*, 6199.

(90)   Biemond, G. J. E.; Feijen, J.; Gaymans, R. J. *Journal of Materials Science* **2008**, *43*, 3689.

(91)   Krijgsman, J.; Gaymans, R. J. *Polymer* **2004**, *45*, 437.

(92)   Niesten, M. C. E. J.; Harkema, S.; van der Heide, E.; Gaymans, R. J. *Polymer* **2001**, *42*, 1131.

(93)   Lips, P. A. M.; Broos, R.; van Heeringen, M. J. M.; Dijkstra, P. J.; Feijen, J. *Polymer* **2005**, *46*, 7823.

(94)   Deshayes, G.; Delcourt, C.; Verbruggen, I.; Trouillet-Fonti, L.; Touraud, F.; Fleury, E.; Degee, P.; Destarac, M.; Willem, R.; Dubois, P. *Macromolecular Chemistry and Physics* **2009**, *210*, 1033.

(95)   Luckachan, G. E.; Pillai, C. K. S. *Journal of Polymer Science Part A: Polymer Chemistry* **2006**, *44*, 3250.

(96)   Lips, P. A. M.; van Luyn, M. J. A.; Chiellini, F.; Brouwer, L. A.; Velthoen, I. W.; Dijkstra, P. J.; Feijen, J. *Journal of Biomedical Materials Research Part A* **2006**, *76A*, 699.

(97)   Pang, X.; Wu, J.; Reinhart-King, C.; Chu, C.-C. *Journal of Polymer Science Part A: Polymer Chemistry* **2010**, *48*, 3758.

(98)   Gaymans, R. J.; van Swaaij, A. W. *Journal of Applied Polymer Science* **2011**, *119*, 23.

(99)   Jeong, H. M.; Moon, S. W.; Jho, J. Y.; Ahn, T. O. *Polymer* **1998**, *39*, 459.

(100)   Palsule, A. S.; Poojari, Y. *Polymer* **2010**, *51*, 6161.

(101)   Sharma, B.; Azim, A.; Azim, H.; Gross, R. A.; Zini, E.; Focarete, M. L.; Scandola, M. *Macromolecules* **2007**, *40*, 7919.

(102) Chromcova, D.; Baslerova, L.; Roda, J.; Brozek, J. *European Polymer Journal* **2008**, *44*, 1733.

(103) Bernaskova, A.; Chromcova, D.; Brozek, J.; Roda, J. *Polymer* **2004**, *45*, 2141.

(104) Lips, P. A. M.; Broos, R.; van Heeringen, M. J. M.; Dijkstra, P. J.; Feijen, J. *Polymer* **2005**, *46*, 7834.

(105) Bera, S.; Jedlinski, Z. *Journal of Polymer Science Part A: Polymer Chemistry* **1993**, *31*, 731.

(106) Liu, S.; Li, C.; Zhao, J.; Zhang, Z.; Yang, W. *Polymer* **2011**, *52*, 6046.

(107) Deshayes, G.; Delcourt, C.; Verbruggen, I.; Trouillet-Fonti, L.; Touraud, F.; Fleury, E.; Degee, P.; Destarac, M.; Willem, R.; Dubois, P. *European Polymer Journal* **2011**, *47*, 98.

(108) Coe, S.; Kane, J. J.; Nguyen, T. L.; Toledo, L. M.; Wininger, E.; Fowler, F. W.; Lauher, J. W. *Journal of the American Chemical Society* **1997**, *119*, 86.

(109) Nguyen, T. L.; Fowler, F. W.; Lauher, J. W. *Journal of the American Chemical Society* **2001**, *123*, 11057.

(110) Schulze, H.; Texaco Development Corp., USA . 1978, p 7 pp.

(111) Benson, K. E.; Hansen, R. G.; Johnson, S. A.; Leir, C. M.; Liu, R. Y.; Purgett, M. D.; Schneider, H. M.; Sherman, A. A.; 3M Innovative Properties Company, USA . 2007, p 45pp.

(112) Benson, K. E.; Hansen, R. G.; Johnson, S. A.; Leir, C. M.; Liu, R. Y.; Purgett, M. D.; Schneider, H. M.; Sherman, A. A.; 3M Innovative Properties Company, USA . 2007, p 31pp.

(113) Leir, C. M.; Benson, K. E.; Hansen, R. G.; Purgett, M. D.; Everaerts, A. I.; 3M Innovative Properties Company, USA . 2007, p 12pp.

(114) Leir, C. M.; Benson, K. E.; Hansen, R. G.; Purgett, M. D.; Everaerts, A. I.; Sherman, A. A.; 3M Innovative Properties Company, USA . 2007, p 16pp.

(115) Sijbrandi, N. J.; Kimenai, A. J.; Mes, E. P. C.; Broos, R.; Bar, G.; Rosenthal, M.; Odarchenko, Y.; Ivanov, D. A.; Dijkstra, P. J.; Feijen, J. *Macromolecules* **2012**, *45*, 3948.

(116) Sijbrandi, N. J.; Kimenai, A. J.; Mes, E. P. C.; Broos, R.; Bar, G.; Rosenthal, M.; Odarchenko, Y. I.; Ivanov, D. A.; Jan, F. J.; Dijkstra, P. J. *Polymer* **2012**, *53*, 4033.

(117) Buckwalter, D. J. H., Amanda G.; Moore, Robert B.; Long, Timothy E. *Submitted to Polymer International* **2013**.

(118) Buckwalter, D. J. I., David; Enokida, Joshua S.; Hudson, Amanda G.; Moore, Robert B.; Long, Timothy E. *Submitted to Macromolecular Chemistry and Physics* **2013**.

(119) Buckwalter, D. J. Z., Mingqiang; Inglefield, David; Moore, Robert B.; Long, Timothy E. *Submitted to Polymer* **2013**.

(120) Henkensmeier, D.; Abele, B. C.; Candussio, A.; Thiem, J. *Polymer* **2004**, *45*, 7053.

(121) Kang, B. M.; Park, Y. W. *Polymer-Plastics Technology and Engineering* **2010**, *49*, 223.

(122) Kishida, A.; Furuzono, T.; Ohshige, T.-a.; Maruyama, I.; Matsumoto, T.; Itoh, H.; Murakami, M.; Akashi, M. *Die Angewandte Makromolekulare Chemie* **1994**, *220*, 89.

(123) Matsumoto, T.; Uchida, T.; Kishida, A.; Furuzono, T.; Maruyama, I.; Akashi, M. *Journal of Applied Polymer Science* **1997**, *64*, 1153.

(124) Furuzono, T.; Kishida, A.; Yanagi, M.; Matsumoto, T.; Kanda, T.; Nakamura, T.; Aiko, T.; Maruyama, I.; Akashi, M. *Journal of Biomaterials Science-Polymer Edition* **1996**, *7*, 871.

(125) Furuzono, T.; Yashima, E.; Kishida, A.; Maruyama, I.; Matsumoto, T.; Akashi, M. *Journal of Biomaterials Science-Polymer Edition* **1993**, *5*, 89.

(126) Gill, R.; Mazhar, M.; Siddiq, M. *Polymer International* **2010**, *59*, 1598.

(127) Saif Ullah Khan, M.; Akhter, Z.; Naz, T.; Bhatti, A. S.; Siddiqi, H. M.; Siddiq, M.; Khan, A. *Polymer International* **2012**, n/a.

(128) Kajiyama, M.; Kakimoto, M. A.; Imai, Y. *Macromolecules* **1989**, *22*, 4143.

(129) Yilgor, I.; Lee, B.; Steckle, W. P., Jr.; Riffle, J. S.; Tyagi, D.; Wilkes, G. L.; McGrath, J. E. *Polymer Preprints (American Chemical Society, Division of Polymer Chemistry)* **1983**, *24*, 35.

(130) Policastro, P. P.; Hernandez, P. K. *Journal of Polymer Science Part A: Polymer Chemistry* **1987**, *25*, 2819.

(131) Furuzono, T.; Seki, K.; Kishida, A.; Ohshige, T.-A.; Waki, K.; Maruyama, I.; Akashi, M. *Journal of Applied Polymer Science* **1996**, *59*, 1059.

(132) Oishi, Y.; Nakata, S.; Kajiyama, M.; Kakimoto, M. A.; Imai, Y. *Journal of Polymer Science Part a-Polymer Chemistry* **1992**, *30*, 2357.

(133) Kishida, A.; Kanda, T.; Furuzono, T.; Maruyama, I.; Akashi, M. *Journal of Applied Polymer Science* **2000**, *78*, 2198.

(134) Furuzono, T.; Senshu, K.; Kishida, A.; Matsumoto, T.; Akashi, M. *Polymer Journal* **1997**, *29*, 201.

(135) Senshu, K.; Furuzono, T.; Koshizaki, N.; Yamashita, S.; Matsumoto, T.; Kishida, A.; Akashi, M. *Macromolecules* **1997**, *30*, 4421.

(136) Kang, E.-C.; Kaneko, T.; Shiino, D.; Akashi, M. *Journal of Polymer Science Part A: Polymer Chemistry* **2003**, *41*, 841.

(137) Matsumoto, T.; Koinuma, Y.; Waki, K.; Kishida, A.; Furuzono, T.; Maruyama, I.; Akashi, M. *Journal of Applied Polymer Science* **1996**, *59*, 1067.

(138) Park, Y. W.; Lee, D. S. *Journal of Applied Polymer Science* **2004**, *93*, 342.

(139) Mallakpour, S.; Rafiemanzelat, F. *High Performance Polymers* **2008**, *20*, 146.

(140) Báez, J. E.; Ramírez, D.; Valentín, J. L.; Marcos-Fernández, Á. *Macromolecules* **2012**, *45*, 6966.

(141) Chapman, T. M.; Marra, K. G. *Macromolecules* **1995**, *28*, 2081.

(142) Nojima, K.; Sanui, K.; Ogata, N.; Yui, N.; Kataoka, K.; Sakurai, Y. *Polymer* **1987**, *28*, 1017.

(143) Kolahdoozan, M.; Mirsafaei, R.; Mallakpour, S. *Polymer Bulletin (Heidelberg, Ger.)* **2012**, *68*, 1239.

(144) Mallakpour, S.; Rafiemanzelat, F. *Reactive and Functional Polymers* **2005**, *62*, 153.

(145) Mallakpour, S.; Khani, M.; Rafiemanzelat, F. *Journal of Applied Polymer Science* **2008**, *108*, 2975.

(146) van der Schuur, M.; Noordover, B.; Gaymans, R. J. *Polymer* **2006**, *47*, 1091.

(147) Mallakpour, S.; Khoee, S. *Journal of Applied Polymer Science* **2004**, *91*, 2288.

(148) Yui, N.; Nojima, K.; Sanui, K.; Ogata, N. *Polymer Journal (Tokyo)* **1985**, *17*, 969.

Chapter 3: Structure Property Relationships of Non-chain Extended Poly(dimethyl siloxane) Poly(bisoxamide) Segmented Copolymers

(From: Buckwalter, D. J.; Inglefield, D.; Enokida, J. S.; Hudson, A. G.; Moore, R. B.; Long, T. E. *Submission in Progress*)

3.1 Abstract

An investigation of the structure-property relationships of poly(dimethyl siloxane) (PDMS) polyoxamide segmented copolymers revealed the impact of oxamide spacing and PDMS molecular weight on physical properties. Varying the length of methylene spacing between oxamide hydrogen bonding groups in the hard segment as well as the PDMS soft segment molecular weight provided insight into the influence on thermal and mechanical properties. Bulk polymerization of ethyl oxalate terminated PMDS oligomers with diamines yielded optically clear thermoplastic elastomers with excellent mechanical properties. Variable temperature FTIR spectroscopy revealed an ordered, hydrogen bonding carbonyl stretching band for each copolymer, and the dissociation temperature for the ordered hydrogen bonding carbonyl decreased with an increase in hard segment oxamide spacing. Dynamic mechanical analysis revealed a decrease in the flow temperature with increased oxamide spacing, while tensile analysis exhibited reduced mechanical properties with longer spacing. Hysteresis experiments demonstrated reduced % hysteresis from cycle to cycle when oxamide spacing decreased. The structure-property investigation revealed optimum mechanical properties of PDMS polyoxamide segmented copolymers occurred with the smallest spacing between oxamide groups in the hard segment.

3.2 Introduction

Segmented copolymers that exhibit thermoplastic elastomer (TPE) behavior are often composed of a polymer backbone containing alternating hard and soft segments covalently linked in a linear fashion. The incompatibility of the two microphases within the copolymer, as well as strong intermolecular interactions, result in microphase separated bulk morphologies, which are essential to the properties commonly associated with TPEs.[1] Physical properties include flexibility, elasticity, large temperature insensitive rubbery plateaus or "service windows", and melt processability, which is a characteristic not observed with conventional rubbers.[2,3] The nature and strength of the intermolecular interactions between hard segments (HS) play a critical role in forming strong physical crosslinks that are necessary to impart microphase separation.[4,5] Many common segmented copolymers rely on HS hydrogen bonding to form physical crosslinks, including polyureas,[6-8] polyurethanes,[9-11] poly(urethane urea)s,[12-14] polyamides,[15-17] and poly(ester amide)s.[18,19] These rigid, highly polarized groups are often immiscible at ambient temperature with soft segments (SS) such as polyethers and poly(dimethyl siloxane) (PDMS), which helps drive the formation of microphase separated morphologies.[20,21] PDMS is an attractive soft segment for segmented copolymers due to its flexibility, hydrophobicity, low surface energy, and high chemical and thermal stability.[22,23] Yilgor et al. published reports on the structure property relationships of segmented copolymers containing uniform, monodisperse HS.[24] Segmented copolymers containing uniform hard segments possessed improved material properties compared to similar segmented copolymers containing polydisperse HSs.[25-27] However, hydrogen bonding strength and hard segment symmetry played a more important role in determining the physical properties associated with the copolymers containing uniform HS than those with polydisperse HS.[28-30]

Oxamide groups possess strong hydrogen bonding interactions that are applicable for incorporation into a wide range of segmented systems.[31,32] The introduction of oxamide hydrogen bonding groups in the HS of segmented copolymers proved possible through the early work of Schulze on polyoxypropylene based polyoxamide segmented copolymers in the late 1970s.[33] More recently, researchers at 3M have developed PDMS based polyoxamide segmented copolymers through bulk polymerization of ethyl oxalate terminated PDMS oligomers with low molar mass diamines that yielded clear films with TPE behavior.[34,35] 3M researchers demonstrated the robustness of the bulk polymerization with various diamines and showed that PDMS polyoxamide copolymers were effective as adhesives and sealants.

Currently, detailed reports of the structure-property relationships for PDMS polyoxamide segmented copolymers do not exist in the literature. Recently, Sijbrandi et al. published a report on the structure-property relationships of poly(tetramethylene oxide) (PTMO) based polyoxamide copolymers.[36] Their study focused on the effects of HS composition through varying the number of oxamide groups and the HS spacing. The DMA flow temperatures (T_f) for the PTMO polyoxamide copolymers decreased from 200 to 140 ˚C with an increase in oxamide spacing from 2 to 10 methylene groups. Tensile analysis did not elucidate an obvious trend with increased oxamide spacer length, but all copolymers exhibited distinctive yield points near 50% strain. The presence of at least two oxamide groups in the HS proved necessary to impart good thermal and mechanical properties.

This report describes the synthesis and characterization of PDMS polyoxamide (PDMS-Ox) segmented copolymers with variable PDMS molecular weights and spacing between oxamide groups in the HS. Our goal was to understand the structure-property relationships of the PDMS-Ox copolymers as well as the effect of HS structural variations on hydrogen bonding

interactions. In each PDMS molecular weight series, spacing between oxamide groups varied from 2 to 8 methylene groups. *m*-xylene diamine provided steric bulk, aromaticity, and an odd spacing between oxamide groups in the HS (Figure 3.1). Varying the HS composition and PDMS molecular weight provided comparisons of the thermal and mechanical properties associated with each copolymer. Increasing the spacing between oxamide groups in the HS led to weaker hydrogen bonding interactions and dramatically affected the mechanical properties. Comparisons provided a fundamental understanding of the structure-property relationships associated with the PDMS-Ox segmented copolymers.
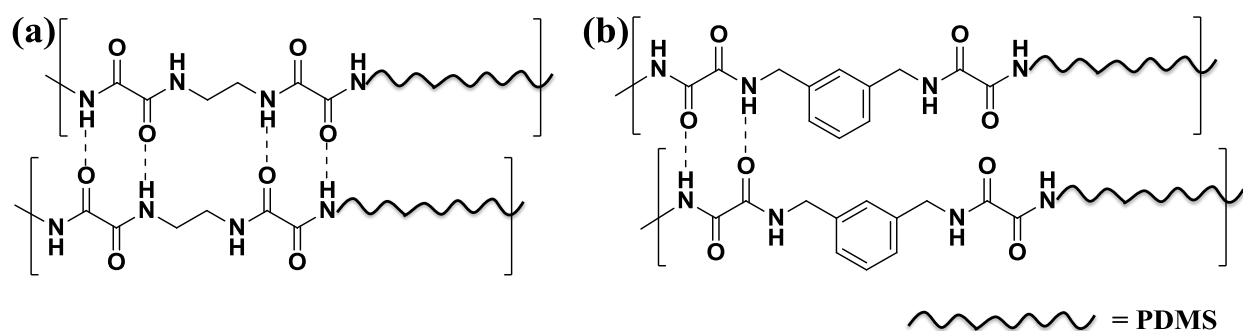
Figure 3.1. Hydrogen bonding interactions of (a) PDMS-Ox2 and (b) PDMS-OxAr hard segment structures

3.3 Experimental

3.3.1 Materials

2,000 and 5,000 g/mol aminopropyl terminated PDMS oligomers were purchased from Gelest, Inc. Wacker Chemie kindly donated the 12,000 g/mol aminopropyl terminated PDMS oligomer. Each PDMS diamine was used after removal of dissolved CO_2 and residual cyclics under heat (100 ˚C) and reduced pressure (0.06 mmHg). *N*-hexylamine (98%), diethyl oxalate (>99%), ethylene diamine (≥99%), 1,4-diamino butane (99%), hexamethylenediamine (99.5%),

1,8-diamino octane (99%), and *m*-xylene diamine (99%) were purchased from Sigma Aldrich and used without further purification.

3.3.2 Polymerization of PDMS Poly(bisoxamide) Copolymers

Each PDMS-Ox copolymer was synthesized using an identical synthetic strategy with differences in temperature and diamine. The following synthesis of a 5K PDMS polyoxamide will serve as an example. Aminopropyl terminated PDMS (24.04 g, 4.77 mmol) was cannulated into a dry, Ar purged round-bottomed flask. Diethyl oxalate (2.44 g, 16.7 mmol) was syringed directly into the reaction flask with stirring. After stirring for 24 h, the end-capped oligomer was placed under high vacuum (0.06 mmHg) and heat (80 ˚C) to remove excess diethyl oxalate and ethanol. Number-average molecular weight of the ethyl oxalate terminated PDMS oligomer was calculated with ^{1}H NMR spectroscopy and end-group analysis. Ethyl oxalate terminated oligomers (5.15 g, 0.95 mmol) were added to a two-necked, round-bottomed flask equipped with a mechanical stirrer and purged with argon. Ethylenediamine (0.06 g, 0.95 mmol) was then pipetted directly into the reaction flask at 23 ˚C and stirred until a solid polymer product was formed. After sitting for 24 h, the solid polymer product was dissolved in $CHCl_3$ at 10 wt% solids and solution cast into Teflon molds to yield a clear, elastic film. Films were subsequently annealed at 100 ˚C under reduced pressure (1 mmHg) for 12 h prior to mechanical or morphological testing. Bulk polymerizations were also conducted at 50 to 120 ˚C depending on the diamine and PDMS molecular weight.

3.3.3 Analytical Methods

^{1}H NMR spectra were collected using an Advance 500 MHz spectrometer in $CDCl_3$ at 27 ˚C. A Malvern Instruments Zetasizer Nano ZS (633 nm) was utilized to check for aggregation in potential SEC solvents. Thermogravimetric analysis (TGA) was performed on a TA Instruments

Q500 TGA with a heating ramp of 10 ˚C/min and constant nitrogen purge. TA Instruments Q1000 differential scanning calorimeter (DSC) measured thermal transitions from -75 to 200 ˚C with a heating rate of 10 ˚C/min and cooling rate of 50 ˚C/min under nitrogen purge. DSC thermal transition values were reported for each sample from the second heat. Dynamic mechanical analysis (DMA) was conducted on a TA Instruments Q800 in tension mode (1 Hz frequency) from -140 ˚C to the temperature of film failure at a rate of 3 ˚C/min. An Instron 4411 universal testing instrument was used for all tensile and hysteresis experiments with samples cut using a Pioneer Dietechs dumbbell cutting die. A crosshead speed of 50 mm/min was set for tensile analysis with values reported as an average of 5 samples. Hysteresis experiments were conducted at a rate of 2%/sec to a maximum strain of 30%, 50%, or 100% over 5 consecutive cycles. The trapezoid method was used to determine the area under the curve, and cycle to cycle comparisons were observed. Variable temperature FTIR spectroscopy was performed using a Varian 670-IR equipped with a PIKE Technologies Heated Stage Diamond GladiATR attachment. Each copolymer was heated over a temperature range of 30 ˚C to 195 ˚C, at a ramp rate of 1 °C/min. Spectra were acquired at 5° intervals, with 32 scans (time required for 32 scans was approximately 1 min) conducted for each spectrum at a resolution of 4 cm^{-1}. Each copolymer sample was dried prior to FTIR analysis during the annealing step.

3.4 Results and Discussion

3.4.1 Synthesis of PDMS Poly(oxamide) Copolymers

Bulk polymerization of PDMS polyoxamide segmented copolymers containing uniform oxamide HSs utilized a previously reported method (Scheme 3.1).[33,35] End-capping aminopropyl terminated PDMS oligomers of varying molecular weights (2, 5, and 12 kg/mol) with diethyl oxalate provided difunctional (f = 2) ethyl oxalate terminated PDMS oligomers with minimal

polymerization. ^{1}H NMR spectroscopy confirmed minimal polymerization during the ethyl oxalate end-capping procedure using integral ratios of the propyl and ethyl ester protons. Bulk polycondensation of ethyl oxalate terminated soft segments with aliphatic and aromatic diamines proved efficient for each PDMS polyoxamide segmented copolymer, which yielded strong, elastic films. Oxamide spacing varied from 2 to 8 methylene groups as well as *m*-xylene, which

Scheme 3.1. Synthesis of PDMS polyoxamide segmented copolymers
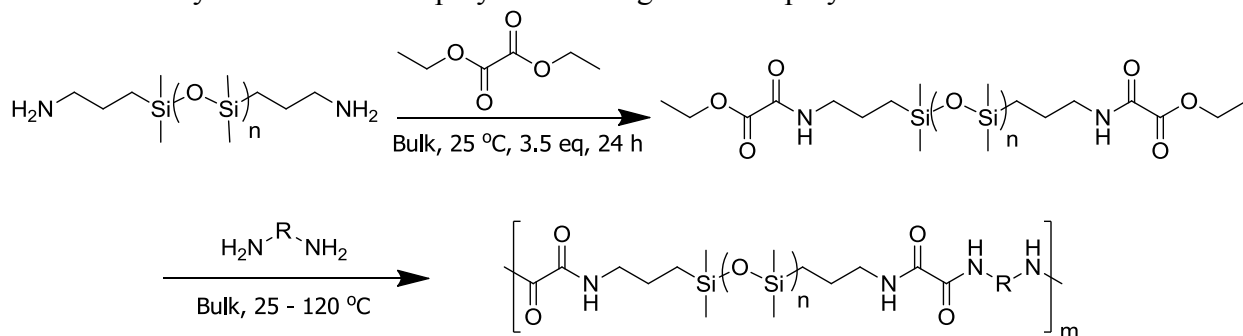
R = -(CH$_2$)$_2$-, -(CH$_2$)$_4$-, -(CH$_2$)$_6$-, -(CH$_2$)$_8$-, *m*-xylene

 provided an odd spacing of 5 between the oxamide groups in the HS. Table 3.1 provides a description of each PDMS-Ox copolymer composition. Polymerization temperature varied from 23 to 120 ˚C. PDMS2K-Ox and PDMS5K-Ox copolymers polymerized well at room temperature or 50 ˚C depending on the diamine monomer. Successful polymerizations demonstrated that efficient bulk polymerization of lower molecular weight ethyl ester terminated PDMS oligomers with low molar mass diamines did not require high heat and catalyst. However, copolymers containing PDMS12K required 120 ˚C to fully homogenize the polymerization, which produced more ductile films compared to those polymerized at lower temperatures.

Bulk polymerizations of the end-capped PDMS oligomers yielded clear, colorless films with TPE behavior that depended on polymer composition. ^{1}H NMR spectroscopy indicated full conversion of the ethyl oxalate terminated PDMS oligomers without ethyl ester resonances remaining in the NMR spectrum. Aggregation in both CHCl$_3$ and THF SEC solvents prevented

Table 3.1. PDMS polyoxamide copolymer composition and thermal degradation values

	Soft Segment M_n (kg/mol)	Hard Segment Content (wt %)	Spacer Length	$T_{d, 5\%}$ (°C)
PDMS2K-Ox2	2	7.5	2	417
PDMS2K-Ox4	2	8.5	4	399
PDMS2K-Ox6	2	9.4	6	392
PDMS2K-Ox8	2	10.3	8	388
PDMS2K-OxAr	2	10.0	5	418
PDMS5K-Ox2	5	3.7	2	424
PDMS5K-Ox4	5	4.2	4	402
PDMS5K-Ox6	5	4.7	6	429
PDMS5K-Ox8	5	5.2	8	386
PDMS5K-OxAr	5	5.0	5	411
PDMS12K-Ox2	12	1.5	2	402
PDMS12K-Ox4	12	1.8	4	416
PDMS12K-Ox6	12	2.0	6	425
PDMS12K-Ox8	12	2.2	8	420
PDMS12K-OxAr	12	2.1	5	426

<u>TGA</u>: N_2, 10 °C/min, 25 − 600 °C

molecular weight determination with SEC analysis. Dynamic light scattering of a 1 mg/mL solution in both SEC solvents revealed scattering peaks of 100 nm or greater. Analysis of these copolymers in the SEC solvents would have resulted in unreliable molecular weight data and possibly contaminate the column due to polymer aggregation. Annealing of each copolymer film at 100 °C for 12 h under vacuum preceded all thermal and mechanical testing to ensure each copolymer possessed identical thermal histories.

3.4.2 Variable Temperature FTIR Spectroscopy

Both the carbonyl and N-H groups participate in hydrogen bonding interactions between amide groups, and hydrogen bonding interactions imparted characteristic changes to the stretching vibrations of both the carbonyl and N-H stretch in the infrared spectrum.[37] Semi-crystalline polyamides typically reveal three distinctive contributions to the carbonyl stretching region that include ordered hydrogen bonding (crystalline), non-ordered hydrogen bonding (amorphous), and free carbonyl groups.[38] Increasing the temperature of the polyamide results in a shift to higher vibrational frequency indicating the presence of less ordered and non-ordered

hydrogen bonding carbonyl groups, and after melting at higher temperatures, ordered carbonyl stretches were not observed.[39] Variable temperature FTIR spectroscopy probed the influence of oxamide spacing in the HS on the hydrogen bonding characteristics of each copolymer. At room temperature, all PDMS-Ox copolymers exhibited ordered, hydrogen bonding carbonyl bands at 1651 cm^{-1}. A gradual loss of the ordered, hydrogen bonding band occurred as the temperature increased from 30 – 195 °C (Figure 3.2). Stretching bands associated with disordered, hydrogen bonding and free carbonyl groups gradually appeared with increased temperature at 1664 – 1673 cm^{-1} and 1685 cm^{-1}, respectively. At 30 °C, N-H stretching vibrations in the ordered, hydrogen bonding state resided at 3297 cm^{-1} and at higher temperatures, the free N-H band appeared at 3398 cm^{-1} (Figure 3.3). Wavenumbers for each state of hydrogen bonding and the thermal dissociation profile agreed well with earlier reports.[36]
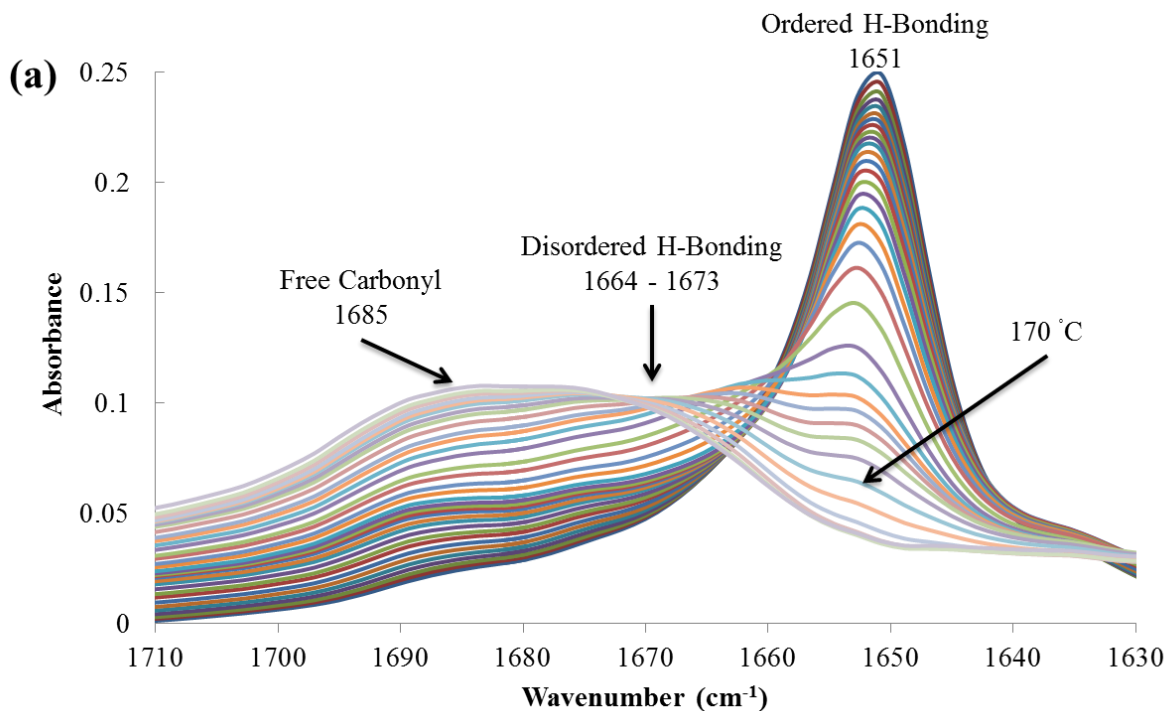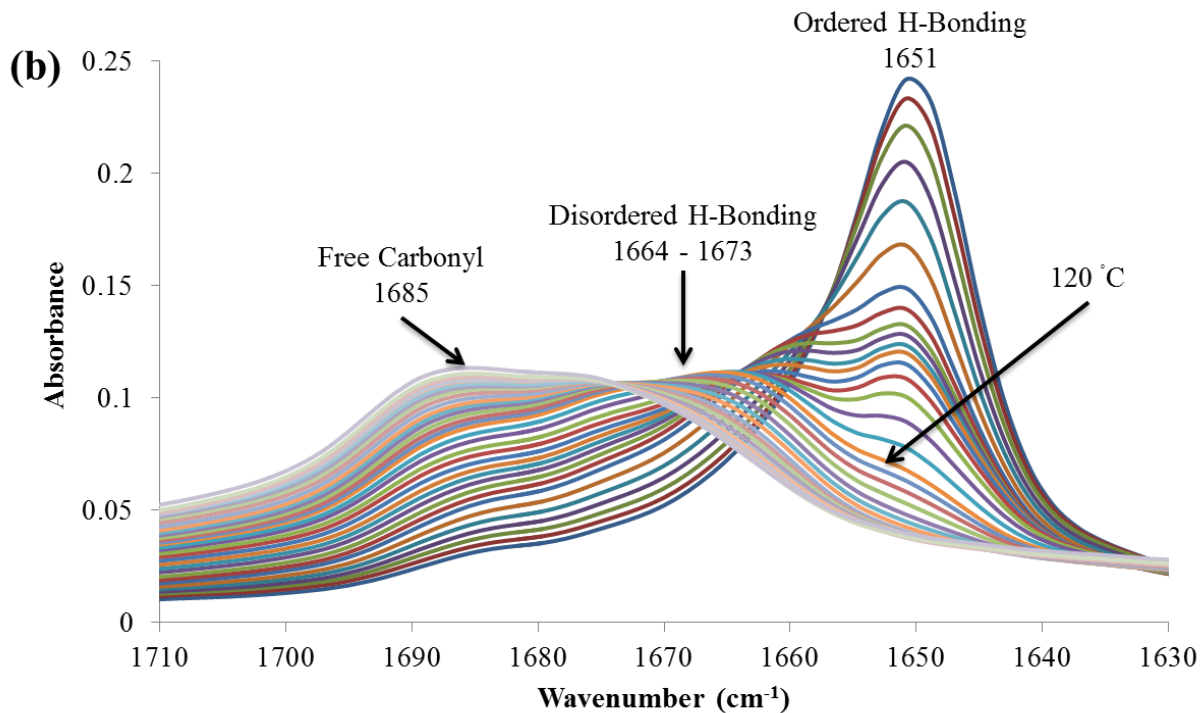
Figure 3.2. Variable temperature FTIR in the carbonyl region for (a) PDMS2K-Ox2 and (b) PDMS2K-Ox 8 copolymers from 30 – 195 ˚C
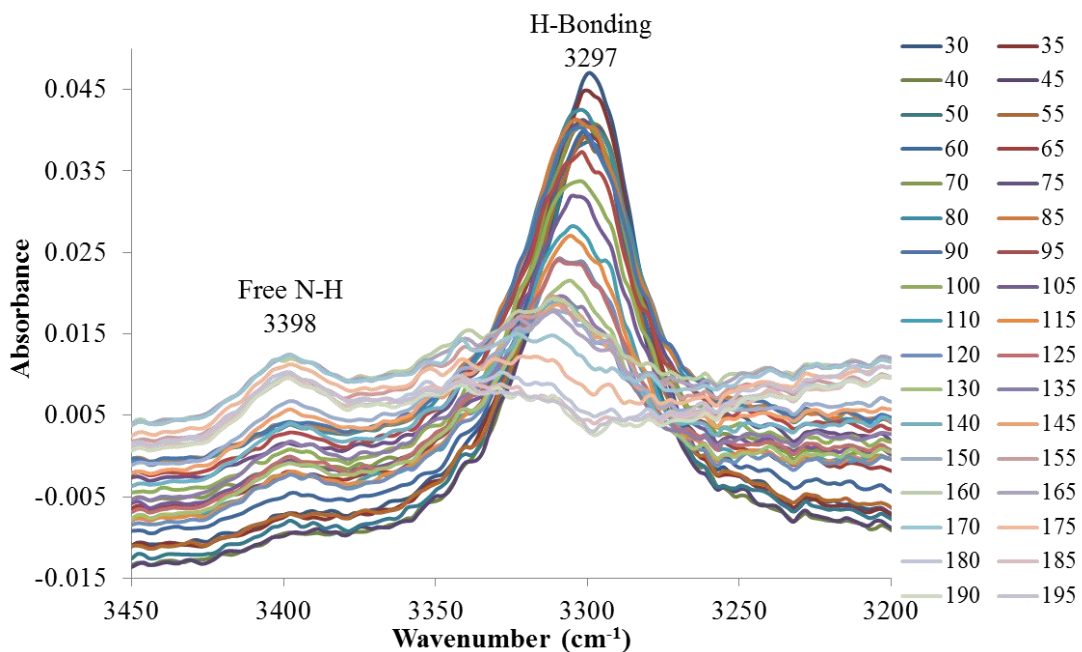
Figure 3.3. Variable temperature FTIR spectra of PDMS2K-Ox2 in the N-H stretch region from 30 – 195 ˚C

Increasing the spacing between oxamide groups revealed a change in the temperature for

ordered, hydrogen bond disruption. Presence of the ordered, hydrogen bonding carbonyl band at

1651 cm^{-1} appeared in the FTIR spectra up to 170 ˚C for PDMS2K-Ox2, which contained two methylene spacers between the oxamide groups (Figure 3.2a). When oxamide spacing increased from 2 to 8 methylene groups (PDMS2K-Ox8) the temperature for complete loss of ordered, hydrogen bonding was 120 ˚C according to the FTIR spectra (Figure 3.2b). Hydrogen bonding in close proximity was more effective at stabilizing the order of hydrogen bonding and when longer, more flexible linkages separated the oxamide groups, the cooperative effect of neighboring hydrogen bonds was diminished. Therefore, a decreased thermal stability of the order within the HS resulted. Figure 3.4 depicts the contribution of ordered, hydrogen bonding at 100 ˚C for PDMS2K-Ox copolymers, which demonstrates the effect of oxamide spacing on the
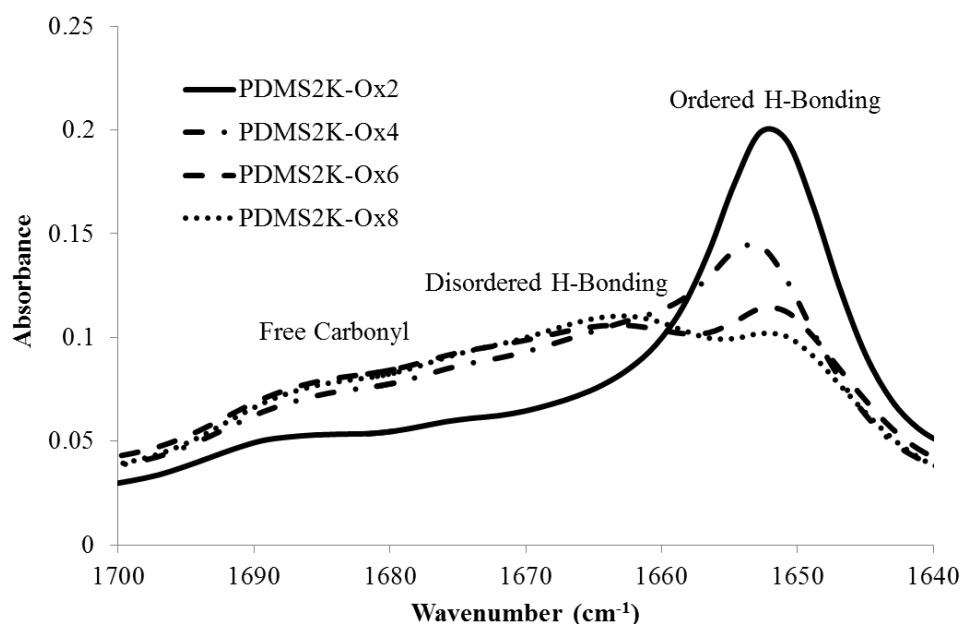
Figure 3.4. FTIR spectra of the carbonyl region at 100 ˚C for PDMS2K-Ox copolymers with increasing oxamide spacing

temperatures for ordered, hydrogen bond disruption. PDMS2K-Ox2, with two methylene groups between oxamides, exhibited a large ordered, hydrogen bonding carbonyl band with minimal contributions from less ordered hydrogen bonding. As the spacing increased to 4, 6, and 8, the contribution of ordered, hydrogen bonding in the FTIR spectra decreased and contributions from

59

non-ordered, hydrogen bonding and free carbonyl increased. PDMS2K-OxAr copolymer, containing an odd numbered spacer as well as an aromatic ring, demonstrated a hydrogen bonding dissociation profile similar to PDMS2K-Ox8 (Figure 3.5). The shortest alkyl spacer provided the strongest HS hydrogen bonding interactions for PDMS-Ox segmented copolymers due to the cooperative effect of neighboring hydrogen bonding.
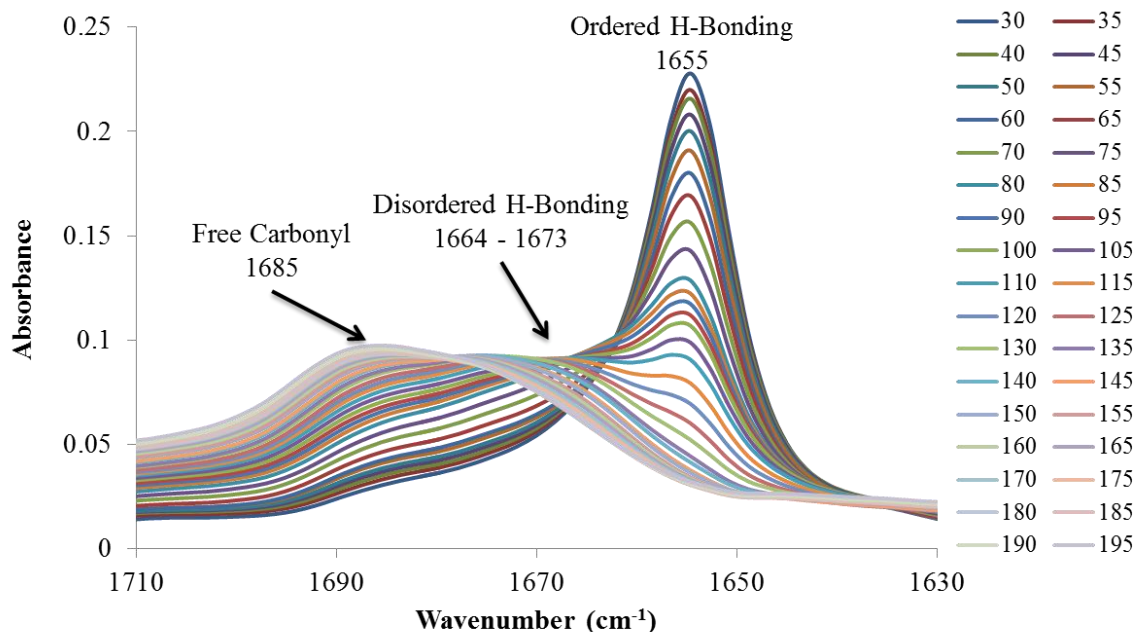
Figure 3.5. Variable temperature FTIR of PDMS2K-OxAr in the carbonyl region from 30 – 195 ˚C

3.4.3 Thermal Properties

TGA of each polyoxamide copolymer demonstrated high thermal stability with temperatures at 5% weight loss from 386 - 429 ˚C under a nitrogen atmosphere (Table 1). Each PDMS-Ox copolymer exhibited a similar thermal degradation profile, irregardless of the spacing between oxamide groups in the HS (Figure 3.6). The T_f of each copolymer resided below the thermal degradation temperatures, which was an important indicator for subsequent melt processability of these segmented copolymers.
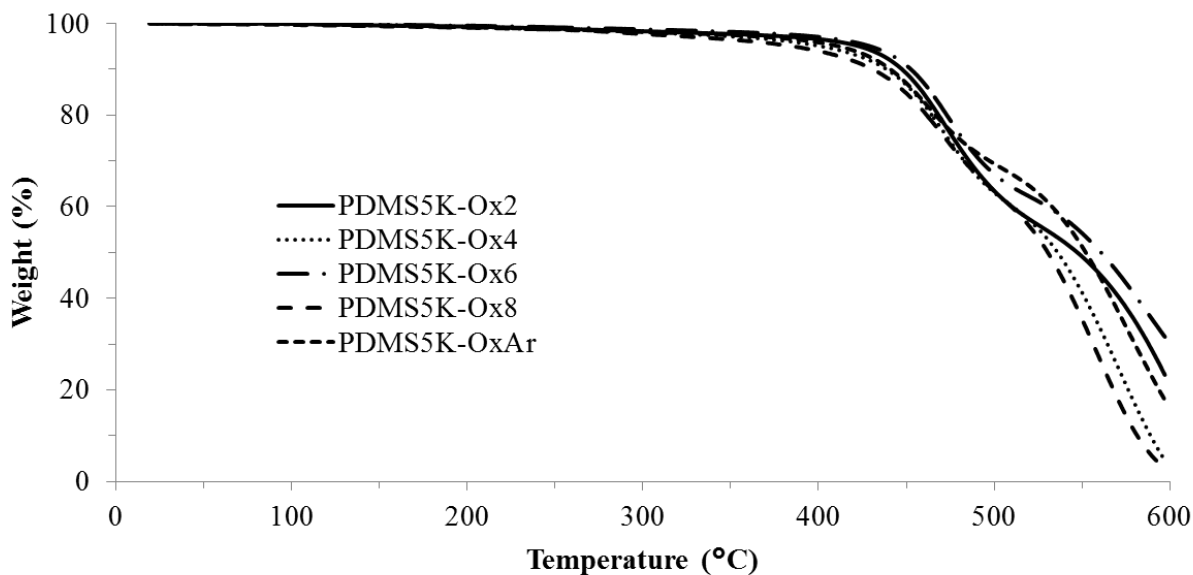
Figure 3.6. TGA trace for PDMS5K-Ox copolymers under N_2 from 25 – 600 ˚C

DSC examined the impact of alkyl spacers and PDMS molecular weight on the thermal transitions of each PDMS-Ox segmented copolymer. PDMS-Ox segmented copolymers exhibited a glass transition temperature (T_g) for the PDMS soft segment at -123 ˚C. Copolymers composed of 2,000 and 5,000 g/mol PDMS SS revealed broad endothermic transitions corresponding to the HS T_m. The endothermic peaks observed with DSC suggested the presence of crystalline HS domains, and previous reports reported the crystallinity of bisoxamide HS structures in segmented copolymers.[36,40] PDMS12K-Ox copolymers failed to exhibit any HS melting transitions due to the very low HS wt% composition, and the only observed thermal transitions were T_g, T_c, and T_m of PDMS. The temperatures of the broad melting transitions decreased as the methylene spacing increased from 2 to 8 (Figure 3.7). The trend in melting transitions correlated well with the variable temperature, FTIR spectroscopic data, which showed the loss of ordered, hydrogen bonding at lower temperatures with increased oxamide spacing.
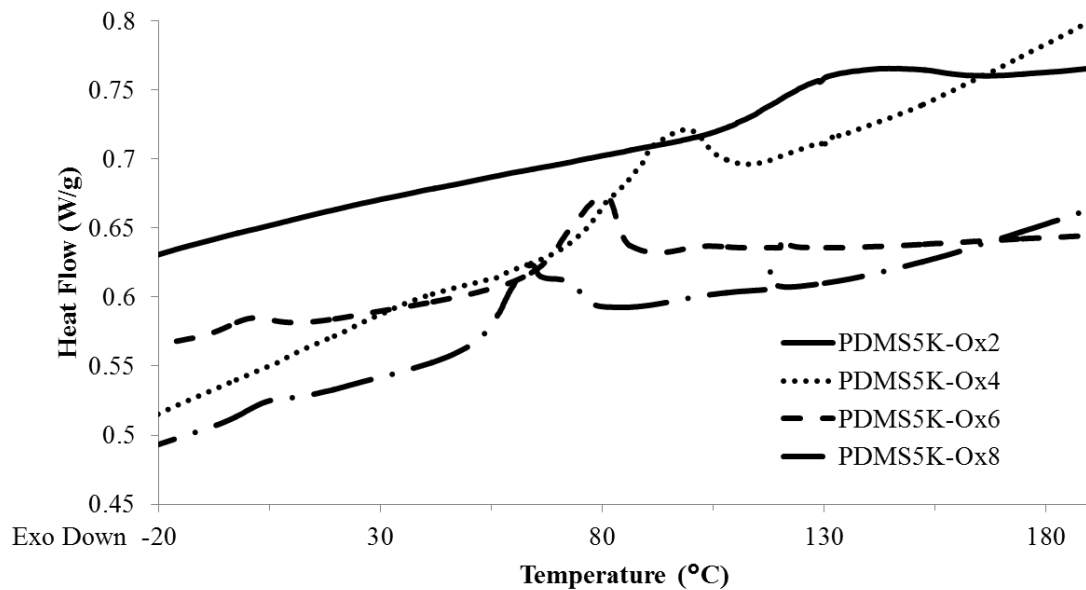
Figure 3.7. Second heat DSC traces of PDMS5K-Ox copolymers containing 2 – 8 methylene spacers between oxamide groups

3.4.4 Dynamic Mechanical Analysis

DMA revealed differences in the thermomechanical behavior of PDMS-Ox segmented copolymers as the oxamide spacing and PDMS molecular weight varied. All copolymers containing two methylene spacers demonstrated higher T_f values compared to copolymers with 4, 6, and 8 methylene groups. The observed DMA T_g values for all PDMS-Ox copolymers resided between -114 and -120 ˚C. PDMS5K-Ox2 possessed a T_f at 117 ˚C and as the oxamide spacer increased, the T_f of each subsequent copolymer decreased to ~80 ˚C (Figure 3.8). The temperature insensitive rubbery plateau region for PDMS5K-Ox copolymers exhibited a storage modulus of 8 – 15 MPa. Polyoxamide copolymers containing 2,000 and 12,000 g/mol PDMS SSs showed a more defined trend of the effect of oxamide spacer length on the DMA T_f. PDMS2K-Ox2 demonstrated a T_f of 139 ˚C and as the spacer increased from 4, 6 , and 8 methylene groups, the T_f decreased to 130, 120, and 91 ˚C, respectively (Figure 3.9). The rubbery plateau storage moduli of PDMS2K-Ox copolymers resided at 70 – 110 MPa with

62
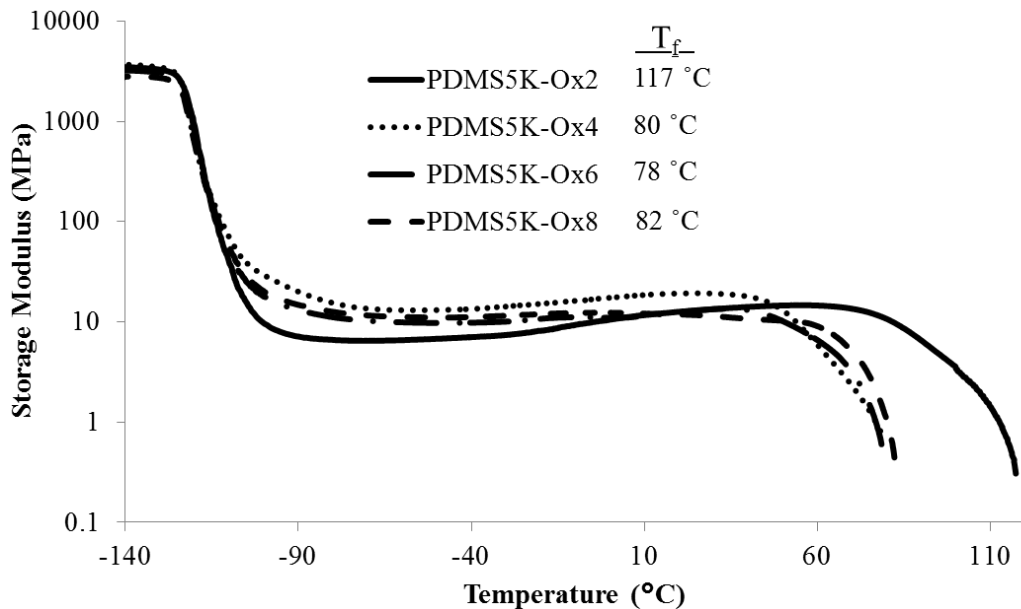
Figure 3.8. Storage modulus as a function of temperature for PDMS5K-Ox segmented copolymers with increasing spacer length
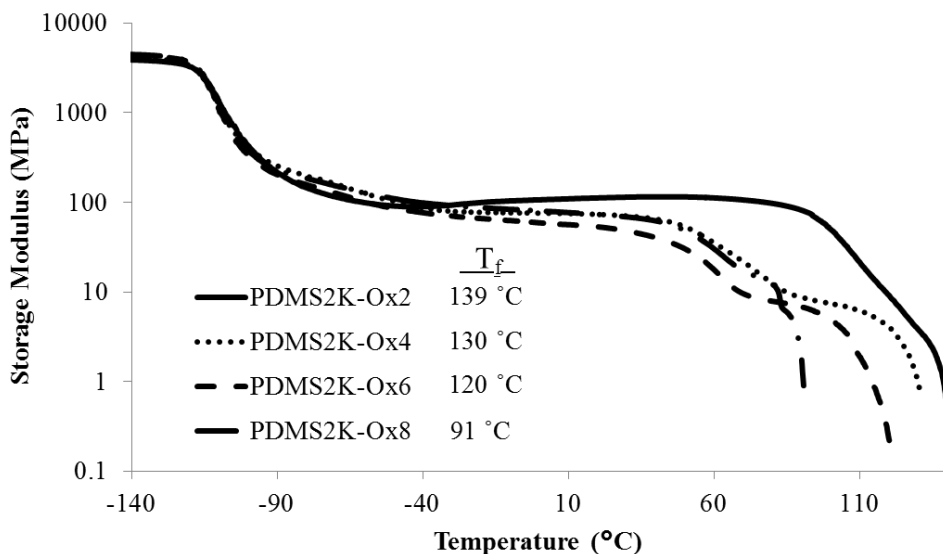
Figure 3.9. DMA trace of PDMS2K-Ox copolymer series

PDMS2K-Ox2 having the highest storage modulus. PDMS12K-Ox copolymers exhibited similar T_f values as PDMS5K-Ox copolymers with PDMS12K-Ox2 showing a T_f of 113 ˚C (Figure 3.10). Increasing the oxamide spacer resulted in a reduction in the T_f, as previously observed, to 78, 70, and 68 ˚C for copolymers PDMS12K-Ox4 − 8. PDMS crystallization and melting

63

transitions limited the rubbery plateau range of PDMS12K-Ox copolymers, which maintained stable storage moduli at ~2MPa after the T_m of PDMS. The dynamic mechanical behavior of PDMS-OxAr copolymers showed similar behavior compared to copolymers with the same PDMS molecular weight. The observed DMA T_f values were comparable to copolymers containing 6 and 8 methylene spacers between oxamide groups.
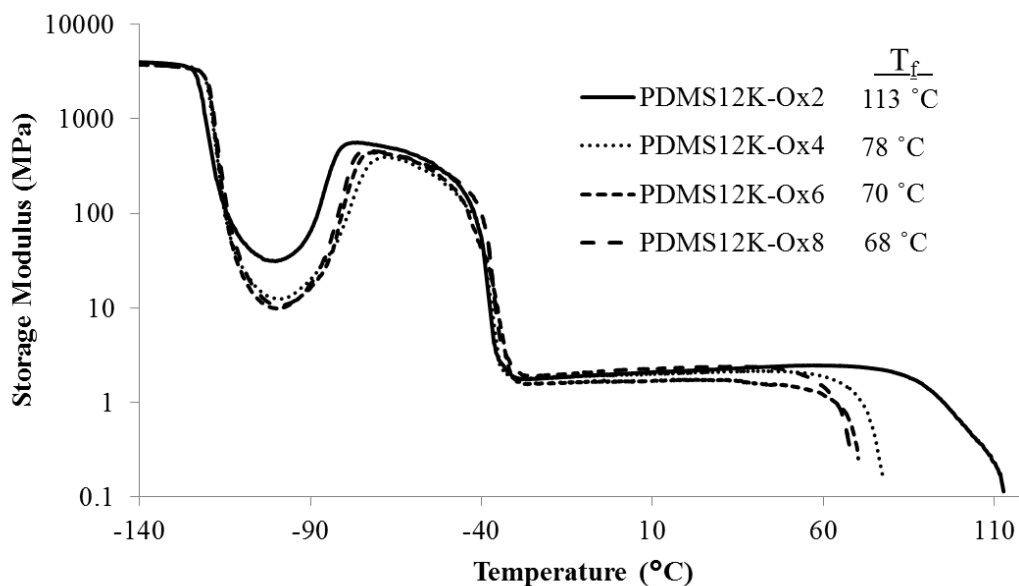
Figure 3.10. DMA trace of PDMS12K-Ox copolymer series

The effects of PDMS molecular weight on dynamic mechanical behavior exhibited a reduction in the rubbery plateau storage moduli and T_f with increasing PDMS molecular weight. Figure 3.11 depicts the effect of PDMS molecular weight for copolymers containing 2 methylenes between oxamide groups. As the wt% HS decreased from 7.5% to 1.5%, the average storage modulus dropped from 100 MPa to 2 MPa, similar to PDMS poly(urea) and poly(urethane) segmented copolymers.[41,42] Copolymer PDMS2K-Ox2 also exhibited the highest T_f of 139 °C when compared to all copolymer compositions, which suggested higher hydrogen bonding concentrations increased the T_f of PDMS-Ox copolymers. PDMS-Ox copolymers

containing the shortest oxamide spacing in the HS yielded materials with the best thermomechanical properties.
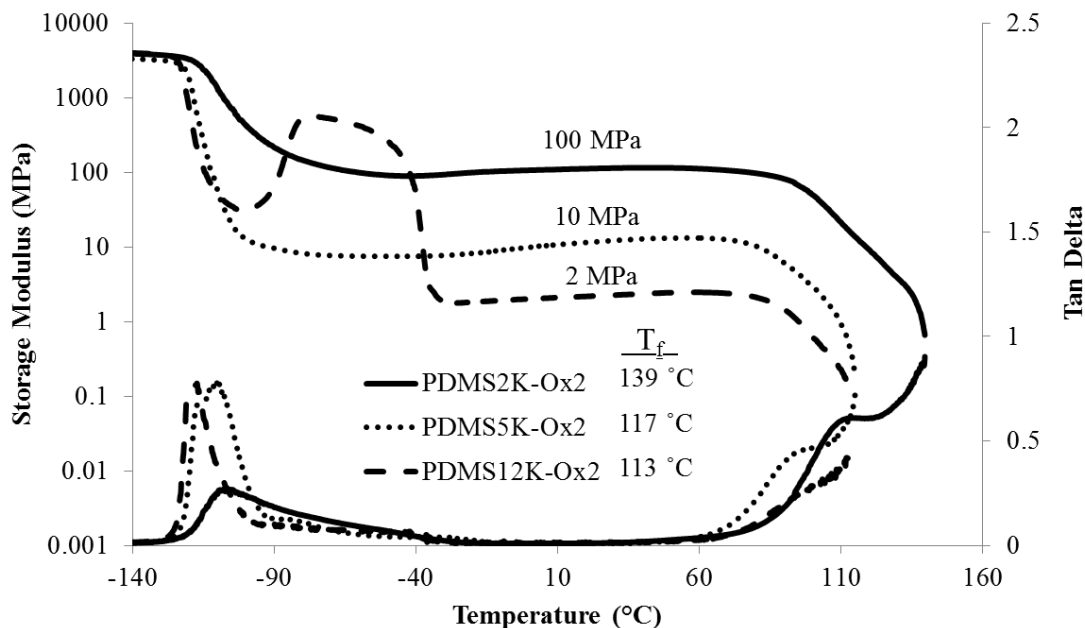
Figure 3.11. DMA traces for PDMS-Ox2 copolymers containing 2,000, 5,000, and 12,000 g/mol PDMS soft segments

3.4.5 Tensile Properties

Tensile analysis of PDMS-Ox copolymers exhibited properties typical of TPEs and tensile values are reported in Table 2 as the average of 5 specimens. PDMS2K-Ox2 showed a yield point at 30% strain and significant necking until film failure at 626 ± 43% strain (Figure 3.12). Stress at break occurred at 8 ± 0.4 MPa for PDMS2K-Ox2 with a measured Young's modulus of 96 ± 8 MPa. PDMS2K-Ox4 also exhibited a yield point at 30% strain without any observed necking. Strain at break occurred at 254 ± 14% with a stress of 2.1 ± 0.1 MPa. A large decrease in the Young's modulus, compared to PDMS2K-Ox2, resulted with a calculated value of 37 ± 2 MPa. The tensile properties decreased further with longer oxamide spacing of 6 and 8 methylene groups. PDMS2K-Ox6 and PDMS2K-Ox8 copolymers exhibited similar tensile

65

Table 3.2. Tensile properties of PDMS-Ox segmented copolymers reported as the average of 5 experiments

	Stress (MPa)	Strain (%)	Young's Modulus (MPa)
PDMS2K-Ox2	7.9 ± 0.39	626 ± 43	96 ± 8
PDMS2K-Ox4	2.1 ± 0.08	254 ± 14	37 ± 2
PDMS2K-Ox6	2.2 ± 0.12	91 ± 6.0	38 ± 3
PDMS2K-Ox8	2.2 ± 0.11	122 ± 10	38 ± 2
PDMS2K-OxAr	1.6 ± 0.08	13 ± 1.0	32 ± 1
PDMS5K-Ox2	2.1 ± 0.06	564 ± 17	14 ± 0.3
PDMS5K-Ox4	1.3 ± 0.07	441 ± 33	12 ± 0.6
PDMS5K-Ox6	1.2 ± 0.06	431 ± 25	10 ± 0.4
PDMS5K-Ox8	1.2 ± 0.04	475 ± 17	11 ± 0.4
PDMS5K-OxAr	0.9 ± 0.03	30 ± 3	19 ± 0.5
PDMS12K-Ox2	0.58 ± 0.06	941 ± 52	1.3 ± 0.1
PDMS12K-Ox4	1.3 ± 0.01	669 ± 28	2.4 ± 0.2
PDMS12K-Ox6	0.69 ± 0.01	503 ± 16	2.6 ± 0.1
PDMS12K-Ox8	0.58 ± 0.03	556 ± 30	3.3 ± 0.3
PDMS12K-OxAr	0.35 ± 0.02	32 ± 7	4.0 ± 0.2
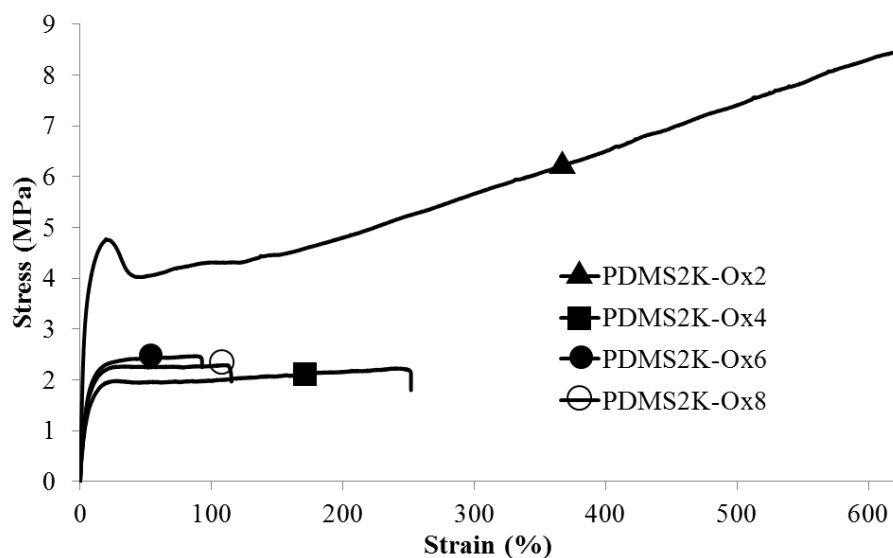
Figure 3.12. Stress-strain curve for PDMS2K-Ox copolymers

properties with stress at break, strain at break, and Young's modulus at ~2.2 MPa, 100%, and 38

MPa, respectively. Increasing oxamide spacing for PDMS5K-Ox copolymers also demonstrated

a decrease in the stress and strain at break. However, an increase in the spacing from 4 to 8 methylene groups resulted in minor changes to the tensile properties, which showed an average stress and strain at break ~1.2 MPa and 450%, respectively. Young's modulus decreased slightly with increased spacing from 14 ± 0.3 to 10 ± 0.4 MPa for the PDMS5K-Ox series. PDMS12K-Ox copolymers exhibited decreased strain at break with increased oxamide spacing without a significant trend in the stress at break. Strain at break for PDMS12K-Ox2 was $941 \pm 52\%$ and gradually decreased to ~500% for both copolymers that contained 6 and 8 methylene groups. Young's moduli gradually increased with increased spacing between oxamide groups for PDMS12K-Ox copolymers, ranging from 1.3 ± 0.1 to 3.3 ± 0.3 MPa for PDMS12K-Ox2 and PDMS12K-Ox8, respectively.

Varying the PDMS molecular weight elucidated the effects of decreased wt% HS copolymer composition on tensile properties. The stress at break decreased with increasing PDMS molecular weight from 8 ± 0.4 to 0.6 ± 0.06 MPa for PDMS2K-Ox2 and PDMS12K-Ox2, respectively (Figure 3.13). Young's moduli scaled with a decrease in copolymer wt% HS at 96 ± 8, 14 ± 0.3, and 1.3 ± 0.1 MPa, similar to the changes in observed DMA storage moduli. PDMS2K-Ox2 exhibited a high strain at break due to necking of the material after an observed yield point. PDMS5K-Ox2 did not show signs of necking during tensile experiments and exhibited a strain at break of $564 \pm 17\%$. PDMS12K-Ox2 with the lowest wt% HS content, demonstrated the highest strain at break near 1000%.

Tensile properties of PDMS-OxAr copolymers containing an odd numbered, aromatic oxamide spacer showed poor tensile properties. Strain at break did not exceed 32% for any of the three copolymers tested. The stress at break was significantly lower than copolymers with an even numbered spacer presumably due to the weaker intermolecular interactions of the aromatic

spacer. However, the presence of the aromatic group in the HS increased the observed Young's modulus compared to copolymers that contained the same PDMS molecular weight. Overall, tensile properties were optimal with the shortest methylene spacer between oxamide groups in the HS due to the increased stability and interactions between oxamide hydrogen bonding groups.
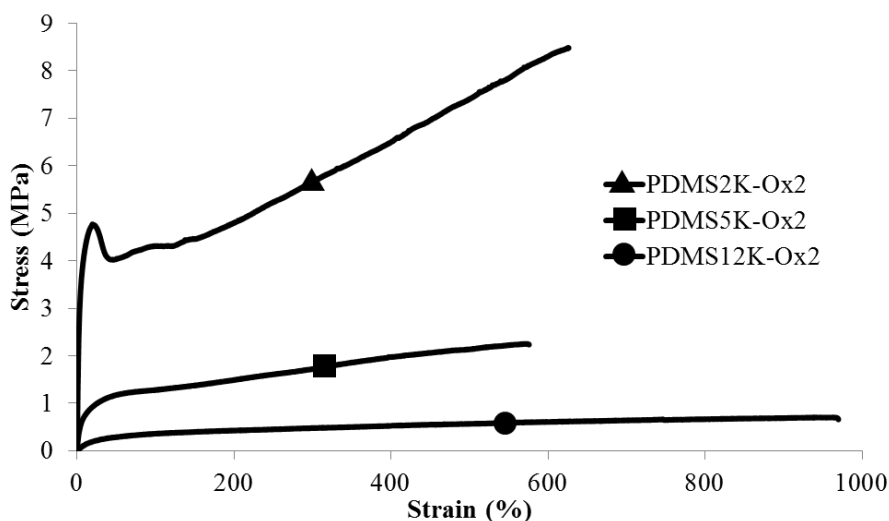
Figure 3.13. Stress-strain curves for PDMS-Ox2 copolymers with increasing soft segment molecular weight

Hysteresis experiments examined the impact of oxamide spacing on the permanent deformation at an applied strain over 5 consecutive cycles. In general, the percentage of hysteresis values were lowest from cycle to cycle with the shortest spacer between oxamide groups in the HS (Table 3.3). At 30% strain, the first cycle % hysteresis increased 10% from 60% for PDMS2K-Ox2 to 70% for PDMS2K-Ox8 as a result of the increase in oxamide spacing. This trend was also valid for the PDMS5K-Ox series where the lowest % hysteresis occurred with the shortest spacer between oxamide groups (Figure 3.14). Hysteresis experiments were not performed for PDMS-OxAr copolymers due to poor tensile properties. Hysteresis experiments suggested that the stronger intermolecular interactions between oxamide containing HSs with

shorter spacers reduced the extent of permanent deformation after an applied strain. As previously shown, PDMS-Ox copolymers containing a 2 methylene spacer between oxamide groups yielded optimal mechanical properties.

Table 3.3. % hysteresis values for copolymers over five cycles at 30%, 50%, and 100% strain respectively

	Max Strain	Cycle				
		1	2	3	4	5
PDMS2K-Ox2	30%	60	45	43	41	41
PDMS2K-Ox4	30%	60	48	46	46	46
PDMS2K-Ox6	30%	67	50	49	48	47
PDMS2K-Ox8	30%	70	54	52	52	51
PDMS5K-Ox2	50%	60	46	43	42	40
PDMS5K-Ox4	50%	61	51	48	47	46
PDMS5K-Ox6	50%	69	55	52	51	50
PDMS5K-Ox8	50%	69	55	53	51	50
PDMS12K-Ox2	100%	48	32	29	27	25
PDMS12K-Ox4	100%	41	28	25	23	22
PDMS12K-Ox6	100%	60	44	41	40	38
PDMS12K-Ox8	100%	63	46	42	40	39
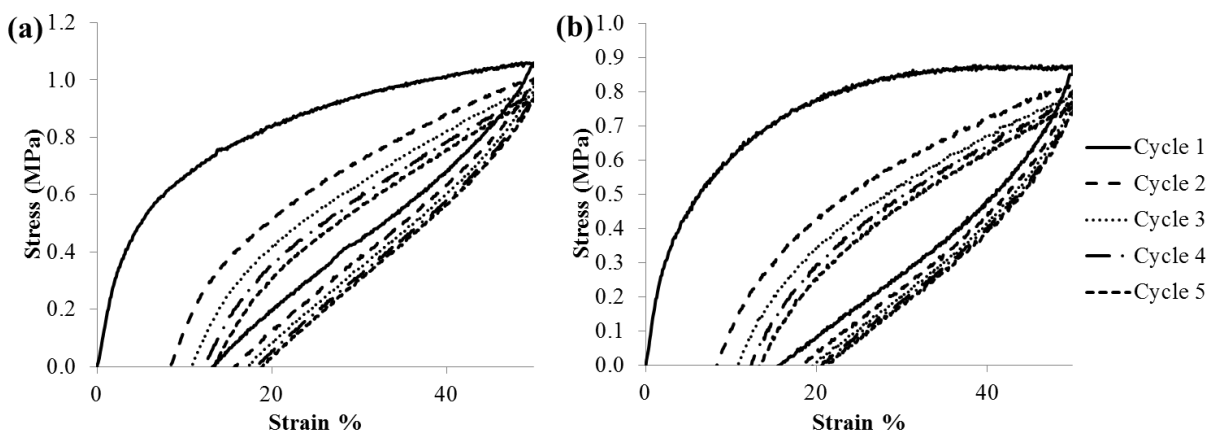
Figure 3.14. Hysteresis profiles for PDMS5K-Ox2 and PDMS5K-Ox8 copolymers over 5 cycles at 50% strain

3.4.6 Atomic Force Microscopy

AFM imaging of PDMS2K-Ox segmented copolymers in tapping mode revealed a microphase separated morphology consisting of a network of needle-like HS domains dispersed in a soft matrix (Figure 3.15). The long needle-like structures are likely the crystalline oxamide HS regions which were observed in a previous report on polyoxamide polyether segmented copolymers.[36] The needle-like crystalline structures in the PDMS2K-Ox2 phase images
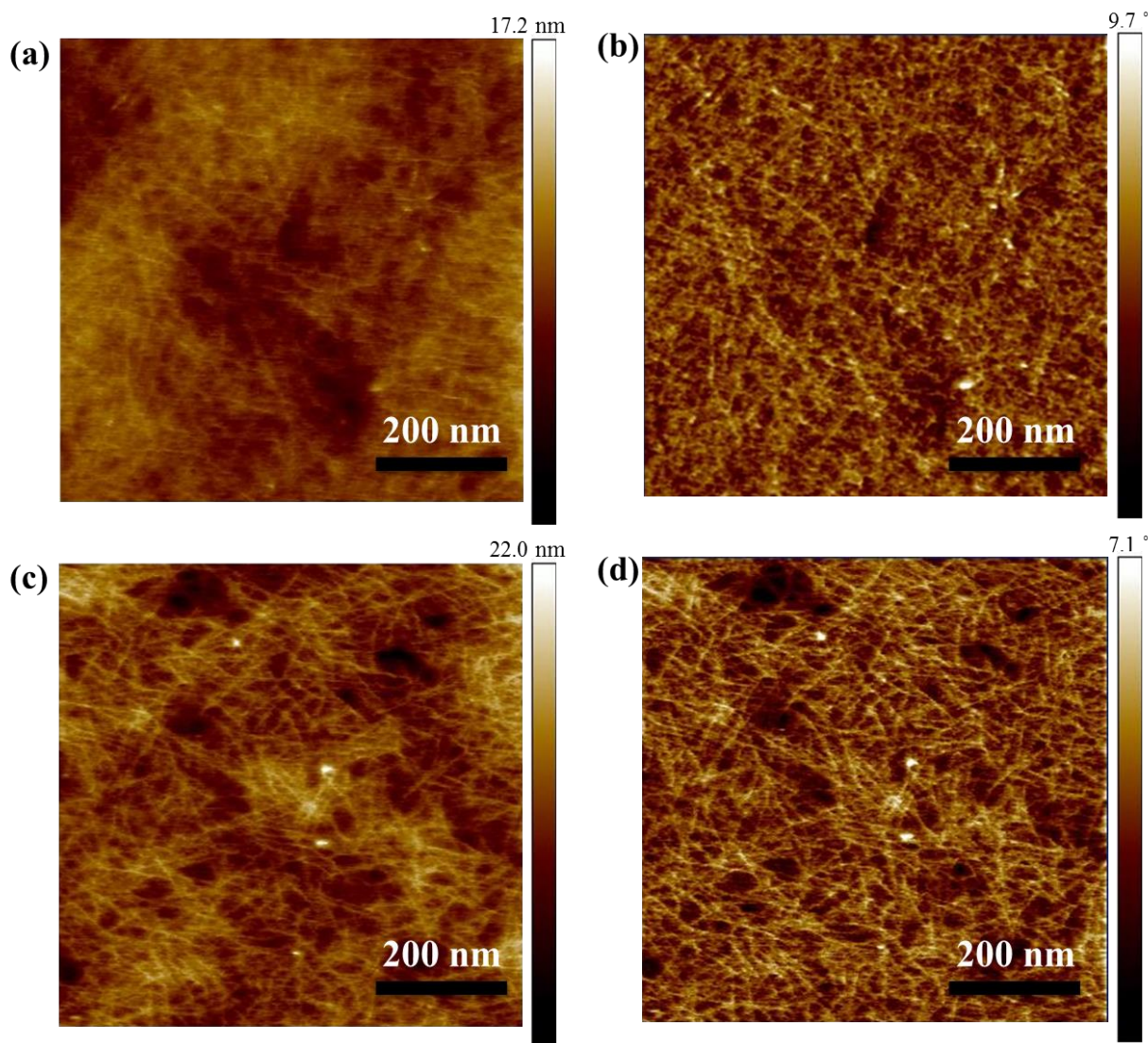
Figure 3.15. AFM (a) height and (b) phase images of PDMS2K-Ox2 and (c, d) PDMS2K-Ox6 segmented copolymers

demonstrated shorter lateral dimensions of the phase separated domains and appeared smaller than in the phase images for PDMS2K-Ox6. The crystalline structures were >100 nm and more apparent in the PDMS2K-Ox6 copolymer and visually confirmed the presence of crystalline regions that DSC analysis and previous reports suggest.

3.5 Conclusions

Bulk polymerization of ethyl oxalate terminated PDMS oligomers with a molecular weight of 2,000, 5,000, and 12,000 g/mol resulted in clear, free standing elastic films. The polymerization temperatures demonstrated the versatility of the bulk polymerization strategy and yielded excellent films after solution casting and annealing. Variable temperature FTIR spectroscopy provided insight into the effect of oxamide spacing on the hydrogen bond dissociation temperatures. FTIR spectroscopy showed that the temperature for ordered, hydrogen bond disruption decreased with an increase in oxamide spacer length. Similarly, DSC revealed a decrease in the HS T_m as the spacing between oxamide groups in the HS increased. Thermomechanical behavior of PDMS-Ox copolymers significantly changed with variations in oxamide spacing. T_f increased with the decrease in oxamide spacing with PDMS2K-Ox2 possessing the highest T_f. The effect of PDMS molecular weight on the thermomechanical behavior revealed a decrease in the rubbery plateau storage moduli with lower wt% HS. Tensile properties were optimal with the shortest 2 methylene spacer between oxamide groups. As the spacer length increased, a significant reduction in the strain at break occurred in each copolymer series as well as a reduction in the stress at break for some of the copolymers studied. A gradual decrease in the stress at break and Young's modulus also occurred with increasing PDMS molecular weight. Copolymers with the shortest oxamide spacing displayed the lowest percentage of hysteresis over 5 consecutive cycles at various % strain. Polymerization with *m-*

xylene diamine yielded copolymers with an aromatic, odd numbered spacer between oxamide groups, and consequently, exhibited poor mechanical properties. Copolymers containing 2 methylenes between the oxamide groups provided the strongest hydrogen bonding interactions, leading to the best combination of tensile and thermomechanical properties.

3.6 Acknowledgments

3.7 References

(1)   Dodge, J.; John Wiley & Sons, Inc.: 2003, p 197.
(2)   Francis, C.; Naba, D.; Namita Roy, C.; Anil, B. In *Current Topics in Elastomers Research*; CRC Press: 2008.
(3)   Versteegen, R. M.; Kleppinger, R.; Sijbesma, R. P.; Meijer, E. W. *Macromolecules* **2006**, *39*, 772.
(4)   ten Cate, A. T.; Sijbesma, R. P. *Macromolecular Rapid Communications* **2002**, *23*, 1094.
(5)   van der Schuur, M. J.; Gaymans, R. J. *Polymer* **2007**, *48*, 1998.
(6)   Jewrajka, S. K.; Yilgor, E.; Yilgor, I.; Kennedy, J. P. *Journal Polymer Science, Part A: Polymer Chemistry* **2008**, *47*, 38.
(7)   Tang, D.; Mulder, D.-J.; Noordover, B. A. J.; Koning, C. E. *Macromolecular Rapid Communications* **2011**, *32*, 1379.
(8)   Wisse, E.; Spiering, A. J. H.; van Leeuwen, E. N. M.; Renken, R. A. E.; Dankers, P. Y. W.; Brouwer, L. A.; van Luyn, M. J. A.; Harmsen, M. C.; Sommerdijk, N.; Meijer, E. W. *Biomacromolecules* **2006**, *7*, 3385.
(9)   Korley, L. T. J.; Pate, B. D.; Thomas, E. L.; Hammond, P. T. *Polymer* **2006**, *47*, 3073.
(10)   Pukánszky Jr, B.; Bagdi, K.; Tóvölgyi, Z.; Varga, J.; Botz, L.; Hudak, S.; Dóczi, T.; Pukánszky, B. *European Polymer Journal* **2008**, *44*, 2431.
(11)   van der Schuur, M.; Noordover, B.; Gaymans, R. J. *Polymer* **2006**, *47*, 1091.
(12)   Klinedinst, D. B.; Yilgör, E.; Yilgör, I.; Beyer, F. L.; Wilkes, G. L. *Polymer* **2005**, *46*, 10191.
(13)   Oprea, S.; Potolinca, V. O. *Designed Monomers and Polymers* **2013**, *16*, 47.
(14)   Strawhecker, K. E.; Hsieh, A. J.; Chantawansri, T. L.; Kalcioglu, Z. I.; Van, V. K. J. *Polymer* **2013**, *54*, 901.
(15)   Huoli; Lihua *Advanced Materials Research (Durnten-Zurich, Switz.)* **2012**, *512-515*, 2185.
(16)   Ijzer, A. C.; Arun, A.; Reijerkerk, S. R.; Nijmeijer, K.; Wessling, M.; Gaymans, R. J. *Journal of Applied Polymer Science* **2010**, *117*, 1394.

(17) Yoshino, M.; Ito, K.; Kita, H.; Okamoto, K.-I. *Journal of Polymer Science Part B: Polymer Physics* **2000**, *38*, 1707.

(18) Lips, P. A. M.; Broos, R.; van Heeringen, M. J. M.; Dijkstra, P. J.; Feijen, J. *Polymer* **2005**, *46*, 7834.

(19) Niesten, M.; Gaymans, R. J. *Journal of Applied Polymer Science* **2001**, *81*, 1372.

(20) Castagna, A. M.; Pangon, A.; Choi, T.; Dillon, G. P.; Runt, J. *Macromolecules* **2012**, *45*, 8438.

(21) Chakrabarty, S.; Nisenholt, M.; Wynne, K. J. *Macromolecules* **2012**, *45*, 7900.

(22) Mark, J. E. *Accounts of Chemical Research* **2004**, *37*, 946.

(23) Yilgor, E.; Yilgor, I. *Polymer* **2001**, *42*, 7953.

(24) Yilgor, I.; Yilgor, E. *Polymer Reviews* **2007**, *47*, 487.

(25) Miller, J. A.; Lin, S. B.; Hwang, K. K. S.; Wu, K. S.; Gibson, P. E.; Cooper, S. L. *Macromolecules* **1985**, *18*, 32.

(26) van der Schuur, M.; de Boer, J.; Gaymans, R. J. *Polymer* **2005**, *46*, 9243.

(27) Yilgor, I.; Shaaban, A. K.; Steckle, W. P.; Tyagi, D.; Wilkes, G. L.; McGrath, J. E. *Polymer* **1984**, *25*, 1800.

(28) Das, S.; Yilgor, I.; Yilgor, E.; Wilkes, G. L. *Polymer* **2008**, *49*, 174.

(29) Sheth, J. P.; Klinedinst, D. B.; Wilkes, G. L.; Iskender, Y.; Yilgor, I. *Polymer* **2005**, *46*, 7317.

(30) Yilgor, E.; Yurtsever, E.; Yilgor, I. *Polymer* **2002**, *43*, 6561.

(31) Coe, S.; Kane, J. J.; Nguyen, T. L.; Toledo, L. M.; Wininger, E.; Fowler, F. W.; Lauher, J. W. *Journal of the American Chemical Society* **1997**, *119*, 86.

(32) Nguyen, T. L.; Fowler, F. W.; Lauher, J. W. *Journal of the American Chemical Society* **2001**, *123*, 11057.

(33) Schulze, H.; Texaco Development Corp., USA . 1978, p 7 pp.

(34) Leir, C. M.; Benson, K. E.; Hansen, R. G.; Purgett, M. D.; Everaerts, A. I.; 3M Innovative Properties Company, USA . 2007, p 12pp.

(35) Leir, C. M.; Benson, K. E.; Hansen, R. G.; Purgett, M. D.; Everaerts, A. I.; Sherman, A. A.; 3M Innovative Properties Company, USA . 2007, p 16pp.

(36) Sijbrandi, N. J.; Kimenai, A. J.; Mes, E. P. C.; Broos, R.; Bar, G.; Rosenthal, M.; Odarchenko, Y.; Ivanov, D. A.; Dijkstra, P. J.; Feijen, J. *Macromolecules* **2012**, *45*, 3948.

(37) Coleman, M. M.; Lee, K. H.; Skrovanek, D. J.; Painter, P. C. *Macromolecules* **1986**, *19*, 2149.

(38) Skrovanek, D. J.; Howe, S. E.; Painter, P. C.; Coleman, M. M. *Macromolecules* **1985**, *18*, 1676.

(39) Skrovanek, D. J.; Painter, P. C.; Coleman, M. M. *Macromolecules* **1986**, *19*, 699.

(40) Sijbrandi, N. J.; Kimenai, A. J.; Mes, E. P. C.; Broos, R.; Bar, G.; Rosenthal, M.; Odarchenko, Y. I.; Ivanov, D. A.; Jan, F. J.; Dijkstra, P. J. *Polymer* **2012**, *53*, 4033.

(41) Sheth, J. P.; Aneja, A.; Wilkes, G. L.; Yilgor, E.; Atilla, G. E.; Yilgor, I.; Beyer, F. L. *Polymer* **2004**, *45*, 6919.

(42) Tyagi, D.; Yilgor, I.; McGrath, J. E.; Wilkes, G. L. *Polymer* **1984**, *25*, 1807.

Chapter 4: Synthesis and Characterization of Poly(dimethyl siloxane) Poly(urea oxamide) Segmented Copolymers

(From: Buckwalter, D. J.; Zhang, M.; Inglefield, D.; Moore, R. B.; Long, T. E. *Submission in Progress*)

4.1 Abstract

An unprecedented family of non-chain extended segmented poly(dimethyl siloxane) poly(urea oxamide) (PDMS-UOx) copolymers displayed thermoplastic elastomeric behavior with improved thermomechanical properties compared to PDMS polyurea (PDMS-U) analogs. A two-step, PDMS end-capping sequence using diethyl oxalate and hydrazine generated difunctional oxamic hydrazide capped oligomers. Polymerization with HMDI provided high molecular weight copolymers, which yielded tough, elastomeric films with monodisperse hard segments. Dynamic mechanical analysis (DMA) of PDMS-UOx copolymers revealed a broad rubbery plateau that extended to 186 ˚C. The PDMS-UOx rubbery plateau extended ~120 ˚C longer than a PDMS-U analog, presumably due to enhanced hydrogen bonding resulting in increased microphase separation. DSC and WAXD elucidated the amorphous character of PDMS-UOx while DMA, SAXS, and AFM confirmed a well-defined microphase separated morphology. Incorporation of urea oxamide groups significantly affected microphase separation and thermomechanical properties, and these copolymers offer impact in adhesive and biomedical technologies due to low temperature formation of unique hydrogen bonding sequences.

4.2 Introduction

Segmented block copolymers typically exhibit microphase separated morphologies due to $\chi*n$ described in the Flory-Huggins equation. The covalently linked segments consist of a low T_g soft segment (SS) and a rigid, often highly polar, hard segment (HS) with a higher T_g.

Poly(dimethyl siloxane) (PDMS) and polyether SSs, such as poly(tetramethylene oxide) (PTMO), provide flexibility and incompatibility with the polar HS sequences.[1,2] PDMS flexibility and other desirable physical properties including hydrophobicity, low surface energy, high gas permeability, coupled with high thermal, UV, and oxidative stability provide a very attractive SS for microphase separated segmented copolymers.[3,4] HSs typically include sequences capable of forming strong, mechanically reinforcing physical crosslinks through intermolecular hydrogen bonding or other forms of non-covalent intermolecular interactions.[5] Typical HSs include polyureas (PU),[6] polyurethanes,[7] polyamides,[8,9] poly(ester amide)s,[10,11] polyimides,[12-14] and polysulfones.[15,16] Most segmented block copolymers display thermoplastic elastomer (TPE) behavior with desirable melt and solution processability.[17]

McGrath et al. first introduced non-chain extended PDMS PU segmented copolymers containing uniform, monodisperse hard segments with low urea HS content down to 6 wt%.[18,19] These early PDMS PU copolymers suggested the design of other non-chain extended segmented copolymers that varied in the soft and hard segment contents. Many reports focus particularly on hard segment architecture and the effect of hydrogen bonding on the corresponding physical properties.[20] Previous in-depth reports of PDMS and PTMO PU segmented copolymers demonstrate well-defined microphase separated morphologies containing urea hard segments possessing strong bidentate urea hydrogen bonding, despite low HS content. However, hydrogen bonding and isocyanate symmetry were more important factors in non-chain extended PU copolymers than traditional chain extended compositions to achieve enhanced thermomechanical performance.[21,22] Isocyanate symmetry of the HS also reduces the hydrogen bonding competition between ether and urea groups.[23] These effects are not quite as evident with PDMS based non-chain extended PU copolymers. It is suggested that the high degree of microphase separation in

PDMS PU copolymers, due to the lack of intermolecular interactions between the urea groups and hydrophobic PDMS, resulted in a reduced sensitivity to HS symmetry.[24] Bidentate urea hydrogen bonding imparts strong physical crosslinking that are well-suited for a broad range of segmented copolymers.

Meijer et al. reported the role of hydrogen bonding strength of a polyether-based segmented copolymer composed of monodisperse PU HSs with 1 to 4 urea hydrogen bonding groups. Optimum mechanical properties and processability were obtained with two urea groups, and in contrast, copolymers containing only one urea resulted in a viscous liquid. Copolymers containing three and four urea groups in the HS yielded insoluble polymers with poor processability due to the strong hydrogen bonding interactions.[25] A similar study of PTMO polyoxamide copolymers revealed similar results when varying the number of hydrogen bonding groups in the monodisperse HS.[26] Polyoxamide copolymers containing a single oxamide unit in the HS yielded a sticky copolymer with poor material properties. Copolymers with HSs containing two or three oxamide groups produced TPEs with good mechanical and thermal properties, which demonstrated the need for higher contents of hydrogen bonding in the HS. This earlier work also demonstrated the ability of oxamides in the segmented copolymer HS to impart strong hydrogen bonding that generated a highly ordered, microphase separated morphology. Oxamides are gaining more attention as an alternative hydrogen bonding groups in segmented copolymers due to several synthetic advantages and the resulting unique hydrogen bonding.

Herein, we report a new family of non-chain extended, segmented copolymers containing both urea and oxamide groups to provide an enhanced hydrogen bonding HS. The copolymers contain a monodisperse bis(urea oxamide) HS and PDMS SS with molecular weights of 2,000, 5,000, and 12,000 g/mol. Oxamic hydrazide terminated PDMS oligomers and stoichiometric

amounts of HMDI yielded PDMS poly(urea oxamide) (PDMS-UOx) segmented copolymers with TPE behavior. The presence of oxamide groups adjacent to the ureas in the HS provided unique hydrogen bonding architectures, as seen in Figure 4.1, compared to non-chain extended segmented PDMS polyurea (PDMS-U) controls. Increasing the hydrogen bonding in the HS with the presence of oxamide groups yielded a new family of segmented copolymers and provided fundamental understanding of the role of hydrogen bonding on thermal and mechanical properties. Varying the copolymers PDMS molecular weight resulted in tailored PDMS-UOx HS contents from 3.6 to 22 wt% HS.
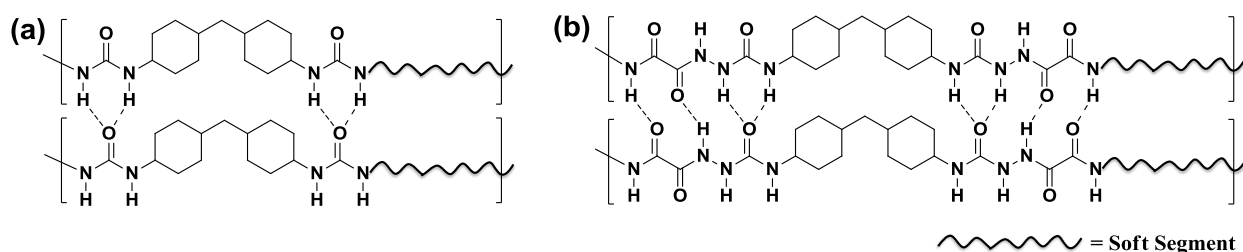
Figure 4.1. Hydrogen bonding interactions of (a) polyurea and (b) poly(urea oxamide) hard segments

4.3 Experimental

4.3.1 Materials

Amino propyl terminated poly(dimethyl siloxane) (AP-PDMS) with M_n's of 1,800 and 5,000 g/mol were purchased from Gelest Inc., and Wacker Chemie kindly donated 12,000 g/mol AP-PDMS. The AP-PDMS oligomers were placed under high vacuum (0.06 mmHg) while heating (90 ˚C) to remove residual cyclics and CO_2 prior to use. Diethyl oxalate (99%) and anhydrous hydrazine (98%) were purchased from Sigma Aldrich and used without further purification. Dibutyltin dilaurate (DBTDL) (95%) was purchased from Aldrich and a 10 wt% solution in dry THF was prepared. Bayer kindly donated 4,4'-methylenebis(cyclohexyl isocyanate) (HMDI), which was used without further purification.

4.3.2 Synthesis of PDMS Poly(urea oxamide) Copolymers

AP-PDMS (18.87 g, 11.3 mmol, 5,000 g/mol) was cannulated into a dry, 100-mL, round bottomed flask equipped with a stir bar and purged with dry argon. Four molar equivalents of diethyl oxalate (6.59 g, 45.2 mmol) was syringed directly into the reaction flask at 0 ˚C, and the solution was stirred for 12 h. Ethanol and excess diethyl oxalate were removed under high vacuum (0.06 mmHg) at 80 ˚C for 2 h. The number-average molecular weight of the ethyl ester capped PDMS oligomer was determined using ^{1}H NMR spectroscopy and end-group analysis. The ethyl ester capped PDMS (13.93 g, 2.59 mmol) was then cannulated into a dry, 100-mL flask equipped with a large stir bar and purged with argon. A slight excess of anhydrous hydrazine (0.25 g, 7.78 mmol) was syringed directly into the reaction flask at 25 ˚C and the solution was stirred for 12 h. Excess hydrazine and ethanol were removed under high vacuum (0.06 mmHg) at 80 ˚C. The molecular weight of the hydrazide-capped PDMS was determined with ^{1}H NMR spectroscopy and end-group analysis. The hydrazide capped PDMS (12.75 g, 2.38 mmol) was added to a dry, two necked, 100-mL round bottomed flask under an argon blanket. THF (60 mL, 20 wt% solids) was added to the flask and the solution was stirred until the polymer dissolved to yield a cloudy, white solution. HMDI (0.63 g, 2.38 mmol) was syringed directly into the reaction flask and then DBTDL (50 ppm) was added. The solution was stirred at 60 ˚C for 48 h. Polymer films were solution cast from the diluted reaction mixture (10 wt % polymer) and allowed to dry overnight at 23 ˚C. The PDMS based films were annealed at 100 ˚C for 4 h then an additional 8 h at 100 ˚C under high vacuum.

4.3.3 Synthesis of Segmented 5K PDMS Poly(urea oxamide)

All poly(urea oxamide) segmented copolymers were synthesized following a similar procedure and the synthesis for a 10.4 wt % hard segment PDMS5K-UOx follows as an

example. The hydrazide capped PDMS oligomers (5.73 g, 1.03 mmol) were dissolved in THF at 10 wt % solids in a dry, two necked round-bottomed flask under argon atm. Oxalic dihydrazide (0.036 g, 0.31 mmol) was added to the reaction flask under an argon blanket while stirring. After the PDMS dihydrazide dissolved in THF, HMDI (0.35 g, 1.33 mmol) and DBTDL catalyst (50 ppm) was syringed directly into the reaction flask while stirring. The reaction was sealed tightly and placed in a 60 ˚C oil bath for 24 h. The reaction mixture was diluted with fresh THF after cooling to 23 ˚C and the polymer film was solution cast into Teflon molds. These films were air dried at 23 ˚C then annealed under the same conditions as previous PDMS-UOx copolymers. The copolymer composed of 14.5 wt% HS was refluxed in a mixture of THF, methanol, and DMF for over 24 h until the copolymer was completely dissolved, then cast into a Teflon® mold and placed directly in the vacuum oven at 100 ˚C to anneal for 12 h.

4.3.4 Synthesis of PDMS Poly(urea) Copolymers

AP-PDMS (10.8 g, 2.14 mmol, 5,000 g/mol) was cannulated into a dry argon purged 100-mL, round-bottomed flask. THF (51 mL, 20 wt% solids) was added and the solution was stirred until homogeneous. HMDI (0.562 g, 2.14 mmol) was syringed directly into the reaction mixture and the polymerization was conducted at 60 ˚C for 24 h. The polymer was then cast directly from the reaction mixture into Teflon® molds and annealed after drying in the same manner as the PDMS-UOx copolymers.

4.3.5 Analytical Methods

Each PDMS-U and PDMS-UOx copolymer was analyzed using ^{1}H NMR spectroscopy in CDCl$_3$ at 27 ˚C with an Avance 500 MHz spectrometer. Size exclusion chromatography (SEC) was conducted at 30 ˚C in THF (HPLC grade containing 250 ppm BHT) at 1.0 mL/min on a Waters 717plus auto sampler equipped with a Waters 515 HPLC pump, Waters 2414 refractive

index detector, and Wyatt Technology miniDawn MALLS detector. Absolute molecular weights were calculated using an offline dn/dc value measured on a Wyatt Optilab T-rEX differential refractive index detector. *In situ* FTIR spectroscopy was performed using a Mettler Toledo ReactIR[TM] equipped with a SiComp probe, monitoring the isocyanate stretching band from 2200-2300 cm^{-1}. FT-IR spectra were collected every 30 s for the first 30 min and then every min subsequently. Thermal gravimetric analysis (TGA) was conducted on a TA Instruments Hi-Res TGA 2950 with a heating ramp of 10 ˚C/min to provide degradation temperatures under a nitrogen purge. Differential scanning calorimetry (DSC) was conducted at a heating rate of 10 ˚C/min under a nitrogen purge of 50 mL/min from -140 to 200 ˚C with a cooling rate of 50 ˚C/min on a TA Instruments Q1000 DSC. Each sample was subjected to a heat/cool/heat cycle with values reported from the second heat. Dynamic mechanical analysis (DMA) was conducted using a TA Instruments Q800 in tension mode 1 Hz with the temperature ramped at a rate of 3 ˚C/min from -140 ˚C to the flow temperature. Flow was defined as the temperature where the storage modulus reached 0.1 MPa. The peak maximum in the tan δ curve was identified as the glass transition temperature for each sample tested. Tensile and hysteresis analysis were performed on an Instron 4411 universal testing instrument. Tensile experiments were performed at a crosshead speed of 50 mm/min with the reported tensile values as an average of 5 samples. Each sample was cut using a Pioneer Dietechs dog bone cutting die. Hysteresis experiments were conducted with a maximum strain of 100% with a rate of 2 %/sec over 5 full cycles. The area under the curve was calculated using the trapezoid method[27] of analysis and compared cycle to cycle. Variable temperature FT-IR experiments were conducted using a Varian 670-IR equipped with a PIKE GladiATR accessory. The temperature was ramped from 35 – 190 ˚C for each copolymer at a rate of 1 ˚C/min, with spectrum being collected every 5 ˚C. Spectral data was

collected with 32 scans and a resolution of 4 cm^{-1}. Small angle X-ray scattering (SAXS) and wide angle X-ray diffraction (WAXD) analysis were performed using a Rigaku S-Max 3000 3 pinhole SAXS system, equipped with a rotating anode emitting X-ray with a wavelength of 0.154 nm (Cu Kα). Scattering from a silver behenate standard was used to calibrate the sample-to-detector distance. For SAXS, the sample-to-detector distance was 1603 mm and for WAXD, the sample-to-detector distance was 82.5 mm. Two-dimensional SAXS patterns were obtained using a fully integrated 2D multiwire, proportional counting, gas-filled detector, with an exposure time of 1 h. SAXS data was corrected for sample thickness, sample transmission, and background scattering. WAXD two-dimensional diffraction patterns were obtained using an image plate with an exposure time of 1 h. All SAXS/WAXD data were analyzed using the SAXSGUI software package to obtain radially integrated SAXS/WAXD intensity versus scattering vector q (SAXS), where q=(4π/λ)sin(θ), θ is one half of the scattering angle and λ is the wavelength of X-ray or 2θ (WAXD) profiles. Variable temperature SAXS experiments were conducted using a Linkam hot stage positioned in the sample chamber. X-ray scattering data was collected every 10 ˚C from 30 – 150 ˚C, every 1 ˚C from 155 – 180 ˚C, and every 5 ˚C from 180 – 200 ˚C. The sample was equilibrated for 1 h at each temperature before acquisition. Melt rheology was conducted on a TA Instruments Ares G2 rheometer equipped with a temperature controlled environmental chamber. Each temperature sweep experiment was conducted from 120 to 200 ˚C at 1 Hz with 1.25% strain and a temperature ramp rate of 1 ˚C/min. Atomic force microscopy phase and height images were obtained using a Vecco multimode AFM in tapping mode with a 42 nN spring constant tip and a set point ratio of 0.68.

4.4 Results and Discussion

4.4.1 Synthesis of PDMS Segmented Copolymers

Polymerization of PDMS-UOx copolymers containing 3.6 – 22 wt% HS content resulted in optically clear, free-standing films with TPE behavior (Scheme 4.1). A four molar excess of diethyl oxalate, during the first end-capping reaction, avoided premature polymerization and yielded a pure ethyl oxalate capped PDMS oligomer. The second end-capping reaction with hydrazine was the key step of the synthetic strategy to obtain a pure, difunctional oxamic hydrazide end-capped PDMS oligomer. Nucleophilic substitution of the ethyl oxalate end groups

Scheme 4.1. Step-growth polymerization of non-chain extended poly(dimethyl siloxane) poly(urea oxamide) segmented copolymers
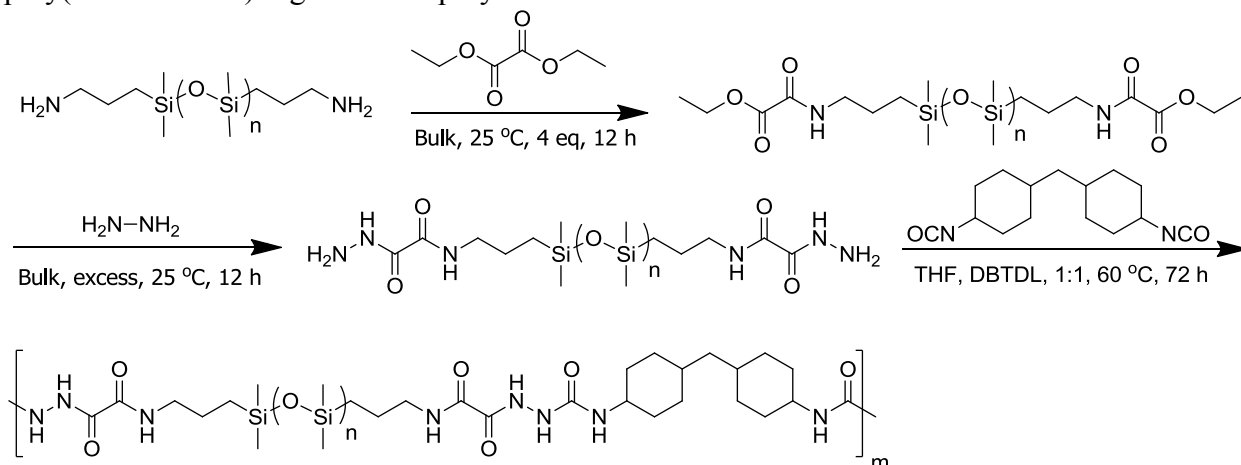
with hydrazine proved very efficient in the absence of polymerization despite high temperatures. Hydrazides lack of reactivity towards ethyl oxalate allowed the oxamic hydrazide-terminated PDMS to efficiently form and become a very useful synthetic handle for new polymerization chemistry. Oxamic hydrazide terminated PDMS oligomers appeared as white, solid to waxy products, with the exception of the 12K PMDS terminated oligomers, which were sticky, soft solids. The polymerization remained heterogeneous for the first hour and then became clear and homogeneous for the duration of the polymerization with a subsequent increase in viscosity. Previous studies demonstrated the influence of thermal annealing on bulk morphology and mechanical properties.[28-31] An annealing study determined the temperature and time for

optimum, stable thermomechanical properties of the PDMS-UOx copolymers. All films were annealed at 100 ˚C for 12 h prior to characterization.

Despite two end-capping reactions, polymerization with HMDI yielded high molecular weight copolymers, as summarized in Table 4.1. THF SEC provided reliable absolute molecular weight data for each segmented copolymer with monomodal light scattering traces, however, SEC solvent solubility issues prevented collection of molecular weight data for PDMS12K-UOx. Molecular weight differences between the PDMS-UOx and PDMS-U analogs will influence physical properties, and multiple polymerizations provided copolymers with similar molecular weights for comparison. Polymerization of the non-chain extended PDMS-PU segmented copolymers, ranging from 2.3 – 15 wt% HS content, (Scheme 4.2) resulted in transparent, free standing films with TPE behavior, consistent with previous studies.[32]

Table 4.1. Molecular weights and thermal degradation values of PDMS-U and PDMS-UOx segmented copolymers

	Soft Segment M_n (kg/mol)	Hard Segment Content (wt %)	M_n (kg/mol)	M_w (kg/mol)	PDI	$T_{d, 5\%}$ (˚C)
PDMS2K-U	2	15	69.3	97.1	1.40	315
PDMS2K-UOx	2	22	71.9	132	1.85	314
PDMS5K-U	5	5.5	32.3	42.7	1.32	305
PDMS5K-UOx	5	8.5	40.2	63.7	1.58	347
PDMS12K-U	12	2.3	52.9	93.4	1.77	316
PDMS12K-UOx	12	3.6	-	-	-	346

<u>SEC</u>: 30 ˚C, THF, 1 mL/min; <u>TGA</u>: N_2, 10 ˚C/min, 25 – 600 ˚C

Scheme 4.2. Synthesis of PDMS polyurea copolymers
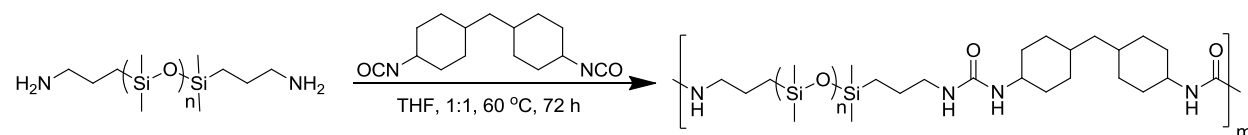
Polymerization of chain extended PDMS5K-UOx segmented block copolymers included oxalic dihydrazide as the chain extender to control the copolymer HS wt% in addition to varying

PDMS SS molecular weight (Scheme 4.3). Segmented PDMS-UOx copolymers, with 5K PDMS SS ranged from 10.4 to 14.5 wt% HS content, and yielded TPE behavior with opaque films. Preparation of these copolymers utilized the same reaction conditions and film casting procedure as the non-chain extended copolymers. Determining the extent of high urea oxamide (UOx) segment incorporation in the chain extended copolymers versus UOx homopolymer impurities was difficult to determine due to the nature of the UOx HS. The observed opaque films may indicate the presence of UOx homopolymer contamination. The segmented copolymer with 14.5 wt% HS content resulted in an insoluble product, requiring a refluxing DMF solution for film casting. Overall, the chain extended polymerization strategy for PDMS-UOx copolymers yielded inferior TPEs compared to the non-chain extended analogs.

Scheme 4.3. Synthesis of segmented PDMS poly(urea oxamide) copolymers for increased weight % hard segment content
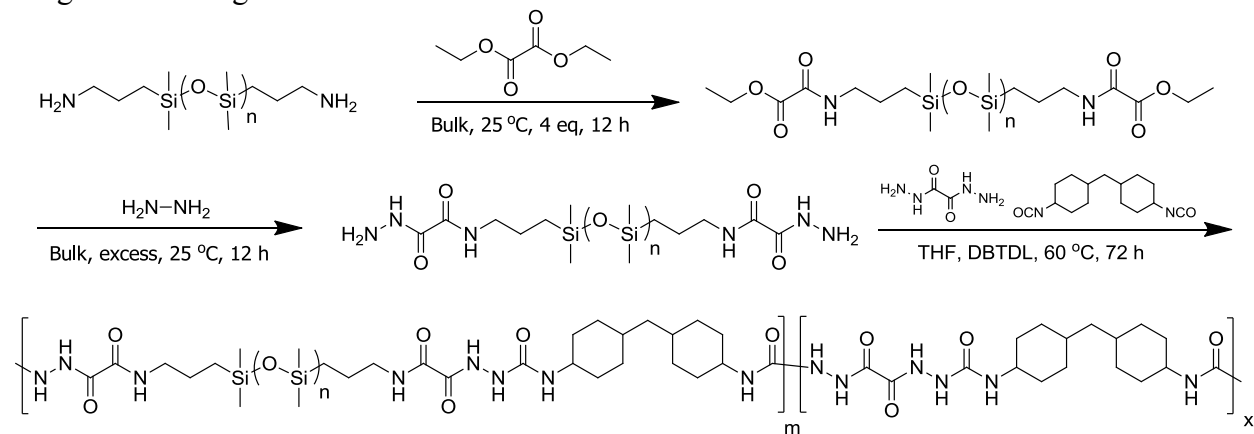
4.4.2 Polymerization Kinetics of 2K PDMS Poly(urea oxamide)

Investigations into the kinetics associated with this new family of segmented copolymers, based on novel polymerization chemistry, is essential in the fundamental understanding of the PUOx containing copolymers. *In situ* FTIR was utilized to monitor the polymerization of PDMS2K-UOx through the disappearance of the HMDI isocyanate stretching band, from 2200 – 2300 cm^{-1}, as the polymerization proceeded. PDMS2K-UOx polymerization was the best choice

for a kinetic study due to the highest wt% HS content, compared to the other copolymers in this study, to provide the strongest isocyanate signal. HMDI concentrations were calculated using the Beer-Lambert equation and the absorbance of the isocyanate stretching band at each time point, which is reported to be accurate at HMDI concentration below 0.4 M.[1] A simple second order kinetic treatment of the data was used due to the equivalent molar ratios used in the polymerization, similar to previously reported urethane kinetic studies.[2,3] Using the integrated rate law seen below (equation 1), a plot of 1/[HMDI] versus polymerization time yielded a rate constant that appeared to change as the polymerization proceeded (Figure 4.2). A rapid consumption of HMDI in the first two minutes of the polymerization corresponds to a rate

$$\frac{1}{[HMDI]_t} = \frac{1}{[HMDI]_o} + kt \quad \text{Equation 1}$$

Constant, k_1, of 0.058 M^{-1} sec^{-1}. The second observed rate constant, k_2, drops to 0.003 M^{-1} sec^{-1} for 1.7 hours into the polymerization and falls further to 0.001 M^{-1} sec^{-1} (k_3) for the duration of the polymerization. The FTIR data suggests high conversion after 6 hours under the reported conditions with the rate constant reaching 0. Ideally the rate constant should not change for
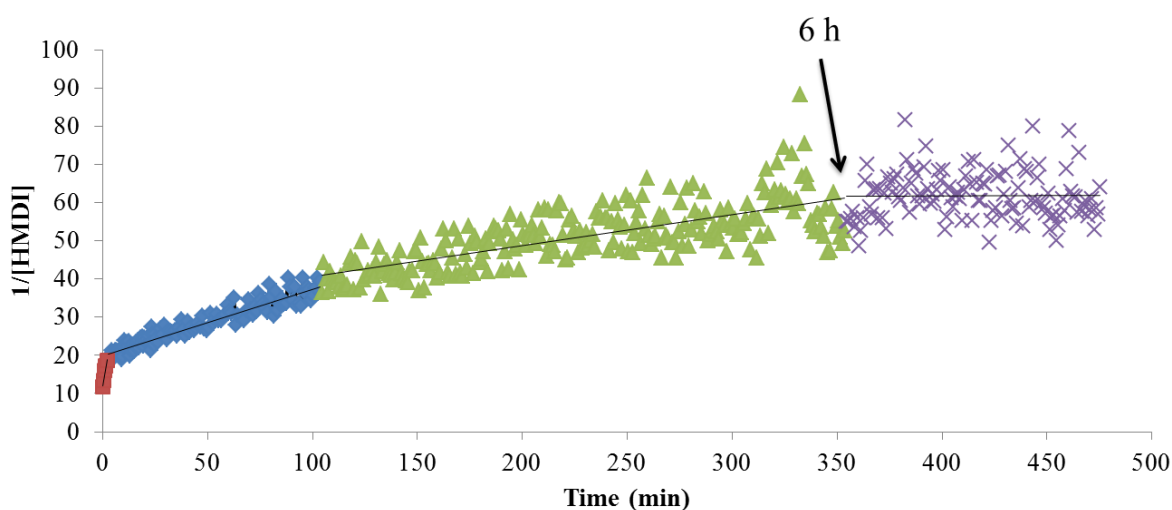
Figure 4.2. Consumption of HMDI as a function of time for the polymerization of PDMS2K-UOx segmented copolymer following 2nd order kinetics

85

the duration of polymerization with the rate only being affected by the concentration of reactive species, but other factors are influencing the reaction to give the observed change in rate constant. As mentioned earlier, the reaction begins as a cloudy mixture in THF and as the polymerization continues the reaction mixture clears up with a corresponding increase in viscosity. This indicates not all the reactive oligomer species are fully solvated and gradually dissolve as the reaction proceeds and is likely the reason for the apparent change in the rate constant as the polymerization proceeds.

A second polymerization of PDMS2K-UOx, with small aliquots taken from the reaction mixture over the duration of the polymerization, provides MW as a function of time utilizing THF SEC (Figure 4.3). Aliquots were obtained every 30 minutes for the first 2.5 hours then every hour for the duration and immediately quenched with wet THF and fully dissolved. After sitting for a short period of time, the THF was evaporated off under a stream of air until a solid
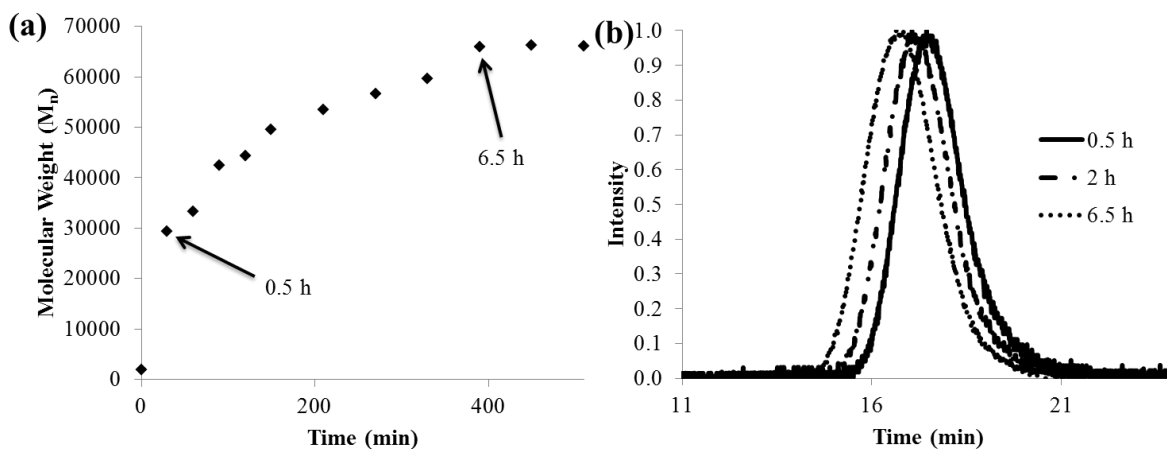
Figure 4.3. Polymerization molecular weight growth for PDMS2K-UOx copolymers (a) with time and (b) THF SEC 90° MALLS traces at 0.5, 2, and 6.5 h

polymer film was obtained. Each solid polymer film was dissolved in the THF used for SEC analysis at 2 mg/mL and injected to give the M_n at each given time point. As seen in Figure 4.3 a

M_n of just under 30 kg/mol was measured after 30 min and gradually increased to a final M_n of 66 kg/mol (M_n), which can also be observed by the shift of the monomodal light scattering trace to higher MW. The measured MW leveled off at 6.5 hours with the previous aliquot taken at 5.5 hours. MW with respect to polymerization time correlates very well with the *in situ* FTIR kinetics experiment and also suggests high conversion is reached after approximately 6 hours.

4.4.3 Effects of Annealing on Copolymer Thermomechanical Properties

An annealing study conducted on the PDMS2K-UOx segmented copolymer provided understanding into the effects annealing time and temperature has on the mechanical properties of PDMS-UOx containing copolymers. In an attempt to reduce as many variables in this study as possible, pieces of a single PDMS2K-UOx copolymer film were taken and annealed at 80, 100, 120, and 160 ˚C for 8 or 24 hours to determine what effect the annealing process has on the dynamic mechanical behavior of the copolymer. A temperature range was chosen based on the initial softening transition at 100 ˚C and the flow temperature. The dynamic mechanical behavior before and after annealing (Figure 4.4) indicated the ideal annealing temperature for the PDMS2K-PUOx was 100 ˚C. The non-annealed film showed a shorter rubbery plateau with no indication of the initial softening transition which suggested a lack of hard segment association or ordering when compared to the annealed samples. After annealing at 80 ˚C for 24 hours the presence of the initial transition appear along with an increase in the rubbery plateau and flow temperature. At 100 ˚C for 24 hours, the initial transition is fully apparent with another increase in the flow temperature and the DMA trace does not change at all when increased to 120 ˚C for 24 hours with little change also observed at 160 ˚C. The results indicate that annealing above the initial transition was required to fully form the physical crosslinks between the hard segment, which maximized phase separation and the resulting mechanical properties.
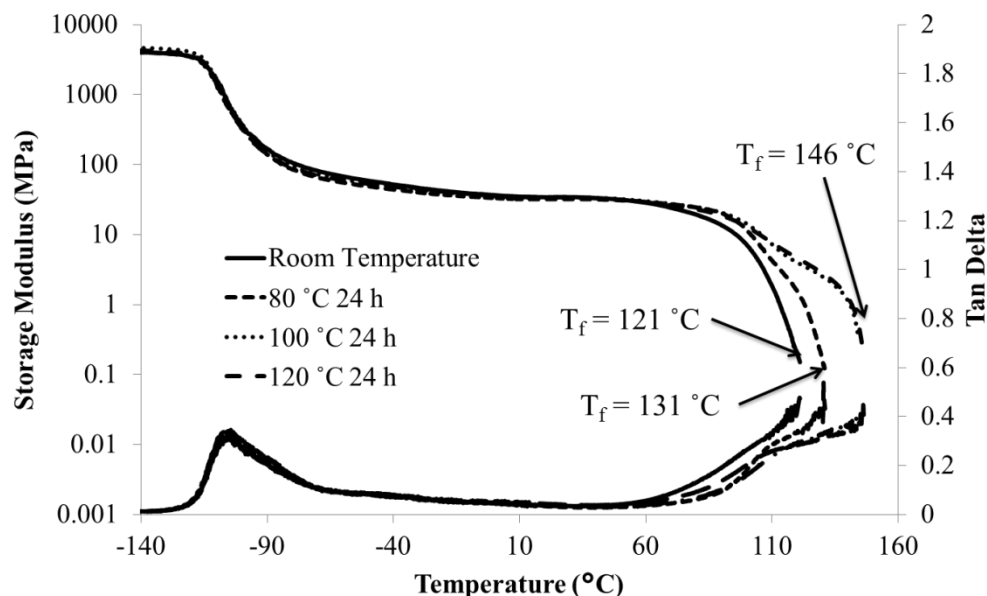
Figure 4.4. Effect of 24 h annealing temperature on the dynamic mechanical behavior of PDMS2K-UOx copolymers

4.4.4 Thermal Properties

Thermal gravimetric analysis (TGA) of the segmented PDMS-U and PDMS-UOx copolymers demonstrated lack of weight loss to 300 °C under a nitrogen purge with the temperature values at 5% weight loss reported in Table 1. PU copolymers exhibited a two-step degradation process with the first and second mass loss corresponding to PU HS and PDMS SS degradation, respectively. The temperatures and thermal degradation profiles corresponded well with previously published PU degradation studies.[33] Degradation of the PDMS-UOx copolymers also showed a two-step degradation profile, but the onset of initial loss in mass resided at a higher temperature (Figure 4.5). This observation was true for all PDMS-UOx copolymers except PDMS2K-UOx, which was equivalent to the PDMS2K-U.

Differential scanning calorimetry (DSC) measured the thermal transitions associated with variations in copolymer structure for each segmented PDMS-U and PDMS-UOx copolymer.
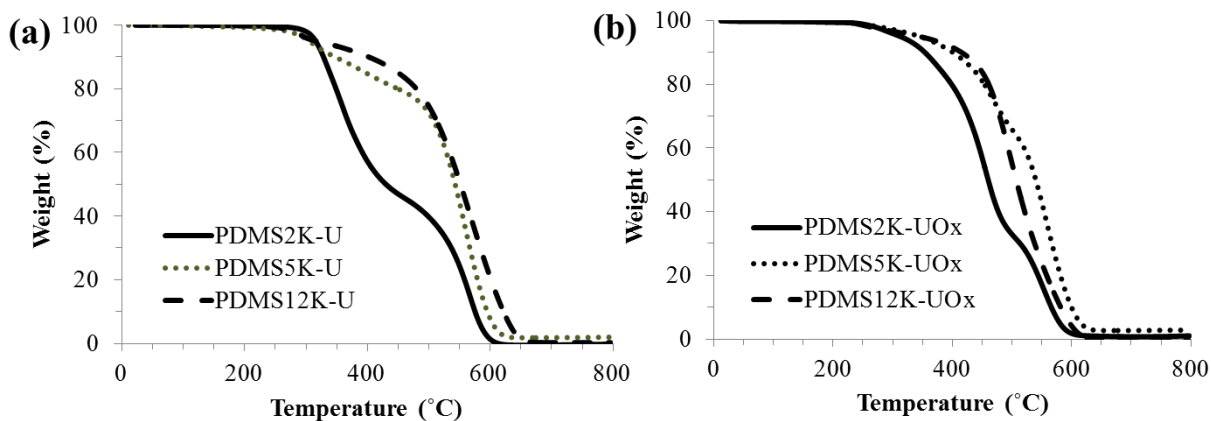
Figure 4.5. TGA degradation curves for (a) PDMS-U and (b) PDMS-UOx segmented copolymers

However, the only observed transitions were the glass transition temperatures (T_g) of the SS for each copolymer and melting of the crystalline PDMS SS for PDMS12K-U and PDMS12K-UOx. T_g values observed for copolymers with SS compositions of PDMS2K and PDMS5K/12K were -117 and -123 ˚C respectively. All copolymers did not exhibit an endothermic transition, which suggested the presence of amorphous HS domains. WAXD analysis verified the absence of any crystalline regions associated with the packing of the hard segment domains for both the 2K and 5K PDMS-UOx and PDMS-U copolymers (Figure 4.6). As expected, WAXD revealed only broad amorphous peaks without any indication of crystallinity. The reason for the lack of crystallinity in the HS was a consequence of the non-aromatic HMDI used for polymerization, which contains a mixture of the cis and trans isomers associated with the cyclohexyl rings. Future work associated with PDMS-UOx copolymers will include studying the effects of an aromatic isocyanate, such as MDI, which may provide crystallinity to the HS as observed with earlier PU compositions.[34]
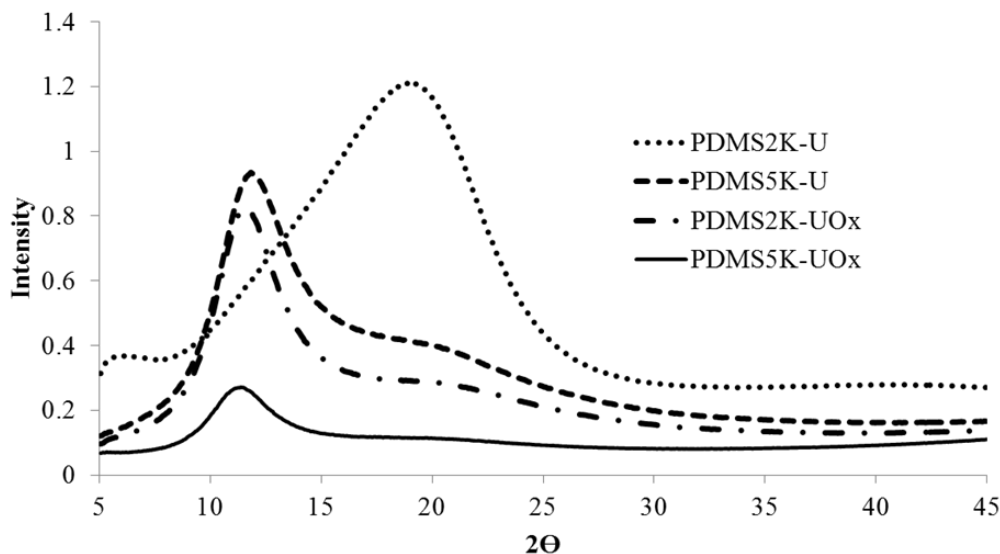
Figure 4.6. WAXD plot for PDMS-U and UOx segmented copolymers

4.4.5 Variable Temperature FTIR

Variable temperature FTIR spectroscopy probed the hydrogen bonding characteristics of the urea and UOx HSs. The broadness of each band represented a diverse population of hydrogen bonding groups that varied in strength. PDMS-UOx copolymers demonstrated similar trends in the peak broadening with an increase in temperature, and also exhibited a complex, broad carbonyl vibrational band residing at 1660 cm^{-1} (Figure 4.7). The broad carbonyl band contained the hydrogen bonding bands for both the urea and oxamide groups. As the temperature increased to 190 ˚C, the broad carbonyl peak shifted to a higher wavenumber of ~1678 cm^{-1} with significant broadening, suggesting the presence of weaker hydrogen bonding, free carbonyl groups, or a combination. The N-H stretch appeared as a single broad peak at 3310 cm^{-1}, which broadened further as temperature increased.

Segmented PU copolymers showed typical urea stretching bands in the N-H and carbonyl spectral regions where the distance and geometry between the hydrogen bonding donor and acceptors strongly influence the vibrational frequency associated with these stretches.[35-37] At 30
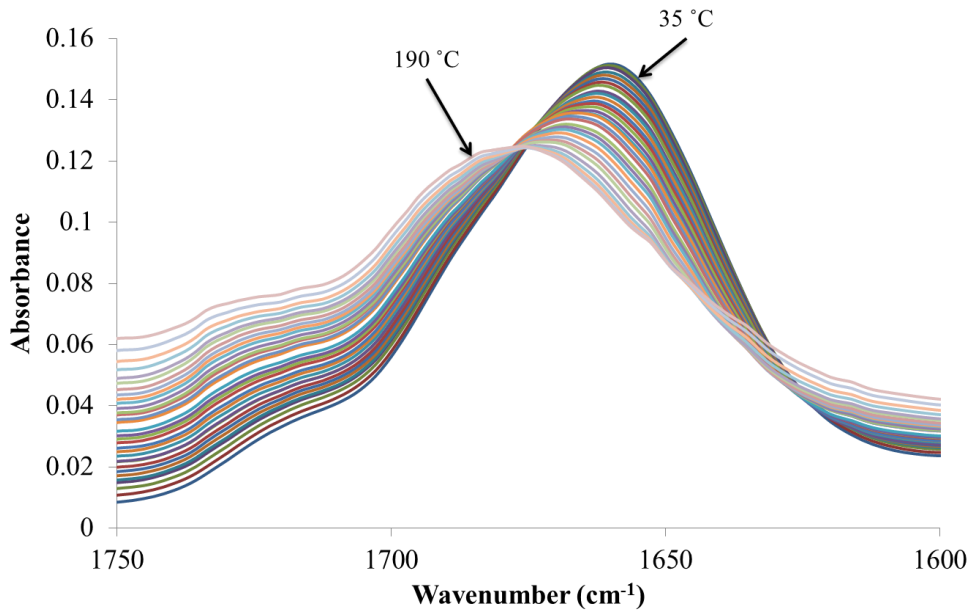
Figure 4.7. Variable temperature FT-IR in the carbonyl region of PDMS2K-UOx copolymer from 35 – 195 ˚C

˚C, the carbonyl vibrational band appeared at ~1630 cm^{-1} and as the temperature increased, the band shifted to 1645 cm^{-1} with significant broadening (Figure 4.8). Small bands also appeared at
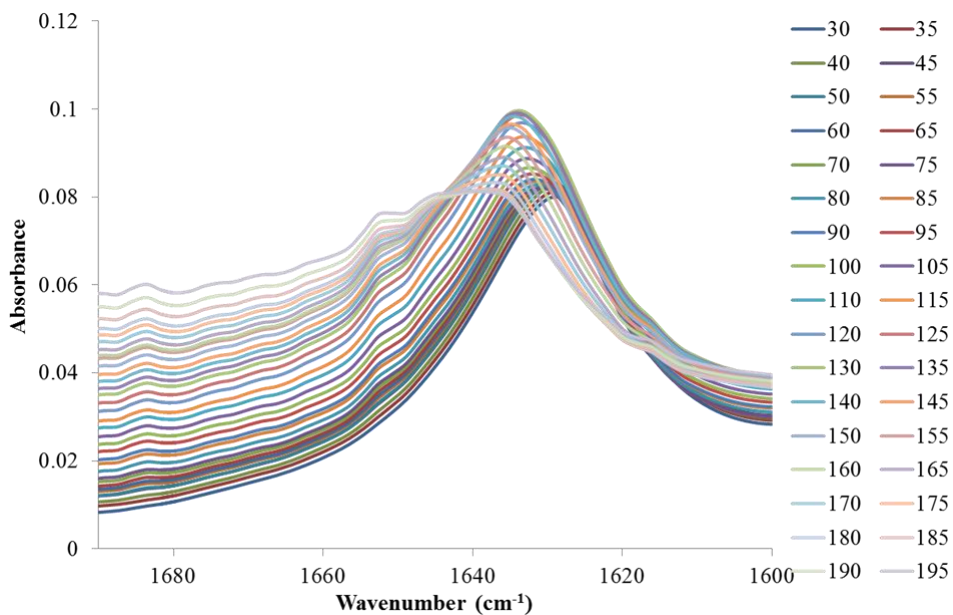
Figure 4.8. Variable temperature FTIR spectroscopy for PDMS2K-U from 30 to 195 ˚C

1650 cm^{-1} and 1684 cm^{-1}, corresponding to weaker hydrogen bonding and free urea groups, respectively. The PU N-H vibrational band occurred as a broad peak at 3320 cm^{-1} indicative of hydrogen bonding with further broadening as the temperature increased. This shift and broadening indicated an increased population of weaker hydrogen bonding as the temperature increased and agreed well with reported literature.[38,39]

4.4.6 Dynamic Mechanical Analysis

DMA of annealed segmented PDMS-U and PDMS-UOx copolymers suggested a significant impact of increased hydrogen bonding for PDMS-UOx copolymers compared to PU analogs. The increase in HS hydrogen bonding leads to a dramatic lengthening of the temperature insensitive rubbery plateau for each PDMS-UOx copolymer, when compared to the respective PU analog. Each segmented PDMS-U copolymer exhibited dynamic mechanical behavior consistent with previous reports of non-chain extended PDMS PU.[40] Tan delta curves provided T_g values for the PDMS2K, 5K, and 12K PU copolymers of -103, -114, and -115 ˚C, respectively, which were slightly higher than DSC values due to a frequency dependence between the two instruments.[41] Each PDMS PU copolymer exhibited a temperature insensitive plateau region with the PDMS5K-U having the longest, ranging from -76 ˚C to 26 ˚C. PDMS2K-U and PDMS12K-U demonstrated similar plateau lengths with varying temperature ranges. Crystallization of the SS in PDMS12K-U copolymer limited the plateau region due to melting of the semi-crystalline SS at -40 ˚C. Higher wt% HS led to higher storage moduli, ranging from 42 MPa for the PDMS2K-U to 1 MPa for the PDMS12K-U copolymers. The softening transition that appeared for each PU near 50 ˚C showed an increased drop in moduli with an increase in HS wt%, which suggested the extent of moduli loss was a function of HS wt%. The initial softening transitions for other urea- and urethane-containing segmented copolymers,[42-45] coupled with the

HS T_g in certain cases, was dependent on HS structure and annealing processes. Previous reports suggested this transition involved a dynamic rearrangement of the hydrogen bonds within the hard segment that leads to softening.[32] Variable temperature FTIR spectroscopy data also indicated a change to less ordered hydrogen bonding and non-bonding interactions in the HS. These changes will lead to a drop in storage modulus. The lack of a HS T_g in the non-chain extended PDMS-U and PDMS-UOx segmented copolymers further supported the role of hydrogen bonding on the initial softening behavior.

The dynamic mechanical behavior of PDMS-UOx copolymers, as indicated previously, showed a large increase in the rubbery plateau compared to the corresponding PDMS-U copolymers. PDMS2K-UOx exhibited a temperature insensitive plateau of 127 °C from -54 to 73 °C with a similar rubbery plateau modulus compared to PDMS2K-U; however, in contrast, the rubbery plateau extended 36 °C longer. DMA traces of PDMS5K-U and PDMS5K-UOx copolymers showed a dramatic increase in the length of the rubbery plateau with the oxamide containing HS (Figure 4.9). The PDMS5K-UOx rubbery region ranged from -92 °C to 75 °C at
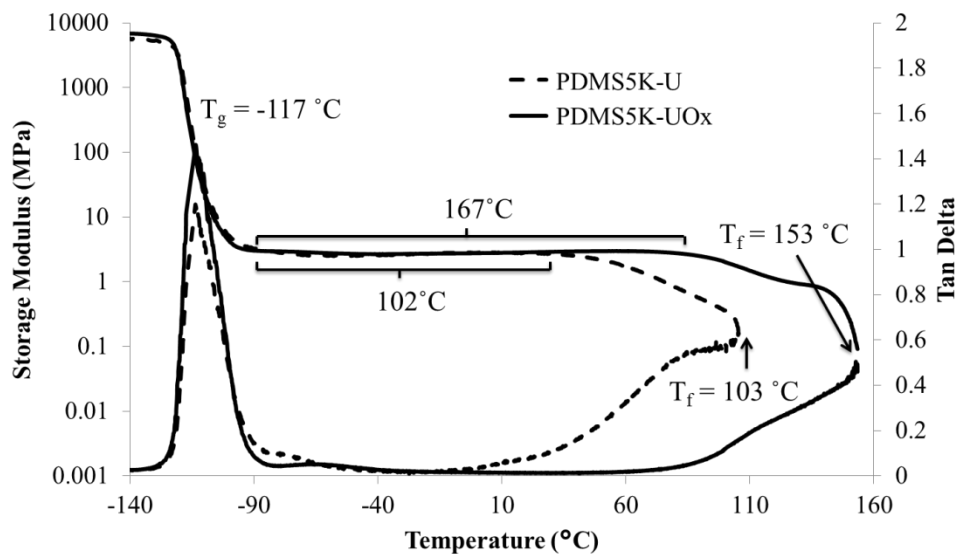
Figure 4.9. Dynamic mechanical analysis of PDMS5K-U and PDMS5K-UOx copolymers

approximately 3 MPa, despite the increase in HS wt%. This corresponded to an increased service

window of 65 °C compared to the PDMS5K-U analog. PDMS12K-U and UOx copolymers

showed a limited rubbery plateau, due to the crystallization and melting of the PDMS SS

beginning at -31 °C and extended to 36 and 155 °C for the PDMS12K-U and PDMS12K-UOx,

respectively. This 119 °C increase in the plateau region was significant and demonstrated a slight

modification to the HS structure will have a large impact on the thermomechanical properties.

Figure 4.10 shows increasing the wt% HS in the PDMS-UOx copolymers follows the same trend
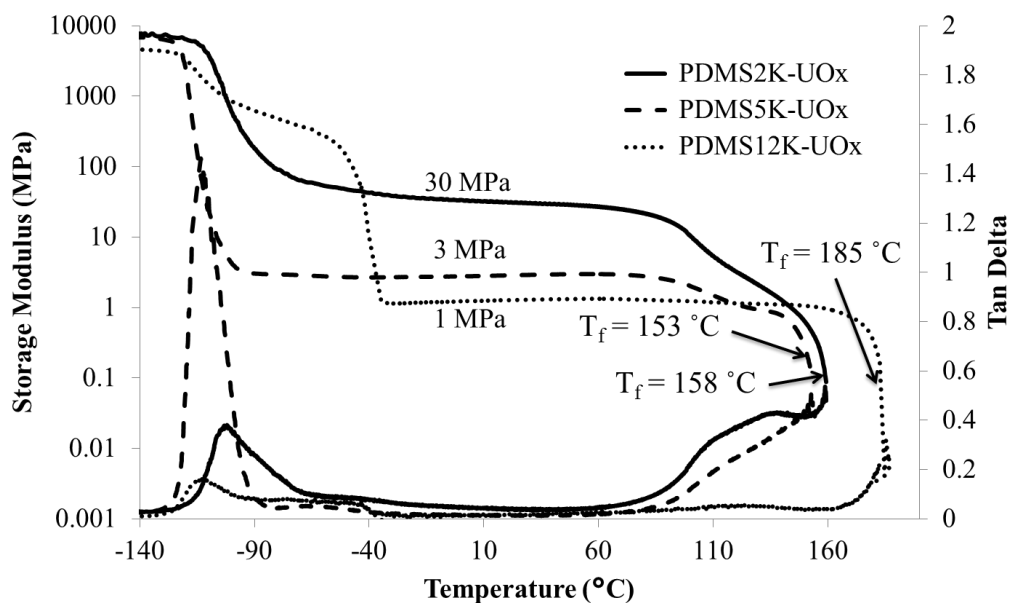
Figure 4.10. Storage and lost modulus of PDMS-UOx segmented copolymers with increased soft segment molecular weight

as the PU analogs with an increase in the rubbery plateau storage modulus from 1 MPa to 30

MPa. The thermomechanical data clearly indicated that the increased hydrogen bonding of the

UOx HS shifts the initial softening transition to a higher temperature, which gives rise to a

longer rubbery plateau range. Increasing the wt% hard segment content of the PDMS5K-UOx

copolymer, using oxalic dihydrazide as a chain extender, slightly increased the plateau length

and T_f, but did not impart significant differences to the thermomechanical properties (Figure 4.11).
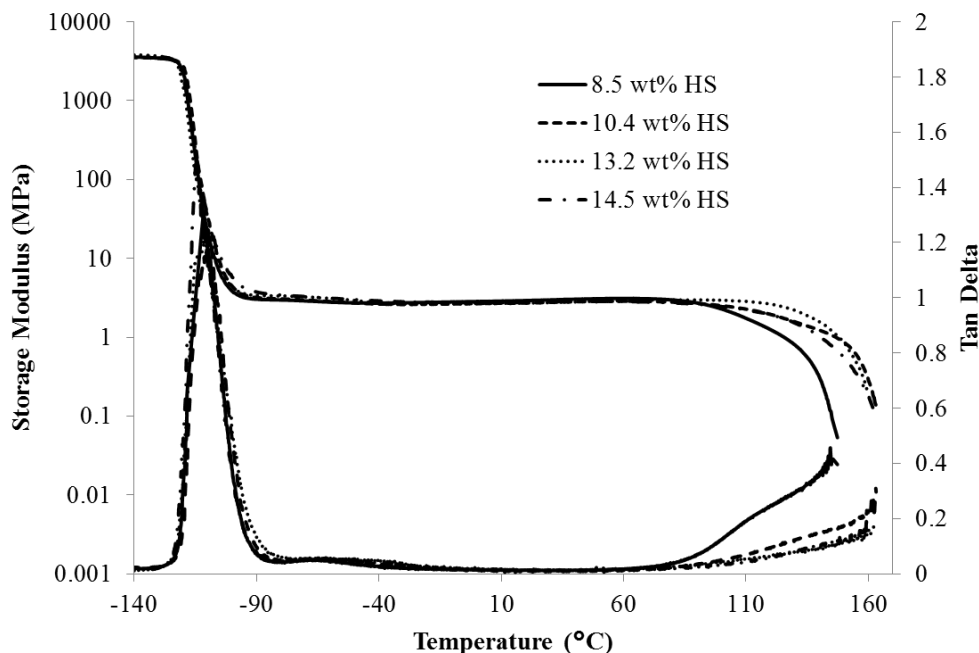
Figure 4.11. DMA of PDMS5K-UOx segmented copolymers with increasing wt% HS content from 8.5 to 174.5 %

4.4.7 Small Angle X-ray Scattering Analysis

DMA of PDMS-UOx segmented copolymers indicated a high degree of phase separation, affording enhanced mechanical properties compared to the non-chain extended PDMS-U analogs. SAXS was essential for verification of the increased microphase separated morphology and provided understanding into the morphological changes that resulted due to the presence of oxamide groups in the hard segment. SAXS profiles of the PDMS-UOx and PDMS-U copolymers both show a clear phase separation at the q range from 0.98 to 2.0 nm^{-1}, and q shifts to lower values as the PDMS MW increases, indicating an increase in inter-domain spacing with an increase in HS length (Figure 4.12). For PDMS-UOx copolymers, a large increase in the intensity as well as the sharpness of this phase separation peak was observed, which confirmed

the enhanced microphase separated morphology. This data confirmed the presence of a highly

microphase separated morphology and fully corroborated the DMA data.
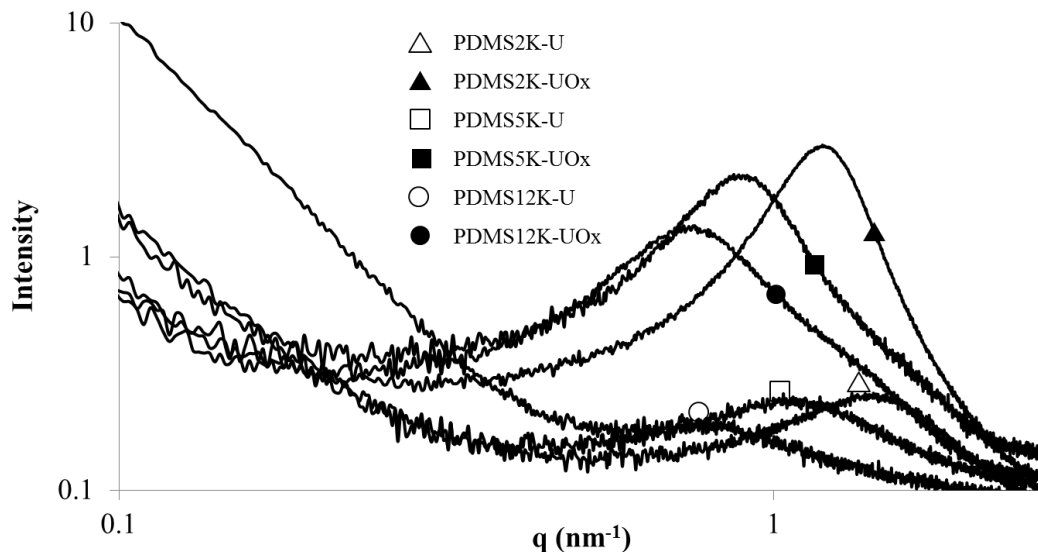
Figure 4.12. SAXS intensity plots for PDMS-U and UOx copolymers varying in hard segment content as well as soft segment molecular weight

Variable temperature SAXS (VT-SAXS) was performed to probe the temperature at

where the ordered phase-separated morphology transitioned to a disordered (phase-mixed)

morphology for PDMS2K-UOx and PDMS2K-U copolymers. Figure 4.13 depicts the 3D VT-
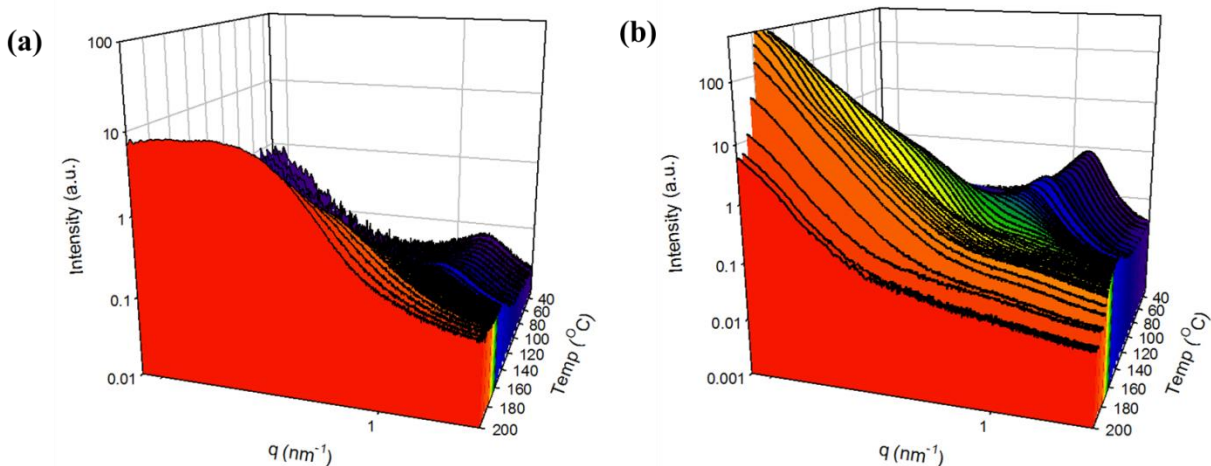
Figure 4.13. Variable temperature SAXS 3D intensity plots from 30 – 200 ˚C for (a) PDMS2K-U and (b) PDMS2K-UOx

SAXS intensity profiles for both segmented copolymers. At temperatures below 150 °C, the scattering peak persisted, indicating a stable phase-separated morphology. Above 150 °C, an abrupt change in the morphology was observed for both copolymers. To further evaluate the morphological transition, the position of the scattering peak (q_{max}) was plotted as a function of temperature (Figure 4.14). For both polymers, q_{max} remained constant up to ~155 °C. When temperatures passed 155 °C, a much sharper change in the slope was observed for PDMS2K-
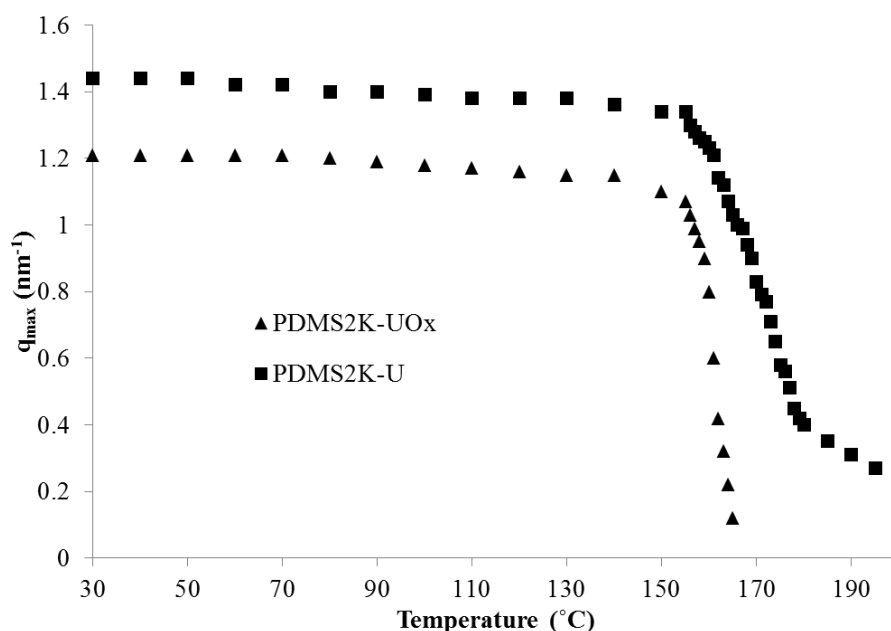
Figure 4.14. q_{max} as a function of temperature for PDMS2K-U and PDMS2K-UOx segmented copolymers

UOx, which indicated the more ordered microphase separated morphology resulted in a sharper morphological transition. The onset of flow for each copolymer, observed with DMA and melt rheology (Figure 4.15), occurred within the order-disorder transition temperature range observed in the VT-SAXS experiments. Initial melt rheology experiments for PDMS-UOx copolymers indicated a crosslinking mechanism or change in HS chemistry occurred at temperatures above 190 ˚C, which requires further analysis to fully understand.
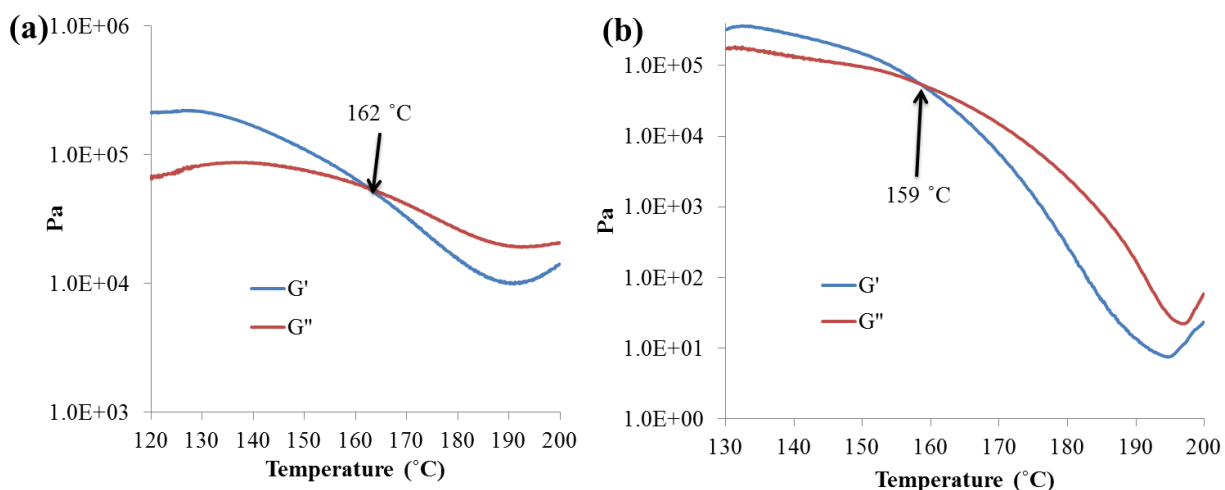
Figure 4.15. Melt rheology temperature sweep of (a) PDMS2K-U and (b) PDMS2K-UOx copolymers

4.4.8 Atomic Force Microscopy

AFM of PDMS5K-U and PDMS5K-UOx copolymers revealed microphase separated surface morphologies consisting of small dark regions corresponding to the PDMS soft phase and lighter HS domains (Figure 4.16). The phase image of PDMS5K-UOx showed similar microphase separated morphology as PDMS5K-U, but the hard and soft domains were better
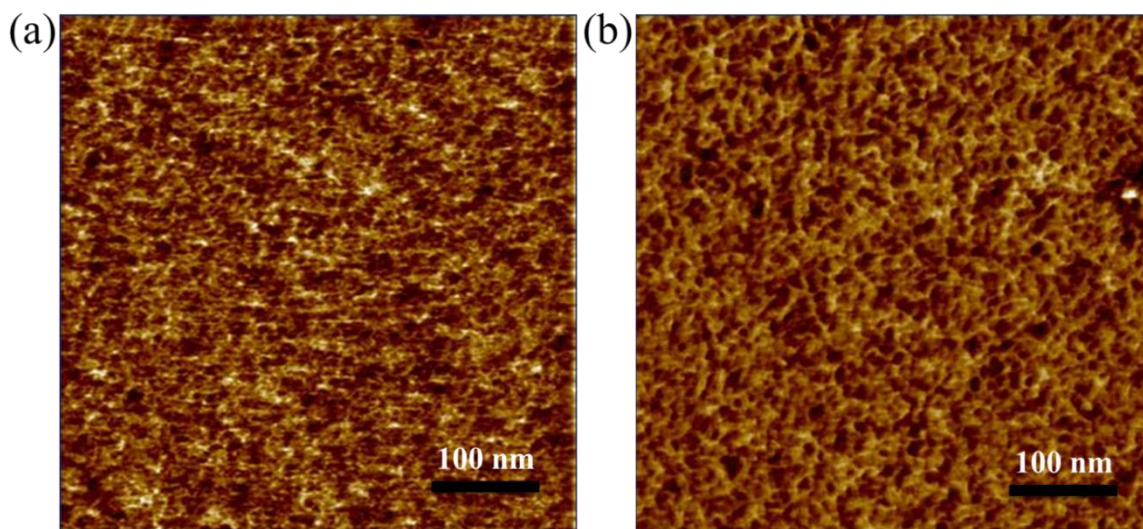
Figure 4.16. AFM phase images of (a) PDMS5K-U and (b) PDMS5K-UOx

defined as a consequence of increased hydrogen bonding with the spacing of the HS domains. This observation was consistent with the observed SAXS data. Unfortunately, transmission electron microscopy (TEM) analysis of PDMS-U and PDMS-UOx copolymers did not provide reliable images. Earlier reports on non-chain extended PDMS-PU segmented copolymers also failed to obtain TEM, presumably due to the small interdomain distances relative to the sample thickness typically needed for TEM.[20]

4.4.9 Tensile Analysis

Tensile analysis for each PDMS-U and PDMS-UOx copolymer revealed typical TPE behavior with values reported as an average of five independent experiments. Comparing the PDMS-UOx copolymers to PU analogs showed a similar trend between all copolymers wherein the PDMS-UOx copolymers displayed higher stress at break and Young's modulus values with a decrease in strain at break. For example, the stress at break slightly increased from 11.9 ± 0.9 to 13.6 ± 1.1 MPa with a corresponding increase in Young's modulus from 27.2 ± 0.5 to 29.8 ± 1.6 MPa for the PDMS2K-U and PDMS2K-UOx, respectively. Both the PDMS5K and PDMS12K copolymers exhibited this trend of increasing stress at break and Young's modulus when comparing PDMS-UOx copolymers to PU analogs. However, the strain at break decreased for the PDMS-UOx copolymers compared to PUs. The increase in HS wt% content, from oxamide units in the HS, resulted in the increased stress at break and Young's modulus of the PDMS-UOx copolymers. As expected, when comparing the PDMS-UOx copolymers, the highest wt% HS demonstrated the higher stress at break and Young's Modulus as seen in Figure 4.17a for the PDMS-UOx copolymers. Chain-extended PDMS5K-UOx copolymers with increasing wt% HS also displayed a similar trend (Figure 4.17b). From 8.5 to 14.5 wt% HS, the stress at break increased from 4.4 ± 0.3 to 6.3 ± 0.8 MPa and the Young's modulus increased from 3.2 ± 0.2 to

4.5 ± 0.4 MPa, respectively. These results demonstrated that varying HS wt% allows for the tunability of tensile properties, either through SS molecular weight or use of a chain extender.
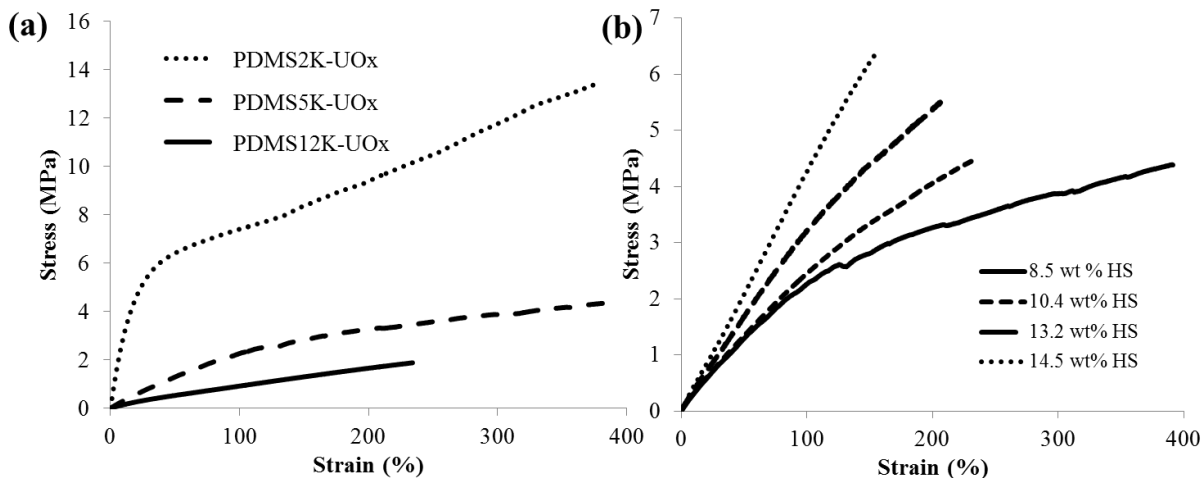
Figure 4.17. Tensile analysis of (a) PDMS-UOx copolymers with increasing soft segment molecular weight and (b) chain-extended PDMS5K-UOx segmented copolymers with increasing weight percent hard segment content

PDMS segmented copolymers subjected to 100% strain over five consecutive cycles yielded hysteresis profiles showing a reduction in the % hysteresis for each PDMS-UOx copolymer compared to the PU control. Table 4.2 reports the hysteresis values for each copolymer over 5 cycles at 100% strain. When comparing PDMS12K-UOx and the PU analog, a decrease was shown in the first cycle hysteresis, from 37% to 9%, for PDMS12K-U and PDMS12K-UOx, respectively (Figure 4.18). Due to the increase in microphase separated morphology, and stronger hydrogen bonding interactions between the HS, it was expected that more energy was required to rupture or deform the microphase separated physical network of PDMS-UOx copolymers, which may explain the large reduction in hysteresis values. The decrease in hysteresis was also more significant with higher PDMS molecular weight. Comparing copolymers with the same HS and higher weight fraction of flexible PDMS showed that hysteresis reduction is also a function of HS wt%, an observation previously reported.[46]

Table 4.2. Percent hysteresis values for segmented PDMS-U and PDMS-UOx copolymers over five cycles at 100% strain

Cycles	1	2	3	4	5
PDMS2K-U	80	66	64	62	62
PDMS2K-UOx	73	54	51	49	48
PDMS5K-U	60	53	52	51	50
PDMS5K-UOx	34	14	13	12	6
PDMS12K-U	37	33	32	31	31
PDMS12K-UOx	9	3	3	3	3
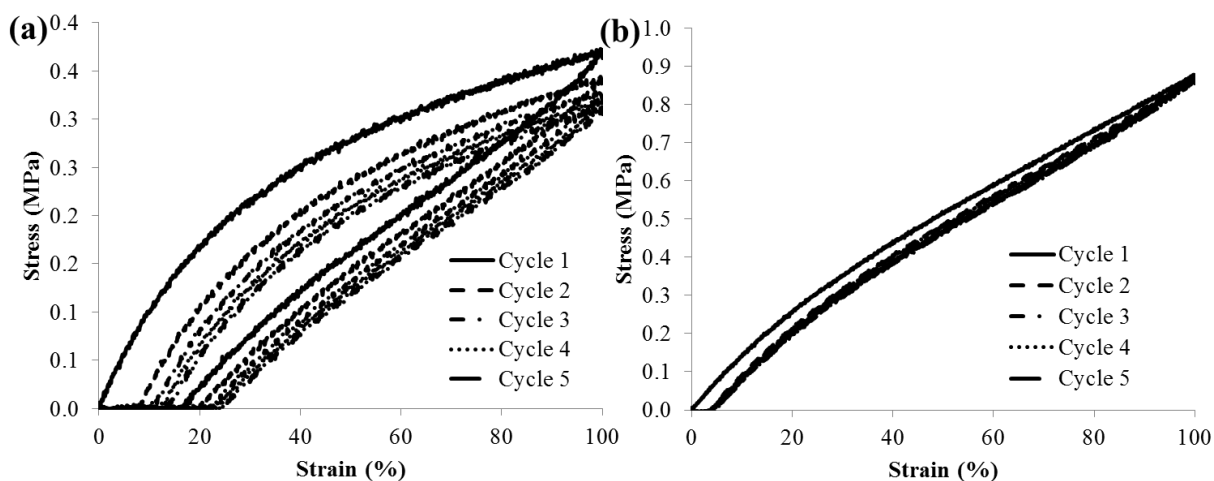
Figure 4.18. Five cycle hysteresis profiles of (a) PDMS12K-U and (b) PDMS12K-UOx at 100% strain

4.5 Conclusions

Successful synthesis of a new family of segmented copolymers composed of a PDMS SS and UOx hard segment yielded copolymers with microphase separated morphologies that lead to improved thermomechanical properties. The PDMS-UOx synthetic pathway resulted in high molecular weight copolymers, despite two end-group modifications. SEC studies revealed PDMS-UOx high molecular weight was achieved after 6 h and annealing studies suggested 100 ˚C for 12 h as ideal annealing conditions. Dynamic mechanical behavior of PDMS-UOx copolymers exhibited temperature insensitive rubbery plateaus that extended for 167 and 186 ˚C for PDMS5K-UOx and PDMS12K-UOx respectively. The extended temperature range of the

service window for PDMS-UOx copolymers, up to 119 ˚C compared to the PDMS12K-U analogs, demonstrated the effect of higher HS hydrogen bonding content, which resulting in increased microphase separated morphologies. SAXS analysis confirmed the change in morphology for PDMS-UOx copolymers through a significant increase in the intensity and sharpness of the X-ray scattering peaks. VT-SAXS revealed a sharp morphological transition above 155 ˚C, for both PDMS-U and PDMS-UOx copolymers, toward a phase-mixed morphology that corresponded to the onset of flow observed with DMA and melt rheology. DSC and WAXD confirmed the amorphous character of PDMS-UOx copolymers. AFM phase images of PDMS5K-UOx copolymers provided visual confirmation of the microphase separated morphology. Utilizing oxalic dihydrazide as a chain extender allowed for the tuning of tensile properties through the change in HS wt% copolymer composition. Higher HS wt% content resulted in a higher stress at break and Young's modulus with a corresponding decrease in strain at break. PDMS-UOx copolymers demonstrated improved hysteresis, compared to PU analogs, as a result of higher hydrogen bonding content. PDMS-UOx segmented copolymers exhibited excellent TPE behavior with enhanced thermomechanical properties and ability to tune tensile properties for potential commercial applications.

4.6 Acknowledgments

4.7 References

(1)   Castagna, A. M.; Pangon, A.; Choi, T.; Dillon, G. P.; Runt, J. *Macromolecules* **2012**, *45*, 8438.
(2)   Chakrabarty, S.; Nisenholt, M.; Wynne, K. J. *Macromolecules* **2012**, *45*, 7900.
(3)   Mark, J. E. *Accounts of Chemical Research* **2004**, *37*, 946.
(4)   Yilgor, E.; Yilgor, I. *Polymer* **2001**, *42*, 7953.
(5)   ten Cate, A. T.; Sijbesma, R. P. *Macromolecular Rapid Communications* **2002**, *23*, 1094.
(6)   Wisse, E.; Spiering, A. J. H.; van Leeuwen, E. N. M.; Renken, R. A. E.; Dankers, P. Y. W.; Brouwer, L. A.; van Luyn, M. J. A.; Harmsen, M. C.; Sommerdijk, N.; Meijer, E. W. *Biomacromolecules* **2006**, *7*, 3385.
(7)   Dodge, J.; John Wiley & Sons, Inc.: 2003, p 197.
(8)   Krijgsman, J.; Biemond, G. J. E.; Gaymans, R. J. *Polymer* **2005**, *46*, 8250.
(9)   van der Schuur, M. J.; Gaymans, R. J. *Polymer* **2007**, *48*, 1998.
(10)   Lips, P. A. M.; Broos, R.; van Heeringen, M. J. M.; Dijkstra, P. J.; Feijen, J. *Polymer* **2005**, *46*, 7834.
(11)   Sijbrandi, N. J.; Kimenai, A. J.; Mes, E. P. C.; Broos, R.; Bar, G.; Rosenthal, M.; Odarchenko, Y. I.; Ivanov, D. A.; Jan, F. J.; Dijkstra, P. J. *Polymer* **2012**, *53*, 4033.
(12)   Mecham, J. B.; Wang, F.; Glass, T. E.; Xu, J.; Wilkes, G. L.; McGrath, J. E. *Polymer Material Science and Engineering* **2001**, *84*, 105.
(13)   Xi, K.; Meng, Z.; Heng, L.; Ge, R.; He, H.; Yu, X.; Jia, X. *Journal of Applied Polymer Science* **2009**, *113*, 1633.
(14)   Yilgor, I.; Yilgor, E.; Eberle, J.; Steckle, W. P.; Johnson, B. C.; Tyagi, D.; Wilkes, G. L.; McGrath, J. E. *Abstracts of Papers of the American Chemical Society* **1983**, *185*, 32.
(15)   Gu, X.; Kuang, Y.; Guo, X.; Fang, J.; Ni, Z. *Journal Controlled Release* **2008**, *127*, 267.
(16)   Lu, Q.; Fang, J.; Yang, J.; Yan, G.; Liu, S.; Wang, J. *Journal of Membrane Science* **2013**, *425-426*, 105.
(17)   Francis, C.; Naba, D.; Namita Roy, C.; Anil, B. In *Current Topics in Elastomers Research*; CRC Press: 2008.
(18)   Tyagi, D.; Wilkes, G. L.; Yilgor, I.; McGrath, J. E. *Polymer Bulletin* **1982**, *8*, 543.
(19)   Yilgor, I.; Riffle, J. S.; Wilkes, G. L.; McGrath, J. E. *Polymer Bulletin* **1982**, *8*, 535.
(20)   Yilgor, I.; Yilgor, E. *Polymer Reviews* **2007**, *47*, 487.
(21)   Das, S.; Yilgor, I.; Yilgor, E.; Wilkes, G. L. *Polymer* **2008**, *49*, 174.
(22)   Sheth, J. P.; Klinedinst, D. B.; Wilkes, G. L.; Iskender, Y.; Yilgor, I. *Polymer* **2005**, *46*, 7317.
(23)   Yilgor, E.; Yurtsever, E.; Yilgor, I. *Polymer* **2002**, *43*, 6561.
(24)   Yilgor, E.; Burgaz, E.; Yurtsever, E.; Yilgor, I. *Polymer* **2000**, *41*, 849.
(25)   Versteegen, R. M.; Sijbesma, R. P.; Meijer, E. W. *Macromolecules* **2005**, *38*, 3176.
(26)   Sijbrandi, N. J.; Kimenai, A. J.; Mes, E. P. C.; Broos, R.; Bar, G.; Rosenthal, M.; Odarchenko, Y.; Ivanov, D. A.; Dijkstra, P. J.; Feijen, J. *Macromolecules* **2012**, *45*, 3948.
(27)   Burden, R. L. J. D. F. *Numerical Analysis*; 7th ed.; Brooks/Cole, 2000.
(28)   Liu, J.; Guo, T.-F.; Yang, Y. *Journal of Applied Physics* **2002**, *91*, 1595.
(29)   Shu, Y.-C.; Lin, M.-F.; Tsen, W.-C.; Chuang, F.-S. *Journal of Applied Polymer Science* **2001**, *81*, 3502.
(30)   Takahashi, A.; Kita, R.; Kaibara, M. *Journal of Material Science: Materials in Medicine* **2002**, *13*, 259.
(31)   Van Bogart, J. W. C.; Bluemke, D. A.; Cooper, S. L. *Polymer* **1981**, *22*, 1428.

(32)   Sheth, J. P.; Aneja, A.; Wilkes, G. L.; Yilgor, E.; Atilla, G. E.; Yilgor, I.; Beyer, F. L. *Polymer* **2004**, *45*, 6919.

(33)   Awad, W. H.; Wilkie, C. A. *Polymer* **2010**, *51*, 2277.

(34)   Das, S.; Yilgor, I.; Yilgor, E.; Inci, B.; Tezgel, O.; Beyer, F. L.; Wilkes, G. L. *Polymer* **2007**, *48*, 290.

(35)   Coleman, M. M.; Lee, K. H.; Skrovanek, D. J.; Painter, P. C. *Macromolecules* **1986**, *19*, 2149.

(36)   Skrovanek, D. J.; Howe, S. E.; Painter, P. C.; Coleman, M. M. *Macromolecules* **1985**, *18*, 1676.

(37)   Skrovanek, D. J.; Painter, P. C.; Coleman, M. M. *Macromolecules* **1986**, *19*, 699.

(38)   Coleman, M. M.; Sobkowiak, M.; Pehlert, G. J.; Painter, P. C.; Iqbal, T. *Macromolecular Chemistry and Physics* **1997**, *198*, 117.

(39)   Versteegen, R. M.; Kleppinger, R.; Sijbesma, R. P.; Meijer, E. W. *Macromolecules* **2006**, *39*, 772.

(40)   Yilgor, I.; Shaaban, A. K.; Steckle, W. P.; Tyagi, D.; Wilkes, G. L.; McGrath, J. E. *Polymer* **1984**, *25*, 1800.

(41)   Tyagi, D.; Yilgor, I.; McGrath, J. E.; Wilkes, G. L. *Polymer* **1984**, *25*, 1807.

(42)   Klinedinst, D. B.; Yilgör, E.; Yilgör, I.; Beyer, F. L.; Wilkes, G. L. *Polymer* **2005**, *46*, 10191.

(43)   Pukánszky Jr, B.; Bagdi, K.; Tóvölgyi, Z.; Varga, J.; Botz, L.; Hudak, S.; Dóczi, T.; Pukánszky, B. *European Polymer Journal* **2008**, *44*, 2431.

(44)   Sheth, J. P.; Yilgor, E.; Erenturk, B.; Ozhalici, H.; Yilgor, I.; Wilkes, G. L. *Polymer* **2005**, *46*, 8185.

(45)   Tyagi, D.; McGrath, J. E.; Wilkes, G. L. *Polymer Engineering and Science* **1986**, *26*, 1371.

(46)   Yilgor, I.; Eynur, T.; Bilgin, S.; Yilgor, E.; Wilkes, G. L. *Polymer* **2011**, *52*, 266.

Chapter 5: Synthesis and Characterization of Poly(ether oxamide) and Poly(ether trioxamide) Segmented Copolymers

(From: Buckwalter, D. J.; Hudson, A. G.; Moore, R. B.; Long, T. E. *Submission in Progress*)

5.1 Abstract

This report describes the synthesis and characterization of unique non-chain extended poly(propylene glycol) (PPG) polytrioxamide (TriOx) and poly(urea oxamide) (UOx) segmented copolymers containing monodisperse hard segments. Synthesis of the segmented copolymers relied on an efficient two-step end-capping sequence, which resulted in novel difunctional oxamic hydrazide terminated polyether oligomers. Polymerization with oxalyl chloride or HMDI provided the desired segmented copolymers displaying thermoplastic elastomeric behavior. Variable temperature FTIR spectroscopy confirmed the presence of HS structures and revealed low energy ordered hydrogen bonding interactions with thermal dissociation profiles similar to polyurea and polyoxamide copolymer analogs. Dynamic mechanical analysis of PPG-UOx exhibited a longer, rubbery plateau with increased moduli compared to PPG polyurea, and tensile analysis revealed a dramatic increase in copolymer toughness due to enhanced hydrogen bonding. This manuscript describes a new step-growth polymerization strategy that is capable of producing tunable hydrogen bonding segmented copolymer architectures.

5.2 Introduction

Segmented thermoplastic elastomers (TPE) rely on the presence of microphase separated morphologies to impart desired physical properties including flexibility, elasticity, and melt processability.[1] Segmented copolymers are commonly comprised of a flexible soft segment (SS), such as PDMS or a polyether, and a covalently linked hard segment (HS) that contains sequences

that are incompatible with the SS.[2,3] Examples of commonly used highly polar HS structures include amides,[4-6] urethanes,[7-10] ureas,[11-13] esters,[14-16] and imides.[17-20] The ability of the HS to self-associate and form strong physical crosslinks through non-covalent intermolecular interactions governs the extent of microphase separation and ultimately thermomechanical properties. The dominating intermolecular interaction in amide-, urea-, and urethane-containing HS structures is hydrogen bonding, which drives HS association leading to microphase separated morphologies.[21-23] Each group displays different hydrogen bonding energies, ranging from the strong bidentate hydrogen bonding of ureas (58.5 kJ/mol) to the monodentate bonding of amides (32.5 kJ/mol).[24] HS symmetry also plays an important role in the association of hydrogen bonding groups, especially in segmented copolymers containing a uniform HS, and provides the prerequisite cohesiveness for optimal physical properties.[25] Furthermore, segmented copolymers containing uniform HSs demonstrate improved mechanical properties compared to those with polydisperse HSs.[26-30]

Oxamide units possess excellent hydrogen bonding characteristics[31,32] that are well suited for incorporation into segmented copolymers. However, current literature contains few examples of oxamide-containing segmented copolymers. Only three research groups have provided literature precedent on polyoxamide segmented copolymers, which include the synthesis and characterization of poly(ether oxamide) and poly(dimethylsiloxane oxamide) copolymers. A patent issued in 1978 described Schulze's work on poly(oxypropylene oxamide) segmented copolymers where the investigators end-capped a poly(propylene glycol) (PPG) diamine with diethyl oxalate and subsequently polymerized with a alkyl diamine in the melt.[33] This method yielded elastic to brittle copolymers with a range of melting temperatures dependent on polymer composition. In 2007, Leir et al. published patents describing the synthesis of polyoxamide

silicone elastomers through a similar ethyl oxalate end-capping scheme and polymerized with small alkyl diamines.[34,35] The optically clear, elastomeric films exhibited Shore A hardness values between 14 and 88 depending on polymer composition. The researchers also reported that polyoxamide PDMS elastomers were effective thermoplastic adhesives. More recently, Sijbrandi et al. published a very detailed study on poly(tetramethylene oxide) (PTMO) segmented copolymers containing uniform oxamide-based HS.[36] PTMO polyoxamide copolymers provided TPEs with good thermal and mechanical properties for copolymers containing two or three oxamide groups in the HS. Varying the methylene spacing between oxamide groups in the hard segment altered the mechanical properties and increased melting temperatures from 140 to 200 ˚C. Morphological studies confirmed highly microphase-separated morphologies with fiber-like nanocrystals dispersed throughout the PTMO matrix. Also, a similar study of poly(ether ester oxamide) copolymers utilizing a glycine or β-alanine containing monomer revealed TPE-like behavior with properties comparable to poly(ether oxamide) segmented copolymers.[37] These limited examples of oxamide-containing segmented copolymers demonstrate the utility and versatility of oxamide hydrogen bonding groups for segmented copolymers.

In this current study, a new polymerization chemistry based on oxamic hydrazide terminated PPG SSs afforded novel, strong hydrogen bonding HS structures. Comparisons between two copolymers and structurally similar analogs revealed interesting differences in the physical properties. PPG polytrioxamide (PPG-TriOx) segmented copolymers contain a uniform HS composed of three oxamide groups that provide a strong hydrogen bonding structure containing 12 hydrogen bond donors and acceptors (Figure 5.1). The HS of PPG poly(urea oxamide) (PPG-UOx) copolymers include 4 oxamide and 2 bidentate urea hydrogen bonding groups resulting in strong intermolecular interactions between the uniform HSs. PPG

polyoxamide (PPG-Ox) and PPG polyurea (PPG-U) segmented copolymer analogs provided useful comparisons of the hydrogen bonding interactions and physical properties of PPG-TriOx and PPG-UOx copolymers. Comparisons between the new copolymers and the respective analogs provided insight into the nature of the hydrogen bonding interactions as well as the impact of enhanced hydrogen bonding on mechanical properties. The successful synthesis of both PPG-TriOx and PPG-UOx copolymers also demonstrated the possibility for exciting HS architectures using oxamic hydrazide terminated oligomers for preparation of segmented copolymers.
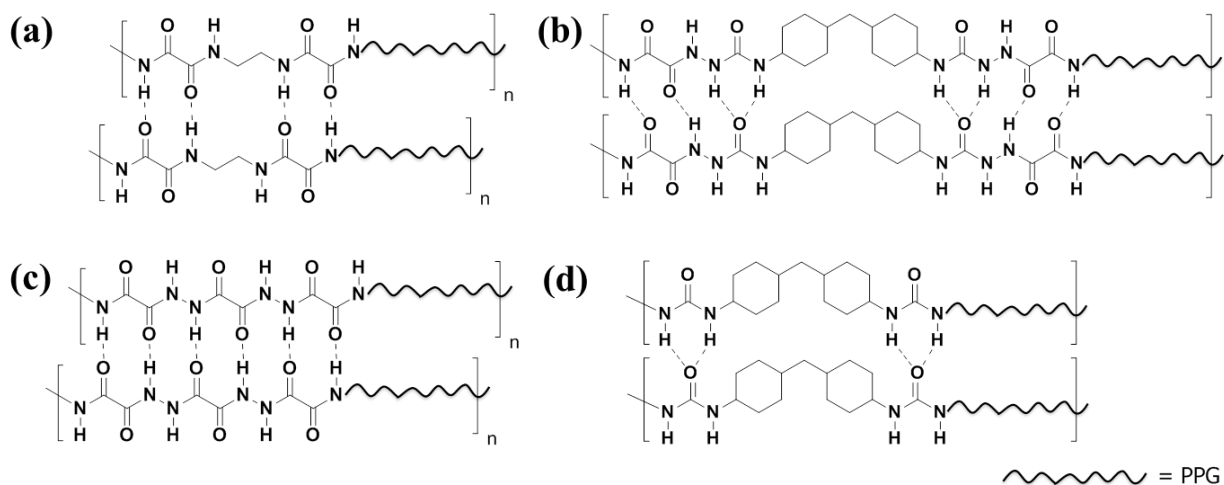
Figure 5.1. Hydrogen bonding interactions of (a) polyoxamide, (b) poly(urea oxamide), (c) polytrioxamide, and (d) polyurea hard segments

5.3 Experimental

5.3.1 Materials

Huntsman graciously donated the Jeffamine® D-2000 (PPG diamine) and all volatiles were removed using heat (80 °C) and high vacuum (0.08 mbar) prior to use. Diethyl oxalate (>99%), anhydrous hydrazine (98%), ethylene diamine (≥99%), and oxalyl chloride (99%) were purchased from Sigma Aldrich and used without further purification. Dibutyltin dilaurate

(DBTDL) (95%) was purchased from Aldrich and a 10 wt% solution in dry THF was prepared. Bayer Material Science kindly provided 4,4'-methylenebis(cyclohexyl isocyanate) (HMDI) and was used without further purification.

5.3.2 Synthesis of PPG Poly(oxamide) Copolymers

PPG diamine (15.12 g, 7.61 mmol, 2,000 g/mol) was cannulated into a dry 100-mL, round-bottomed flask equipped with a stir bar, purged with dry argon, and cooled in an ice bath. A four molar excess of diethyl oxalate (4.45 g, 30.5 mmol) was syringed directly into the reaction flask at 25 °C and left to stir for 12 h. Ethanol and excess diethyl oxalate were removed under high vacuum (0.06 mmHg) at 80 °C until distillate was not observed. Number-average molecular weight of the ethyl oxalate capped PPG oligomer was determined through end-group analysis and ^{1}H NMR spectroscopy. The ethyl ester capped PPG (4.24 g, 1.91 mmol) was added to a dry, 100-mL, flask equipped with a large stir bar and purged with argon. Ethylenediamine (0.114g, 1.91 mmol) was pipetted directly into the reaction mixture and stirred until the polymerization fully solidified. After sitting at room temperature for 24 h, the solid polymer product was dissolved in CHCl$_3$ at 10 wt % solids and cast into a Teflon$^®$ mold then allowed to air dry. The films were then annealed at 80 °C for 8 h under reduced pressure (1 mmHg), prior to mechanical testing.

5.3.3 Synthesis of PPG Poly(trioxamide) Copolymers

PPG diamine (8.77 g, 4.39 mmol, 2,000 g/mol) was cannulated into a 100-mL, round-bottomed flask equipped with a stir bar and purged with argon. Diethyl oxalate (2.56 g, 17.6 mmol) was added directly to the ice bath cooled reaction flask and stirred for 12 h while allowing the reaction to slowly reach ambient temperature. After removal of ethanol and excess diethyl oxalate under vacuum (0.06 mmHg) and heat (80 °C), the number-average molecular

weight was determined through ^{1}H NMR spectroscopy and end-group analysis. The ethyl ester capped PPG (9.7 g, 4.39 mmol) was reacted in the bulk at 25 ˚C with hydrazine (0.42 g, 13.2 mmol) in a 100-mL, round bottomed flask for 12 h. Ethanol and excess hydrazine were removed under high vacuum (0.06 mmHg) at 80 ˚C which yielded a white viscous polymer product. Polymerization was conducted through dissolving the oxamic hydrazide capped PPG (9.48 g, 3.7 mmol) in dry $CHCl_3$ (26.7 mL, 20 wt % solids) in a sealed, 100-mL, round-bottomed flask equipped with a large stir bar. While stirring the PPG hydrazide solution, an equimolar amount of oxalyl chloride (0.47 g, 3.7 mmol) was syringed into the reaction mixture and allowed to react at room temperature while gently purging the generated HCl. After stirring for 12 h, the reaction mixture was poured into a glass dish and allowed to air dry. The polymer film was soaked in distilled water for 8 h to sequester any remaining HCl, then dried under vacuum. The solid polytrioxamide polymer was dissolved in $CHCl_3$ at 10 wt% solids and solution cast into Teflon$^®$ molds. After air drying, the films were annealed at 80 ˚C for 8 h under reduced pressure (1 mmHg).

5.3.4 Synthesis of PPG Poly(urea oxamide) Copolymers

Synthesis of PPG poly(urea oxamide) utilized the same oxamic hydrazide-terminated PPG as in the polytrioxamide synthesis. Polymerization of poly(urea oxamide) was conducted as follows. PPG oxamic hydrazide (8.18 g, 3.15 mmol) was added to a dry, two-necked, flask under an argon purge. The oxamic hydrazide PPG oligomer was dissolved in THF (37 mL, 20 wt% solids) to yield a heterogeneous solution. HMDI (0.83 g, 3.15 mmol) was syringed directly in the reaction mixture and then DBTDL (50 ppm) catalyst in dry THF. The polymerization was placed in a 60 ˚C oil bath and stirred for 48 h, eventually becoming homogeneous. Films were obtained

through solution casting directly from the reaction mixture and air dried overnight. Films were annealed at 80 ˚C for 8 h under reduced pressure (1 mmHg).

5.3.5 Synthesis of PPG Poly(urea) Copolymers

PPG diamine (10.4 g, 5.21 mmol) was added to a dry flask after a thorough argon purge. The PPG diamine was subsequently dissolved in THF (17.6 mL, 40 wt% oligomer) and stirred until fully dissolved. HMDI (1.37 g, 5.21 mmol) was added directly to the reaction mixture then placed in a 60 ˚C oil bath and stirred for 24 h. Polymerization mixtures were cast directly into Teflon® molds and allowed to air dry overnight. Films were annealed at 80 ˚C for 8 h under reduced pressure (1 mmHg).

5.3.6 Analytical Methods

^{1}H NMR spectra of each PPG copolymer was collected in CDCl$_3$ at 27 ˚C using an Advance 500 MHz spectrometer. Molecular weight data was obtained through size exclusion chromatography (SEC) conducted at 30 ˚C in THF (HPLC grade containing 250 ppm BHT). The flow rate was maintained at 1.0 mL/min on a Waters 515 HPLC pump equipped with a Waters 717plus auto sampler, Waters 2414 refractive index detector, and Wyatt Technology miniDawn MALLS detector. An offline dn/dc value measured with a Wyatt Optilab T-rEX differential refractive index detector was used to calculate absolute molecular weights. The hydrodynamic radius of the copolymers in THF were measured on a Malvern Instruments Zetasizer Nano ZS (633 nm) to ensure the absence of polymer aggregation before SEC analysis. The degradation profiles, under a nitrogen purge, were collected on a TA Instruments Hi-Res TGA 2950 with a heating ramp of 10 ˚C/min. Thermal transitions were measured on a TA Instruments Q1000 differential scanning calorimeter (DSC) from -75 to 200 ˚C with a heating rate of 10 ˚C/min and cooling rate of 50 ˚C/min under nitrogen purge. Heat/cool/heat cycles were conducted for each

sample with values reported from the second heat. Dynamic mechanical analysis (DMA) was conducted on a TA Instruments Q800 in tension mode (1 Hz frequency). Films were cooled and held for 5 min at -75 °C, and the temperature was increased at a rate of 3 °C/min until flow. Tensile experiments were conducted on an Instron 4411 universal testing instrument. A crosshead speed of 50 mm/min was set for tensile analysis with values reported as an average of 5 samples. Film samples for tensile experiments were cut using a Pioneer Dietechs dumbbell cutting die. Variable temperature FTIR spectroscopy was collected with a Varian 670-IR equipped with a PIKE Technologies Heated Stage Diamond GladiATR attachment. Each copolymer was heated over a temperature range of 30 °C to 195 °C, at a ramp rate of 1 °C/min. Spectral data was acquired at 5° intervals, with 32 scans (The time required for 32 scans was approximately 1 min.) each at a resolution of 4 cm^{-1}. Samples were dried before analysis and the heat-cool-heat experiment was conducted through a gradual cooling of the sample in ambient conditions after the first heating cycle and subsequently heated in the exact same manner as the first heat.

5.4 Results and Discussion

5.4.1 Synthesis of PPG Copolymers

All four PPG based segmented copolymers described below contained a monodisperse HS ranging from 9.2 to 19 wt%. Each copolymer included an ethyl oxalate end-capping reaction, except for PPG-U, which yielded a difunctional PPG oligomer without polymerization. Polymerization of PPG-Ox resulted in clear tough, free-standing films with TPE behavior. The two step synthesis of PPG-Ox (Scheme 5.1) began with ethyl oxalate end-capping of the PPG diamine in the bulk using a four molar excess of diethyl oxalate. An equimolar bulk polycondensation of ethyl oxalate terminated PPG with ethylenediamine afforded the PPG-Ox

Scheme 5.1. Two step synthesis of PPG polyoxamide copolymers

Jeffamine D-2000
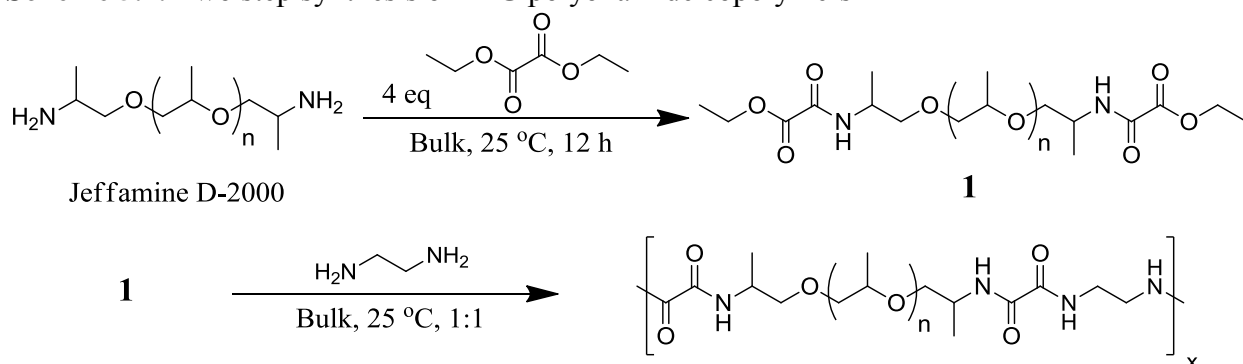
copolymer analog under very mild conditions, which proceeded rapidly at room temperature without the use of solvent, heat, low pressure, or catalyst. After direct addition of ethylenediamine, the reaction solidified within minutes yielding a solid, clear product. Solution casting and annealing under reduced pressure afforded colorless, transparent free-standing PPG-Ox films. ^{1}H NMR spectroscopy of the PPG-Ox copolymer confirmed the structure, and integration of each resonance matched well with expected values (Figure 5.2). Aggregation in both THF and CHCl$_3$ SEC solvents, as observed with dynamic light scattering, prevented molecular weight determination. Any attempts at SEC analysis in these solvents would lead to inaccurate molecular weights and possible column contamination.
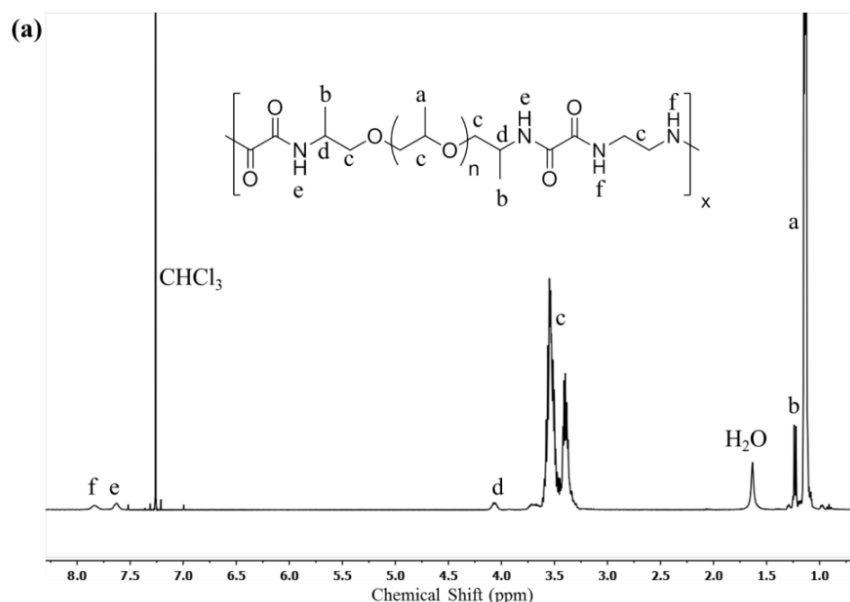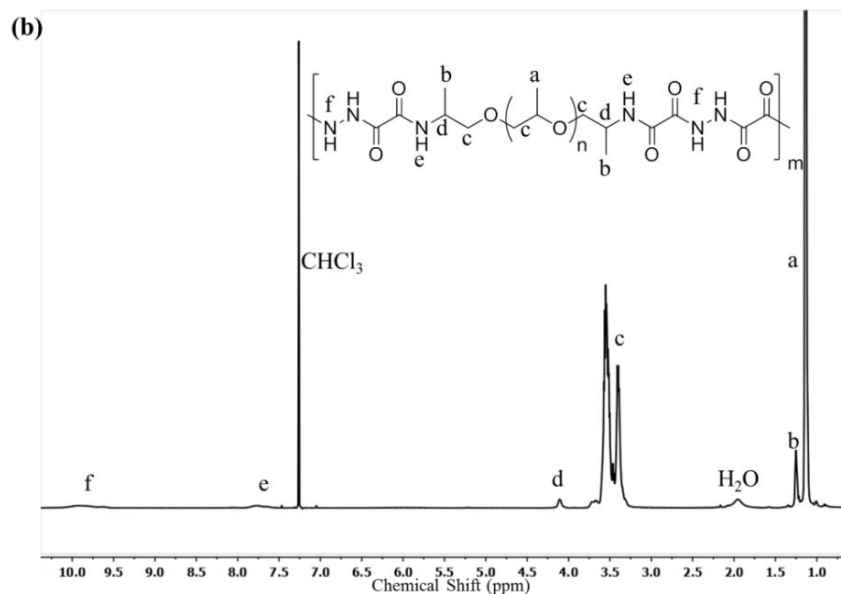
Figure 5.2. ^{1}H NMR of (a) PPG-Ox and (b) PPG-TriOx copolymers

Synthesis of PPG-TriOx copolymers that contained 12 wt% HS proved challenging and required a two-step end-capping procedure of the PPG oligomers before polycondensation with oxalyl chloride (Scheme 5.2). Reacting ethyl oxalate terminated PPG with hydrazine during the second end-capping reaction afforded difunctional, oxamic hydrazide oligomers. Oxamic hydrazide terminated PPG appeared as a white, waxy solid that flowed with minimal heat. Exploring various methods for polymerization of the oxamic hydrazide terminated PPG with oxalyl chloride revealed the best method for dealing with the HCl produced during polymerization. The presence of a base, such as triethylamine, during polymerization consistently afforded yellow, sticky polymers without mechanical integrity. Polycondensations conducted in the absence of an acid scavenger with a gentle argon purge into a base trap to remove the gaseous HCl yielded a solid polymer product after removal of CHCl$_3$. However, low levels of HCl may remain in the polymer film and slowly degrade the PPG backbone over time if not removed. Clear, free-standing films resulted from solution casting in CHCl$_3$ at 5 wt%

114

Scheme 5.2. Three step (a) PPG polytrioxamide and (b) PPG poly(urea oxamide) copolymer synthetic scheme

(a)

(b)
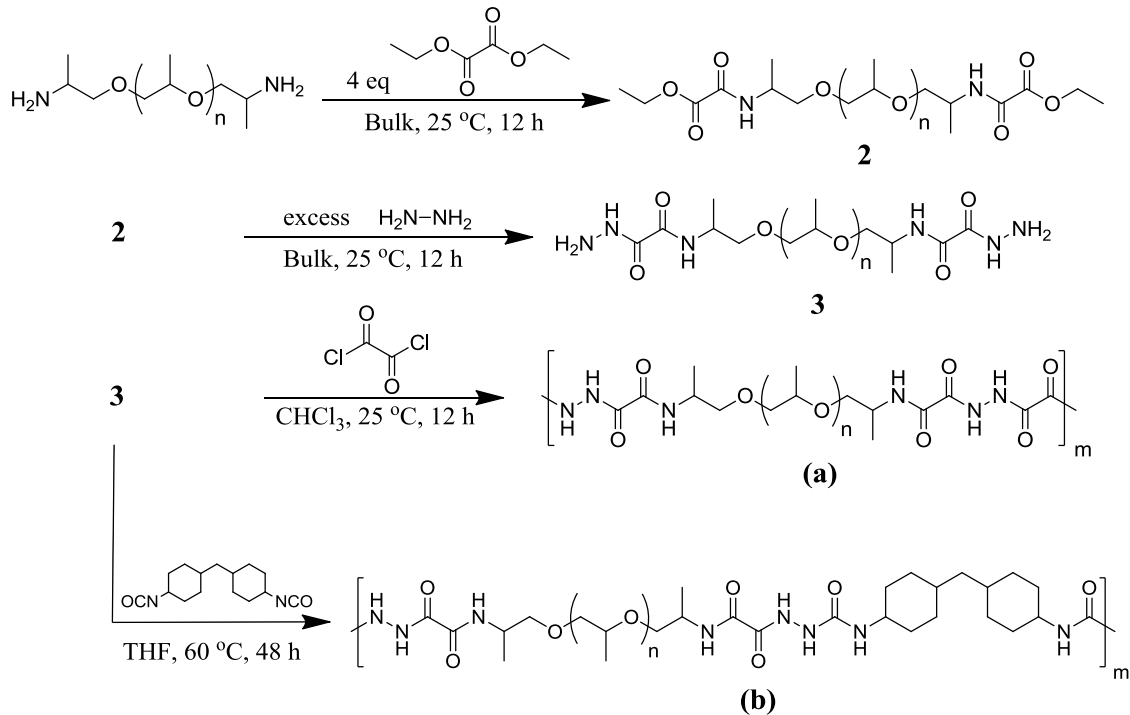
polymer and annealing. ^{1}H NMR spectroscopy confirmed the PPG-TriOx structure and revealed oxamide protons residing at 7.7 and 9.9 ppm integrating to 2 and 4 protons, respectively (Figure 5.2). PPG-TriOx showed persistent aggregation in CHCl$_3$ and THF SEC solvents, similar to PPG-Ox copolymers, preventing SEC analysis. Poor mechanical properties, as discussed below, suggested low molecular weights for PPG-TriOx. Despite the difficult synthesis, polymerization with oxalyl chloride proved successful in yielding trioxamide HS architecture and provided free-standing polymer films with mechanical integrity.

Polymerization conditions for the synthesis of PPG-UOx copolymers required solvent, heat, and a catalyst (Scheme 5.2) unlike PPG-TriOx and PPG-Ox. Polymerization of the oxamic hydrazide terminated PPG oligomer with HMDI yielded high molecular weight, free-standing polymer films with TPE behavior. Solution polymerization of PPG-UOx was cloudy in THF and cleared as polymerization progressed to yield a homogeneous, viscous solution. The initial

heterogeneous polymerization solution suggested the oxamic hydrazide oligomers were not fully dissolved and gradually solvated as polymerization proceeded. Synthesis of PPG-U with PPG diamine and HMDI remained homogenous throughout polymerization, and yielded a soft, sticky film with poor mechanical integrity (Scheme 5.3). PPG-U films were tacky and difficult to

Scheme 5.3. Synthesis of PPG polyurea segmented copolymer
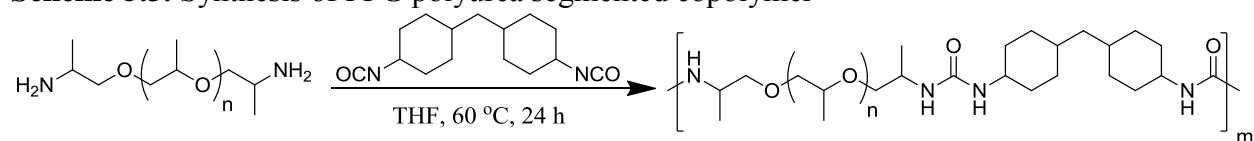
handle due to poor mechanical properties. The two bidentate urea hydrogen bonding groups in the monodisperse HS did not provide sufficient physical crosslinking to induce sufficient microphase separation from the PPG SS. Competition between ether and urea groups for hydrogen bonding may have also played a role in reducing the extent of physical crosslinking between the HSs.[24] DLS of both PPG-U and PPG-UOx segmented copolymers indicated the absence of aggregation in the SEC solvent unlike the PPG-Ox and PPG-TriOx copolymers. THF SEC provided reliable absolute M_n's, over 35,000 g/mol (Table 5.1) and demonstrated monomodal light scattering peaks for both copolymers.

Table 5.1. Molecular weights and thermal degradation values of PPG segmented copolymers

	Hard Segment Content (wt %)	M_n (kg/mol)	M_w (kg/mol)	PDI	$T_{d,5\%}$ (˚C)
PPG-U	13	36	48	1.33	277
PPG-UOx	19	39	57	1.47	300
PPG-Ox	9.2	-	-	-	338
PPG-TriOx	12	-	-	-	356

<u>SEC</u>: 30 ˚C, THF, 1 mL/min; <u>TGA</u>: N$_2$, 10 ˚C/min, 25 – 600 ˚C

5.4.2 FTIR Spectroscopy

Hydrogen bonding interactions of amide groups include both the N-H and carbonyl groups. This strong intermolecular interaction resulted in characteristic shifts in the vibrational frequency associated with the carbonyl and N-H stretching in the infrared spectrum. Carbonyl

stretching vibrations are sensitive to changes in dipole-dipole interactions due to differences in hydrogen bonding conformations or degree of order. However, the N-H stretch is insensitive to the conformation of hydrogen bonding segments and only shows a shift to higher wavenumber when transitioning from hydrogen bonded to non-bonded.[38] For this reason, probing changes in the carbonyl region provided more useful information about the nature of hydrogen bonding in a polyamide. FTIR spectroscopy of polyamides containing semicrystalline, hydrogen bonding segments exhibited ordered, hydrogen bonding (crystalline), non-ordered hydrogen bonding (amorphous), and non-bonded carbonyl groups in the infrared spectrum.[39] Calculations presented in previous literature have shown that the hydrogen-bond geometries present in ordered (crystalline) and disordered (amorphous) polymer have a significant effect upon the force constant of the carbonyl stretch vibrational frequency.[40] The force constant is mathematically related to the transition dipole coupling of the carbonyl stretching, which is sensitive to the packing of the hydrogen-bonded structure.[41] A transition from an ordered to disordered state results in an increased force constant and consequently an increased vibrational frequency. As the temperature is increased, a gradual increase in the vibrational frequency occurs as conformations of hydrogen bonding segments shift to a less ordered state and as more thermal energy is applied to the system, contributions of non-ordered hydrogen bonding and free carbonyl became significant.[42]

Variable temperature FTIR spectroscopy probed the hydrogen bonding of the PPG copolymers and suggested the formation of an ordered, trioxamide HS structure through the observed ordered hydrogen bonding vibrational frequency at a very low wavenumber. PPG-Ox copolymers exhibited a carbonyl stretching band at 1649 cm^{-1}, corresponding to a ordered hydrogen bonding state consistent with literature values.[36] The carbonyl ordered hydrogen

bonding peak for PPG-TriOx resided at 1618 cm^{-1}, which indicated the formation of an ordered, trioxamide HS structure. The large decrease in wavenumber for the PPG-TriOx ordered hydrogen bonded carbonyl stretching band, compared to PPG-Ox, suggested the trioxamide HS packing resulted in a more ordered structure than that of PPG-Ox copolymers. At 30 ˚C, the PPG-Ox analog exhibited a large ordered, hydrogen bonded carbonyl stretching band at 1649 cm^{-1} and a small free carbonyl band at 1684 cm^{-1}. PPG-TriOx spectra showed a large ordered band at 1618 cm^{-1} and small disordered, hydrogen bonded band at 1673 cm^{-1} (Figure 5.3). At 120 °C, a dramatic decrease occurred in the contribution of the ordered hydrogen bonded carbonyl band during heating of both PPG-Ox and PPG-TriOx copolymers. A corresponding increase in the disordered hydrogen bonding and free carbonyl absorbances was observed. At temperatures above 120 ˚C, primarily only non-ordered and free carbonyl absorbances were present. After cooling, a second heating cycle was performed for PPG-TriOx, resulting in an identical set of spectra to the first heating cycle (Figure 5.4). This indicated that the disruption of hydrogen bonding was reversible, but also heating of the polymer will not damage the copolymer in any way that would alter the hydrogen bonding. The N-H stretching bands in the hydrogen bonded state for PPG-Ox and PPG-TriOx resided at 3292 and 3216 cm^{-1}, respectively, revealing a similar lower vibrational frequency associated with the hydrogen bonding trioxamide HS (Figure 5.5). FTIR spectroscopy revealed the same trend of hydrogen bond disruption in the N-H stretch region as in the carbonyl region for PPG-Ox and PPG-TriOx, and the spectra at 120 ˚C revealed free N-H stretching bands at 3394 cm^{-1} for both copolymers.
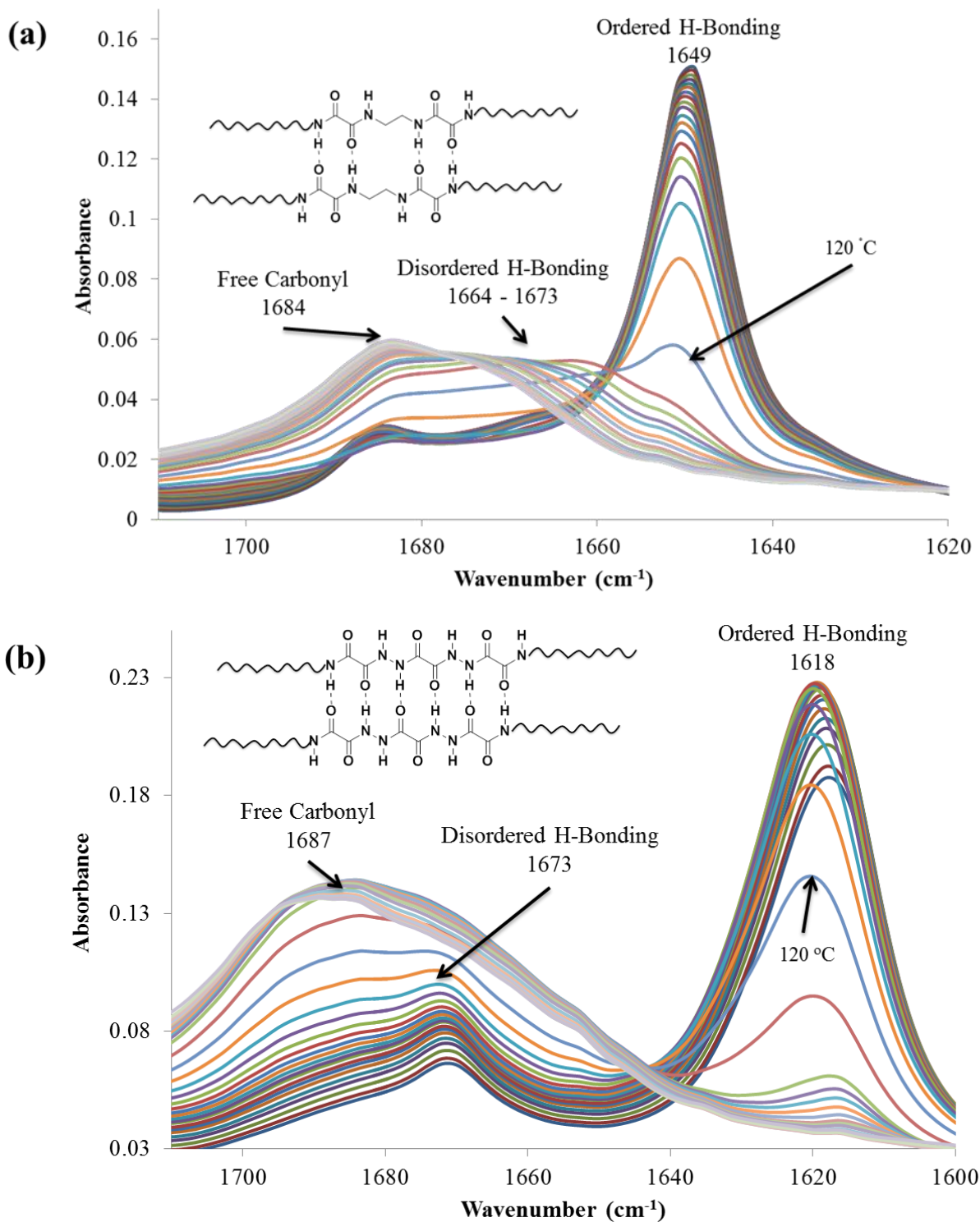
Figure 5.3. Variable temperature FTIR spectroscopy of (a) PPG-Ox and (b) PPG-TriOx copolymers in the carbonyl region from 30 ˚C to 195 ˚C
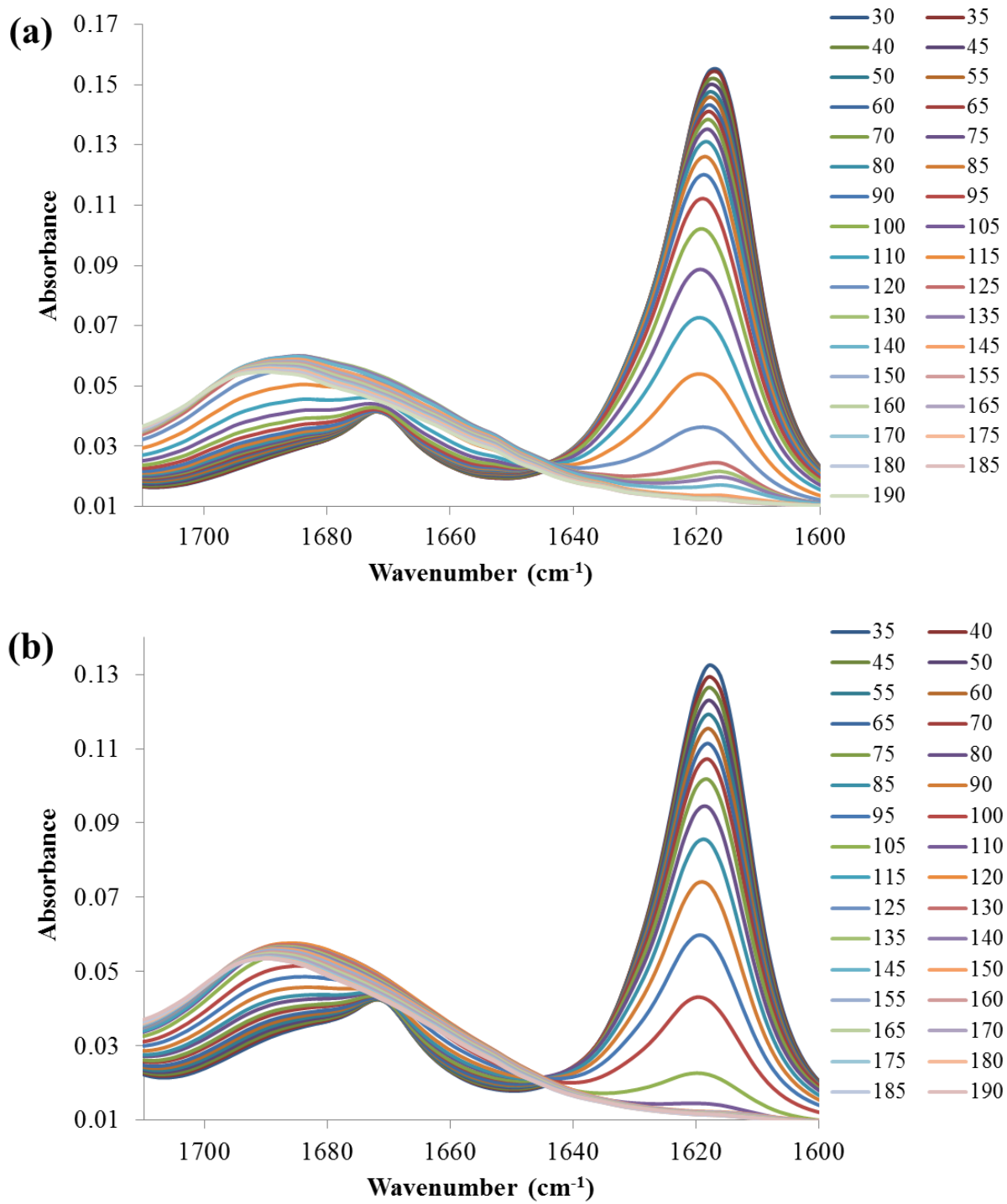
Figure 5.4. Variable temperature FTIR (a) first heat and (b) second heat for PPG-TriOx copolymer
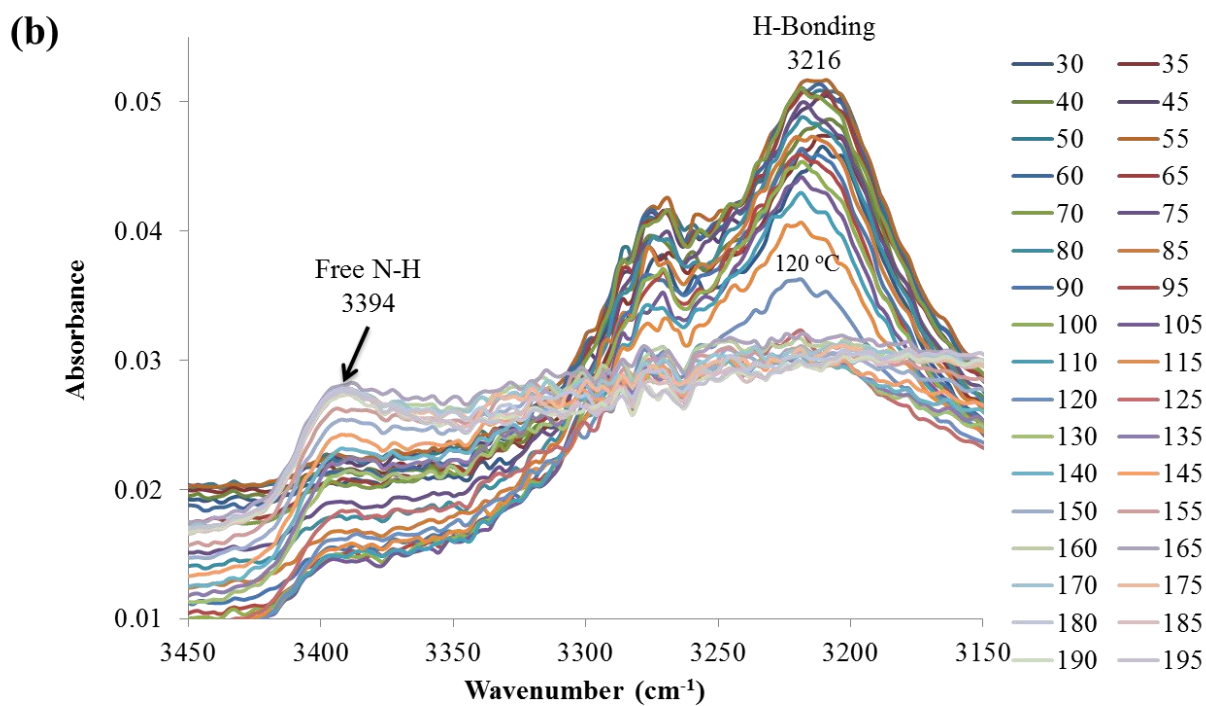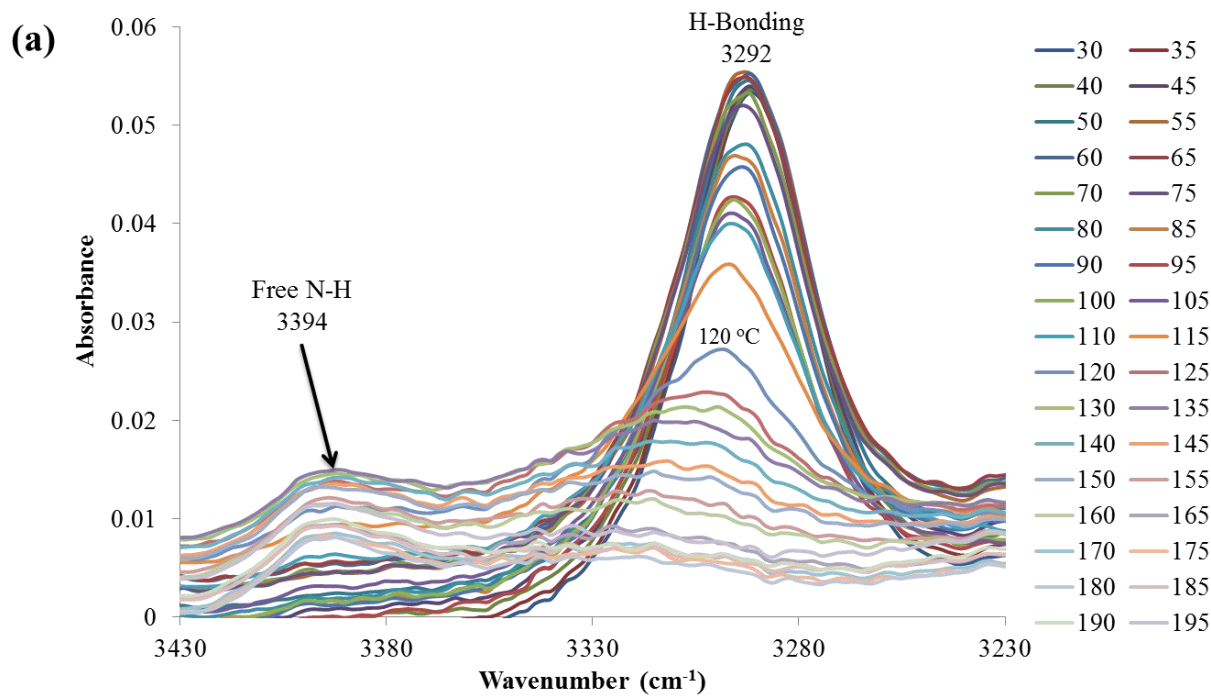
Figure 5.5. Variable temperature FTIR looking at the N-H stretching region for (a) PPG-Ox and (b) PPG-TriOx copolymers from 30 ˚C – 195 ˚C

PPG-UOx and the PPG-U analog exhibited different variable temperature FTIR profiles compared to PPG-Ox and PPG-TriOx copolymers. Carbonyl stretching bands for both copolymers were comprised of one large, broad band. FTIR spectroscopy revealed a gradual shift and broadening of the carbonyl band from 1629 to 1652 cm^{-1} for the PPG-U segmented copolymer as the temperature increased (Figure 5.6a). In contrast to the visible free band in the PPG-Ox and PPG-TriOx copolymers, the free urea band was likely convoluted with the broad band, contributing to the overall shift toward higher wavenumber. PPG-UOx copolymers exhibited the same trend and shifted from 1668 cm^{-1} at 30 °C to 1683 cm^{-1} at 190 °C (Figure 5.6b). Presence of the oxamide group linked directly to the urea group in the HS displayed a higher vibrational frequency carbonyl band than the PPG-U copolymer and included both the oxamide and urea carbonyl stretching bands.
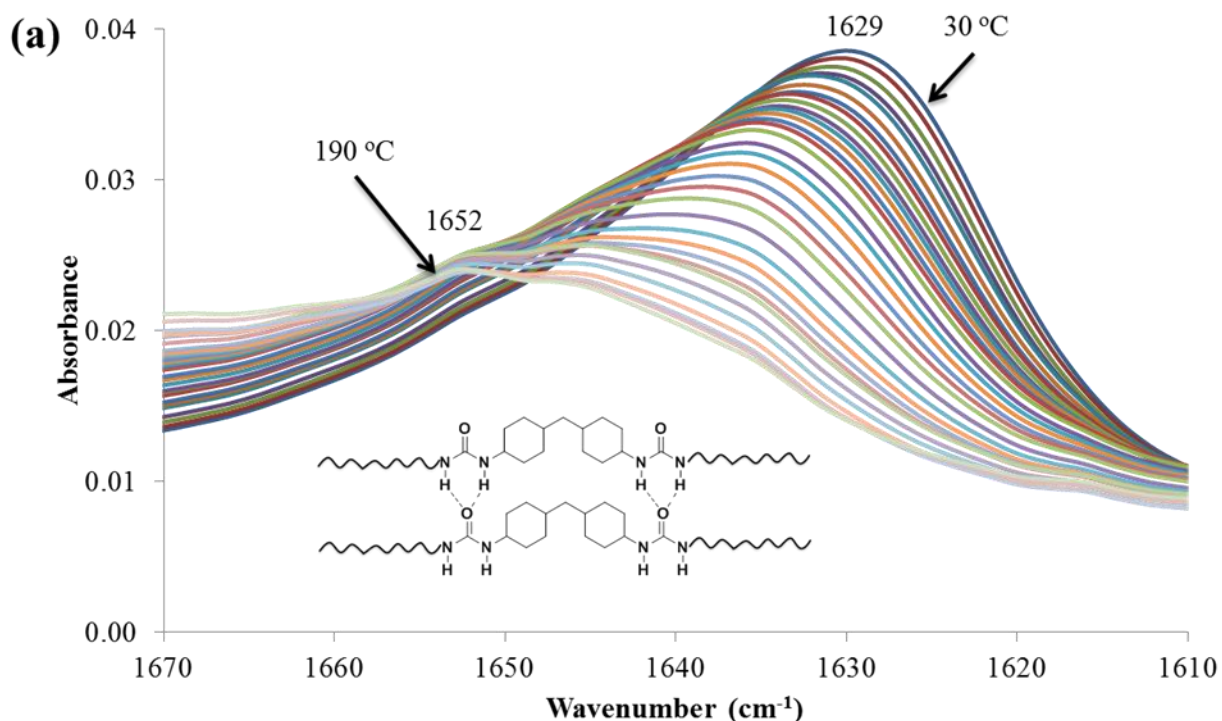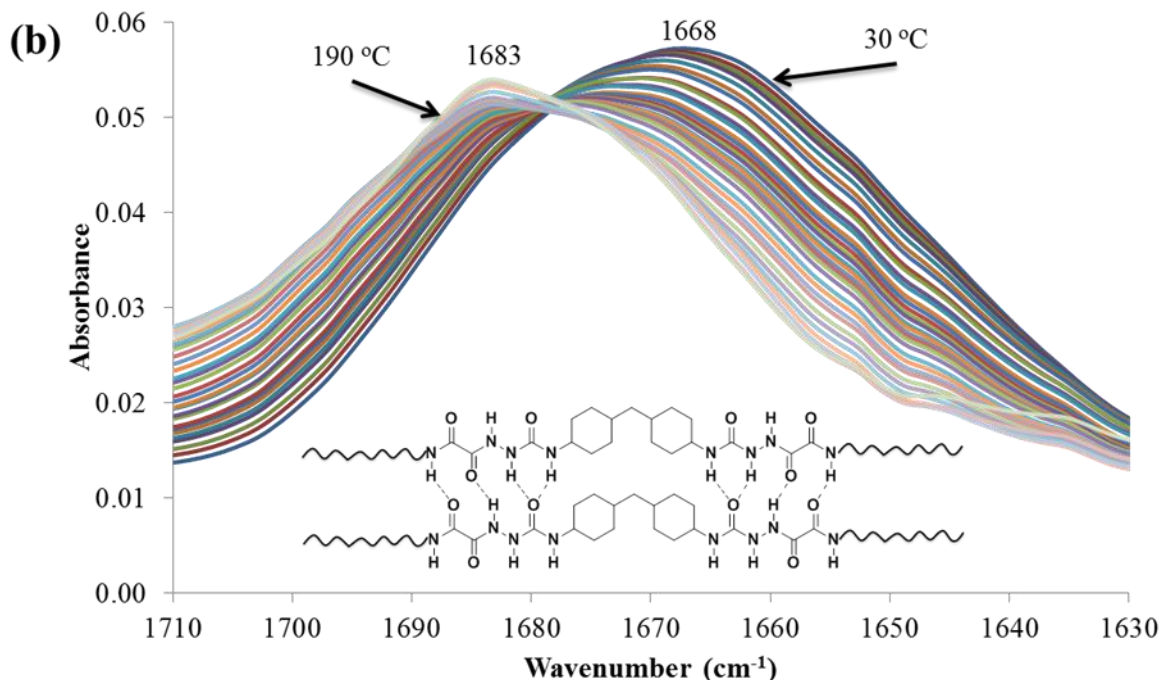
Figure 5.6. Variable temperature FTIR spectroscopic shifts in the carbonyl region for (a) PPG-U and (b) PPG-UOx copolymers from 30 ˚C to 195 ˚C

5.4.3 Thermal Analysis

Measuring the thermal stability of each copolymer using TGA showed each PPG copolymer did not lose weight to 300 ˚C under nitrogen except PPG-U, which displayed a temperature at 5% weight loss ($T_{d,5\%}$) of 277 ˚C (Table 5.1). Presence of an oxamide group in the HS resulted in a slight increase of the degradation temperature when comparing the $T_{d,5\%}$ of PPG-U and PPG-UOx copolymers. Similarly for PPG-Ox and PPG-TriOx, the presence of an additional oxamide group in the HS resulted in similar $T_{d,5\%}$ values. All non-chain extended PPG copolymers revealed a single step degradation profile.

DSC measured the thermal transitions associated with both copolymers revealing similar DSC traces for PPG-Ox and PPG-TriOx non-chain extended segmented copolymers. Figure 5.7 depicts the second heat DSC traces for both PPG-Ox and PPG-TriOx, revealing an endothermic transition at 120 ˚C for both copolymers. The endotherm corresponded to melting of the
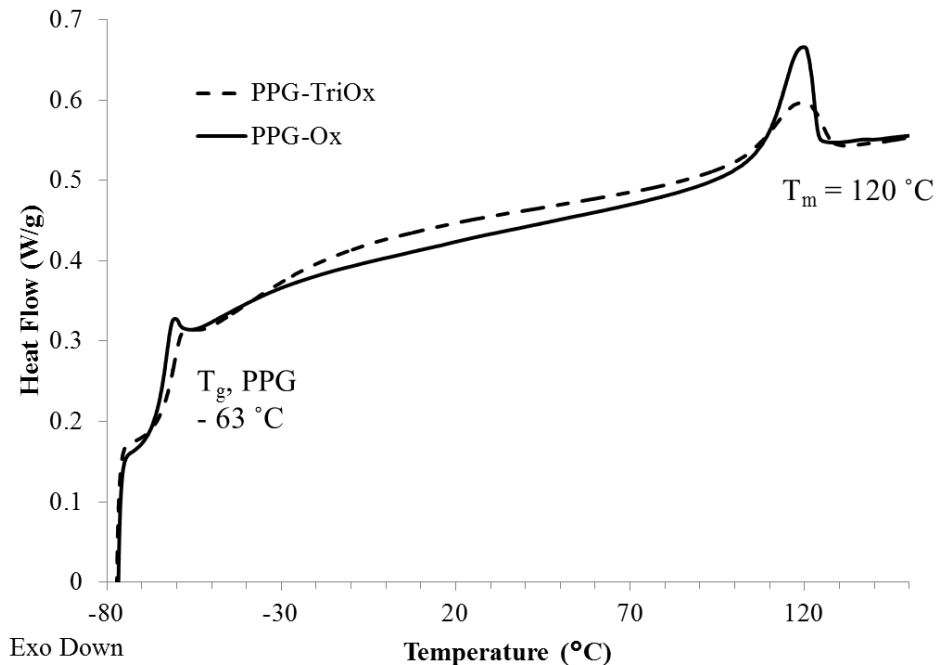
Figure 5.7. Second heat DSC traces for PPG-Ox and PPG-TriOx copolymers from – 75 ˚C to 150 ˚C with a rate of 10 ˚C/min

crystalline HS in both copolymers, consistent with earlier reports of polyoxamide copolymers that confirmed the crystalline structure of the polyoxamide HS.[36] PPG-TriOx exhibited a similar T_m and hydrogen bonding dissociation temperature as PPG-Ox. Increasing the HS hydrogen bonding with a third oxamide unit for PPG-TriOx did not change the HS T_m from the PPG-Ox, which was consistent with variable temperature FTIR experiments. PPG-U and PPG-UOx copolymers exhibited only a SS T_g. The absence of an endothermic response for PPG-U and PPG-UOx suggests a lack of crystallinity associated with the HS. Current studies of non-chain extended PDMS based polyurea and poly(urea oxamide) segmented copolymers verified the amorphous nature of the UOx HS with WAXD analysis. HMDI presumably imparted the amorphous character to the HS due to a mixture of cis and trans conformations associated with the cyclohexyl rings. All four PPG based copolymers exhibited a SS T_g of -63 ˚C.

5.4.4 Dynamic Mechanical Analysis

Distinct differences between annealed PPG based copolymers were observed when comparing dynamic mechanical behavior. PPG-Ox and PPG-TriOx copolymers both exhibited temperature insensitive rubbery plateau regions of 127 ˚C for PPG-Ox and 105 ˚C for PPG-TriOx (Figure 5.8). The PPG-Ox copolymers also had a higher rubbery plateau moduli of 42 MPa compared to 18 MPa for PPG-TriOx copolymer despite the lower wt% HS content. The poor mechanical performance suggested a low molecular weight PPG-TriOx copolymer. Since polymer aggregation prevented any reliable SEC molecular weight data for PPG-TriOx, physical properties provided the only indication of poor molecular weight. The critical molecular weight for optimum mechanical properties of PPG-TriOx segmented copolymers were not obtained with the current synthetic strategy. However, flow temperatures for both segmented copolymers resided at 122 and 124 ˚C for PPG-TriOx and PPG-Ox respectively. DSC and FTIR spectroscopy both indicated a major HS transition near 120 ˚C corresponding to HS melting and hydrogen bonding dissociation, disrupting the copolymers physical crosslinks and resulting in film failure.

DMA of PPG-U revealed the lack of a significant rubbery plateau region with a softening transition observed at 0 ˚C and eventual film failure occurred at 31 ˚C. The presence of oxamide groups in the HS imparted a rubbery plateau with a range of -15 to 40 ˚C and average storage moduli of 7 MPa for PPG-UOx copolymers. The increased thermomechanical properties of PPG-UOx, compared to the PPG-U analog, suggested an increase in the microphase separation due to stronger hydrogen bonding interactions between copolymer HSs. Also, the presence of oxamide groups in the HS likely reduced the competition for hydrogen bonding between ether linkages and urea groups through increased HS hydrogen bonding interactions resulting in better microphase separation.
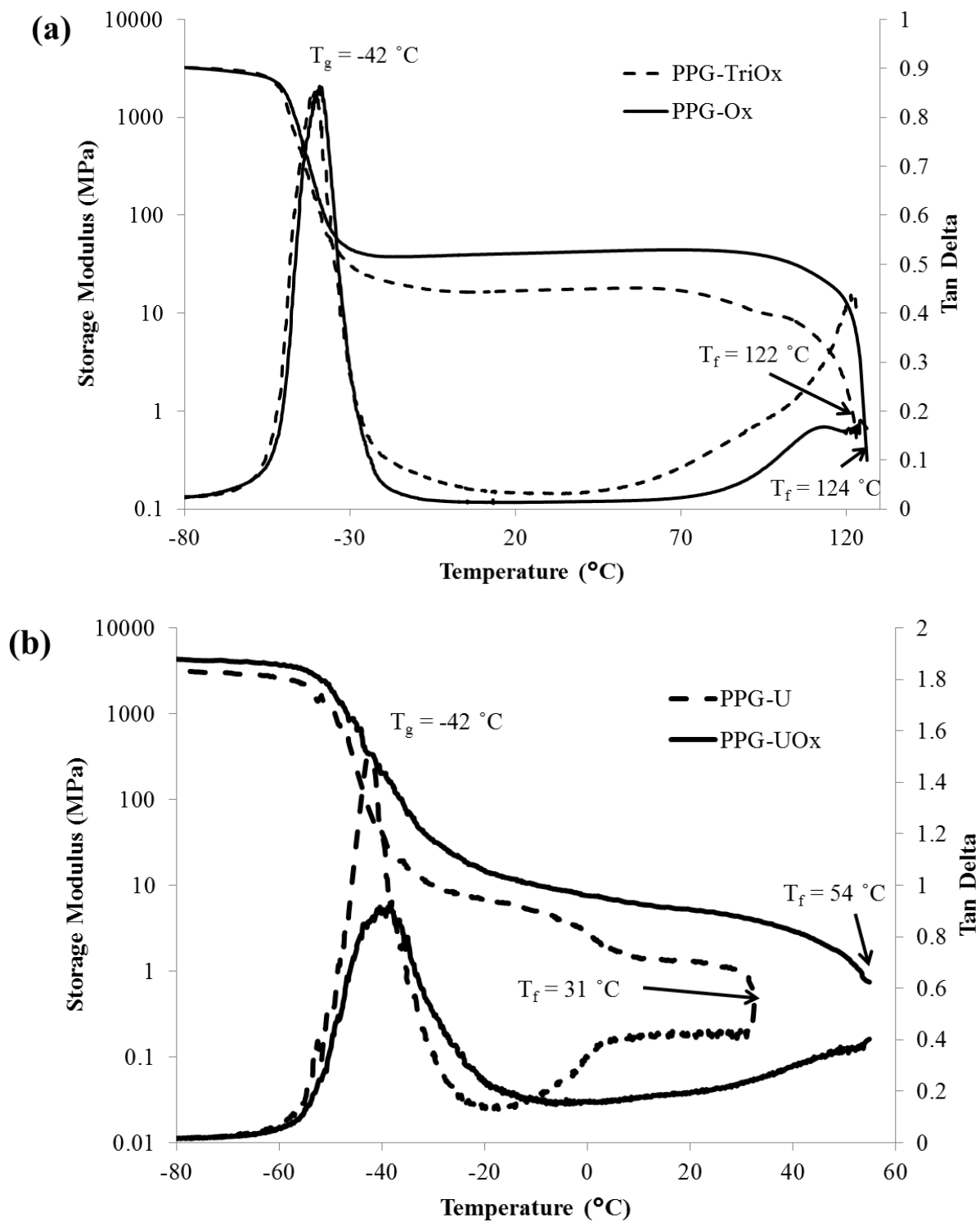
Figure 5.8. DMA traces of (a) PPG-TriOx, PPG-Ox, (b) PPG-U, and PPG-UOx segmented copolymers

5.4.5 Tensile Testing

Uniaxial tensile testing of PPG-TriOx and PPG-Ox provided further evidence for a low molecular weight effect for PPG-TriOx copolymers. Measuring five independent PPG-Ox samples demonstrated good tensile properties with a stress at break of 4.2 ± 0.3 MPa and strain at break of $196 \pm 27\%$ (Figure 5.9a). PPG-Ox and PPG-TriOx exhibited Young's moduli of 43 ± 3 and 18 ± 2 MPa respectively, similar to the observed DMA rubbery plateau storage modulus. PPG-TriOx exhibited poor tensile properties with a stress and strain at break of 1.2 ± 0.3 MPa and $19 \pm 3\%$, respectively. The poor tensile properties also indicated the lack of a critical molecular weight needed for optimal mechanical properties for PPG-TriOx copolymers.
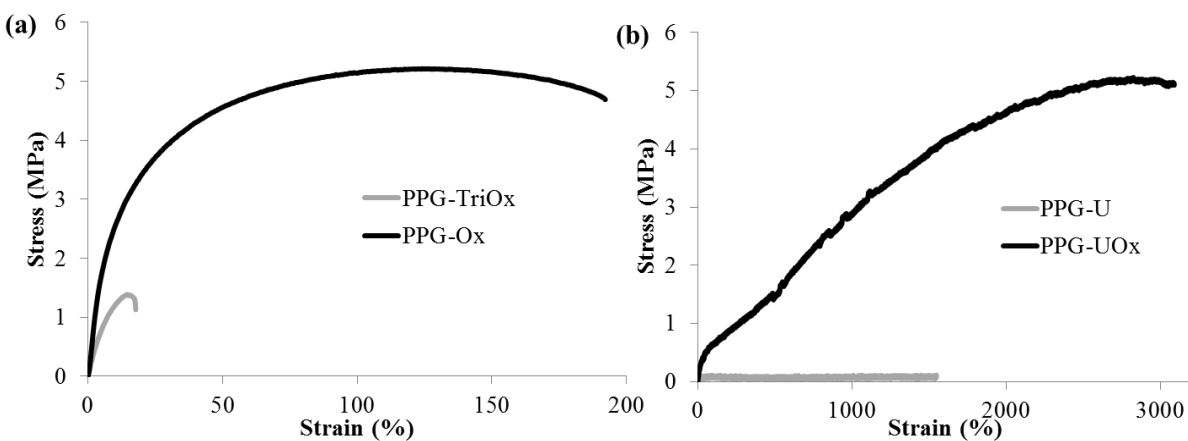
Figure 5.9. Stress-strain curves for (a) PPG-TriOx, PPG-Ox, (b) PPG-U, and PPG-UOx copolymers

PPG-UOx displayed a dramatic improvement in tensile properties compared to the PPG-U analog. Reliable comparisons of the tensile properties for PPG-UOx and PPG-U proved possible despite the challenging sample preparation. PPG-U exhibited very poor mechanical properties with a stress at break of 0.1 ± 0.01 MPa and strain at break of $1588 \pm 83\%$ (Figure 5.9b). Excellent tensile properties resulted due to the enhanced hydrogen bonding in the uniform HS of PPG-UOx. The stress at break increased over 50 times to 5.3 ± 0.5 MPa with a

corresponding increase in Young's Modulus of 1.7 ± 0.4 MPa, compared to 0.5 ± 0.1 MPa for PPG-U. Strain at break doubled to >3000% demonstrating the increase in tensile properties as a result of oxamide groups in the HS. Stronger hydrogen bonding interactions between the HSs of segmented polymer chains significantly improved physical properties. Meijer et al. also demonstrated the dramatic effects on physical properties that increasing HS hydrogen bonding had on poly(ether urea) segmented copolymers.[43] Incorporation of oxamide groups into the HS of a PPG polyurea segmented copolymer provided adequate hydrogen bonding to impart sufficient physical crosslinking and enhanced mechanical properties.

5.5 Conclusions

^{1}H NMR and FTIR spectroscopy analysis confirmed the successful synthesis of new PPG based segmented copolymers containing enhanced hydrogen bonding architectures. The two-step end-capping synthetic strategy yielded a difunctional oxamic hydrazide oligomer that provided a new synthetic pathway to unique, strong hydrogen bonding polymer architectures. Synthesis of PPG-TriOx through solution polymerization of oxamic hydrazide terminated PPG oligomers and oxalyl chloride proved challenging and resulted in low molecular weight copolymers with poor mechanical properties. However, PPG-TriOx copolymers possessed a low energy ordered, hydrogen bonding HS that exhibited a similar hydrogen bond disruption profile compared to PPG-Ox. DSC showed a HS T_m for both PPG-TriOx and PPG-Ox copolymers at 120 ˚C. Solution polymerization of PPG oxamic hydrazide with HMDI proved efficient for the synthesis of PPG-UOx copolymers, which yielded a transparent, tough thermoplastic elastomer with a M_n ~ 40,000 g/mol. PPG-U analogs displayed poor physical properties due to the insufficient hydrogen bonding strength of the HS. Variable temperature FTIR spectroscopy of PDMS-UOx copolymers showed a gradual shift to less ordered hydrogen bonding of the HS in a single

complex carbonyl stretching band. DMA of PPG-UOx revealed a significant service window and increased moduli compared to the PPG-U analog. Tensile testing of PPG-U and PPG-UOx revealed the impact of hydrogen bonding on mechanical properties. PPG-UOx displayed a stress at break over 50 times that of PPG-U and twice the strain at break (>3000%). PPG-TriOx and PPG-UOx segmented copolymers highlighted the hydrogen bonding structural possibilities with the new oxamic hydrazide polymerization chemistry and demonstrated the impact of oxamide hydrogen bonding on copolymer physical properties.

5.6 Acknowledgments

5.7 References

(1)   Holden, G.; Legge, N. R.; Quirk, R. P.; Schroeder, H. E.; Editors *Thermoplastic Elastomers, 2nd Edition*; Hanser/Gardner, 1996.
(2)   Castagna, A. M.; Pangon, A.; Choi, T.; Dillon, G. P.; Runt, J. *Macromolecules* **2012**, *45*, 8438.
(3)   Chakrabarty, S.; Nisenholt, M.; Wynne, K. J. *Macromolecules* **2012**, *45*, 7900.
(4)   Krijgsman, J.; Biemond, G. J. E.; Gaymans, R. J. *Polymer* **2005**, *46*, 8250.
(5)   Lips, P. A. M.; Broos, R.; van Heeringen, M. J. M.; Dijkstra, P. J.; Feijen, J. *Polymer* **2005**, *46*, 7834.
(6)   van der Schuur, M. J.; Gaymans, R. J. *Polymer* **2007**, *48*, 1998.
(7)   Fragiadakis, D.; Dou, S. C.; Colby, R. H.; Runt, J. *Macromolecules* **2008**, *41*, 5723.
(8)   Gao, R. L.; Zhang, M. Q.; Dixit, N.; Moore, R. B.; Long, T. E. *Polymer* **2012**, *53*, 1203.
(9)   Korley, L. T. J.; Pate, B. D.; Thomas, E. L.; Hammond, P. T. *Polymer* **2006**, *47*, 3073.
(10)   van der Schuur, M.; Noordover, B.; Gaymans, R. J. *Polymer* **2006**, *47*, 1091.
(11)   Jewrajka, S. K.; Yilgor, E.; Yilgor, I.; Kennedy, J. P. *Journal Polymer Science, Part A: Polymer Chemistry* **2008**, *47*, 38.
(12)   Tang, D.; Mulder, D.-J.; Noordover, B. A. J.; Koning, C. E. *Macromolecluar Rapid Communications* **2011**, *32*, 1379.
(13)   Wisse, E.; Spiering, A. J. H.; van Leeuwen, E. N. M.; Renken, R. A. E.; Dankers, P. Y. W.; Brouwer, L. A.; van Luyn, M. J. A.; Harmsen, M. C.; Sommerdijk, N.; Meijer, E. W. *Biomacromolecules* **2006**, *7*, 3385.

(14)   June, S. M.; Bissel, P.; Long, T. E. *Journal of Polymer Science Part a-Polymer Chemistry* **2012**, *50*, 3797.
(15)   Schmidt, F. G.; Droescher, M. *Makromolecular Chemistry* **1983**, *184*, 2669.
(16)   Zhang, M.; Moore, R. B.; Long, T. E. *Journal of Polymer Science, Part A: Polymer Chemistry* **2012**, *50*, 3710.
(17)   June, S. M.; Suga, T.; Heath, W. H.; Long, T. E.; Lin, Q.; Puligadda, R. *Journal of Adhesion* **2010**, *86*, 1012.
(18)   Mecham, J. B.; Wang, F.; Glass, T. E.; Xu, J.; Wilkes, G. L.; McGrath, J. E. *Polymer Materials Science and Engineering* **2001**, *84*, 105.
(19)   Xi, K.; Meng, Z.; Heng, L.; Ge, R.; He, H.; Yu, X.; Jia, X. *Journal of Applied Polymer Science* **2009**, *113*, 1633.
(20)   Yilgor, I.; Yilgor, E.; Eberle, J.; Steckle, W. P.; Johnson, B. C.; Tyagi, D.; Wilkes, G. L.; McGrath, J. E. *Abstracts of Papers of the American Chemical Society* **1983**, *185*, 32.
(21)   Yilgor, E.; Burgaz, E.; Yurtsever, E.; Yilgor, I. *Polymer* **2000**, *41*, 849.
(22)   Yilgor, E.; Yilgor, I. *Polymer* **2001**, *42*, 7953.
(23)   Yilgor, E.; Yurtsever, E.; Yilgor, I. *Polymer* **2002**, *43*, 6561.
(24)   Yilgor, I.; Yilgor, E. *Polymer Reviews* **2007**, *47*, 487.
(25)   Sheth, J. P.; Klinedinst, D. B.; Wilkes, G. L.; Iskender, Y.; Yilgor, I. *Polymer* **2005**, *46*, 7317.
(26)   Miller, J. A.; Lin, S. B.; Hwang, K. K. S.; Wu, K. S.; Gibson, P. E.; Cooper, S. L. *Macromolecules* **1985**, *18*, 32.
(27)   Niesten, M.; Gaymans, R. J. *Journal of Applied Polymer Science* **2001**, *81*, 1372.
(28)   van der Schuur, M.; de Boer, J.; Gaymans, R. J. *Polymer* **2005**, *46*, 9243.
(29)   Versteegen, R. M.; Kleppinger, R.; Sijbesma, R. P.; Meijer, E. W. *Macromolecules* **2006**, *39*, 772.
(30)   Yilgor, I.; Shaaban, A. K.; Steckle, W. P.; Tyagi, D.; Wilkes, G. L.; McGrath, J. E. *Polymer* **1984**, *25*, 1800.
(31)   Coe, S.; Kane, J. J.; Nguyen, T. L.; Toledo, L. M.; Wininger, E.; Fowler, F. W.; Lauher, J. W. *Journal of the American Chemical Society* **1997**, *119*, 86.
(32)   Nguyen, T. L.; Fowler, F. W.; Lauher, J. W. *Journal of the American Chemical Society* **2001**, *123*, 11057.
(33)   Schulze, H.; Texaco Development Corp., USA . 1978, p 7 pp.
(34)   Leir, C. M.; Benson, K. E.; Hansen, R. G.; Purgett, M. D.; Everaerts, A. I.; 3M Innovative Properties Company, USA . 2007, p 12pp.
(35)   Leir, C. M.; Benson, K. E.; Hansen, R. G.; Purgett, M. D.; Everaerts, A. I.; Sherman, A. A.; 3M Innovative Properties Company, USA . 2007, p 16pp.
(36)   Sijbrandi, N. J.; Kimenai, A. J.; Mes, E. P. C.; Broos, R.; Bar, G.; Rosenthal, M.; Odarchenko, Y.; Ivanov, D. A.; Dijkstra, P. J.; Feijen, J. *Macromolecules* **2012**, *45*, 3948.
(37)   Sijbrandi, N. J.; Kimenai, A. J.; Mes, E. P. C.; Broos, R.; Bar, G.; Rosenthal, M.; Odarchenko, Y. I.; Ivanov, D. A.; Jan, F. J.; Dijkstra, P. J. *Polymer* **2012**, *53*, 4033.
(38)   Coleman, M. M.; Lee, K. H.; Skrovanek, D. J.; Painter, P. C. *Macromolecules* **1986**, *19*, 2149.
(39)   Skrovanek, D. J.; Painter, P. C.; Coleman, M. M. *Macromolecules* **1986**, *19*, 699.
(40)   Pollack, S. K.; Shen, D. Y.; Hsu, S. L.; Wang, Q.; Stidham, H. D. *Macromolecules* **1989**, *22*, 551.

(41)   Krimm, S.; Abe, Y. *Procedings of the National Acadamy of Sciences U S A* **1972**, *69*, 2788.

(42)   Skrovanek, D. J.; Howe, S. E.; Painter, P. C.; Coleman, M. M. *Macromolecules* **1985**, *18*, 1676.

(43)   Versteegen, R. M.; Sijbesma, R. P.; Meijer, E. W. *Macromolecules* **2005**, *38*, 3176.

Chapter 6: Part I Overall Conclusions

The intermolecular hydrogen bonding interactions between oxamide-containing segmented copolymers was manipulated through HS structural modifications, and the effects that each modification displayed on the copolymers physical properties was measured. First, the structure-property relationships of PDMS-based poly(oxamide) segmented copolymers were studied through varying the alkyl spacer length between oxamide groups in the hard segment, and also changing PDMS molecular weight. Optically clear, ductile films were obtained after the bulk polymerization of ethyl oxalate terminated PDMS oligomers (2,000, 5,000, and 12,000 g/mol) with various alkyl diamines. The bulk polymerization strategy was tolerant of various temperatures demonstrating the synthetic versatility. Variable temperature FTIR spectroscopy probed the influence of oxamide spacing on the thermal stability of the bisoxamide HS. The FTIR studies revealed that disruption of ordered, hydrogen bonding interactions occurred at lower temperatures as the length of alky spacer increased. DSC also showed a decrease in HS T_m with an increase in oxamide spacing. Significant changes in copolymer thermomechanical properties were observed with oxamide spacing, in particular the T_f decreased as the spacer length increased. Increased PDMS molecular weight, thereby decreasing HS wt% content, led to lower moduli of the large temperature insensitive service window observed for each PDMS poly(oxamide) copolymer. Tensile testing revealed reduced tensile properties with the increase in oxamide spacing primarily with a reduction in the strain at break. Hysteresis experiments also mirrored the poor performance with longer oxamide linkages exhibiting high % hysteresis values for longer oxamide spacing. Poly(oxamide) copolymers synthesized with *m*-xylene diamine demonstrated poor properties due to the odd spacing and steric bulk. Copolymers synthesized

with the shortest alkyl spacer (ethylene) provided the strongest hydrogen bonding interactions leading to optimal mechanical properties.

A new family of segmented copolymers were developed through a novel polymerization chemistry based on oxamic hydrazide terminated oligomers. The new polymerization chemistry allowed for incorporation of oxamide hydrogen bonding groups into urea containing hard segments to yield high molecular weight poly(urea oxamide) segmented copolymers, even after two end-group modifications. These PDMS-based poly(urea oxamide) copolymers possessed well defined microphase separated bulk morphologies, which led to improved mechanical properties when compared to PDMS polyurea analogs. SEC studies showed that high molecular weight copolymers were produced after 6 h and annealing studies suggested 100 °C as the optimum annealing temperature. DMA of the PDMS poly(urea oxamide) copolymers showed a long service window, which extended up to 186 °C for PDMS12K-UOx. When compared to the polyurea analogs, a dramatic increase in the temperature insensitive service window was observed due to increased hydrogen bonding in the hard segment that the oxamide groups provided. SAXS analysis confirmed the increased microphase separation, compared to polyurea analogs. Variable temperature SAXS experiments elucidated a sharp morphological transition at 155 °C for PDMS2K-UOx copolymers, which led to phase mixing and subsequently the onset of flow. Tuning of the tensile properties was demonstrated through changes in PDMS molecular weight and use of a dihydrazide chain extender. The higher HS wt% contents resulted in higher stress at break and Young's moduli values, but a decrease in the strain at break always resulted from higher HS wt%. Overall, PDMS poly(urea oxamide) copolymers possessed TPE behavior and tunable mechanical properties superior to polyurea analogs.

The last project focused on synthesis of more novel segmented copolymers based on the oxamic hydrazide polymerization chemistry. PPG-based copolymers containing a trioxamide and urea oxamide HS were synthesized and compared to oxamide and urea containing analogs. Synthesis of PPG poly(trioxamide) copolymers was carried out through solution polymerization of a oxamic hydrazide terminated oligomer with oxalyl chloride and proved difficult due to the nature of the reactants and HS properties. Poly(trioxamide) copolymers had a low energy ordered hydrogen bonding HS that exhibited a similar thermal stability as the PPG poly(oxamide) analog. However, the mechanical properties of PPG poly(trioxamide) copolymers were poor, presumably due to low molecular weight copolymers. PPG poly(urea oxamide) segmented copolymers afforded optically clear, elastic films with TPE behavior. Both the poly(urea oxamide) and polyurea copolymers were high molecular weight, but the polyurea copolymers exhibited poor mechanical properties. Incorporation of the oxamide group in the HS significantly improved the thermomechanical properties of the copolymers and demonstrated a large service window for poly(urea oxamide) copolymers. The tensile properties were the most affected when comparing the poly(urea oxamide) to the polyurea analog with a 50x increase in the stress at break and 2x the strain at break (>3000%). These copolymers exemplified the structural possibilities for segmented copolymers when utilizing the oxamic hydrazide polymerization chemistry.

Chapter 7: Suggested Future Work

7.1 Comparison of Hard Segment Aromaticity and Symmetry in Poly(dimethyl siloxane) Poly(urea oxamide) Segmented Copolymers

PDMS poly(urea oxamide) segmented copolymers described in chapter four demonstrated excellent physical properties especially when compared to the PDMS poly(urea) counterparts. The success of this segmented system warrants further investigation into the structure property relationships of the urea oxamide hard segment. The reported synthesis utilized 4,4′-methylenebis(cyclohexyl isocyanate) (HMDI), which contained a mixture of cis and trans isomers. The presence of the cyclohexyl isomer mixture in the poly(urea oxamide) hard segment imparts an amorphous character to the copolymers. However, synthesis of PDMS poly(urea oxamide) copolymers through the step-growth polymerization of the oxamic hydrazide terminated PDMS oligomers and 4,4′-methylenebis(phenyl isocyanate) (MDI) may yield a more uniform urea oxamide hard segment (Scheme 7.1). The uniformity imposed through

Scheme 7.1. Synthesis of PDMS poly(urea oxamide) containing an aromatic hard segment
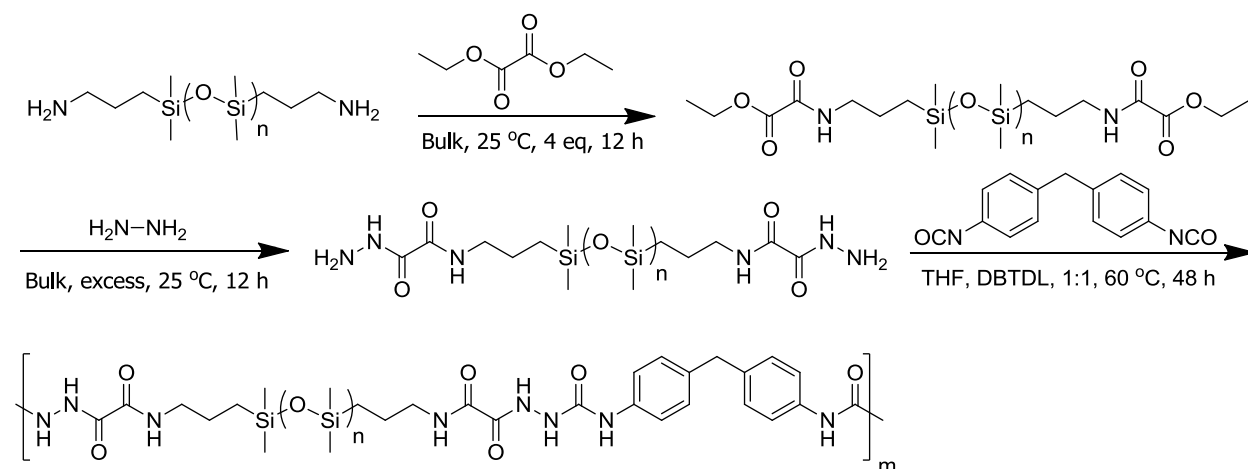
incorporation of the aromatic groups may impart a crystalline nature to the hard segment and significantly affect the materials physical properties. Future studies should include full polymer

characterization and in-depth morphological studies to probe the nature of crystallinity, if any, to fully understand its influence on the physical properties.

Symmetry of the hard segment in segmented copolymers containing a uniform hard segment can have a dramatic effect on the physical crosslinks and subsequent material properties of a given copolymer. The asymmetry of the hard segment will affect hard segment packing and significantly reduce crystallinity. Solution polymerization with a series of symmetric and unsymmetrical diisocyanate monomers will provide insight into the role of diisocyanate symmetry on the physical properties of poly(urea oxamide) segmented copolymers (Figure 7.1). Full morphological analysis and mechanical testing of each copolymer will provide a reliable comparison of the effects of diisocyanate symmetry.
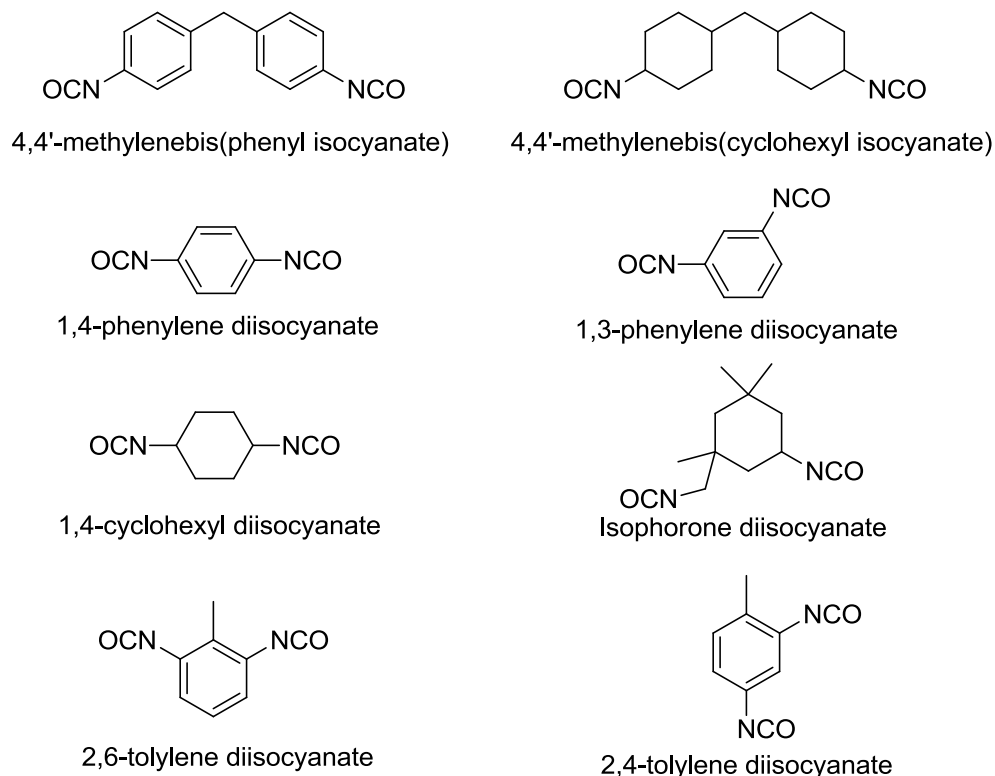
Figure 7.1. Structures of possible diisocyanates for polymerization of poly(urea oxamide) copolymers to study the effect of diisocyanate symmetry on physical properties

7.2 Synthesizing Functional MWCNT-Poly(urea oxamide) Composites

Incorporating functionalized nano carbon materials into poly(urea oxamide) segmented copolymer films would likely yield useful composite materials with enhanced thermal and mechanical properties. A six-step oxamide urea functionalization of MWCNT would provide an excellent choice for the production of poly(urea oxamide)-nanotube composites (Scheme 7.2). The urea oxamide functionality covering the nanotubes provides multiple hydrogen bonding sites for the hard segments of a poly(urea oxamide) segmented copolymer to bind. The strong intermolecular interactions of the copolymer and functionalized carbon nano tubes would impart a significant reinforcing effect on the material and demonstrate enhanced mechanical properties over the copolymers alone.

Scheme 7.2. Urea oxamide functionalization of MWCNT for poly(urea oxamide) composites
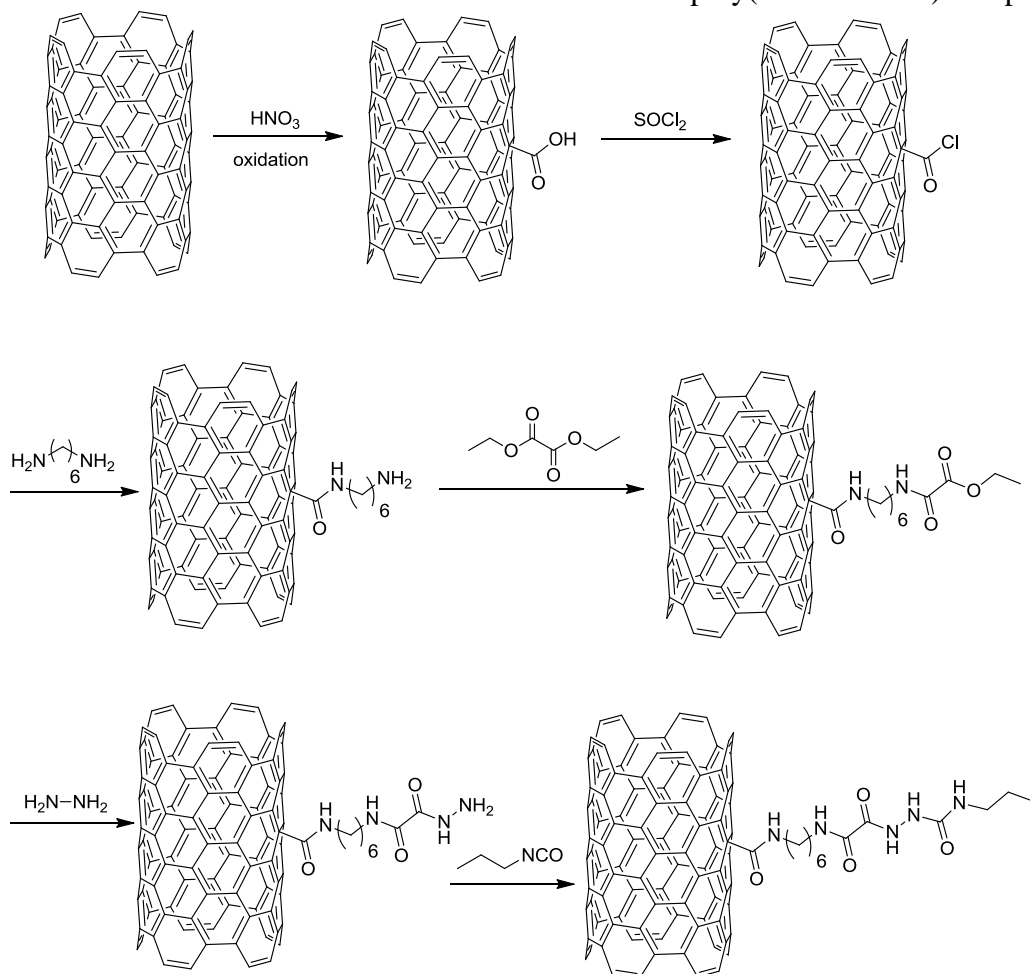
7.3 Effect of Deformation on the Crystalline Morphology of PDMS Poly(oxamide) Copolymers

Morphological studies in chapter three and other literature reports verified the crystalline nature of poly(oxamide) hard segments in the cases where oxamide groups were connected through a linear alkyl chain. An in-depth morphological study of the effects of mechanical deformation on the ribbon-like crystalline morphology of poly(oxamide) segmented copolymers would provide a fundamental understanding into the role that crystallites play in the mechanical properties. Elucidation of the mechanism in which a morphological breakdown occurs, and eventual film fracture will aid in the understanding and future design of strong hydrogen bonding segmented copolymers. SAXS and WAXD analysis at various elongations would allow for probing into the changes to the crystalline domains associated with tensile elongation and AFM would provide real-space resolution of the changes to the surface morphology during elongation. Characterization of elongated films with techniques such as DSC and polarized light microscopy could also provide useful information in conjunction with SAXS and AFM.

7.4 Rheological Characterization of PDMS Poly(urea oxamide) Segmented Copolymers

The thermal stability and rheological behavior of PDMS poly(urea oxamide) is not well understood to date and an in-depth investigation into the rheological properties of the poly(urea oxamide) copolymers is needed. A key property of poly(urea oxamide) segmented copolymers is the melt processability and the stability of the copolymers in the melt is essential for processing in the melt. Initial studies have suggested poly(urea oxamide) copolymers are not fully stable at high temperatures (>180 ˚C) for extended periods of time. The first set of experiments should include time sweeps at various temperatures to understand the temperature range, if any, that the

copolymers remain stable in the melt. After determining the temperature range where the copolymers remained thermally stable, further investigation into the linear viscoelastic properties of the poly(urea oxamide) copolymers would be warranted. Rheological experiments would include frequency sweeps, time-temperature superposition experiments, as well as the effect of large-amplitude oscillation shear pretreatment of the copolymers.

7.5 Synthesis of Biodegradable, Cationic Poly(oxalate) Copolyesters for Non-viral Gene Delivery Applications

All of the work described above utilized the oxalyl chemistry for the synthesis and characterization of poly(oxamide) containing segmented copolymers. Polymerization of the oxalate end-functionalized oligomers with diamines proved efficient and useful for obtaining high molecular weight segmented copolymers. The use of diols for polymerization yields poly(oxalate) copolymers that are water soluble and easily hydrolyzed. The use of bulky, asymmetric diols are favorable for inhibiting crystallinity in poly(oxalate)s. The major application for poly(oxalate) copolymers is use in biodegradable drug delivery systems due to the hydrolysis of the oxalate group and the potential for biocompatible degradation products (Scheme 7.3). Currently no literature exist for the use of poly(oxalate)s in the non-viral gene delivery field. The ability of a delivery vector to degrade into biocompatible degradation products could provide a non-toxic delivery vehicle as well as a mechanism for release of the nucleic acid payload after endocytosis into the cell. The drop in pH of the endosome would likely promote the degradation of the cationic poly(oxalate) and aid in DNA release.

Scheme 7.3. Hydrolysis of poly(oxalate) copolymer
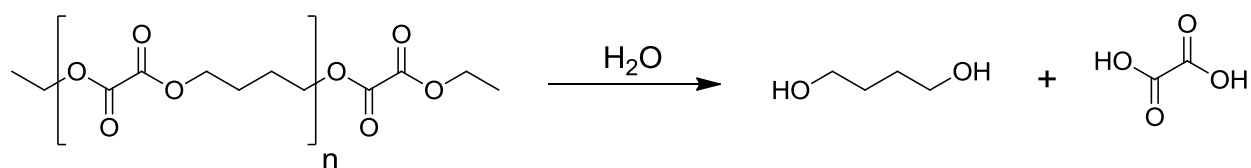
The initial investigation into the development of a cationic poly(oxalate) copolymer would include synthesis of a simple poly(oxalate) (Scheme 7.4) to work out the polymerization conditions and probe the rate of hydrolysis under various conditions. Step growth polymerization

Scheme 7.4. Step-growth polymerization of diethyl oxalate and 1,4-butane diol to provide the initial poly(oxalate) copolymer
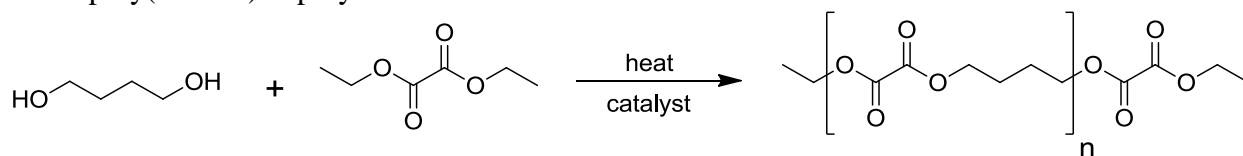
of the initial poly(oxalate) would include attempts at both bulk and solution polymerization to identify the optimal conditions for polymerization. After the polymerization conditions were worked out, incorporation of a phosphonium containing diol to provide a cationic charge to the poly(oxalate) would be investigated. Zhang et al. have developed phosphonium containing segmented copolymers for non-viral gene delivery using a trialkyl(3-hydroxy-2-(hydroxymethyl)-2-methylpropyl)phosphonium monomer (ethyl, propyl, and butyl). Synthesis of phosphonium containing poly(oxalate) copolymers for non-viral gene delivery would include diethyl oxalate, 1,4-butane diol, and the phosphonium diol to provide a positively charged, degradable poly(oxalate) polymer (Scheme 7.5). After a high molecular weight polymer is produced, then degradation and DNA complexation studies could begin with subsequent biological evaluations to follow. Investigating the effects of phosphonium trialkyl arm length on DNA complexation, cellular uptake, transfection efficiency, and cellular toxicity would provide interesting structure-property relationships to aid in further development of phosphonium containing poly(oxalate) copolymers.

Scheme 7.5. Synthesis of a cationic copolyester based on poly(oxalate) for non-viral gene delivery
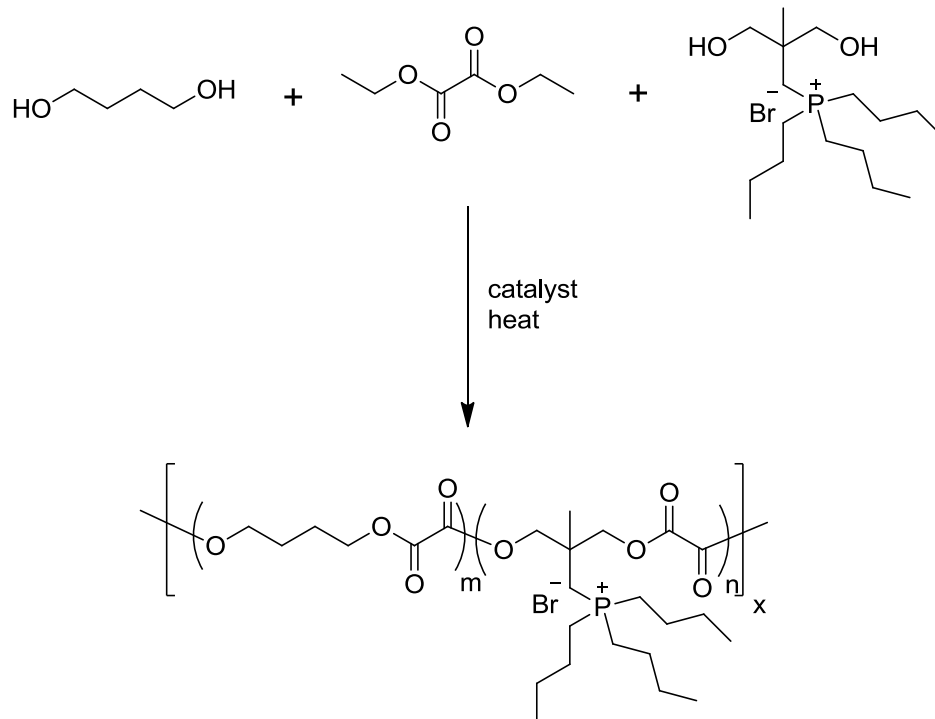
Part II

Chapter 8: Non-viral Delivery of Nucleic Acids

8.1 Abstract

Non-viral gene delivery of nucleic acids is a hot field of research which has received a lot of attention in the past 15 years. The need for novel therapeutics for the treatment of various diseases is desired for many applications, in particular a strategy which can be tailored for a specific disease such as a specific type of cancer. Non-viral gene delivery provided a therapeutic platform to which a large variety of nucleic acids can be utilized for gene therapy with a single non-viral delivery vector. This review discusses a variety of delivery vehicles which have been reported in literature and are well understood. Synthesis, toxicity, and transfection efficiency were included for each delivery vector. The use of theranostic materials and various delivery vector targeting strategies are an important aspect of the non-viral gene delivery field with examples of each and the future outlook included.

8.2 List of Abbreviations Used

PEI – Poly(ethyelenimine)
PGAA – poly(glycoamidoamine)
mRNA – messenger RNA
pDNA – plasmid DNA
RNAi – RNA interference
dsRNA – double stranded RNA
siRNA – small interfering RNA
PEG – poly(ethylene glycol)
ODN – oligodeoxynucleotides
AFM – atomic force microscopy
PAMAM – poly(amidoamines)
TAT – trans-activating transcriptional activator
RLU – relative light units
β-CD – β-cyclodextrin
AD-PEG – PEG with terminal adamantane

8.3 Introduction

8.3.1 Non-viral Gene Delivery

The field of non-viral nucleic acid delivery is fast growing and utilizing many unique types of nucleic acid delivery vehicles that have the capability to efficiently delivery therapies to specific cells. The expansion and growth of this area took off in 1995 when Behr, et al. showed how polyethylenimine (PEI) complexed with DNA and demonstrated excellent transfection efficiency.[1] These observations led the way for further investigations of macromolecules as therapeutic non-viral nucleic acid delivery vehicles. Strategies using small molecule therapeutics have been met with many problems that led to many failures in clinical trials such as poor pharmacokinetics and lack of efficacy.[2] There are a countless number of different delivery vehicles, each having its own properties. Some of the successful delivery vehicles that have been commercialized are PEI, which has high transfection efficiency but shows some cytotoxicity,[3] and chitosan. Chitosan has very low if any cytotoxicity, but poor delivery efficiency.[4] A polymeric non-viral delivery vehicle developed by Reineke, et al. termed PGAA (poly(glycoamidoamine)s), is in the process of being commercialized. PGAAs utilized the high delivery efficiency of PEI and the biocompatibility of chitosan.[5] These delivery vehicles, among others, have become the standard in many research institutions and laboratories.

All of these delivery vehicles have various extracellular and intracellular barriers to overcome on their way to deliver the nucleic acid payload. The extracellular barrier that needs to be considered first and foremost is the ability to compact nucleic acids into small nanosized particles, and protect the payload from degradation by nucleases. These nanoparticles need to avoid stimulating any immune response and any type of aggregation with itself or other non-targets. It is important to recognize, or target, a specific cell type and avoid non-specific binding.

143

Once the nanoparticle has reached the target cell there is an array of intracellular barriers to overcome. The nanoparticle must be internalized into the cell by receptor-mediated endocytosis or by interactions with the proteoglycans on the cell surface. Once inside the cell, the particle must escape the endosome before getting degraded and releasing its nucleic acid payload in the cytoplasm.[5,6] Once the nucleic acid is free in the cytoplasm, it must find its way to the nuclear envelope and pass through the nuclear pore complexes, which are only ~40 nm in diameter.[7] Once inside, the gene can be transcribed and eventually expressed in the cell.

Even though the viral approach to nucleic acid delivery shows excellent transfection efficiencies that exceed those of any non-viral delivery vehicle, there are still many problems that keep it from being clinically used. Issues such as targeting specific cell types and tissues have proved problematic.[8] Viral methods can elicit unwanted immune responses and tend to have problems with pathogenicity. There is also the risk of oversaturation of pathways that are essential in the production of certain proteins or function of the organism.[9] Viral approaches are also limited due to the size and amount of nucleic acids that can be delivered. These viruses tend to be expensive and difficult to produce.[10] These problems alone demonstrate the need for the development of non-viral delivery vehicles for nucleic acids that are biocompatible and very cell specific when delivering its cargo. The cell specificity is especially important in order to avoid non-specific interactions with healthy normal cells that could be damaged by the vehicles payload. The cellular specificity will also reduce the amount of the therapeutic that is necessary for treatment. The goal of the delivery vehicle is to enter into only the cells of interest and deliver the payload, which is why the incorporation of targeting moieties into the delivery vehicle is so important.

8.3.2 Nucleic Acids for Non-viral Delivery

144

The biological process of gene expression has been extensively studied and has become well understood. DNA in the nucleus of the cell is transcribed into messenger RNA (mRNA), which codes for proteins, by RNA polymerase. These mRNAs make their way to the cytoplasm where they are translated by ribosomes into the corresponding proteins.[11] Plasmid DNA (pDNA), which is a circular piece of double stranded DNA, has become a common nucleic acid used in many research and development institutions and has been utilized in studying transfection efficiency and pharmacokinetics.[12,13] pDNA can contain a gene of interest that codes for a specific protein, independent from the chromosomal DNA. RNA interference (RNAi) pathways can be exploited to disrupt this flow of genetic information, at mRNA level for example. This method of gene silencing was first recognized when studying nematodes and its biological response to double stranded RNA (dsRNA) which won the Nobel Prize in 2006.[14-16] One of the most popular technologies to exploit the RNAi pathways today is the use of small interfering RNA (siRNA). Long double stranded RNA molecules will get chopped into smaller dsRNA, around 21-23 nucleotides long, by the dicer enzyme. This creates two single stranded siRNAs which will attach to silencing complex called RISC. The activated RISC complex will then seek out and degrade the complementary mRNA.[17] The non-viral delivery of siRNA has had success in many different types of delivery vehicles such as a RGD peptide targeted poly(ethylene glycol) (PEG) PEI conjugate[18] and cyclodextrin containing cationic polymers, where both targeted cancer.[2] There are a few drawbacks to siRNA delivery that need to be considered when designing a siRNA system. There have been "off-target" interactions observed with some of these siRNA systems that have initiated immune response that can lead to many undesirable effects,[19] and some desired anti-tumor effects.[20]

Nucleic acids with catalytic effects such as DNAzymes have also been used in targeted non-viral delivery. Pun et al. demonstrated the effectiveness of DNAzymes as anti-cancer treatments.[21] Oligodeoxynucleotides (ODN) are sequences of nucleic acids that can have effective antisense activity or even immunostimulatory effects. These ODNs have been extensively studied to investigate their therapeutic possibilities including anti-tumor effects using a targeted liposome based delivery vehicle.[22] There are many opportunities for all these and other classes of nucleic acids to play an important role in complexing with various types of non-viral nucleic acid delivery for medicinal use.

8.3.3 Mechanisms of Endocytosis and Therapeutic Release

In order for the nucleic acid to do its job, it must be able to enter into the cell and deliver its nucleic acid payload. This entails an endocytosis mechanism by which the cell can internalize the polyplex, lipoplex, or another type of complexed system. The most studied mechanism for endocytosis involves a clathrin-dependent pathway and also a clathrin-independent pathway.[23] The clathrin mediated endocytosis usually involves a receptor-ligand type interaction, which is often termed receptor mediated endocytosis. Most receptors are internalized by the clathrin pathway, but there are some other pinocytic pathways that are capable of receptor mediated endocytosis.[24] The particles will start to accumulate on the surface of the cell then eventually a coated pit will form. This pit is coated with clathrin and eventually will get pinched off of the plasma membrane by dynamin and taken into the cell. This vesicle will eventually turn into an early endosome after the clathrin "coat" is shed. These endosomes will then fuse with others and form a lysosome. There are other possible pathways that have been studied for the internalization of these nucleic acid containing nanoparticles such as the caveolae mediated endocytosis. Caveolae are hydrophobic flask shaped invaginations on the cell surface, which are marked by a

membrane protein called caveolin. These caveolae will then be pinched off and become caveolar vesicles which are trafficked through the cell on microtubules. They will eventually reach a microtubule organizing center where the vesicle will potentially be taken into recycling endosomes. Caveolae mediated endocytosis is much different than the clathrin mechanism in that it is slow and there is no change in the pH of the caveolar vesicles once internalized.[24,25] There is still so much that is not known about how these nanoparticles are taken into the cell, such as what factors influence which uptake mechanism is used for nanoparticle uptake. Further understanding of these mechanisms will be essential in designing novel delivery vehicles.

Once these nanoparticles are taken into the cell by clathrin mediated endocytosis, they will experience a drop in the pH from 7.4 to about 6 in the lumen of the early endosomes. The pH will drop further to around pH 5 in the late endosome and lysosomes.[23] This gradual drop in pH, as the polyplex or lipoplex travels to the nucleus, has been visualized in real time by Davis et al. They were able to visualize, through confocal laser scanning microscopy, the pH change as the particle traveled through the cytoplasm to the nucleus in a single cell. A pH sensitive fluorophore called SNARF-4F was used to monitor the pH.[8]   At physiological pH, roughly 15%-20% of the secondary amines on linear PEI are protonated and carry a positive charge. When the pH drops to 5, this will increase to around 45%.[26] The delivery vehicle's cationic charge will start to increase with this decrease in pH. As this happens there will be a rush of negatively charged Cl^- ions coming into the cell to maintain the electroneutrality inside the endosome. It is proposed that the polyplex might start to swell as it gains the positive charge. It is this swelling and the influx of the Cl^- ions that will increase the osmotic pressure inside the endosome and cause it to become unstable. Eventually it will rupture and release the polyplex and cargo into the cytoplasm.[23,26] This is commonly known as the "proton sponge" effect. The exact mechanisms

for endocytosis and the release of the nucleic acid payload are still largely unknown. It has been demonstrated that the good buffering capacity of cationic delivery vehicles and imidazole substituents does not automatically correlate with better transfection efficiency.[8,10] A study done by May et al. suggests that in order for the proton sponge hypothesis to work, there must be some amount of free or uncomplexed polymer in the endosome along with the complexed polymer.[26] Substituents attached to the delivery vehicle such as histidine or imidazoles have been shown to act as efficient proton buffers and promote endosomal escape.[2,8,23]

8.4 Polymer Delivery Vectors

The use of cationic polymers has been an important tool in the field of non-viral delivery ever since it was shown how well PEI condenses DNA into small nanoparticles (polyplexes).[1] These cationic polymers interact with the anionic backbone of DNA through electrostatic interactions that allow the DNA to be compacted down into a nanoparticle.[5-7,23] The assembly, or compaction process, between a cationic polymer and DNA has been studied and visualized with atomic force microscopy (AFM). AFM experiments show how particles form different types of condensates and aids in the understanding of this compaction process.[27] The size of these polyplexes can range anywhere from 70 nm up to hundreds of nm depending on the cationic polymer, payload, and surrounding environment.[2] Changing the amounts of nucleic acid that is included in the polyplex will not only change the size of the particle, but also the N/P ratio. This molar ratio of nitrogen atoms on the cationic polymer to the phosphate groups in the DNA backbone will affect the transfection efficiency and gene expression. This could be due to the amount of charge, or zeta potential, that the polyplex will have. If the polyplex carries a strong positive zeta potential, this can cause non-specific interactions with plasma proteins and the cell surface. On the other hand it can also be detrimental to have a strongly negative charged particle

due to the increased risk of phagocytosis.[6] For these reasons a zeta potential of -10 mV to +10 mV is a reasonable range to use.[2] Each different polymer can vary on the optimum N/P ratio for effective gene expression or knockdown, but they usually fall in the range of N/P 5-10.[13,26] There has been an extensive amount of research done with cationic polymers, such as PEI and its derivatives,[3,8,10,28,29] poly(glycoamidoamine)s (PGAAs),[5,30-32] cyclodextrin containing polymers,[2,8,21,33,34] polyamidoamines (PAMAM),[27,35] and others.

8.4.1 Poly(ethylenimine)

Polyethylenimine (PEI) has been one of the most extensively studied cationic polymers in the field of non-viral delivery. PEI tends to have excellent transfection efficiency, but there is often a problem with high levels of cytotoxicity.[5,28] The cytotoxicity of PEI is affected by the molecular weight of the polymer. PEI with a low molecular weight, around 10,000, will still show high transfection efficiency, but with less toxic effects than PEI with MW of 25,000.[6,28] PEI can be in a linear or branched form, both having different delivery properties. Branched PEI inherently has much higher polydispersity than linear PEI, which is undesirable when developing a polymer delivery system. A recent study compared linear to branched PEI *in vivo* and *in vitro* and found that the transfection efficiency was highly dependent on the zeta potential and size of the particle. Some results suggest that branched PEI has the ability to compact DNA into a smaller particle and also have a higher zeta potential. This can increase the transfection efficiency, but it can also inhibit the gene expression due to the zeta potential being too high to allow for efficient unpacking of the DNA.[36] Linear PEI often demonstrates greater transfection efficiency, which could be due to a kinetic instability under physiological salt conditions.[37]

Linear PEI is commonly made through the polymerization of 2-methyl-2-oxazoline followed by the alkaline hydrolysis of the amide group on the secondary amine.[38] As for the

branched PEI, it usually is made by the acid catalyzed ring-opening polymerization of aziridine.[39] These can be prepared with varying molecular weights and degrees of branching. Degradable linear PEIs can be synthesized using a small molecular weight PEI and a diacrylate cross-linker. This Michael type addition, as seen in Scheme 8.1, will form ester linkages through the backbone of the polymer which provides degradation through hydrolysis.[40]

Scheme 8.1. Synthetic scheme for degradable linear PEI[40]
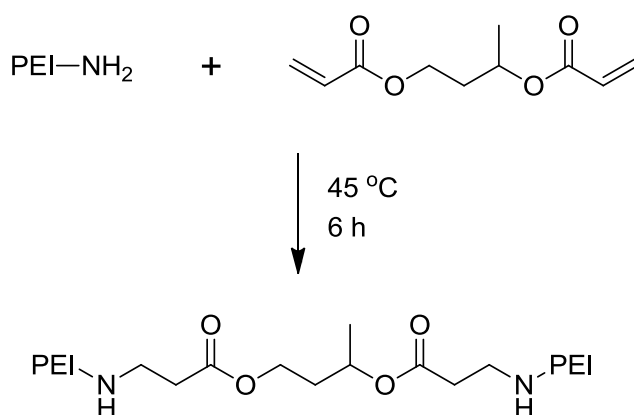
PEI has been modified to increase its biocompatibility as well as adding targeting moieties. For example, PEGylated PEI that is conjugated to small peptides such as the RGD peptide (Arg-Gly-Asp) shows increased tumor uptake and reduced toxicity.[18] A very recent study utilized a trans-activating transcriptional activator (TAT) peptide linked to PEG_{5000} and then conjugated to both linear and branched PEI. The use of TAT was inspired by the HIV virus that uses it for translocation across the cellular membrane. Incorporation of the TAT-peptide into the polyplex significantly enhanced the transfection efficiency, which was also influenced by the length of the linker. When the PEG_{5000} was incorporated, over the short propyl linker, there was almost a two fold increase in the relative light units (RLU) per mg of protein, which demonstrated much higher transfection efficiency.[41] Block copolymers of PEI and PEG, that

include various sizes of each block, have been shown to have transfection efficiency similar to that of a 25 kg/mol molecular weight branched PEI.[42] Park et al. used a PEG diacrylate and a 423 molecular weight PEI, as seen in Scheme 8.2, to synthesize a PEG-PEI copolymer. These copolymers demonstrated effective transfection efficiency, low cytotoxicity (over 80% viability), and readily degraded in PBS buffer at 37° C.[43]

Scheme 8.2. The proposed reaction scheme for formation of PEG-PEI copolymer[43]

PEI linear (Mn : 423)   PEG diacrylate (Mn : 258, 575 and 700)

PEI-*alt*-PEG

*Degree of polymerization

1 ≅ 9.43 (Mn : 423)
m ~ 3   (Mn : 258)
   ≅ 10   (Mn : 575)
   ≅ 13.5 (Mn : 700)
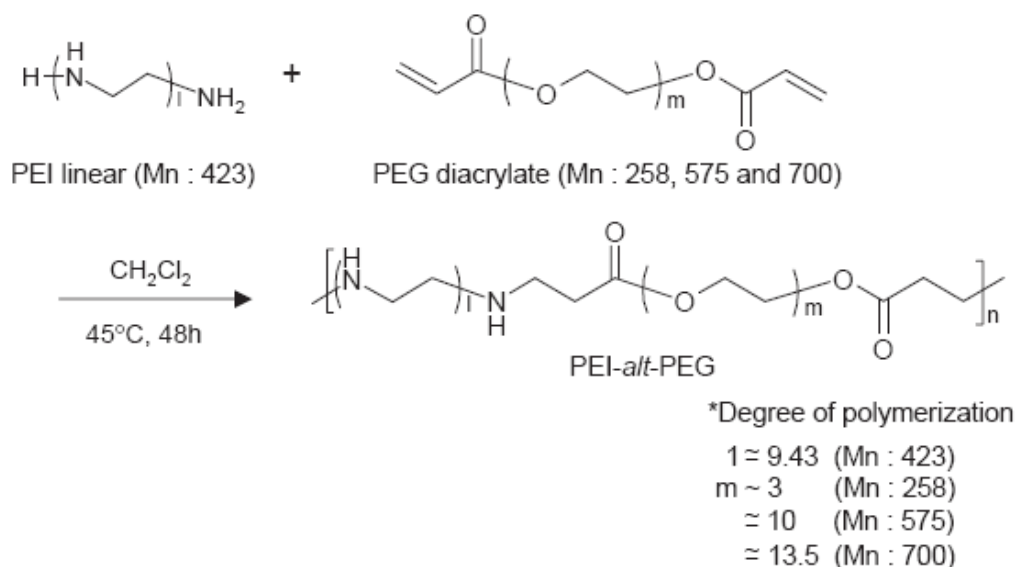
Other modifications include crosslinking low molecular weight PEI using cross-linkers that contain disulfide linkages, this makes the crosslinking reversible.[28] There are so many ways to modify PEI that they are too numerous to list, but many of these derivatives show efficient transfection, various amounts of cytotoxicity, and high endosomal buffering capacity.

8.4.2 Chitosan

Another cationic polymer that has been extensively studied and found in nature is chitosan. It is found in high concentrations in organisms such as crustaceans. It has been studied for many years due to its good biocompatibility and has the opposite transfection properties than

PEI.[44] The PEI has good transfection efficiencies but tends to be toxic and chitosan is low in toxicity but has poor transfection efficiency.[5] Chitosan is a cationic, biodegradable polysaccharide polymer[45] that shows no significant toxicity *in vivo* and *in vitro*[46] and can effectively bind and compact DNA. The polysaccharide structure of chitosan contains (1,4) linkages of D-glucosamine and *N-acetyl*-D-glucosamines.[47] Mao, et al. prepared their chitosan-DNA nanoparticles by a coacervation process and studied all the factors that influence particle size, zeta potential, protection capability, and transfection efficiency. Chitosan polymers are cationic at pH lower than 6.0, but tend to be close to neutral around physiological pH. In one study the observed zeta potential for these nanoparticles was +12 to +18 mV for a complex that contained a 2:1 ratio of chitosan to DNA at pH 6. The sizes of the particles were in the range of 100 to 250 nm in diameter. When targeting moieties were added there was an observed increase in transfection efficiency, as commonly seen with cationic polymers.[44]

8.4.3 Poly(glycoamidoamine)

As seen with the cases of PEI and chitosan, each cationic polymer exhibits a desirable and undesirable property. Reineke, et al. took up the challenge of developing a cationic polymer that took the desirable properties of both PEI and chitosan and incorporated it into a novel cationic polymer, poly(glycoamidoamines) (PGAAs). These PGAAs were synthesized using four different carbohydrates that included D-glucarate derivatives (D), galactarate derivative (G), D-mannaro1,4:6,3-dilactone (M), and L-tartarate (T). These carbohydrates contained ester groups and lactones that reacted with primary amines on oligoethylenamines to form the PGAA polymers through condensation polymerization.[48] The number of secondary amines on the oligoethylenamine molecules ranged from 1 to 4, as shown in Figure 8.1. With this design, the biocompatibility of carbohydrates will be exploited, as seen in chitosan. Properties such as

endosomal buffering and DNA compaction, which is seen with PEI, will be utilized via the oligoethylenamines. The PGAAs that contained four secondary amines had increased transfection efficiency and gene expression over those with fewer secondary amines.[13] The stereochemistry of the hydroxyl groups in the carbohydrates did have a significant effect on the gene expression as well as the transfection efficiency. Transfection efficiencies into HeLa cells were highest with G4, which were two fold greater than D4 and three fold higher than M4. The G4 stereochemistry also showed the highest luciferase gene expression around 10^9 RLU, which
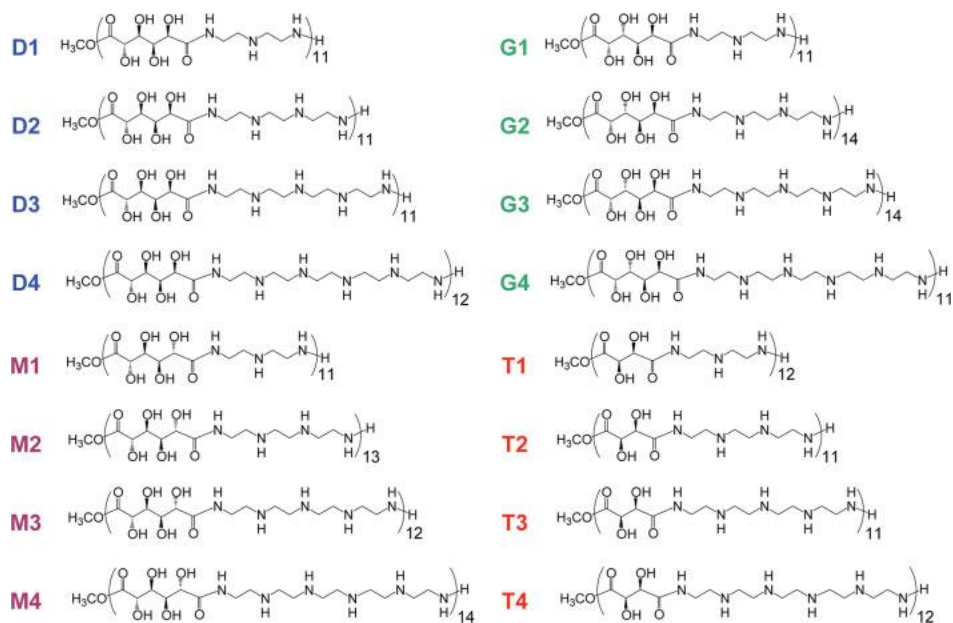
Figure 8.1. The 16 different PGAA polymers that were studied[5]

was about two fold greater than M4 and one fold greater than D4 at N/P 20.[13] G4 and T4 were shown to bind pDNA tighter and protect the nucleic acid from degradation which is thought to contribute to its higher gene expression.[48] These PGAAs showed little to no cytotoxicity, with most having greater than 90% viability.[5,13] Branched and linear PGAAs were compared to see if there is any increase in nucleic acid delivery properties as well as increasing the number of secondary amines in the oligoethylenamine structure. The same sugar units were used with the

branched and linear PGAAs and compared to the earlier generations seen in Figure 8.1. The number of secondary amines was increased from four to five and six, with branching occurring from these secondary amines. The branched PGAAs showed less toxicity and lower delivery efficiency which is also seen with PEI. The linear PGAAs demonstrated higher delivery efficiency, but the increase from four to five and six secondary amines increased the toxicity of the delivery vehicle.[49] Other structural variations that were studied include increasing the number of methylene units between the secondary amines. When a propylene and butylene spacer was used, versus the ethylene spacer, there was a dramatic increase in toxicity.[50] These results suggest that the previous G4 PGAA, with four secondary amines and ethylene spacers, is the most effective nucleic acid delivery vehicle in the series. Indeed, these PGAAs capture the benefits of both chitosan and PEI, which demonstrates the potential of this class of non-viral nucleic acids delivery vehicles. Other applications using these PGAAs include multilayer films composed of poly(L-tartaramidopentaethylenetetramine) (T4), which can be used for localized controlled release of nucleic acids.[32]

A novel PGAA polymer composed of trehalose and oligoethylenamine monomers was designed by Srinivasachari, et al. after the impressive results of the previous PGAA series. These click polymers, as seen in Figure 8.2, are polymerized via an alkyne-azide click reaction.[31] This polymer contains a trehalose structure to increase water solubility and improve the biocompatibility of the molecule. An oligoethylenamine chain is utilized for nucleic acid compaction and endosomal buffering. The amide triazole functionality that results from the alkyne-azide click reaction will aid in binding of nucleic acids through hydrogen bonding.[31]
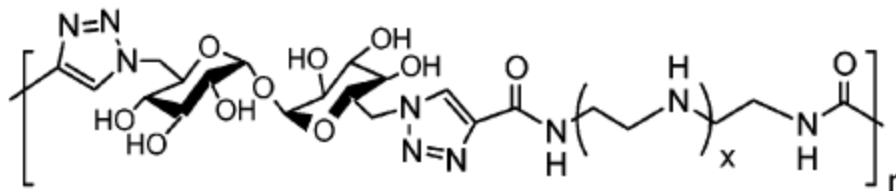
Figure 8.2. Structure of poly(trehalose) click polymer where x = 1-3 and n = 56-61[31]

The binding mechanism of pDNA with these click polymers varies with the number of secondary amines. Click polymers with only one secondary amine have higher protonation fractions and bind primarily through electrostatic interactions. As for the click polymers with more secondary amines, these bind pDNA through stronger hydrogen bonding interactions.[51] The delivery vehicles were able to compact pDNA into polyplexes with a particle size ranging from 100 nm in water up to large aggregates in Opti-MEM and DMEM serum media. The polymer that contained three secondary amines did not show any aggregation in serum. HeLa cell transfection efficiency for the polymers was highest for the polymer with the most secondary amines and demonstrated higher cellular uptake than commerically available Jet-PEI, at N/P 5, under all conditions tested. Jet-PEI did show higher luciferase gene expression in serum containing DMEM at N/P 3 − 15, but showed the same or less gene expression at N/P 15 and 25 in Opti-MEM. These click polymers showed cell viability greater than 80% where Jet-PEI only had around 50% cell viability at best.[31] The degree of polymerization, 35, 53, 75, and 100, of click polymers that contained four secondary amines had an effect on aggregation and serum stability. Polyplexes with a degree of polymerization of 35 would aggregate fast while the polyplexes formed with the larger polymers inhibited aggregation. There was no significant effect on pDNA compaction and protection as well as the cellular uptake with longer chains. Other than serum stability, the luciferase gene expression and toxicity was effected by the change in molecular weight of the polymer. The click polymers with greater degrees of polymerization showed higher

toxicity, but always less than PEI, and an increase in gene expression with the increase in polymer size. This suggests that the endosomal release could be affected by the length of the click polymers.[30]

8.4.4 Cyclodextrin Containing Polymers

The incorporation of β-cyclodextrin (β-CD) into the backbone of cationic polymers for nucleic acid delivery has become a hot area of research in recent years. One of the reasons for this is when β-CD is incorporated into a polymers backbone, there has been a decrease in the cytotoxicity when compared to the same polymers without the β-CD.[33] There is also an increase in solubility of the polymer when the β-CD is incorporated.[2] The most useful aspect of β-CD containing polymers is the inclusion complexes that can be formed with the β-CD structure. β-CD is a cup shaped molecule which has a hydrophobic interior and hydrophilic exterior.[52] β-CD has the ability to form strong inclusion complexes with hydrophobic "guest" molecules such as adamantane or cholesterol.[52-54]

Davis, et al. introduced a novel class of β-CD containing polymers in 1999 which has led the way in β-CD containing polymers.[2,52] They demonstrate that the linker between the β-CD has a dramatic influence on the capability to bind DNA. This is due to the steric hindrance that is involved when the linker between the β-CD components is short.[2,33] The β-CD containing polymers were synthesized by a condensation reaction between a di-amino β-CD monomer and a diimidate comonomer. The transfection efficiencies were dramatically affected with the different lengths of the linkers. The linker that contained six methylene units showed the best transfection efficiency in the series.[33] These β-CD containing polymers were included in a formulation with a PEG$_{5000}$ chain equipped with an adamantane head group (AD-PEG). These AD-PEG agents would strongly bind with the β-CD units in the backbone creating inclusion complexes and

provide a strong stabilization effect. The polyplexes formed had a particle size around 100 nm with a tunable zeta potential. Some of the AD-PEG molecules were conjugated with targeting moieties that eventually lead to targeted delivery of siRNA in humans.[2] Another β-CD containing polymer that was developed by Srinivasachari, et al. employed a backbone composed of β-CD separated by a oligoethylenamine spacer which contained one to four secondary amines (Figure 8.3). They were synthesized via the alkyne-azide click reaction between diazide functionalized β-CDs and terminal alkyne functionalized oligoethylenamines. These polymers were able to efficiently compact pDNA and formed polyplexes with a diameter of $70 - 120$ nm in water. The polymers with four secondary amines demonstrated the best delivery efficiency and lowest toxicity. They also showed cellular uptake two fold higher than that of Jet-PEI, but slightly lower gene expression than the PEI at N/P 5 and 10. One of the most promising results was from the toxicity studies. The β-CD containing polymers showed very little, if any, toxicity
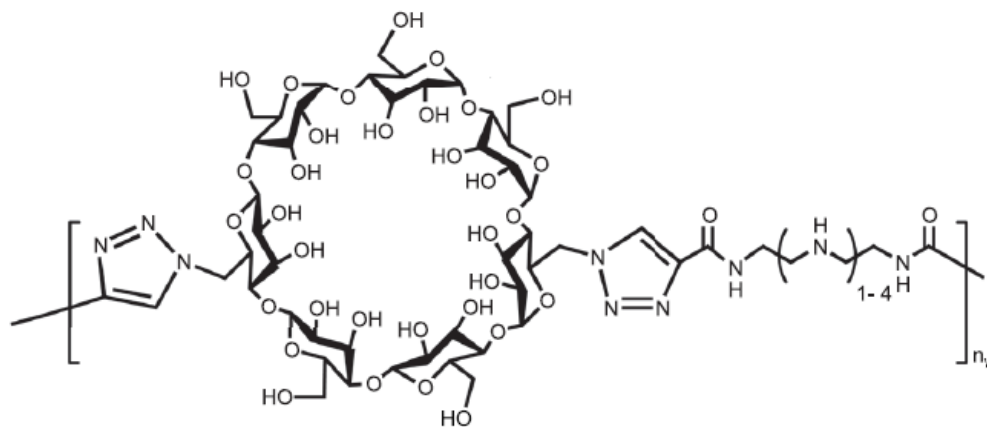
Figure 8.3. β-CD click copolymer developed by Srinivasachari et. al[34]

for the various sized polymers while Jet-PEI had around 55% cell viability.[34] These β-CD click polymers proved to be efficient delivery vehicles that warrant further study into its structure and function as well as targeted inclusion complexes. Burckbuchler, et al. used a β-CD polymer

157

made from β-CD and epichlorohydrin. They then employed cationic adamantyl derivatives to form inclusion complexes with the β-CD components that would in turn bind with DNA and form polyplexes.[55] There are many types of β-CD containing polymers that have been studied as potential delivery vehicles including polymers with pendent chains that contain β-CD.[56] Many of these β-CD polymers have proved to be effective nucleic acid delivery vehicles and can play an important role in the development of very effective non-viral delivery vehicles. One recent success in the specific targeting of cells using these β-CD containing polymers is demonstrated in work done by Dr. Mark Davis. The siRNA delivery system developed by his lab can deliver its cargo specifically to tumor cells and efficiently inhibit tumor growth. It is now in phase I clinical trials. This study marks the first time siRNA has successfully been delivered to a human using a synthetic targeted delivery system.[2]

8.5 Dendrimer Delivery Vectors

8.5.1 Poly(amidoamines)

The use of dendrimers as a delivery vehicle for nucleic acids has been investigated and shown to be effective. Macromolecules such as poly(amidoamine) (PAMAM) dendrimers have been shown to compact nucleic acids and deliver them into the cell, which was first studied by Haensler and Szoka in 1993.[47] These well-defined dendritic structures are synthesized using methyl acrylate and ethylenediamine as seen in Figure 8.4. Traditionally an ammonia core is used to build the dendrimer, but other cores such as tris(2-aminoethyl)amine[57] and
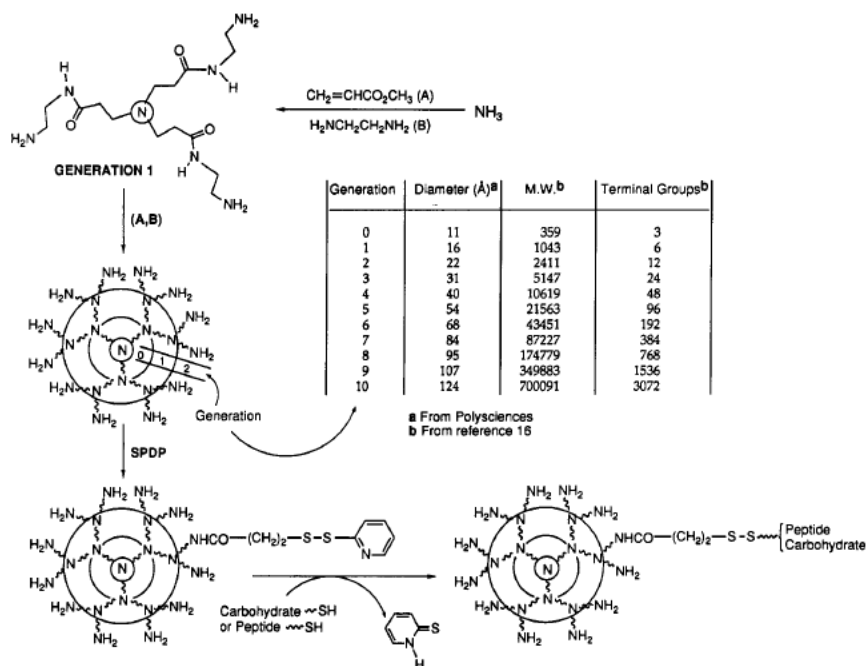
Figure 8.4. Synthetic scheme and size of multiple generations of PAMAM dendrimers[57]

triethanolamine[58] have also shown to be effective cores in the synthesis of PAMAM. They can be built up via generations to give a desired size and molecular weight. The N/P ratios for successful complexation with DNA have been reported to be from 6 to 10.[35,57] The size, or generation, of the PAMAM dendrimer had a large effect on the transfection efficiency. Generations of dendrimers such as G5 to G10 all showed the high transfection efficiency, but the efficiency was cell dependent.[47] It was found that these large dendrimers had optimal properties at an N/P of around 6. These PAMAM-nucleic acid complexes showed minimal to no cytotoxicity and are very well tolerated by the cells.[57,58] Tang, et al. created impure degraded PAMAM dendrimers by heating them in n-butanol and water. These degraded structures exhibited higher transfection efficiencies than the previous PAMAM molecules.[59] Many different PAMAM conjugates have been made and studied over the years. For example Huang, et al. developed a PAMAM-PEG-Lactoferrin conjugate for targeted delivery to the brain. Lactoferrin receptors have been shown to be over expressed in the blood-brain barrier area and

overexpressed in people with Parkinson's disease. This lactoferrin receptor targeted conjugate showed a 2.2 fold increase in brain uptake over PAMAM-PEG-Transferrin and around a 4 fold increase over PAMAM alone.[35]

8.5.2 Click Clusters

Another class of macromolecules that have shown potential to be efficient delivery vehicles is the "click clusters" produced by Srinivasachari et al (Figure 8.5). These "click clusters" are dendrimers built off a β-CD scaffold, which is very stable and biocompatible. β-CD, as described earlier, has a hydrophobic cup that has been used to increase the solubility of hydrophobic drugs by forming an inclusion complex and protecting them from degradation.[60] These click clusters were synthesized by first functionalizing the β-CD at carbon 6 of each of the glucose units in the structure (Scheme 8.3). The hydroxyl group at carbon 6 is replaced by an azide group after a series of reactions giving an acetylated per-azido-β-CD. This is "clicked" with an alkyne functionalized dendron, which contains 0 to 4 secondary amines that are needed for the compaction of nucleic acids, through the azide alkyne click reaction (Scheme 8.4). These "click clusters" efficiently compacted DNA to form particles that ranged from 80 nm to 120 nm in size and exhibited a zeta potential from 0 mV to around 24 mV. The results indicated that the "click cluster" with the largest number of secondary amines provided the most efficient delivery vehicle. These vehicles exhibited transfection efficiencies in the range of 10^4 to 10^5 RLU, which was comparable to Jet-PEI and Superfect transfection reagent, at an N/P of 20. The "click cluster" with 4 secondary amines exhibited gene expression that was similar or better than that of Jet-PEI and Superfect, as well as showing cell viability close to 100%.[61] A PEG molecule conjugated to an adamantane could provide steric stabilization of the nanoparticle. The AD-PEG
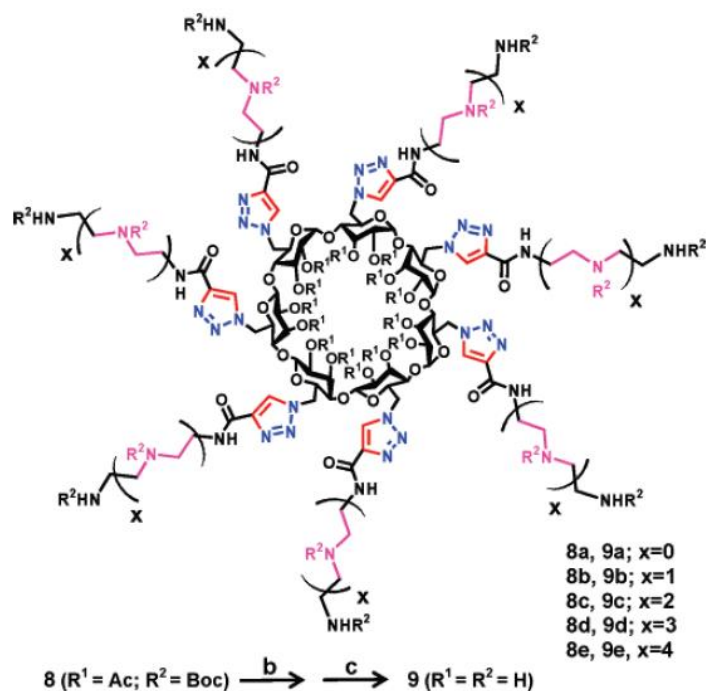
Figure 8.5. The series of "Click Clusters" synthesized that vary in the number of secondary amines in the dendron arm. (b) NaOMe/MeOH, pH = 9, RT; (c) 4 M HCl/dioxane[61]

Scheme 8.3. Synthetic scheme of acetylated per-azido-β-CD. (a) PPh$_3$/I2, DMF, 80 °C, 18 h; (b) NaN$_3$, DMF, 80 °C, 24 h; (c) Ac$_2$O, Pyr, 24 h, RT[61]
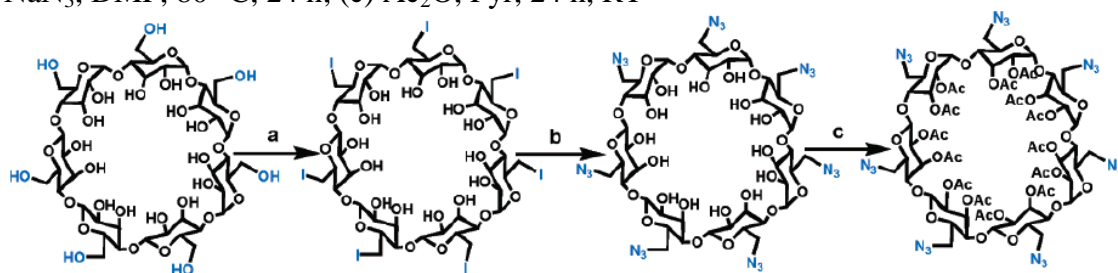
Scheme 8.4. Synthesis of alkyne dendrons. (a) CF$_3$COOEt, MeOH; (b) (Boc)$_2$O, CH$_2$Cl$_2$, TEA; (c) K$_2$CO$_3$, 20:1, MeOH: H$_2$O; (d) propiolic acid, DCC, CH$_2$Cl$_2$[61]

5a, 6a, 7a; x=0
5b, 6b, 7b; x=1
5c, 6c, 7c; x=2
5d, 6d, 7d; x=3
5e, 6e, 7e; x=4

161
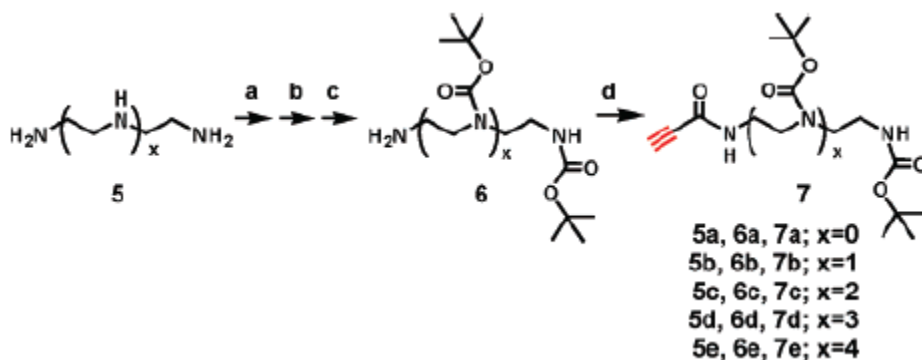
conjugate could also be modified to include a targeting moiety to improve cellular uptake and specificity.[2,34] These types of macromolecules that were discussed above, among others, demonstrate yet another class of delivery vehicles that can efficiently deliver nucleic acids into the cell. There is much more work to be done in the optimization of dendritic type delivery vehicles with an almost endless possibility of novel structures and functions.

8.6 Theranostics

The goal of many delivery vehicle designs is the incorporation of some type of imaging agent on the delivery vehicle. This would allow for the delivery of the nucleic acids to be visualized using methods such as MRI, PET, or fluorescent dyes. The advantage is the noninvasive visualization of the delivery of therapeutics into a target cell type. The specificity and localization of the particles can then be investigated to help assess the delivery vehicles'
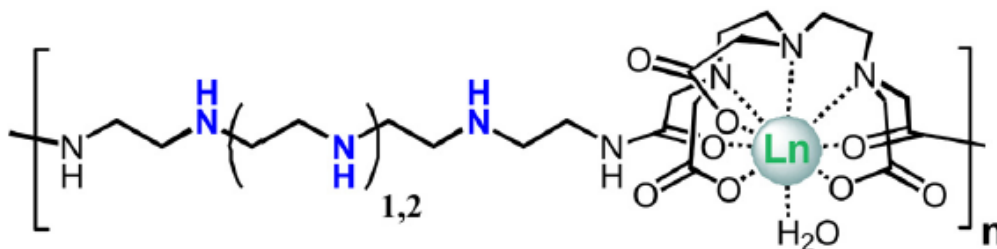
Figure 8.6. The polymer structure of the theranostic delivery vehicle. Ln = Eu3+ (luminesces red) or Gd3+ (MRI active)[62]

efficiency. A recent example of this is work done by Santra et al where they developed a paramagnetic iron oxide nanoparticle with therapeutic and dual imaging properties. A polymer coating over the iron oxide nanoparticle provides a carrier for the therapeutic drug and a NIR dye. This gives the nanoparticle a therapeutic capability, MRI imaging, and optical imaging of the internalization of the particle into the cell.[63] Bryson, et al. developed a set of novel theranostic agents that are composed of two different monomers (Figure 8.6). One monomer in

the chain contained secondary amines that can be positively charged at physiological pH, which is necessary for the compaction of nucleic acids. The second monomer contained a lanthanide chelating agent. Gadolinium (Gd^{3+}) or europium (Eu^{3+}) will bind very well with the chelating monomer to provide two different types of diagnostic properties. The Eu^{3+} will provide a luminescent property for microscopy, while the Gd^{3+} provides an excellent paramagnetic center for MRI. These will allow for the visualization of the delivery vehicle and provide a powerful theranostic tool.[62] These new designs, among others, will change the way many non-viral nucleic acid delivery vehicles are designed and further our understanding of how these vehicles work.

8.7 Delivery Vector Targeting Strategies

Developing delivery vehicles that have the ability to target specific cell types to deliver the nucleic acid payload has become an important aspect of non-viral delivery. When adding a target to the delivery system, a very significant increase in cellular uptake and RNA interference is observed over the untargeted system.[2] Depending on the nature of the nucleic acid payload, it might be detrimental for the delivery vehicle to interact or be endocytosed by any other cell but the target cell. These reasons alone demonstrate the importance of specific targeting and localization.

Many of the targeted non-viral delivery systems have traditionally utilized transferrin protein and folate as targeting groups covalently attached to the delivery vehicle. Tumor cells can proliferate very quickly, which requires a high activity of the ribonucleotide reductase protein. This protein catalyzes the conversion of ribonucleotides to deoxyribonucleotides which plays an important role in cell proliferation. In order for the activity of the reductase protein to continue, there must be iron present in the surrounding environment. If the tumor is going to have enough iron present in the cells to keep up with the reductase activity, there must be a large

amount of iron uptake into the cell. This rapid iron uptake requires an over expression of the transferrin receptor on the tumor cell membrane.[64] This is a reason why using transferrin as a targeting group has been so popular over the years. It has been recently shown that the transferrin receptor plays more of a role in tumor growth than just regulating the iron uptake. It has been shown to play an important role in the production of E-twenty six transcription factors as well as affecting the neuron mass in glioma cells. This reduction of surrounding neuron cells is completed by the *N*-methyl-D-aspartate receptor that is turned on by glutamate. The transferrin receptor will then promote glioma spreading by increasing the proliferation rate and also the amount of glutamate released.[65]

The over expression of the folate receptor is another common feature in many different cancer cells. This receptor is a glycosylphosphatidylinositol-anchored membrane protein that is responsible for the uptake of folic acid.[66] Folates are brought into the cell by receptor mediated endocytosis, and are an essential nutrient for eukaryotic cells. It is present on every cell to some concentration, but at much higher concentrations on cancer cells to provide a growth advantage. Eukaryotic cells don't have the necessary components to synthesize these folates so the ability of the cancer cells to scavenge all the surrounding folates keeps it proliferating at a fast rate. There are two types of folate receptors, a low and high affinity receptor. The low affinity receptor injects the folates directly into the cytoplasm while the high affinity receptor takes the folate into the cell by endocytosis. It is the high affinity receptor that is over expressed on many cancers.[67]

There have been a lot of new technologies associated with cell specific targeting in recent years. One popular design for specific targeting is the use of antibody fragments. Antibodies are proteins used by the immune system to identify and destroy bacteria, viruses, and other foreign substance in the body. They contain four parts, two longer heavy chains and two shorter smaller

chains. The whole antibody or fragments of it can be used to specifically target types of cells. For example, antibody fragments that are specific for cell adhesion molecules can be targeted and tend to be internalized into the cell very fast. This happens when the size of the particle it is attached to is around 100 to 500 nm.[68,69] There is a wide variety of these types of anti-bodies which gives the ability to be very selective in the targeting. It is commonly known that the transferrin receptor is over expressed in tumor cells as previously discussed. This over expression can be exploited using antibody fragments instead of the transferrin protein. An anti-transferrin receptor single-chain antibody fragments has been shown to efficiently target tumor. Increases in the delivery of siRNA and tumor suppression were observed.[70] Fab fragments of an HIV-1 envelope antibody have also been used to silence a F105-P protein in cells expressing HIV-1 envelope and not effecting normal cells. These along with many other cancer targeting antibodies have proved useful.[71] An antibody, either being whole or a fragment, can often be developed to target receptors or other plasma membrane components. This offers a powerful tool in non-viral nucleic acid delivery that can be used to deliver payloads specific to a targeted cell.

Peptide sequences, other than those used in antibodies, offer many useful targeting agents. A targeting agent that has been used recently called transactivator of transcription (TAT), which is used by the HIV virus.[41] This acts as a protein transduction domain that will mediate the binding to negatively charged components of the plasma membrane. This will promote cellular uptake and trafficking to the nucleus.[68] It has been shown that the conjugation of this TAT peptide to branched PEI-PEG polymer significantly increases the gene transfection over that of the unconjugated PEI-PEG, Lipofectamine 2000, and PEI.[41]

Integrins play a very important role in angiogenesis and are over expressed in tumor cells in order to provide more blood to the tumor. A handful of these integrins have been studied

extensively.[72] Some small peptides have been developed to exploit this over expression such as the RGD peptide. This peptide is composed of an Arg-Gly-Asp which will target the tumor neovasculature that is expressing the integrins.[18] The RGD peptide is recognized by the αvβ3 and αvβ5 intergins, which are questionable as to their role in tumor growth.[72] Another very similar targeting peptide is a RGDK peptide (Arg-Gly-Asp-Lys). This RGDK ligand is recognized by the αvβ1 integrin, which is has been shown to definitely be a proangiogenic integrin receptor. The used of this targeting peptide has been shown to have remarkable selectivity for the αvβ1 integrin receptor and directed the delivery vehicle in the inhibition of certain cancer models.[72] There are so many new receptors and targets being discovered for specific cell types. This will provide powerful tools for those in the field of non-viral nucleic acid delivery because it demonstrates an almost countless number of potential targets for the delivery vehicles.

A common way of attaching a targeting group to a system is incorporating PEG to the delivery vehicle. PEG serves a few different functions when attached to a delivery system. The targeting ligand is then attached to the opposite side of the PEG linker with respect to the delivery vehicle. The method of PEGylation will improve the solubility and biocompatibility of the vehicle as well as providing a "masking" of the cationic or anionic nature of the delivery vehicle.[73] PEGylation will also reduce unintended interactions with negatively charged blood components and non-targeted cells.[29] In some systems the PEGylation can provide a stabilization effect that helps control the size of the nanoparticle.[2] PEGylation has also been used in many systems and will continue to be a useful linker to connect the targeting moieties onto.[18,21,29,35,74]

8.8 References

(1)   Boussif, O.; Lezoualch, F.; Zanta, M. A.; Mergny, M. D.; Scherman, D.; Demeneix, B.; Behr, J. P. *Proceedings of the National Academy of Science U. S. A.* **1995**, *92*, 7297.
(2)   Davis, M. E. *Molecular Pharmacology* **2009**, *6*, 659.
(3)   Chollet, P.; Favrot, M. C.; Hurbin, A.; Coll, J. L. *Journal of Gene Medicine* **2002**, *4*, 84.

(4)   MacLaughlin, F. C.; Mumper, R. J.; Wang, J. J.; Tagliaferri, J. M.; Gill, I.; Hinchcliffe, M.; Rolland, A. P. *Journal of Controlled Release* **1998**, *56*, 259.

(5)   Reineke, T. M. *Journal of Polymer Science Polymer Chemistry* **2006**, *44*, 6895.

(6)   Davis, M. E. *Current Opinion in Biotechnology* **2002**, *13*, 128.

(7)   Lentacker, I.; Vandenbroucke, R. E.; Lucas, B.; Demeester, J.; De Smedt, S. C.; Sanders, N. N. *Journal of Controlled Release* **2008**, *132*, 279.

(8)   Kulkarni, R. P.; Mishra, S.; Fraser, S. E.; Davis, M. E. *Bioconjugate Chemistry* **2005**, *16*, 986.

(9)   Grimm, D.; Streetz, K. L.; Jopling, C. L.; Storm, T. A.; Pandey, K.; Davis, C. R.; Marion, P.; Salazar, F.; Kay, M. A. *Nature* **2006**, *441*, 537.

(10)   Forrest, M. L.; Meister, G. E.; Koerber, J. T.; Pack, D. W. *Pharmaceutical Research* **2004**, *21*, 365.

(11)   Sarkar, S. *Trends In Biochemical Sciences* **1998**, *23*, 312.

(12)   Moriguchi, R.; Kogure, K.; Harashima, H. *International Journal of Pharmaceutics* **2008**, *363*, 192.

(13)   Liu, Y. M.; Reineke, T. M. *Journal of the American Chemical Society* **2005**, *127*, 3004.

(14)   Hannon, G. J.; Rossi, J. J. *Nature* **2004**, *431*, 371.

(15)   Fire, A.; Albertson, D.; Harrison, S. W.; Moerman, D. G. *Development* **1991**, *113*, 503.

(16)   Fire, A.; Xu, S. Q.; Montgomery, M. K.; Kostas, S. A.; Driver, S. E.; Mello, C. C. *Nature* **1998**, *391*, 806.

(17)   Akhtar, S.; Benter, I. F. *The Journal of Clinical Investigation* **2007**, *117*, 3623.

(18)   Schiffelers, R. M.; Ansari, A.; Xu, J.; Zhou, Q.; Tang, Q.; Storm, G.; Molema, G.; Lu, P. Y.; Scaria, P. V.; Woodle, M. C. *Nucleic Acids Research* **2004**, *32*, e149.

(19)   Robbins, M.; Judge, A.; MacLachlan, I. *Oligonucleotides* **2009**, *19*, 89.

(20)   Poeck, H.; Besch, R.; Maihoefer, C.; Renn, M.; Tormo, D.; Morskaya, S. S.; Kirschnek, S.; Gaffal, E.; Landsberg, J.; Hellmuth, J.; Schmidt, A.; Anz, D.; Bscheider, M.; Schwerd, T.; Berking, C.; Bourquin, C.; Kalinke, U.; Kremmer, E.; Kato, H.; Akira, S.; Meyers, R.; Hacker, G.; Neuenhahn, M.; Busch, D.; Ruland, J.; Rothenfusser, S.; Prinz, M.; Hornung, V.; Endres, S.; Tuting, T.; Hartmann, G. *Nature Medicine* **2008**, *14*, 1256.

(21)   Pun, S. H.; Tack, F.; Bellocq, N. C.; Cheng, J. J.; Grubbs, B. H.; Jensen, G. S.; Davis, M. E.; Brewster, M.; Janicot, M.; Janssens, B.; Floren, W.; Bakker, A. *Cancer Biology and Therapy* **2004**, *3*, 641.

(22)   Hamzah, J.; Altin, J. G.; Herringson, T.; Parish, C. R.; Hammerling, G. J.; O'Donoghue, H.; Ganss, R. *Journal of Immunology* **2009**, *183*, 1091.

(23)   Midoux, P.; Pichon, C.; Yaouanc, J.-J.; Jaffrès, P.-A. *British Journal of Pharmacology* **2009**, *157*, 166.

(24)   Khalil, I. A.; Kogure, K.; Akita, H.; Harashima, H. *Pharmacological Reviews* **2006**, *58*, 32.

(25)   Medina-Kauwe, L. K.; Xie, J.; Hamm-Alvarez, S. *Gene Therapy* **2005**, *12*, 1734.

(26)   Yang, S.; May, S. *J. Chem. Phys.* **2008**, *129*.

(27)   Martin, A. L.; Davies, M. C.; Rackstraw, B. J.; Roberts, C. J.; Stolnik, S.; Tendler, S. J. B.; Williams, P. M. *FEBS Letters* **2000**, *480*, 106.

(28)   Gosselin, M. A.; Guo, W.; Lee, R. J. *Bioconjugate Chemistry* **2001**, *12*, 989.

(29)   Ogris, M.; Walker, G.; Blessing, T.; Kircheis, R.; Wolschek, M.; Wagner, E. In *2nd International Symposium on Tumor Targeted Delivery Systems*; Sp. Iss. SI ed.; Elsevier Science Bv: Bethesda, Maryland, 2002; Vol. 91, p 173.

(30)   Srinivasachari, S.; Liu, Y. M.; Prevette, L. E.; Reineke, T. M. *Biomaterials* **2007**, *28*, 2885.
(31)   Srinivasachari, S.; Liu, Y. M.; Zhang, G. D.; Prevette, L.; Reineke, T. M. *Journal of the American Chemical Society* **2006**, *128*, 8176.
(32)   Taori, V. P.; Liu, Y. M.; Reineke, T. M. *Acta Biomaterialia* **2009**, *5*, 925.
(33)   Hwang, S. J.; Bellocq, N. C.; Davis, M. E. *Bioconjugate Chemistry* **2001**, *12*, 280.
(34)   Srinivasachari, S.; Reineke, T. M. *Biomaterials* **2009**, *30*, 928.
(35)   Huang, R. Q.; Ke, W. L.; Liu, Y.; Jiang, C.; Pei, Y. Y. *Biomaterials* **2008**, *29*, 238.
(36)   Intra, J.; Salem, A. K. *Journal of Controlled Release* **2008**, *130*, 129.
(37)   Wightman, L.; Kircheis, R.; Rossler, V.; Carotta, S.; Ruzicka, R.; Kursa, M.; Wagner, E. *Journal of Gene Medicine* **2001**, *3*, 362.
(38)   Akiyama, Y.; Harada, A.; Nagasaki, Y.; Kataoka, K. *Macromolecules* **2000**, *33*, 5841.
(39)   Fischer, D.; Bieber, T.; Li, Y. X.; Elsasser, H. P.; Kissel, T. *Pharmaceutical Research* **1999**, *16*, 1273.
(40)   Jiang, H. L.; Arote, R.; Jere, D.; Kim, Y. K.; Cho, M. H.; Cho, C. S. *Journal of Materials Science and Technology* **2008**, *24*, 1118.
(41)   Roy, R.; Jerry, D. J.; Thayumanavan, S. *Biomacromolecules* **2009**, *10*, 2189.
(42)   Zhong, Z. Y.; Feijen, J.; Lok, M. C.; Hennink, W. E.; Christensen, L. V.; Yockman, J. W.; Kim, Y. H.; Kim, S. W. *Biomacromolecules* **2005**, *6*, 3440.
(43)   Park, M. R.; Han, K. O.; Han, I. K.; Cho, M. H.; Nah, J. W.; Choi, Y. J.; Cho, C. S. *Journal of Controlled Release* **2005**, *105*, 367.
(44)   Mao, H. Q.; Roy, K.; Troung-Le, V. L.; Janes, K. A.; Lin, K. Y.; Wang, Y.; August, J. T.; Leong, K. W. *Journal of Controlled Release* **2001**, *70*, 399.
(45)   Onishi, H.; Machida, Y. *Biomaterials* **1999**, *20*, 175.
(46)   Aspden, T. J.; Mason, J. D. T.; Jones, N. S.; Lowe, J.; Skaugrud, O.; Illum, L. *Journal Pharmaceutical Sciences* **1997**, *86*, 509.
(47)   Mintzer, M. A.; Simanek, E. E. *Chemical Reviews* **2009**, *109*, 259.
(48)   Liu, Y. M.; Reineke, T. M. *Bioconjugate Chemistry* **2006**, *17*, 101.
(49)   Lee, C. C.; Liu, Y.; Reineke, T. M. *Bioconjugate Chemistry* **2008**, *19*, 428.
(50)   Liu, Y. M.; Reineke, T. M. *Bioconjugate Chemistry* **2007**, *18*, 19.
(51)   Prevette, L. E.; Lynch, M. L.; Kizjakina, K.; Reineke, T. M. *Langmuir* **2008**, *24*, 8090.
(52)   Pack, D. W.; Hoffman, A. S.; Pun, S.; Stayton, P. S. *Nature Reviews Drug Discovery* **2005**, *4*, 581.
(53)   Wintgens, W.; Amiel, C. *Journal Photochemistry and Photobiology A-Chemistry* **2005**, *173*, 228.
(54)   Shu, H. J.; Zeng, C. M.; Wang, C.; Covey, D. F.; Zorumski, C. F.; Mennerick, S. *British Journal of Pharmacology* **2007**, *150*, 164.
(55)   Burckbuchler, V.; Wintgens, V.; Leborgne, C.; Lecomte, S.; Leygue, N.; Scherman, D.; Kichler, A.; Amiel, C. *Bioconjugate Chemistry* **2008**, *19*, 2311.
(56)   Ren, S. D.; Chen, D. Y.; Jiang, M. *Journal Polymer Science Polymer Chemistry* **2009**, *47*, 4267.
(57)   Haensler, J.; Szoka, F. C. *Bioconjugate Chemistry* **2002**, *4*, 372.
(58)   Liu, X. X.; Rocchi, P.; Qu, F. Q.; Zheng, S. Q.; Liang, Z. C.; Gleave, M.; Iovanna, J.; Peng, L. *ChemMedChem* **2009**, *4*, 1302.
(59)   Tang, M. X.; Redemann, C. T.; Szoka, F. C. *Bioconjugate Chemistry* **1996**, *7*, 703.

(60)   Cryan, S. A.; Holohan, A.; Donohue, R.; Darcy, R.; O'Driscoll, C. M. *European Journal of Pharmaceutical Sciences* **2004**, *21*, 625.

(61)   Srinivasachari, S.; Fichter, K. M.; Reineke, T. M. *Journal of the American Chemical Society* **2008**, *130*, 4618.

(62)   Bryson, J. M.; Fichter, K. M.; Chu, W. J.; Lee, J. H.; Li, J.; Madsen, L. A.; McLendon, P. M.; Reineke, T. M. *Proceedings of the National Academy of Science U. S. A.* **2009**, *106*, 16913.

(63)   Santra, S.; Kaittanis, C.; Grimm, J.; Perez, J. M. *Small* **2009**, *5*, 1862.

(64)   Testa, U.; Pelosi, E.; Peschle, C. *Critical Reviews in Oncogenesis* **1993**, *4*, 241.

(65)   Chirasani, S. R.; Markovic, D. S.; Synowitz, M.; Eichler, S. A.; Wisniewski, P.; Kaminska, B.; Otto, A.; Wanker, E.; Schafer, M.; Chiarugi, P.; Meier, J. C.; Kettenmann, H.; Glass, R. *Journal Molecular Medicine* **2009**, *87*, 153.

(66)   Parker, N.; Turk, M. J.; Westrick, E.; Lewis, J. D.; Low, P. S.; Leamon, C. P. *Analytical Biochemistry* **2005**, *338*, 284.

(67)   Leamon, C. P.; Low, P. S. *Drug Discovery Today* **2001**, *6*, 44.

(68)   Ding, B. S.; Dziubla, T.; Shuvaev, V. V.; Muro, S.; Muzykantov, V. R. *Molecular Interventions* **2006**, *6*, 98.

(69)   Wiewrodt, R.; Thomas, A. P.; Cipelletti, L.; Christofidou-Solomidou, M.; Weitz, D. A.; Feinstein, S. I.; Schaffer, D.; Albelda, S. M.; Koval, M.; Muzykantov, V. R. *Blood* **2002**, *99*, 912.

(70)   Pirollo, K. F.; Rait, A.; Zhou, Q.; Hwang, S. H.; Dagata, J. A.; Zon, G.; Hogrefe, R. I.; Palchik, G.; Chang, E. H. *Cancer Research* **2007**, *67*, 2938.

(71)   Song, E. W.; Zhu, P. C.; Lee, S. K.; Chowdhury, D.; Kussman, S.; Dykxhoorn, D. M.; Feng, Y.; Palliser, D.; Weiner, D. B.; Shankar, P.; Marasco, W. A.; Lieberman, J. *Nature Biotechnology* **2005**, *23*, 709.

(72)   Pramanik, D.; Majeti, B. K.; Mondal, G.; Karmali, P. P.; Sistla, R.; Ramprasad, O. G.; Srinivas, G.; Pande, G.; Chaudhuri, A. *Journal of Medicinal Chemistry* **2008**, *51*, 7298.

(73)   McNeeley, K. M.; Karathanasis, E.; Annapragada, A. V.; Bellamkonda, R. V. *Biomaterials* **2009**, *30*, 3986.

(74)   Nie, Y.; Zhang, Z. R.; Li, L.; Luo, K.; Ding, H.; Gu, Z. W. *Journal of Material Science-Materials in Medicine* **2009**, *20*, 1849.

Chapter 9: Interaction of Poly(glycoamidoamine) DNA Delivery Vehicles with Cell Surface Glycosaminoglycans, a Quartz Crystal Microbalance Study

9.1 Abstract

Being able to understand the mechanism of cellular internalization of polymer-nucleic acids complexes (polyplexes) is very important for the further design of polymers for nucleic acid delivery applications. In this report, we investigated the interactions of poly(glcoamidoamine) (PGAA)-pDNA complexes and glycosaminoglycans (GAGS) to probe the role, or lake thereof, of charge on PGAA-GAG interactions. The PGAA poly(galactaramidopentaethylenetetramine) (G4) was the only PGAA used for polyplex formation and subsequent quartz crystal microbalance (QCM) experiments. QCM was utilized to measure the relative amount of GAG that bound to G4-pDNA polyplexes. Six different GAGs were used for the QCM studies which varied in structure and charge. The results from the QCM relative binding study of the GAGs with G4 polyplexes suggested the affinities for the positively charged polyplex is not solely mediated through electrostatics. The results indicated other factors contribute to the interaction of polyplexes with GAGs other than charge and provided some insight into the role of cell surface GAGs on the internalization of polyplexes into a cell.

9.2 Introduction

Non-viral nucleic acid delivery has shown great potential as a therapeutic strategy that can greatly impact disease treatment.[1] Non-viral delivery vehicles are useful alternatives for DNA carriers compared to virus based systems due to delivery vehicle versatility, modification

potential for various targets, and ability to circumvent the immunogenic responses.[2] Modification of non-viral gene delivery vehicles can also impart enhanced blood stream retention,[3] include cell specific targeting,[4] and allow for *in vitro* and *in vivo* delivery monitoring.[5] However, the delivery efficiency of non-viral delivery systems is not optimal and not anywhere close to that of the viral counterparts. The understanding of the molecular mechanism of delivery to cells must be further understood in order to develop better nucleic acids carriers. Studies into the trafficking mechanisms of various non-viral gene delivery vehicles were reported in an effort to understand the complex process of delivery and nucleic acid release.[6-8] Understanding these delivery mechanisms as a function of subtle chemical structural changes is necessary for the further development of delivery vehicles which allow proper release kinetics, intracellular localization, and offer control over cell specific entry.

Cationic glycopolymers termed poly(glycoamidoamine)s (PGAA) were developed by Reineke et al. and were reported to deliver nucleic acids to the cells without cellular toxicity.[9-11] These short glycopolymers, or oligomers, are comprised of a carbohydrate moiety and oligo ethyleneamine with four secondary amines per repeat unit. Endocytosis of PGAA polyplexes occurred through multiple endocytic pathways and the intracellular trafficking involved various mechanisms. The primary uptake route of PGAA polyplexes into the cell was through a caveolae/raft mediated endocytosis.[12]

In this study we investigated the interactions of D4-pDNA polyplexes with GAGs to probe the influences of GAG charge and structure on the association with PGAA based polyplexes to further understand polyplex interactions with cell surface GAGs. GAGs are linear polysaccharides which exist on the cell surface and are a major component of the extracellular matrix. GAGs play an important role in cell migration, differentiation, cell to cell

communication, and are vital to tissue function.[13,14] GAGs carry a negative charge due to post-translational N- and O-sulfation on the sugar units and are the most anionic component in the cellular membrane.[15] The anionic nature of the GAGs on the surface provided an electrostatic draw for the positively charged G4-pDNA polyplexes. Previously reported studies have suggested the anionic cell surface GAGs served as receptors for endocytosis of cationic non-viral delivery vehicle complexes including polymer,[16-19] peptide,[20-24] and lipid[25-27] based systems.

The six GAGs used in this study are present in mammalian cells and include heparin sulfate (HS), hyaluronate (HA), heparin (Hep), dermatan sulfate (DS), and two forms of chondroitin sulfate (CSA and CSC). Each one of these GAGs carries a different anionic strength with HS having the highest charge density and HA the lowest (Figure 9.1). Quartz crystal
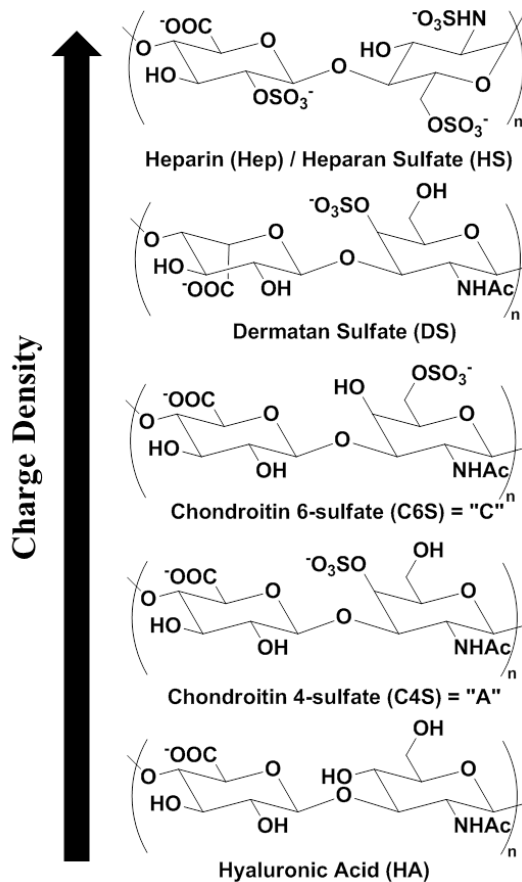

Figure 9.1. Structures of the GAGs used in the QCM study with the trend of increasing charge density indicated

172

microbalance provided a very sensitive technique which allowed for the measurement of the weight of GAGs which irreversibly bound to a polyplex monolayer to provide a relative association between the structurally different GAGs.

9.3 Experimental Section

9.3.1 Materials

All of the reagents used in this study were purchased from Sigma-Aldrich and used without further purification. The PGAA G4 was synthesized according to previously published reports.[9-11] The pCMVβ plasmid DNA was purchased from Aldevron. All polyplex formulations and all other dilutions were made in Gibco DNase/RNase free H_2O.

9.3.2 Polyplex Formation

All G4-pDNA polyplexes were prepared in the exact same manner from experiment to experiment. In each experiment the G4-pDNA polyplexes were formulated at an N/P ratio of 20. A solution of pCMVβ pDNA was diluted with H_2O to 0.02 mg/mL and an equal volume of polymer solution was then added to the pDNA solution and gently vortexed. The polyplex solutions were covered and incubated at room temperature for 1 hour prior to use. The size and zeta potential of each G4-pDNA polyplex was measured using a Malvern Instruments Zetasizer Nano ZS (633 nm) to ensure uniform polyplex hydrodynamic radius and surface potential from experiment to experiment.

9.3.3 Quartz Crystal Microbalance Experiments

All the QCM experiments were carried out on a Q-sense E4 QCM using gold coated quartz crystals and the presented data is an average of two independent QCM experiments. GAG solutions were prepared at 40 µg/mL in the same H_2O as polyplex formation and used shortly

after preparation. The crystal cleaning procedure was a very important step to obtaining consistent results for the QCM experiments. First the gold plated crystals were irradiated with UV/ozone for 10 min. The crystal was then placed in a 5:1:1 mixture of water, 25% ammonia, and 30% hydrogen peroxide at 75 °C for 5 min. Sensors were then submersed in pure H_2O and rinsed with an excess of pure H_2O. Nitrogen gas was then used to dry the crystals followed by another 10 min irradiation with UV/ozone. The clean gold sensors were placed in the clean flow module and equilibrated in air and then in pure H_2O. The G4-pDNA polyplex solution was applied across the gold sensor at 0.2 mL/min until a stabilization of the frequency measurements was observed. After a steady frequency is reached, pure water was flushed through the flow module and over the gold sensor to rinse away any unbound polyplexes and to ensure the polyplexes were irreversibly bound to the sensor surface. The GAG solution was then applied at the same rate of 0.2 mL/min until the frequency measurements stabilized. Again, pure H_2O was used to rinse away any and weakly associated GAGs, leaving only the irreversible bound GAGs to the polyplex later (Figure 9.2). The observed change in frequency with polyplex-GAG
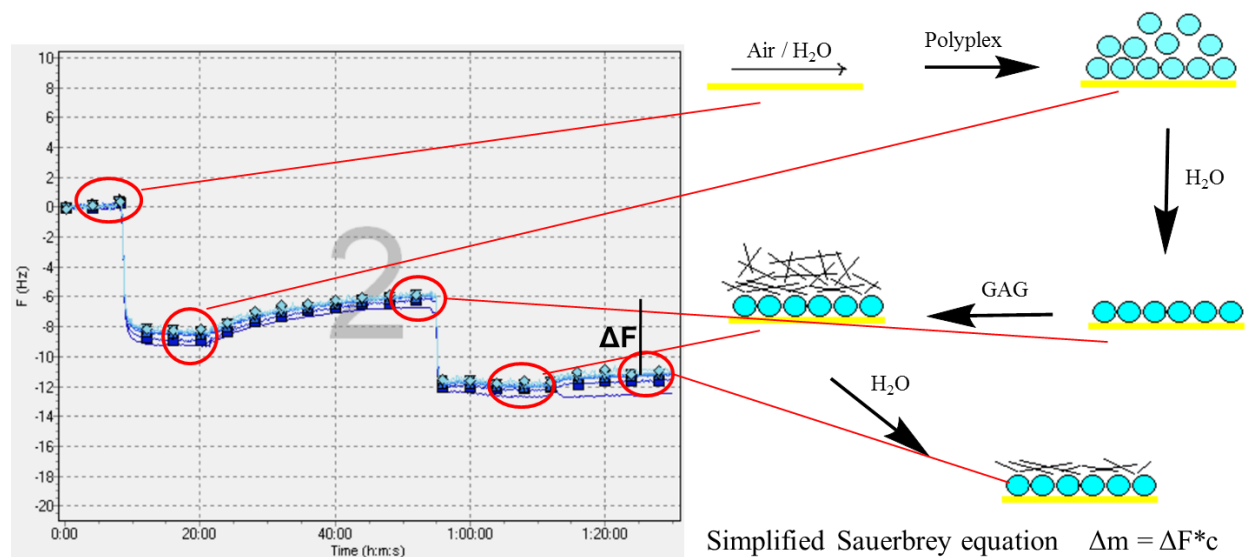

Figure 9.2. A schematic representation of the QCM experiments measuring the relative affinity of GAGs to a G4-pDNA monolayer

174

interactions is directly related to the increase in mass of the bound GAGs. The Sauerbrey equation ($\Delta m = \Delta f c$) was used to calculate the change in mass associated with each change in frequency of the fifth harmonic where c = 17.7 ng cm^{-2} Hz^{-1}, which is specific for the crystal.

9.4 Results and Discussion

Preparation of G4-pDNA polyplexes were reproducible from one experiment to the next and exhibited a diameter around 98 nm with a measured zeta potential near 17 mV. The direct measurement of polyplex-GAG interaction was carried out with QCM experiments which provided the relative affinity of each GAG with the G4-pDNA polyplexes. All the variables associated with the QCM experiments were kept constant except for the GAG solution used to flow across the polyplex monolayer. After applying the GAG solution over the polyplex layer, a measureable increase in the crystal mass was observed and related to the polyplex affinity for the GAGs. HA demonstrated the highest mass increase to the G4 polyplexes and heparin showed the lowest (Figure 9.3). HS and CSA also exhibited a higher mass increase for the G4 polyplexes
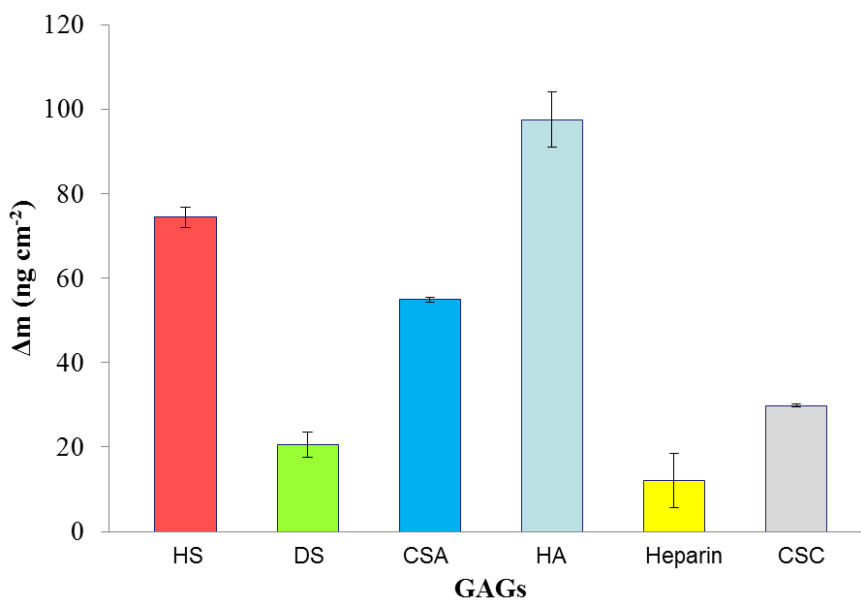

Figure 9.3. The measured change in mass for each of the GAGs studied indicating the relative association of each GAG with G4-pDNA polyplexes

and the observed mass increase for DS and CSC GAGs were low. The trend for the observed mass increase, after exposer of G4 polyplexes to the GAG solution, was HA > HS > CSA > CSC > DS > heparin. The trend observed in the QCM experiment does not correlate with the trend of GAG charge which suggested the polyplex-GAG interaction is mediated through another mechanism besides electrostatic interactions. This evidence that GAG charge does not solely mediate the affinity for G4 polyplexes provided another important piece of information toward understanding of the interaction of polyplexes with cell surface GAGs and the role they play in polyplex endocytosis.

9.5 Conclusions

The relative affinity of six different glycosaminoglycans (GAG) for polyplexes composed of poly(galactaramidopentaethylenetetramine) (G4) copolymers and pDNA was investigated to provide an understanding of the nature of polyplex interactions with cell surface GAGs. QCM experiments provided insight into the relative affinity of GAGs for the polyplexes in an attempt to elucidate the role of GAG charge on interactions with polyplexes. The increase in mass of the GAGs, measured with QCM, provided the relative affinities for the polyplexes and revealed the trend of affinity to be HA > HS > CSA > CSC > DS > Hep. HA possessed the lowest charge density of all the GAGs tested, but showed the highest mass increase after exposer to polyplexes. The data indicated GAGs affinity for G4 polyplexes is not solely mediated through electrostatic interactions. This study warrants further investigations into the mechanisms of GAG and polyplex interactions to better understand the role of cell surface GAGs and to aid in future polymer design.

9.6 Acknowledgments

9.7 References

(1)   Verma, I. M.; Somia, N. *Nature* **1997**, *389*, 239.
(2)   Mintzer, M. A.; Simanek, E. E. *Chemical Reviews* **2009**, *109*, 259.
(3)   Pun, S. H.; Davis, M. E. *Bioconjugate Chemistry* **2002**, *13*, 630.
(4)   Zanta, M. A.; Boussif, O.; Adib, A.; Behr, J. P. *Bioconjugate Chemistry* **1997**, *8*, 839.
(5)   Bryson, J. M.; Fichter, K. M.; Chu, W. J.; Lee, J. H.; Li, J.; Madsen, L. A.; McLendon, P. M.; Reineke, T. M. *Proceedings of the National Academy of Sciences of the United States of America* **2009**, *106*, 16913.
(6)   Khalil, I. A.; Kogure, K.; Akita, H.; Harashima, H. *Pharmacological Reviews* **2006**, *58*, 32.
(7)   Medina-Kauwe, L. K.; Xie, J.; Hamm-Alvarez, S. *Gene Therapy* **2005**, *12*, 1734.
(8)   Midoux, P.; Breuzard, G.; Gomez, J. P.; Pichon, C. *Current Gene Therapy* **2008**, *8*, 335.
(9)   Liu, Y. M.; Reineke, T. M. *Journal of the American Chemical Society* **2005**, *127*, 3004.
(10)   Liu, Y. M.; Reineke, T. M. *Bioconjugate Chemistry* **2006**, *17*, 101.
(11)   Liu, Y. M.; Wenning, L.; Lynch, M.; Reineke, T. M. *Journal of the American Chemical Society* **2004**, *126,* 7422.
(12)   McLendon, P. M.; Fichter, K. M.; Reineke, T. M. *Molecular Pharmaceutics* **2010**, *7*, 738.
(13)   Kjellen, L.; Lindahl, U. *Annual Review of Biochemistry* **1991**, *60*, 443.
(14)   Mislick, K. A.; Baldeschwieler, J. D. *Proceedings of the National Academy of Sciences of the United States of America* **1996**, *93*, 12349.
(15)   Park, P. W.; Reizes, O.; Bernfield, M. *Journal of Biological Chemistry* **2000**, *275*, 29923.
(16)   Hess, G. T.; Humphries, W. H.; Fay, N. C.; Payne, C. K. *Biochimica Et Biophysica Acta-Molecular Cell Research* **2007**, *1773*, 1583.
(17)   Kopatz, I.; Remy, J. S.; Behr, J. P. *Journal of Gene Medicine* **2004**, *6*, 769.
(18)   Ruponen, M.; Honkakoski, P.; Tammi, M.; Urtti, A. *Journal of Gene Medicine* **2004**, *6*, 405.
(19)   Ruponen, M.; Ronkko, S.; Honkakoski, P.; Pelkonen, J.; Tammi, M.; Urtti, A. *Journal of Biological Chemistry* **2001**, *276*, 33875.
(20)   Fuchs, S. M.; Raines, R. T. *Biochemistry* **2004**, *43*, 2438.
(21)   Kosuge, M.; Takeuchi, T.; Nakase, I.; Jones, A. T.; Futaki, S. *Bioconjugate Chemistry* **2008**, *19*, 656.
(22)   Nascimento, F. D.; Hayashi, M. A. F.; Kerkis, A.; Oliveira, V.; Oliveira, E. B.; Radis-Baptista, G.; Nader, H. B.; Yamane, T.; Tersariol, I. L. D.; Kerkis, I. *Journal of Biological Chemistry* **2007**, *282*, 21349.
(23)   Sandgren, S.; Cheng, F.; Belting, M. *Journal of Biological Chemistry* **2002***, 277*, 38877.
(24)   Suzuki, T.; Futaki, S.; Niwa, M.; Tanaka, S.; Ueda, K.; Sugiura, Y. *Journal of Biological Chemistry* **2002**, *277*, 2437.
(25)   Belting, M.; Petersson, P. *Biochemical Journal* **1999***, 342*, 281.

(26)   Mounkes, L. C.; Zhong, W.; Cipres-Palacin, G.; Heath, T. D.; Debs, R. J. *Journal of Biological Chemistry* **1998**, *273*, 26164.

(27)   Ruponen, M.; Yla-Herttuala, S.; Urtti, A. *Biochimica Et Biophysica Acta-Biomembranes* **1999**, *1415*, 331.

Chapter 10: MAG vs. PEG: Incorporating poly(MAG) Layer for Increased Colloidal Stability of Nucleic Acid/"Click Cluster" Complexes

10.1 Abstract

This work demonstrated the use of adamantane-terminated poly(2-deoxy-2-methacrylamido glucopyranose) (Ad-pMAG) glycopolymers as a stabilizing nano-layer through an inclusion complex between adamantane (Ad) and the β-cyclodextrin (βCD) core of click cluster nucleic acid delivery vehicles. Herein we demonstrate the reversible addition fragmentation chain transfer (RAFT) synthesis and incorporation of an adamantane-conjugated pMAG (Ad-pMAG) as a hydrophilic coating for click cluster-pDNA complexes. Ad-pMAG incorporation was favorable over Ad-poly(ethylene glycol) (Ad-PEG) due to the increased colloidal stability of the click cluster/pDNA polyplex under physiological salt conditions as well as providing 'masking' effect when transfecting HeLa cells *in vitro*. Differences in the physical and biological properties of the polyplexes containing either Ad-PEG or Ad-pMAG are investigated.

10.2 Introduction

Poly(ethylene glycol) (PEG) has become a widely used polymer for incorporation of hydrophilic nanoparticle layers and in many cases for increased colloidal stability, reduced toxicity, and imparting passive targeting.[1-4] Although PEG conjugation is successful in providing many systems with the desired properties, as in the case with Davis' success with Ad-PEG inclusion,[5,6] it is not the case for all systems. Recent studies have also addressed the concerns of

accelerated blood clearance (ABC) phenomenon when using PEGylated systems, which is a big concern for therapies that involve repetitive administrations of drugs.[7-9] PEG, being well suited for many delivery systems, does have drawbacks which warrant investigations into alterative polymers for use as nanoparticle coatings. The aim of this initial investigation is to study the difference in physical and biological properties of polyplex formulations that include PEG or poly(2-deoxy-2-methacrylamido glucopyranose) (pMAG).
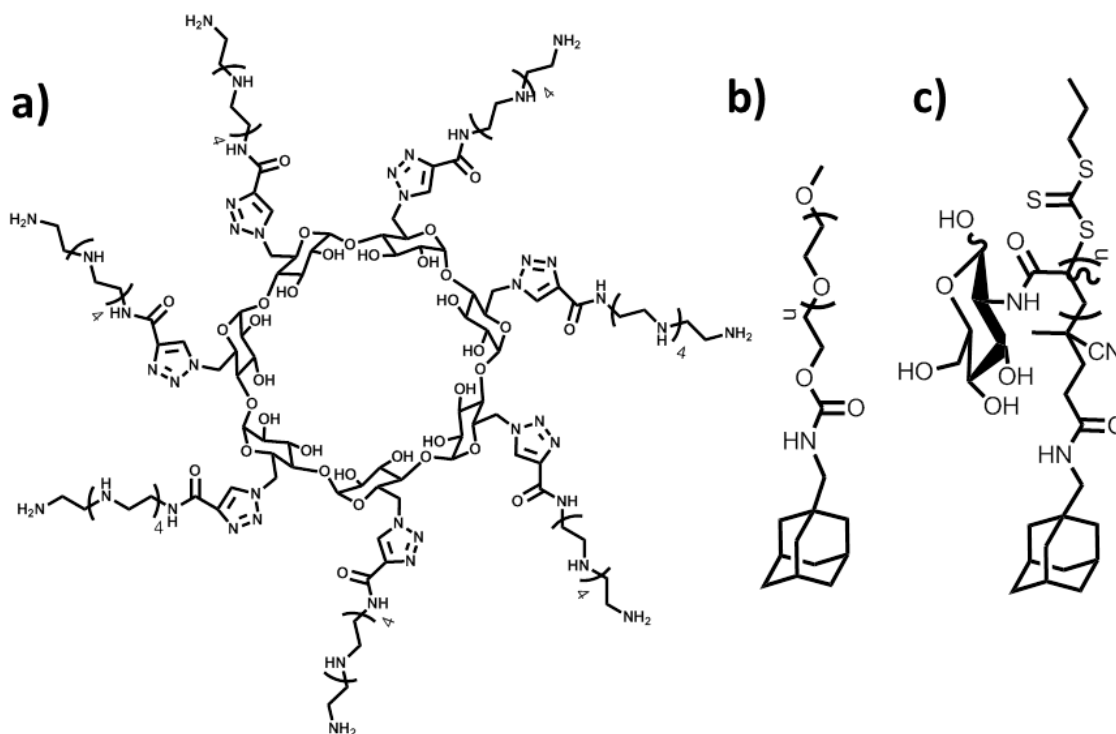
Figure 10.1. Structures of (a) click clusters, (b) Ad-PEG, and (c) Ad-pMAG

Click cluster delivery vehicles, developed by Srinivasachari et al,[10] are utilized in this study to form non-covalent inclusion complexes with the Ad-X polymers (Figure 10.1), which are investigated as pDNA delivery vehicles. Previous studies with HeLa (human adenocarcinoma) cells have demonstrated high transfection efficiency and low toxicity of the click cluster-induced polyplexes. Although these click cluster/pDNA polyplexes are colloidally stable in water, there is a high tendency for them to aggregate in physiological conditions, such

as salt- and serum-containing media, which can be detrimental for *in vivo* delivery applications. Therefore these polyplexes provide a suitable system for comparison of the Ad-p(MAG) and Ad-PEG effects on the polyplex properties (Figure 10.2).
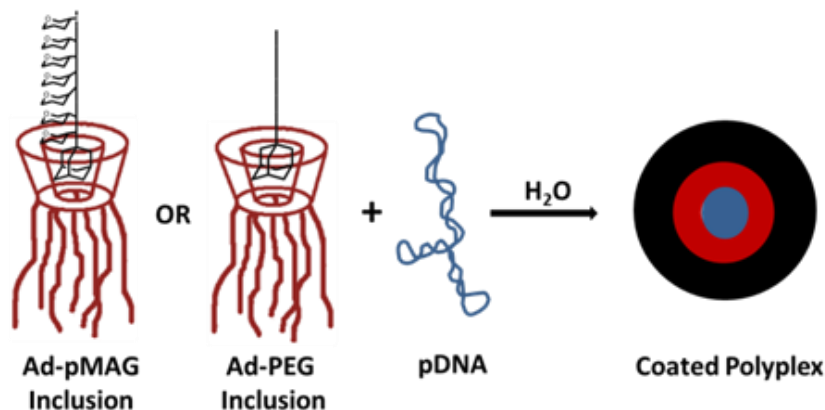
Figure 10.2. A schematic representation of the polyplexes formed with Ad-X inclusion

10.3 Experimental Section

10.3.1 Materials

Pentaethylenehexamine, iodine, and *N*-hydroxy succinimide were purchased from Sigma Aldrich (St. Louis, MO) and used as received unless otherwise noted. Pentaethylenehexamine was purified through double distillation prior to use. *N,N′*-Dicyclohexylcarbodiimide (DCC), adamantane methylamine, ethyl trifluoroacetate, triphenylphosphine, sodium azide, β-cyclodextrin, and acetic anhydride were purchased from Acros Organics (Thermo Fisher Scientific, New Jersey, NJ) and used without purification. β-cyclodextrin was dried by dissolving in dry DMF followed by evaporation and drying under vacuum. Propiolic acid was purchased from Alfa Aesar (Ward Hill, MA) and used without further purification. The NHS activated polyethylene glycol (PEG-SC) was purchased from NOF America Corporation (White Plains, NY) and used without purification. The heptakis{6-[4-(2-

pentaethylenepentaminoethylcarbamoyl)-1*H*-1,2,3-triazol-1-yl]}cycloheptaamylose (click clusters) were synthesized and purified using previously reported methods. All the dilutions of the plasmid DNA and N/P dilutions of the click clusters were done using UltraPure™ DNase⁄RNase-Free Distilled Water (Gibco, Carlsbad, CA). All the cell culture reagents such as Dulbecco's Modified Eagles Medium containing GlutaMAX™ (DMEM), reduced serum media OptiMEM™, phosphate buffered saline at pH 7.4 (PBS), trypsin, heat-inactivated fetal bovine serum (FBS), antibiotic and antimycotic (AB/AM), DNase RNase Free Ultrapure Water were purchased from GIBCO, Invitrogen (Carlsbad, CA). The cell culture supplies from Corning, Inc. (Lowell, MA), such as cell culture plates and 75 cm^2 flasks, were purchased from Fisher Scientific. All of the cell lines used in this study (human adenocervical carcinoma cell line (HeLa), and human glioblastoma cell lines U251 and U-87 MG) were purchased from American Type Cell Culture Collection (Manassas, VA). jetPEI™ was purchased from Polyplus-transfection, Inc. (New York, NY). The polymer Glycofect™ was generously donated by Techulon, Inc. (Blacksburg, VA). The nucleic acid gWiz™ High-Expression Luciferase plasmid DNA (6732 bp) was purchased from Aldevron, Inc. (Fargo, ND). This same plasmid DNA labeled with Cy5™ dye was purchased from Mirus Bio (Madison, WI). The [3-(4,5-dimethylthiazol-2-yl)-2,5-diphenyltetrazolium bromide (MTT) powder was purchased from Invitrogen, Inc. (Carlsbad, CA).

10.3.2 Synthesis of Click Clusters

Experimental details for preparation of click clusters can be found in previously reported publication by Srinivasachari et al. A brief description of the click cluster synthesis is as follows. Pure, dried β-cyclodextrin was reacted with triphenyl phosphine and iodine to afford the fully 6-substituted per-iodo β-cyclodextrin. A nucleophilic substitution using sodium azide was then

used followed by protection of the hydroxyl groups using acetic anhydride to afford the acetylated per-azido-β-cyclodextrin core. Next, the oligoethyleneamine arms were synthesized by first reacting the double distilled pentaethylenehexamine with one equivalent of ethyl trifluoroacetate to protect one of the primary amines. The resulting free internal secondary amines and primary amine were protected *in situ* with (Boc)$_2$O to afford the fully protected pentaethylenehexamine. Deprotection of the primary amine was performed by cleavage of the trifluoroacetyl group in basic aqueous methanol and the desired Boc derivative was obtained via column chromatography. The Boc protected monoamines were then conjugated to propiolic acid using DCC coupling. The pure oligoethyleneamine alkyne arm was obtained after silica gel column chromatography followed by recrystallization with 29% overall yield.

The final click cluster was synthesized by utilizing the azide-alkyne 1,3-dipolar cycloaddition reaction using copper sulfate/sodium ascorbate in ^{t}BuOH/H$_2$O at a ratio of 1:1. The fully protected click cluster was precipitated and washed with a 10% ammonium hydroxide solution multiple times to remove the copper, then rinsed with pure H$_2$O. Without any further purification the Boc and acetyl protecting groups were removed followed by extensive dialysis against pure H$_2$O followed by ion exchange chromatography with an increasing gradient of NH$_4$HCO$_3$ aqueous solutions to elute the pure click clusters. This yielded a white, fluffy product after lyophilization. The click clusters were analyzed by MALDI-TOF mass spectrometry using an Applied Biosystems 4800 MALDI TOF/TOF operated in reflective positive mode. The matrix for click cluster analysis was comprised of 2,5-dihydroxybenzoic acid in acetone with 5 mg/ml of NaI. The click cluster structure was also confirmed by ^{1}H, ^{13}C NMR with peak assignments determined with 2D COSY and HSQC NMR experiments.

10.3.3 Synthesis of Adamantane Terminated Polymers

Preparation of the Ad-PEG molecules was completed using a method similar to one by Pun et al. In brief, PEG_{5000}-SC, in a vial, was dissolved in $CHCl_3$ after which 5 equivalents of adamantane methylamine were added and stirred at room temperature for 24 h. All $CHCl_3$ was then removed under vacuum and ultra-pure H_2O was added to dissolve this residue. The aqueous solution was centrifuged at 4000 rpm for 30 min to separate the excess adamantane methylamine. The supernatant was removed and dialyzed against ultra-pure H_2O, then finally freeze dried to yield white product with near quantitative yield. The PEG derivatives were analyzed by MALDI-TOF in a matrix consisting of 4 mg/mL alpha-cyano-4-hydroxy-cinnamic acid in 50:50 water:acetonitrile supplemented with 0.2% trifluoroacetic acid and 20 mM ammonium citrate. Product purity was analyzed by HPLC using an Agilent 1100 series pump (ACN: H_2O gradient) equipped with C18 column and Alltech ELSD detector. ^{1}H NMR ($CDCl_3$): δ = 1.61 (s, 6H), 1.70-1.90 (dd, 6H), 2.09 (s, 3H), 2.94 (s, 2H), 3.52 (s, 3H), 3.84 (PEG peak), 4.34 (t, 2H)

Synthesis of the Ad-CTA was as follows: 199.5 mg (8.77×10^{-4} mol, 1.1 eq) of 4-cyano-4-(propylsulfanylthiocarbonyl) sulfanyl pentanoic acid (CPP) CTA and 332.7 mg (8.77×10^{-4} mol, 1.1 eq) of HBTU were dissolved in 3 mL of DMSO. After stirring at room temperature for 10 min, 131.7 mg (7.97×10^{-4} mol, 1.0 eq) of adamantane methylamine, dissolved in 1 mL of DMSO, were added to the reaction and stirred at room temperature for 3 h. The reaction mixture was then poured into 40 mL of pH 4 water, extracted with DCM, and organic extracts were dried over Na_2SO_4. The product was isolated by silica gel column purification with DCM:ethyl acetate (9.5:0.5) eluent. The isolated Ad-CTA was purified by recrystallization in CCl_4. ^{1}H NMR ($CDCl_3$): δ = 1.02 (t, 3H), 1.48 (d, 6H), 1.60-1.71 (dd, 6H), 1.75 (m, 2H), 1.90 (s, 3H), 2.04 (s,

3H), 2.35-2.58 (m, 4H), 2.97 (d, 2H), 3.32 (t, 2H). LC-MS: Calcd. for $(M+H)^+$ 425.71 g/mol, found 425.20 g/mol.

The MAG monomer was synthesized according to previously published procedures. Monomer consumption rate was determined by NMR analysis using the following reaction conditions: 210 mg (0.849 mmol, 1.04 eq) of 2-deoxy-2-methacrylamide-glucopyranose (MAG) and 0.238 mg (8.49×10^{-4} mol, 0.104 eq) of V-501 were dissolved in 1.521 mL of D_2O and 0.234 mL of 0.1 M acetate buffer. 3.48 mg (.819 mmol, 1.00 eq) of Ad-CTA was dissolved in 1.755 mL of *d6*-DMSO. Flasks containing these solutions and empty NMR tubes were capped with septa connected with cannula and deoxygenated in line by bubbling N_2 through the solutions for 45 min at room temperature. Solution of MAG and initiator was cooled down in ice-bath and DMSO solution of Ad-CTA was pushed in with nitrogen pressure. This resulted in formation of a milky suspension which was further pushed with nitrogen into NMR tube. The NMR tube was placed in a NMR spectrometer preheated to 70 °C. The progress of monomer consumption was assessed by monitoring the disappearance of the vinyl peak at 5.60 ppm.

Ad-pMAG polymer was synthesized following the established kinetics as follows: 1.653 g (6.685 mmol, 104 eq) of 2-deoxy-2-metacrylamide-glucopyranose (MAG) and 1.87 mg (6.67×10^{-3} mmol, 0.104 eq) of V-501 were dissolved in 11.976 mL of H_2O and 1.842 mL of 0.1M acetate buffer. 27.4 mg (6.45×10^{-2} mmol, 1.00 eq) of Ad-CTA were dissolved in 13.818 mL of DMSO. Flasks containing these solutions were capped with septa, connected with cannula, and deoxygenated in line by bubbling N_2 through the solutions for 45 min at room temperature. The solution of MAG and initiator was cooled down in ice-bath and DMSO solution of Ad-CTA was pushed in with nitrogen pressure. This resulted in formation of a milky suspension. The reaction flask was disconnected from the nitrogen line and placed in oil bath

pre-heated to 70 °C. The solution became clear after ~1 minute of stirring. Reaction was allowed to proceed for 3.5 h and was stopped by removing the septum and cooling the reaction mixture in ice/water bath. The reaction mixture was diluted with 25 mL of water and dialyzed against 4 L x 9 of ultra-pure water for 72 h using dialysis membrane with 3500 Da molecular weight cut-off. Dialyzed polymer solution was freeze-dried to yield 0.584 g of fluffy solid.

10.3.4 NMR Titration Experiments

NMR titration experiments were carried out on a Varian MR400 NMR in D_2O. The relative association constants (K_a) were determined by titration of the click clusters into an Ad-PEG stock solution. The data was analyzed using Conner's Method and TableCurve 2D® data analysis software (Systat Software Inc., San Jose, CA). The titration was carried out by first preparing a stock solution of the guest molecule (Ad-PEG, 1.2 mM) in UltraPure™ DNase/RNase-Free distilled water. A series of click cluster (guest) concentrations were subsequently made using the Ad-PEG stock solution, to keep adamantane polymer concentration constant, ranging from 0 to 6.7 mM. Each sample was prepared in a clean 5mm NMR tube with a final volume of 700 μL each. NMR was then used to acquire the ^{1}H spectra of each of the ten samples under identical conditions. The chemical shift of the tertiary proton on the adamantane head group was identified and the difference in chemical shift of this proton between the uncomplexed and complexed Ad-PEG was recorded. The data was then fit with the Conner's equation[16] using non-linear regression with the Table Curve data analysis software to obtain the K of adamantane/CD complexation.

10.3.5 Polyplex Formulation

All polyplexes were formed in DNase/RNase-Free Distilled Water, at N/P ratio of 5, 7, 10, and 20, and then diluted with water, DMEM, or Opti-MEM™ before use. All polyplexes

were incubated for 1 h at room temperature before use. Click cluster-pDNA polyplexes were prepared at various N/P ratios by adding click cluster solution of appropriate concentration to equal volume of pDNA solution. Polyplexes formulated with either Ad-PEG or Ad-MAG were prepared in the same manner except a pre-complexed Ad-X/click cluster solution containing a 1:1 molar ration of the adamantyl terminated polymer and click cluster was used. Final pDNA concentration in polyplex formulation solutions was 0.1 mg/mL for gel electrophoresis experiment and 0.02 mg/ml for all other experiments. JetPEI^{TM} polyplexes were formulated at an N/P of 5 and Glycofect^{TM} polyplexes at N/P of 20 following the manufacturer protocols

10.3.6 Polyplex Characterization

Polyplexes, formulated at N/P of 5, 7, 10, and 20, were diluted with 700 µL of pure water and transferred in cuvettes. Hydrodynamic diameters were measured at 25 °C using a Zetasizer Nano ZS DLS (Malvern Instruments, Malvern, UK) at a detection angle of 173°. Polyplex solutions were transferred in zeta potential cuvettes and zeta potential measurements were carried using the same instrument at 25 °C. To investigate the stability of these polyplexes in more physiologically relevant conditions, the polyplexes were diluted with 700 µL of either Opti-MEM^{TM} or DMEM containing 10% FBS. Hydrodynamic diameters were measured at different time points between 0 to 4 hours. All measurements were done at 25 °C with a detection angle of 173°. In order to get a better picture of the very slow aggregation taking place with Ad-p(MAG)$_{52}$ at N/P of 20 in salt conditions, the size measurements were done every 15 min up to 9 h.

Gel electrophoresis (60V) was carried out on Agarose gel (0.6%, w/v) containing ethidium bromide (0.6 µg/mL) made with 1x TAE buffer (40 mM Tris-acetate, 1 mM EDTA). 2 µL of BlueJuice^{TM} loading buffer was added to each polyplex solution, and 15 µL of resulting

mixture were loaded onto the gel for analysis. Gels were visualized using a UV (ultra violet) gel box.

10.3.7 Cell Culture and Biological Evaluations

The HeLa, U-87 MG, and U-251 cells were cultured in 75 cm^2 flasks in DMEM containing 10% FBS and 5% AB/AM (hereafter referred as 10% FBS DMEM) in incubator at 37 °C and 5% CO_2. The cells were cultured in 24-well plates for (1) MTT cell viability assay and (2) DC Protein Assay (Bio-Rad Laboratories, Hercules, CA) and luciferase expression assay 'Luciferase Assay System' (Promega, Madison, WI). The cells were cultured in 6-well plates for the uptake experiment. The cells were seeded at a cell density of 50,000 cells/well in 24 well plates at 24 h prior to transfection in 10 % FBS DMEM for both (1) MTT assay and (2) protein and luciferase expression assay. In the case of the uptake experiment, the cells were seeded in 6-well plates at a 250,000 cells/well density 24 h prior to transfection.

The polymer solution 50 µL/well was prepared at pre-determined N/P ratios in UltraPure™ DNase⁄RNase-Free Distilled Water. 50 µL/well pDNA solutions were prepared at a concentration of 0.02 µg/µL in UltraPure™ DNase⁄RNase-Free Distilled Water. The resulting mixture of solution was allowed to incubate at room temperature for 1 h. The polyplexes were then diluted in 200 µL/well OptiMEM^{TM} immediately before adding to the wells during transfection. Thus a final solution of 300 µL/well of diluted polyplex solution was added to the wells. After transfection the cells were incubated in the incubator at 37 °C and 5% CO_2 for 4 h. After which 1 mL/well of 10% FBS DMEM was added to each well and again incubated for another 20 h. Further at 24 h post transfection time point the media in the wells was aspirated and replaced with 1 mL/well fresh 10% FBS DMEM and incubated for another 24 h. After 48 h post-transfection, the cells were assayed.

In case of uptake experiment Cy5^{TM} labeled gWiz^{TM}-luciferase plasmid DNA was used. The polyplexes were prepared by adding 250 µL/well polymer solution at predetermined N/P ratio to 250 µL/well Cy5^{TM} labeled-pDNA solution at 0.02 µg/µL and incubation in dark for 1 h. The polyplexes were diluted in 1000 µL/well OptiMEM^{TM} immediately before adding to the wells during transfection. Thus the final solution of diluted polyplex added to each well was 1500 µL/well. The cells were then incubated at 37 °C and 5% CO_2 for 4 h. After that the cells were washed with 500 µL/well PBS and again washed with 500 µL/well CellScrub^{TM} Buffer (Gelantis, Gene Therapy Systems, Inc., San Diego, CA) to remove polyplexes that may be adhering to outside surface of the cells plasma membrane. Later, the cells were centrifuged and washed three times with PBS before running on BD FACS Canto^{TM} II (BD Bioscience, San Jose, CA). The data was analyzed using BD FACS Diva^{TM} software. The Cy5^{TM} fluorescence was gated using a cells-only control. Cellular uptake studies were carried out using Cy5^{TM}-labeled pDNA for polyplex formation and subsequently used in transfections of each cell line at N/P 10. Cells were incubated with the labeled polyplexes for 4 h before washing with PBS buffer and CellScrub^{TM} to remove any cell surface-bound polyplexes. The number of cells positive for Cy5^{TM} fluorescence was measured on a BD FACS Canto^{TM} II using BD FACSDiva^{TM} software.

For protein and luciferase assays the cells were lysed with 100 µL/well of 1x dilution of Luciferase Cell Culture Lysis 5X Reagent (Promega, Madison, WI). The protein assay was performed using 5 µL of cell lysate to clear 96 well plates and absorbance at 750 nm was measured using a TECAN Genios Pro plate reader (TECAN US, Inc., Durham, NC) at room temperature using Magellan^{TM} software. The luciferase assay was performed on the same plate reader. The experiment consisted of adding 5 µL/well of cell lysate to an opaque (white) 96-well plate and then 95 µL/well of luciferase substrate (Promega, Madison, WI) was added using auto

injector. The luminescence was measured using XFluor4[TM] software with an integration time of 10000 ms. Gene expression was evaluated by transfecting cells with polyplexes formed with gWiz[TM] luciferase pDNA for 4 h in reduced-serum medium then in 10% FBS-containing DMEM medium for 42 h. 48 h after transfection, luciferin was added to cellular lysate and fluorescence was measured with a TECAN Genios Pro plate reader. Gene expression was evaluated based on the fluorescence normalized to a total amount of proteins present.

Toxicity was measured using an MTT (3-(4,5-Dimethylthiazol-2-yl)-2,5-diphenyltetrazolium bromide) assay after 48 h incubation of cells with treatments. Transfection and incubation was carried out identical to that of the luciferase transfection experiments except the transfected cells were incubated with MTT for 1 h at 37 °C and 5% CO_2 then lysed with DMSO (dimethyl sulfoxide). The absorbance was measured at 570 nm, using the same plate reader, to determine the relative cell viability of transfected cells. In case of the MTT assay, 1 mL/well of 0.5 mg/mL MTT containing Opti-MEM[TM] was added to each well and the cells were incubated for 1 hour at 37 °C and 5% CO_2. After 1 h the cells were washed with 500 µL/well PBS and lysed with 600 µL/well dimethyl sulfoxide (DMSO). Then 200 µL/well of the violet-colored cell lysis solution was then added to a clear 96-well plate and absorbance was measured at 570 nm using plate reader TECAN Genios Pro (TECAN US, Inc., Durham, NC) at room temperature.

10.4 Results and Discussion

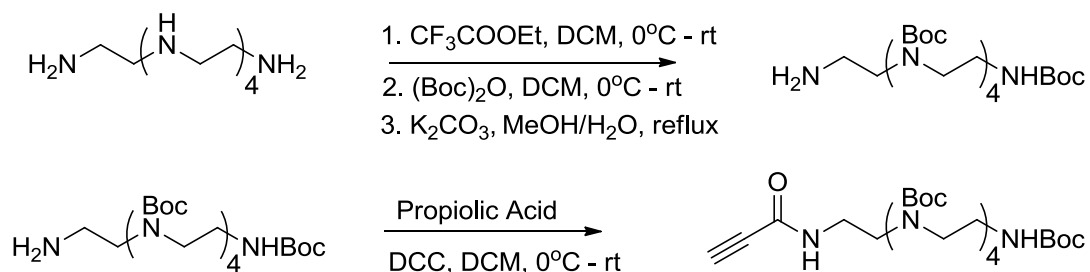### 10.4.1 Synthesis of Click Cluster Delivery Vectors

The previously published synthesis of click clusters was completed after 10 steps which included synthesis of the acetylated per-6-azido βCD core (Scheme 10.1) and an alkyne terminated Boc-protected oligoethyleneamine (Scheme 10.2). It was very important for the

190

removal of H_2O from the βCD before the reaction with PPh_3 and I_2 in order to obtain fully functional per-iodo- βCD. The acetylated per-6-azido βCD synthesis yielded a fully functional core for click cluster synthesis. Synthesis of the alkyne terminated Boc_5N_6 yielded a nice white
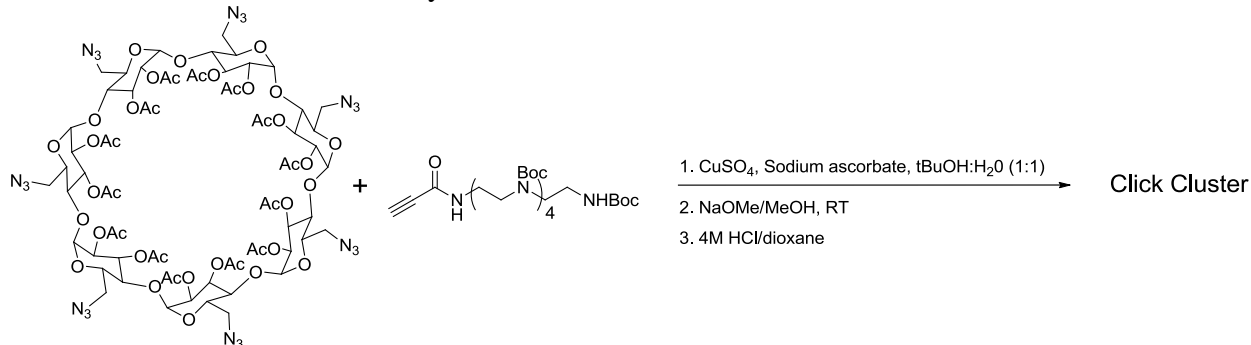
Scheme 10.1. Synthesis of acylated per azido βCD
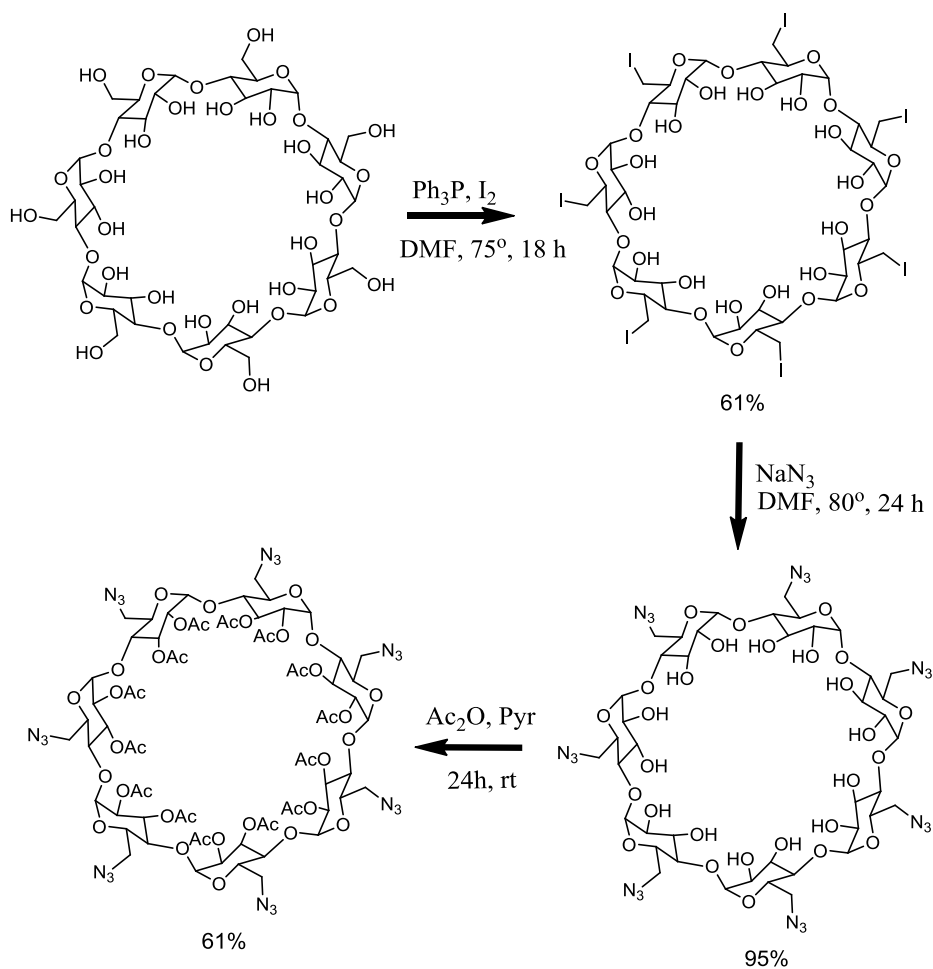
Scheme 10.2. Synthesis of Boc_5N_6 alkyne

Scheme 10.3. Azide-alkyne click reaction of acylated per-azido βCD with Boc$_5$N$_6$ alkyne for the formation of click cluster delivery vectors

solid product, but the overall yield was quite low (<20% yield). The Cu(II) catalyzed azide-alkyne click reaction between the acetylated per-azido βCD and alkyne terminated Boc$_5$N$_6$ gave an off white solid product (Scheme 10.3). A portion of the copper catalyst was removed through washes with ammonium hydroxide solutions but much of the copper persisted after the initial washes. It was very important to remove this copper since the materials are meant for *in vitro* use in this study. After deacylation and Boc deprotection, a greenish solid residue was obtained. Copper removal with an ion-exchange column and ammonium bicarbonate gradient followed by
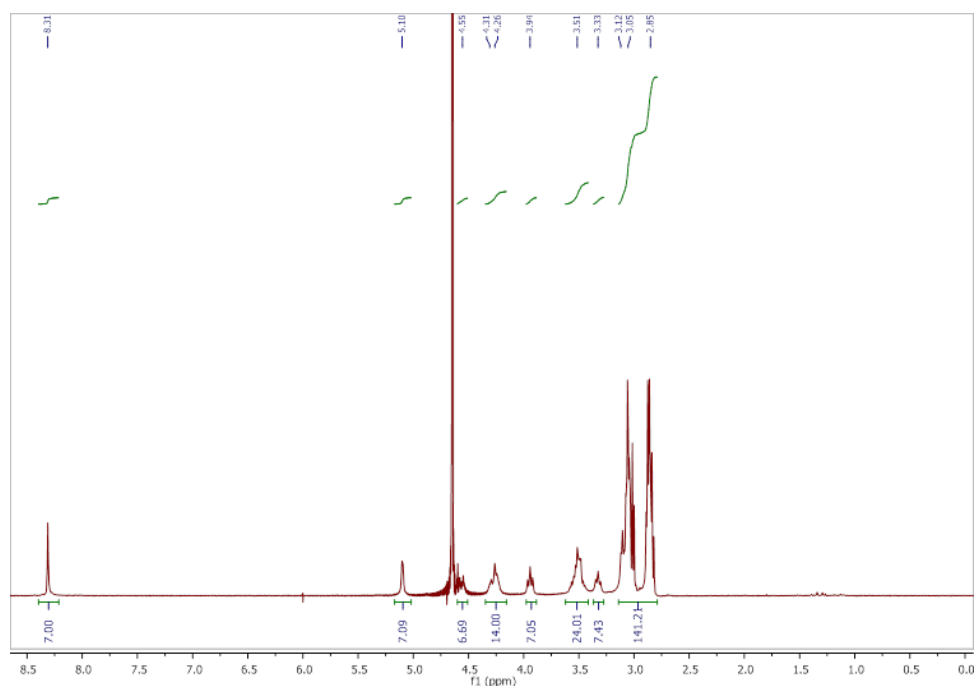
Figure 10.3. ^{1}H spectra of pure click cluster delivery vectors in D$_2$O

dialysis in ultra-pure H_2O yielded click clusters in high purity. MALDI-TOF, ^{1}H NMR (Figure 10.3), and ^{13}C NMR analyses verified the click cluster structure and purity. HSQC and COSY 2D NMR experiments confirmed the chemical shift assignments for each proton and carbon (Figure 10.4).
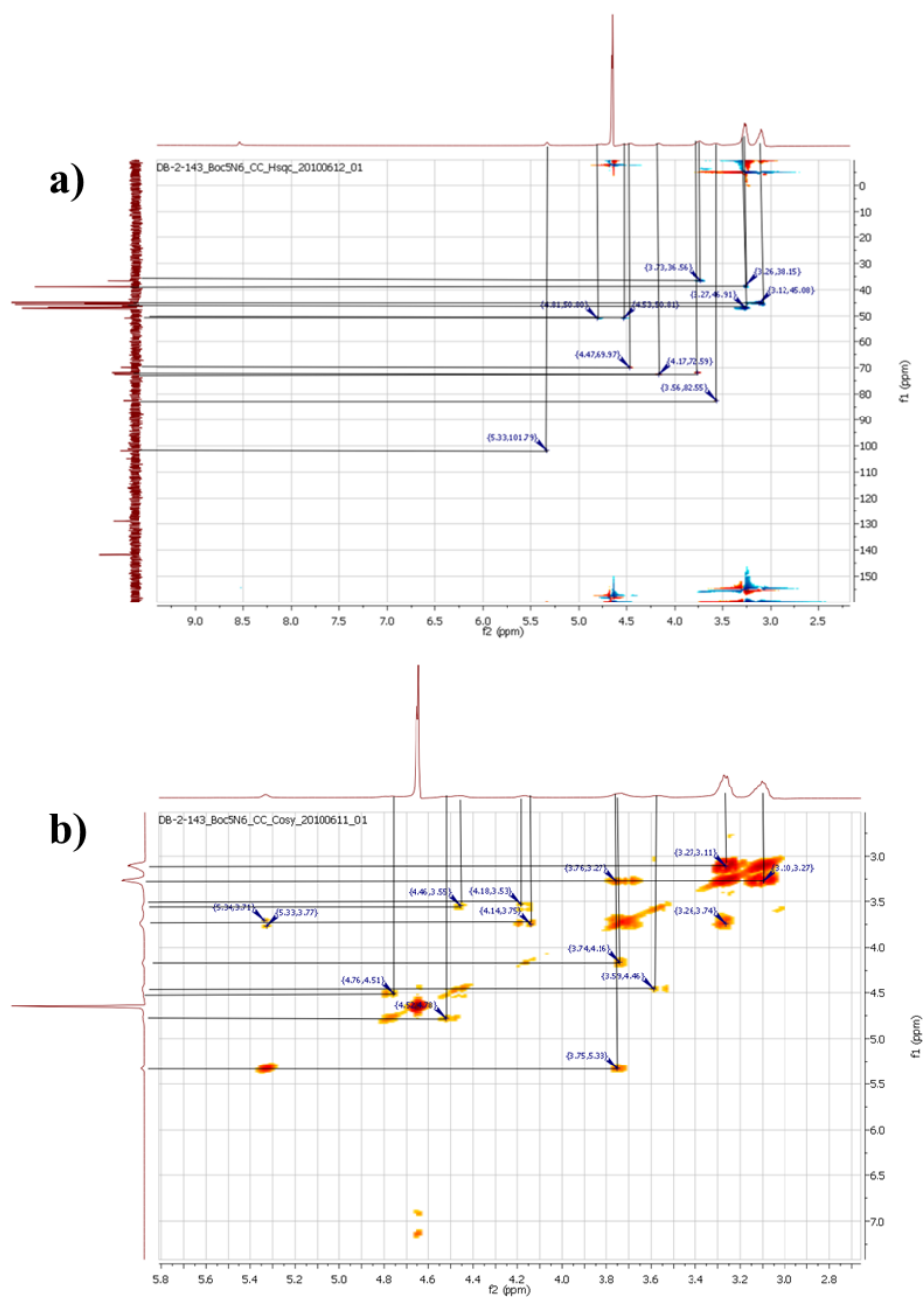

Figure 10.4. 2D (a) HSQC and (b) COSY NMR experiments for proper chemical shift assignment of click clusters in D_2O

10.4.2 Synthesis of Ad-PEG and Ad-pMAG

The Ad-pMAG polymer used in the polyplex formulations was synthesized through a reversible addition fragmentation chain transfer (RAFT) polymerization technique using an adamantane derivative of 4-cyano-4-(propylsulfanylthiocarbonyl) sulfanyl pentanoic acid (CPP). Chain transfer agent (CTA) and 2-deoxy-2-methacrylamido glucopyranose (MAG) monomers which were synthesized according to previously published procedures.[14] The CPP, synthesized according to a published procedure,[15] was reacted with adamantane methylamine and HBTU coupling reagent to yield the Ad-CTA derivative, compound 2. Ad-CTA was subsequently used in the synthesis of Ad-pMAG in a mixture of deoxygenated water, acetate buffer, and DMSO using a V-501 initiator at 70 °C (Scheme 10.4). The monomer consumption and kinetics were studied in order to target a particular DP (Figure 10.5 and 10.6).

Scheme 10.4. Synthesis of Ad-CTA and RAFT polymerization of Ad-pMAG
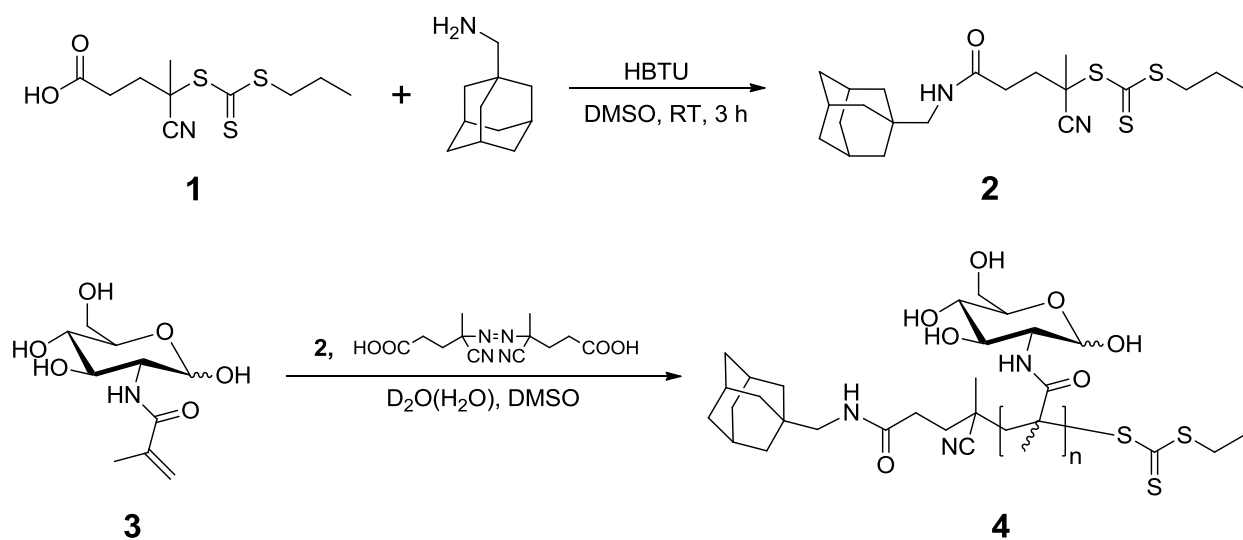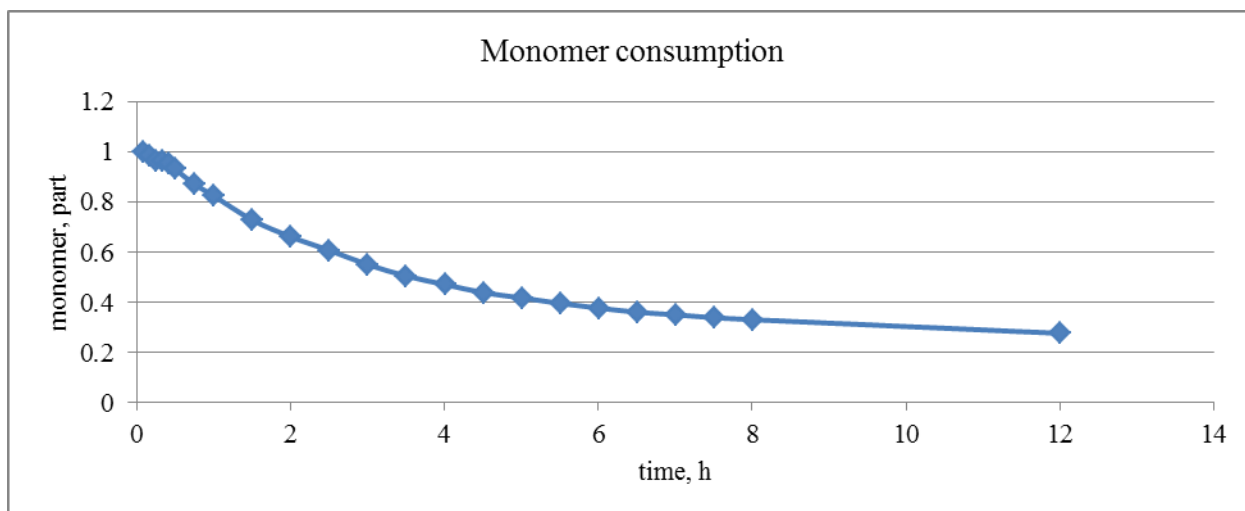
Figure 10.5. Part monomer was calculated by normalizing integration value for 5.51-5.68 ppm (corresponds to one of the vinyl protons), against integration value for 4.42-5.10 ppm (corresponds to anomeric hydrogen's protons of both α and β forms combined)
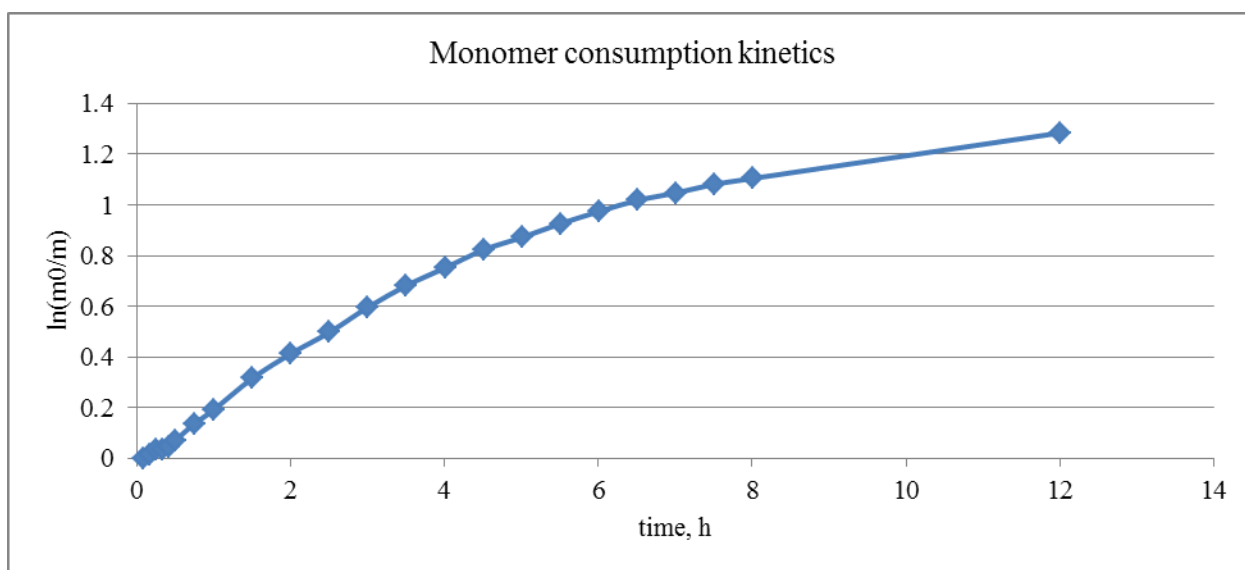

Figure 10.6. Monomer consumption kinetics. $\ln(m_0/m)$ was calculated as natural logarithm of the ratio between normalized integration values 5.51-5.68 ppm (corresponds to one of the vinyl protons) at time t=0 and time t

We targeted the degree of polymerization (DP) of 50 and this choice was based on the previous successful use of pMAG having DP=46 in nucleic acid delivery vehicles.[11] The DP = 52 was calculated from NMR analysis as the integral ratio between the signals of terminal adamantane-CH_2-NHR and anomeric hydrogen protons as shown below (Figure 10.7). Ad-

pMAG polymer was purified by dialyzing the reaction mixture against ultrapure water and yielded a white fluffy powder.
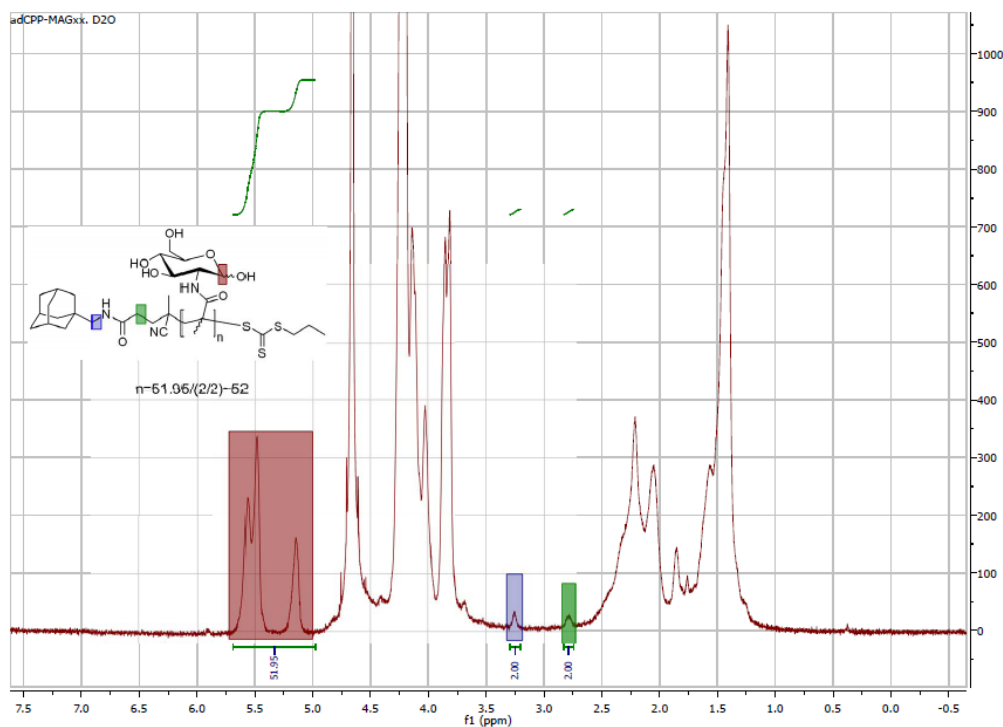

Figure 10.7. Determination of the degree of polymerization of Ad-pMAG through NMR integration

Ad-PEG was synthesized using a commercially-available, mono-NHS-activated PEG_{5000} and adamantane methylamine according to a previously-published procedure (Scheme 10.5).[12] The polymers were produced in high yields and purity as determined through ^{1}H NMR and HPLC analysis. After removal of the excess adamantane methylamine through centrifugation and dialysis against ultrapure H_2O, the pure, fluffy polymers were obtained.

Scheme 10.5. Synthesis of Ad-PEG through terminal NHS activated PEG$_{5000}$

PEG MW = 5000

CHCl$_3$, RT, 24 hr
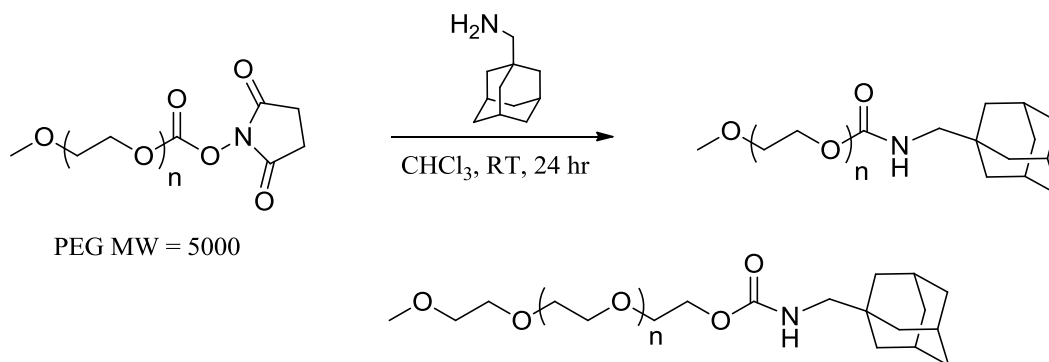
10.4.3 Determination of Ad-PEG Association Constants

It was essential for these Ad-X polymers to form strong inclusion complexes with the hydrophobic cyclodextrin (CD) core of the click clusters in order to impart any effect on the polyplexes. To quantify this interaction, NMR titration experiments were utilized to verify efficient binding of the adamantane moiety with the βCD core. Inclusion complexation of the Ad-X polymer with the βCD core of click clusters resulted in a shift of the tertiary proton toward a higher chemical shift, indicating the presence of adamantane complexation with the click clusters (Figure 10.8). Analysis of three independent titrations resulted in a binding constant (*K*)
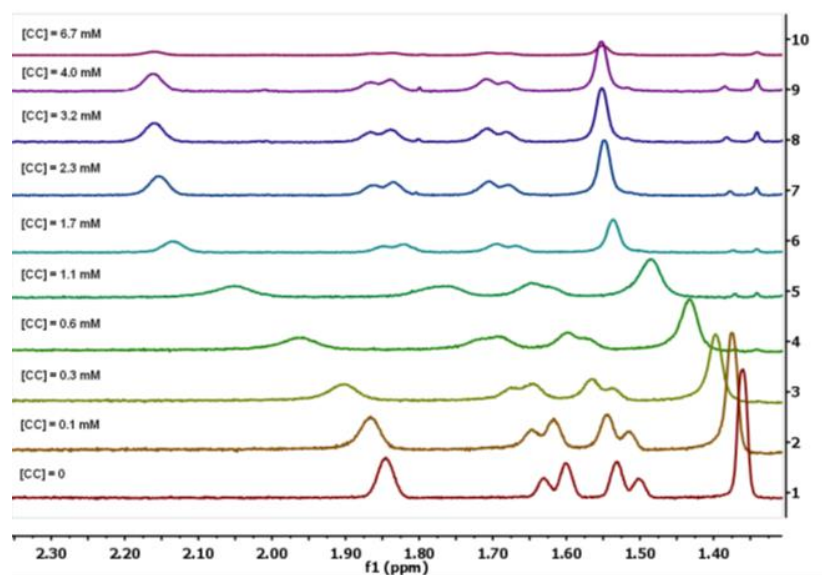

Figure 10.8. Stacked ^{1}H NMR of Ad-PEG/click cluster NMR titration experiments

197

of approximately 36,000 M^{-1} for the Ad-PEG inclusion with click clusters after a non-linear fit of

the obtained data (Figure 10.9). While we had speculated that the seven cationic arms of the click

cluster may distort the CD cup in a way that would hinder the inclusion complexation of

adamantane, the high K value indicated that this was not the case and correlated well with

published values for a similar polymeric system.[13] This method was not suitable for

measurement of the Ad-p(MAG)$_{52}$ polymer, however, due to overlapping NMR resonance peaks.

Due to the similarity in adamantane-polymer linkages, it was assumed that the Ad-p(MAG)$_{52}$

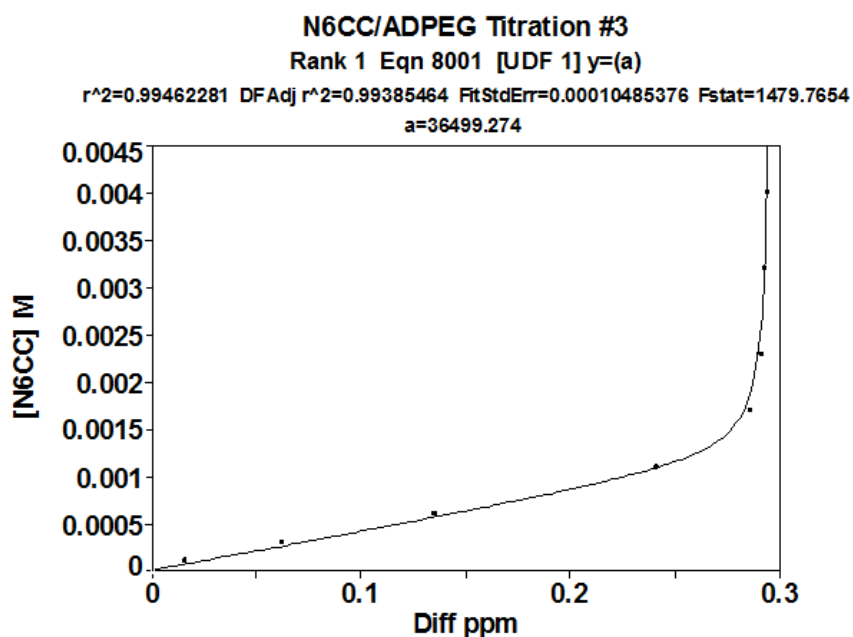would exhibit similar binding interactions to click clusters.

Figure 10.9. Non-linear regression analysis using Table Curve for data fitting of Conner's equation

10.4.4 Gel Binding Assays

Gel electrophoresis assays were performed for polyplexes that contained click clusters

only, AD-PEG-click cluster, or Ad-pMAG-click cluster complexes in order to measure the

minimum N/P ratio (click cluster amines/phosphate units in pDNA backbone) which is necessary

to fully complex the pDNA. Polyplexes that were formulated with pDNA and click cluster only, as well as a formulation which included Ad-PEG, appeared to fully retard the pDNA movement at an N/P = 1. When Ad-p(MAG)$_{52}$ is introduced into the polyplex formulation at a 1:1 molar ratio (mol Ad : mol βCD), the pDNA complexation was not completed until N/P=5, at which pDNA migration was fully retarded (Figure 10.10). This unexpected decrease in pDNA binding ability suggests that pMAG may sterically hinder the click cluster pDNA compaction to a significantly larger extent than PEG causing.
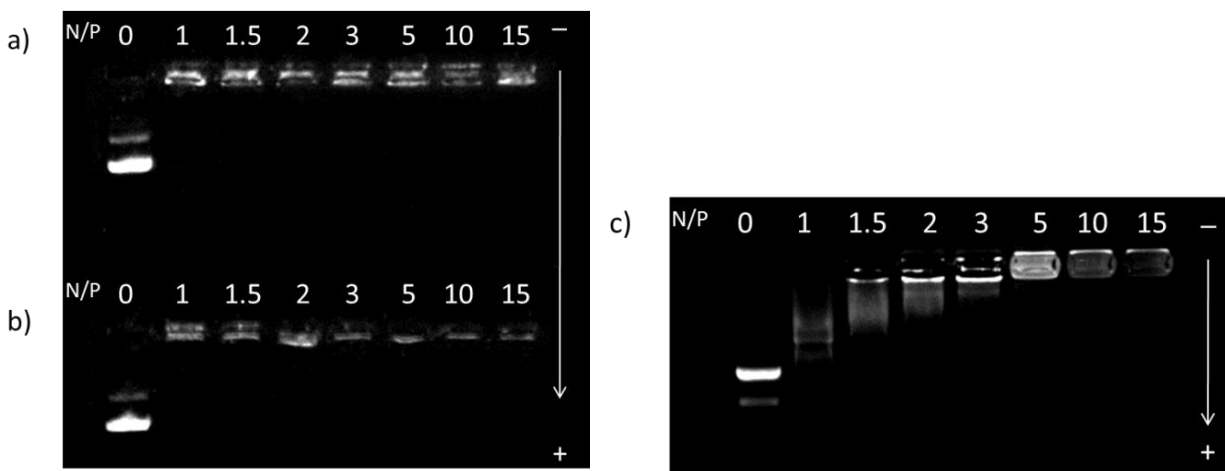

Figure 10.10. Gel binding assay results for a) click cluster/pDNA only, b) Ad-PEG, and c) Ad-p(MAG)$_{52}$ polyplex formulations

10.4.5 Polyplex Size and Zeta Potential

If Ad-p(MAG)$_{52}$ inclusion complex formation with click clusters affects their binding to pDNA, this interaction could presumably impact the size of the polyplex nanoparticles. Dynamic light scattering (DLS) was used to determine the size of polyplexes for each different formulation in pure water (Figure 10.11). There was no significant difference in polyplex size between unmodified and Ad-PEG-containing polyplexes, both of which ranged from 40 nm to 60 nm in hydrodynamic diameter at N/P ratios of 5 to 20. Interestingly, a formulation including Ad-

p(MAG)$_{52}$ showed larger polyplexes, ranging from 90 nm to 110 nm in size. This result agrees with that from gel electrophoresis in that it indicates weaker interactions between click cluster and pDNA in the presence of pMAG, which could lead to a more relaxed polyplex core and, thus increased polyplex size.
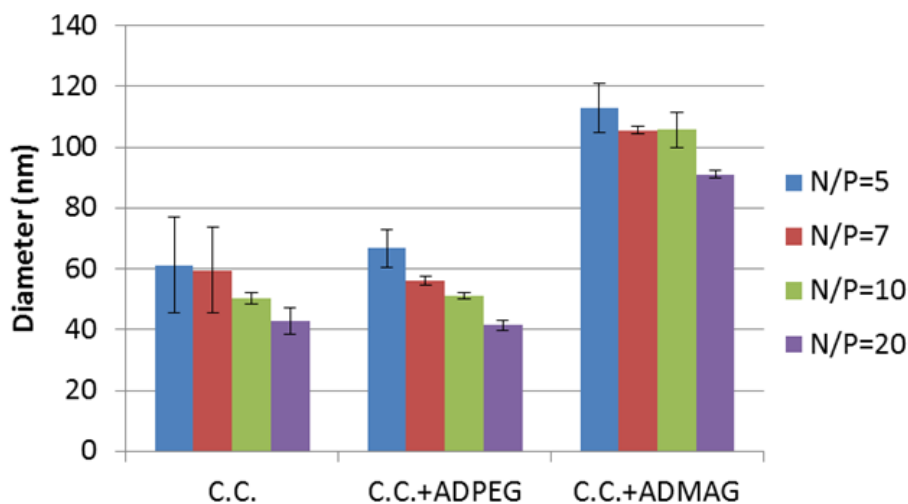

Figure 10.11. Polyplex size of each formulation at various N/P ratios in pure H$_2$O

Zeta potential measurements also revealed a difference in the surface charge of the nanoparticles upon modification (Figure 10.12). Zeta potential of unmodified polyplexes increased with increasing N/P ratio, reaching a value of 52 mV at N/P = 20. Ad-PEG inclusion reduced zeta potential values, which was especially noticeable at higher N/P ratios (10 and 20). The influence of Ad-pMAG$_{52}$ was more profound, when it was included into the polyplex formulation the zeta potential remained between 22-30 mV at all tested N/Ps.
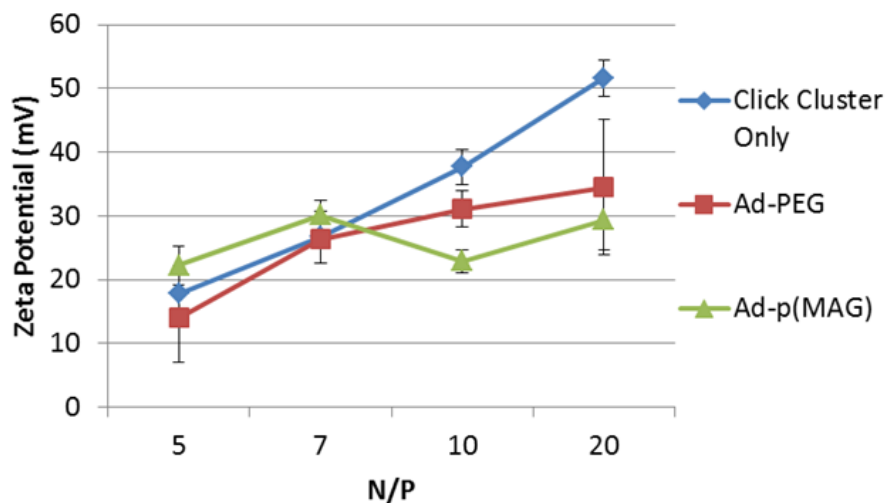
Figure 10.12. Polyplex surface zeta potential of each formulation at various N/P ratios in H_2O

10.4.6 Polyplex Stability in Salt and Serum Conditions

One of the primary functions of Ad-PEG/Ad-pMAG is to promote colloidal stability of polyplexes in physiologically-relevant conditions. We used DLS to measure the polyplex size over time after dilution with salt- (reduced-serum Opti-MEM™) or serum-containing media (DMEM+10%FBS). Upon dilution of unmodified polyplexes (N/P = 5 or N/P = 20) with reduced-serum medium (Opti-MEM), there is a dramatic increase in polyplex size from around 50 nm to over 1 µm after 4 h incubation, as seen in Figure 10.13. The inclusion of Ad-PEG into the formulations did not impart any evident colloidal stability to the delivery system—similar rapid increases in size were observed upon dilution into OptiMEM. When Ad-p(MAG)$_{52}$ was added instead, there was an increase in the colloidal stability for up to 2 hours (Figure 10.13). This is likely due to the increased bulk of pMAG vs. PEG due to the sugar units along its backbone. The size of the Ad-pMAG-modified polyplexes at N/P = 20 remains steady, around 100 nm, for 2 hours until the size gradually increases (Figure 10.14). The size reaches a maximum between 5-8 hours. At an N/P = 5, the colloidal stability of Ad-pMAG-modified
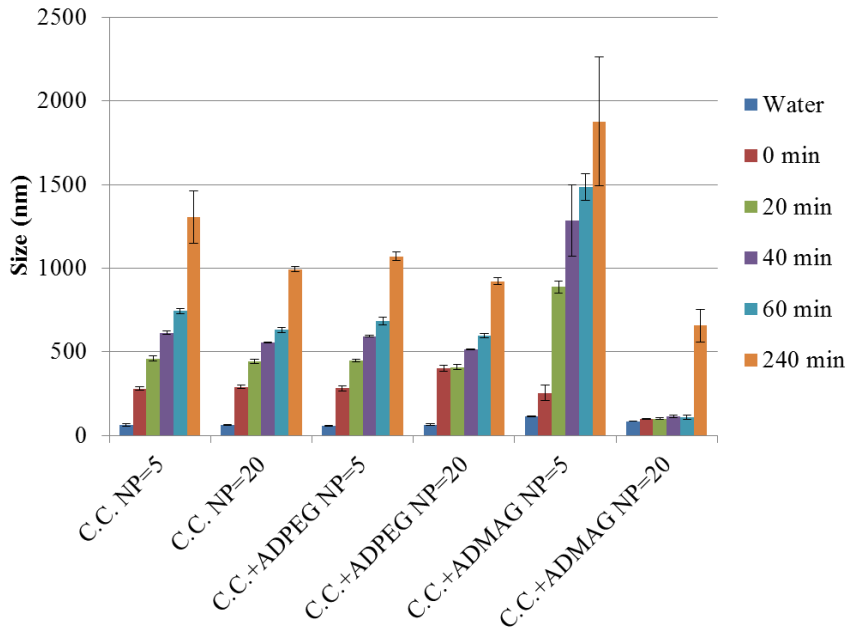
201

Figure 10.13. Hydrodynamic diameters of polyplexes after dilution with 700 µL of Opti-MEM^{TM} of each different formulation
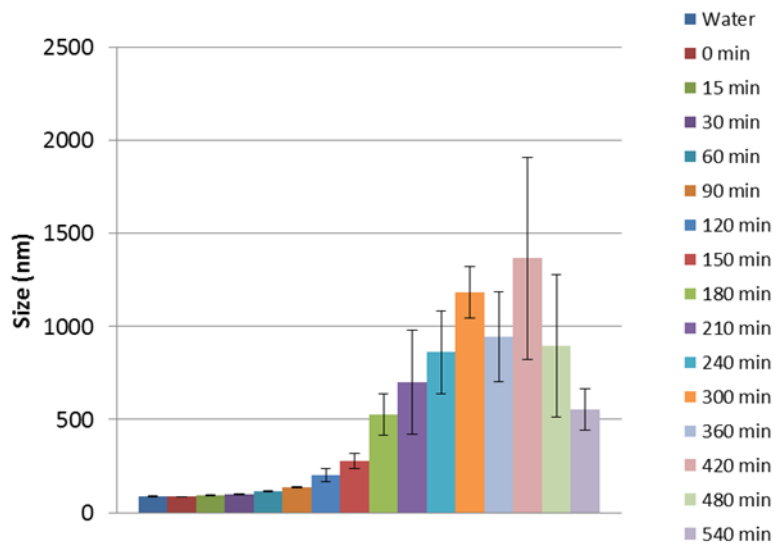

Figure 10.14. Hydrodynamic diameter of Ad-p(MAG)$_{52}$ polyplexes, at N/P 20, after dilution with Opti-MEM^{TM}

polyplexes actually decreases compared to unmodified and Ad- PEG-modified analogues, exhibiting rapid aggregation. At this N/P the polyplex is weakly held together, as observed with

gel electrophoresis, so we speculate that a small amount of charge screening by the salt can cause the rapid aggregation. Also, it is likely at an N/P=5 there is not a sufficient number of CD moieties present on the polyplex surface for Ad-p(MAG)$_{52}$ complexation to provide enough colloidal stability. In the case of N/P=20 there are likely more CD cups present on the surface and thus more Ad-p(MAG)$_{52}$ can coat the polyplex leading to an increase in colloidal stability.

When diluted into serum-containing medium, the stabilizing effects of modification with Ad-pMAG were not observed (Figure 10.15). Again, Ad-PEG did not demonstrate any difference in colloidal stability when introduced into the polyplex formulations, and there was no increase in colloidal stability upon incorporation of Ad-p(MAG)$_{52}$, either. Further studies would be needed to provide a more complete understanding of the dynamics of aggregation in salt and serum conditions as well as to test the effects of pMAG molecular weight on the colloidal stability of click cluster polyplexes.
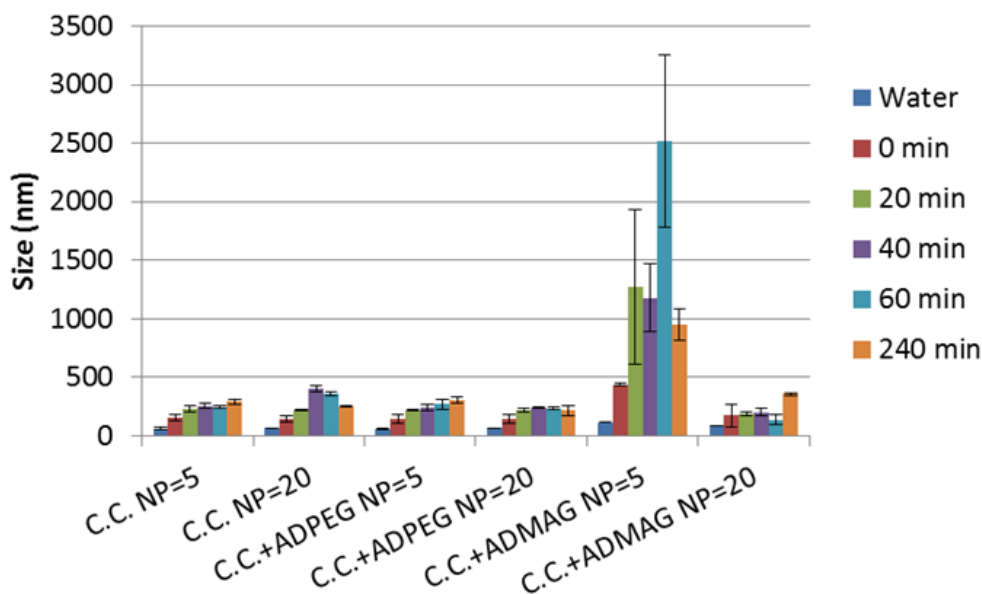

Figure 10.15. Hydrodynamic diameters of polyplexes after dilution with 700 μL of DMEM of each different polyplex formulation

10.4.7 Cellular Uptake Studies

The data shown thus far indicated that inclusion of Ad-p(MAG)$_{52}$ in polyplex formulations causes a significant impact on the physical properties of the pDNA/click cluster polyplexes. In order to probe how these effects may influence nucleic acid delivery properties of the click cluster, several biological assays were conducted using three human cell lines: HeLa (human cervical cancer) and U-251 and U-87 MG (human glioblastoma multiforme (GBM)) cell lines.

To investigate the effect that PEG and pMAG might have on polyplex endocytosis, polyplexes were prepared with Cy5^{TM}-labeled pDNA and incubated with each of these three cell types. Flow cytometry was utilized to quantify the number of cells positive for the presence of Cy5 (Cyanine5: excitation/emission: 649 nm/ 670 nm)-labeled pDNA. Figure 10.16 depicts both
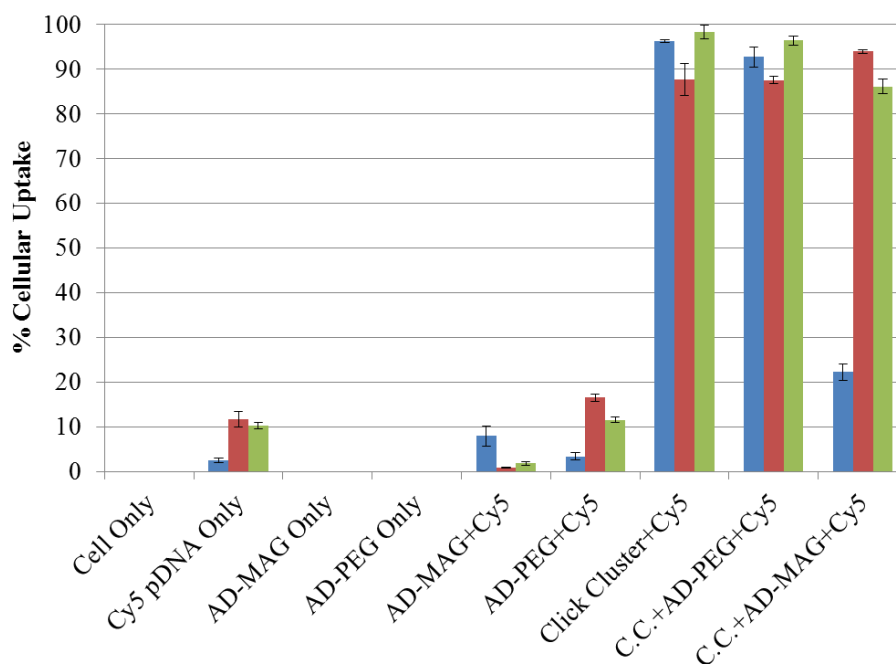

Figure 10.16. Cellular uptake (percent Cy5^{TM} positive cells) of each polyplex formulation at N/P = 10 in HeLa (in blue), U-87 MG (in red), and U-251 (in green) cell lines

of the GBM cell lines have around 90% cellular uptake for all polyplex formulations. HeLa cells, on the other hand, largely reject the polyplexes formulated with Ad-p(MAG)$_{52}$—only a little more than 20% of the HeLa cells treated with Ad-pMAG-modified polyplexes were positive for Cy5. This "stealth" effect, with respect to HeLa cells, should be further investigated with other cell lines to determine whether Ad-p(MAG)$_{52}$ can be used for reducing non-specific cellular uptake when cell targeting groups are used within polyplex formulations.

10.4.8 Transfection and MTT Assay

Delivery of gWiz^{TM} luc-pDNA, which encodes for the luciferase protein, was carried out on all three cell lines to study the effect that Ad-PEG and Ad-p(MAG)$_{52}$ inclusion had on luciferase gene expression efficiency. After 4 h incubation in reduced-serum medium followed by 42 h in 10% FBS-containing DMEM medium, incorporation of Ad-PEG in polyplex formulations had no profound effect on gene expression in U-251 and HeLa cells and was minimal in U-87 cells.
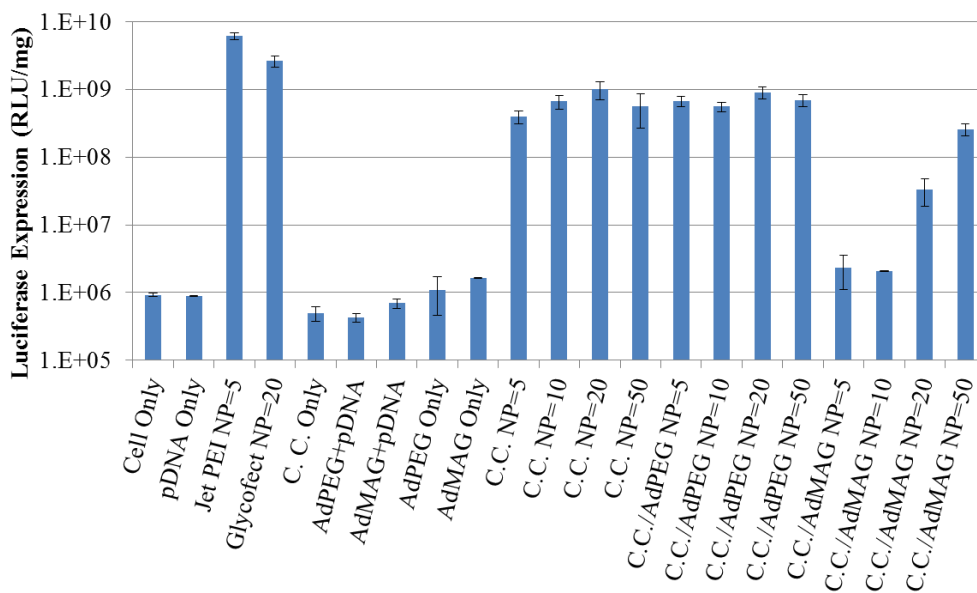

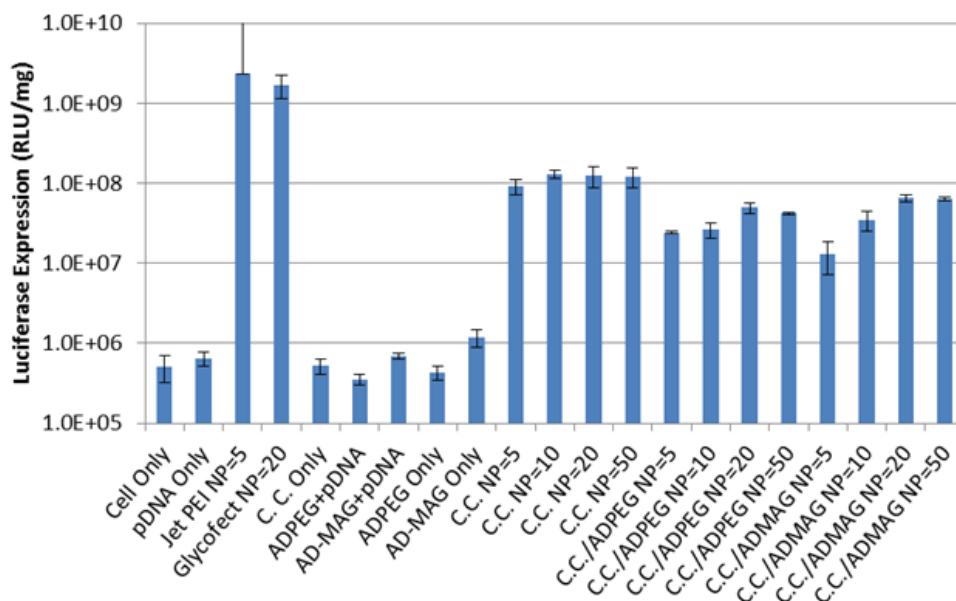**Figure 10.17.** Transfection efficiency of the three polyplex formulations using gWiz^{TM}-luciferase plasmid DNA in U-251 cells

Figure 10.18. Transfection efficiency of the three polyplex formulations using gWiz^{TM}-luciferase plasmid DNA in U-87 MG cells

Ad-p(MAG)$_{52}$ incorporation, on the other hand, does impact the transfection efficiency of U-251 cells. There appears to be little to no transgene expression at N/P 5 and 10, whereas luciferase levels increase for N/P 20 and 50, reaching gene expression levels similar to those of unmodified polyplexes (Figure 10.17). Interestingly, cell line dependence for Ad-p(MAG)$_{52}$ containing polyplexes, along with the uptake, influences also the gene expression. U-87 MG cells do not show any dramatic difference in transfection efficiency among all of the polyplex formulations tested (Figure 10.18). The transfection results for HeLa cells reveal a decrease in transfection efficiency when using Ad-p(MAG)$_{52}$, compared to Ad-PEG and unmodified polyplexes (Figure 10.19). This was expected based on the low cellular uptake of Ad-p(MAG)$_{52}$ containing polyplexes by HeLa cells. These studies suggested there may be a cell type dependence on transfection when using Ad-p(MAG)$_{52}$ in the polyplex formulations, which is likely due to differences in the cell surface chemistry between the cell types studied.
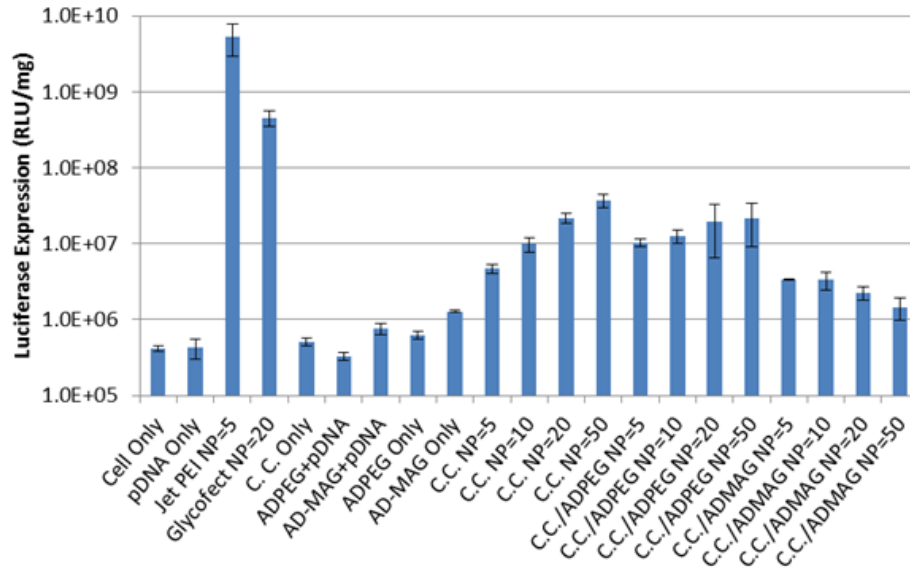
Figure 10.19. Transfection efficiency of the three polyplex formulations using gWiz[TM]-luciferase plasmid DNA in HeLa cells

MTT toxicity assays confirmed the previously-reported[10] trend of increased cellular toxicity with the increase in N/P for unmodified polyplexes (Figure 10.20). However this was not the case when incorporating Ad-p(MAG)$_{52}$ into the formulations. Remarkably, all three cell lines
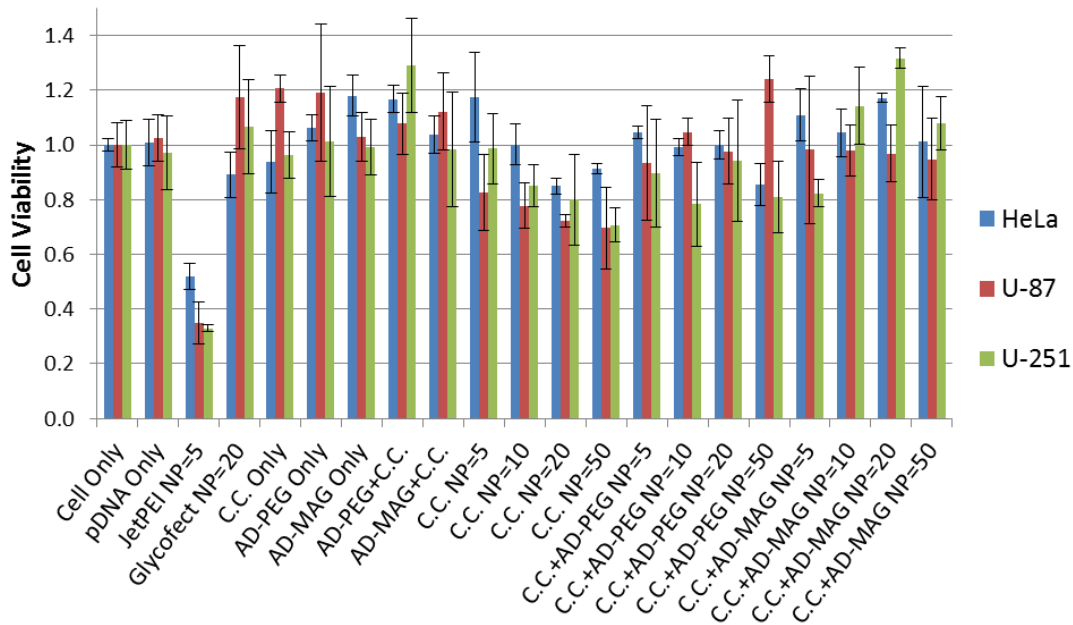

Figure 10.20. MTT toxicity assay of the three polyplex formulations using gWiz[TM]-luciferase plasmid DNA in all three cell lines

showed little to no toxicity for AD-pMAG-modified polyplexes at all N/Ps tested (up to N/P 50) and were comparable to that of Glycofect[TM].

10.5 Conclusions

We have shown in this study the successful polymerization of Ad-p(MAG)$_{52}$ and that incorporation of Ad-p(MAG)$_{52}$ into click cluster/pDNA polyplexes provided increased colloidal stability under physiological salt conditions up to 2 h. The length of pMAG used in this study was not optimized and additional studies need to be conducted to probe the effect of Ad-pMAG molecular weight on the colloidal stability. pMAG significantly decreased the toxicity of click clusters, showing no change in cell viability even at high N/P of 50. This lack of cellular toxicity, along with a trithiocarbonate 'handle' useful for chemical modifications, make pMAG a good candidate for incorporation of targeting groups. There was a significant effect of Ad-pMAG on polyplex biological properties which appeared to be dependent on the cell type studied. Ad-p(MAG)$_{52}$-containing polyplexes were poorly taken up by HeLa cells, exhibiting a 'stealth' effect. Cellular internalization in both GBM cell lines, however, was very efficient. Cell type dependence will be further investigated in future studies to reveal the full potential of pMAG as a coating layer for click cluster-pDNA polyplexes. Overall, the use of pMAG, instead of PEG, could be advantageous in some applications in order to impart colloidal stability, hydrophilicity, and a terminal thiol for facile inclusion of targeting moieties.

10.6 Acknowledgments

10.7 References

(1) Fant, K.; Esbjörner, E. K.; Jenkins, A.; Grossel, M. C.; Lincoln, P.; Nordén, B. *Molecular Pharmacology* **2010**, *7*, 1734.
(2) Pun, S. H.; Bellocq, N. C.; Liu, A.; Jensen, G.; Machemer, T.; Quijano, E.; Schluep, T.; Wen, S.; Engler, H.; Heidel, J.; Davis, M. E. *Bioconjugate Chemistry* **2004**, *15*, 831.
(3) Rieger, J.; Passirani, C.; Benoit, J. P.; Van Butsele, K.; Jérôme, R.; Jérôme, C. *Advanced Functional Materials* **2006**, *16*, 1506.
(4) Aissaoui, A.; Chami, M.; Hussein, M.; Miller, A. D. *Journal of Controlled Release* **2011**, *154*, 275.
(5) Davis, M. E. *Molecular Pharmacology* **2009**, *6*, 659.
(6) Davis, M. E.; Zuckerman, J. E.; Choi, C. H. J.; Seligson, D.; Tolcher, A.; Alabi, C. A.; Yen, Y.; Heidel, J. D.; Ribas, A. *Nature* **2010**, *464*, 1067.
(7) Ishihara, T.; Takeda, M.; Sakamoto, H.; Kimoto, A.; Kobayashi, C.; Takasaki, N.; Yuki, K.; Tanaka, K.-i.; Takenaga, M.; Igarashi, R.; Maeda, T.; Yamakawa, N.; Okamoto, Y.; Otsuka, M.; Ishida, T.; Kiwada, H.; Mizushima, Y.; Mizushima, T. *Pharmaceutical Research* **2009**, *26*, 2270.
(8) Tagami, T.; Nakamura, K.; Shimizu, T.; Yamazaki, N.; Ishida, T.; Kiwada, H. *Journal of Controlled Release* **2010**, *142*, 160.
(9) Tagami, T.; Uehara, Y.; Moriyoshi, N.; Ishida, T.; Kiwada, H. *Journal of Controlled Release* **2011**, *151*, 149.
(10) Srinivasachari, S.; Fichter, K. M.; Reineke, T. M. *Journal of the American Chemical Society* **2008**, *130*, 4618.
(11) Smith, A. E.; Sizovs, A.; Grandinetti, G.; Xue, L.; Reineke, T. M. *Biomacromolecules* **2011**, *12*, 3015.
(12) Pun, S. H.; Davis, M. E. *Bioconjugate Chemistry* **2002**, *13*, 630.
(13) Bartlett, D. W.; Davis, M. E. *Bioconjugate Chemistry* **2007**, *18*, 456.
(14) Ting, S. R. S.; Min, E. H.; Zetterlund, P. B.; Stenzel, M. H. *Macromolecules* **2010**, *43*, 5211.
(15) Xu, X.; Smith, A. E.; Kirkland, S. E.; McCormick, C. L. *Macromolecules* **2008**, *41*, 8429.
(16) Khemtong, C.; Banerjee, D.; Liu, Y. B.; El Khoury, J. M.; Rinaldi, P. L.; Hu, J. *Supramolecular Chemistry* **2005**, *17*, 335.

Chapter 11: Part II Overall Conclusions

Understanding the complex interactions of pDNA-polymer complexes (polyplex) with components of the cell surface was essential for the future design of more efficient non-viral nucleic acid delivery vehicles. Interactions of a poly(glycoamidoamine) copolymer containing polyplex with six different glycosaminoglycans (GAG) that are present on mammalian cell surfaces was examined. Measuring the relative affinities of heparin sulfate (HS), hyaluronate (HA), heparin (Hep), dermatan sulfate (DS), and two forms of chondroitin sulfate (CSA and CSC) for poly(galactaramidopentaethylenetetramine) (G4) copolymer-pDNA polyplexes with quartz crystal microbalance (QCM) was investigated. The QCM experiments provided the relative affinities of GAGs for the G4 polyplexes to provide insight into the role of GAG charge on polyplex interactions. The measured increase in mass associated with the absorption of GAGs onto a polyplex monolayer provided the relative affinity of each GAG. The trend of GAG affinity was HA > HS > CSA > CSC > DS > Hep which suggested the affinity of polyplexes for anionic GAGs is independent of GAG charge density (HS > Hep > DS > CSC > CSA > HA). HA showed the highest mass increase for G4 polyplexes despite having the lowest charge density of the GAGs in this study. The presented data indicated GAG affinity is not completely mediated through electrostatic interactions and warrants continued investigations into GAG-polyplex interactions. The GAG-polyplex interaction and role of charge is an important piece to the puzzle of understanding the complex cell surface interactions and endocytosis mechanism.

Development of a targeting strategy for click cluster non-viral delivery vehicles was undertaken in order to specifically target glioblastoma multiform (GBM) cancer cells in the future. To do so, a new targeting strategy platform was introduced based on an adamantane terminated poly(2-deoxy-2-methacrylamido glucopyranose) (pMAG), which formed a non-

covalent inclusion complex with the βCD core of click cluster delivery vehicles. The polyplex properties and biological effect of Ad-p(MAG) was investigated and compared to those which included poly(ethylene glycol) (PEG). The successful polymerization of Ad-p(MAG), with a DP = 52, and incorporation into click cluster-pDNA formulations was demonstrated. The presence of Ad-p(MAG)$_{52}$ imparted an increased colloidal stability to the polyplexes under physiological salt conditions up to 2 h, whereas Ad-PEG showed no effect on the colloidal stability under the same conditions. Further studies into the molecular weight effect of pMAG on polyplex colloidal stability is needed. Click cluster toxicity was significantly reduced upon Ad-p(MAG)$_{52}$ polyplex incorporation, even at high N/P ratios of 50. Ad-p(MAG)$_{52}$ proved to be a good platform for an active targeted strategy due to the reduced toxicity and the trithiocarbonate synthetic handle for targeting ligand incorporation. However, the *in vitro* biological properties appeared cell type dependent where HeLa cells exhibited poor cellular uptake and therefore poor transfection efficiency. Cellular internalization of the Ad-p(MAG)$_{52}$ containing polyplexes that both GBM cell lines exhibited was very efficient with over 90% of cells positive for polyplexes. Future studies into the cell dependence of the polyplexes containing Ad-p(MAG) will provide a better understanding of the potential for Ad-p(MAG) as a coronal layer for click cluster-pDNA polyplexes. The use of pMAG instead of PEG has its advantages that included increased colloidal stability, hydrophilicity, and the terminal thiol functionality for targeting groups.

Chapter 12: Suggested Future Work

12.1 Synthesis of Cbz Protected Click Clusters for Post-click Modifications

The ability to perform modifications to click cluster non-viral nucleic acid delivery vehicles after the azide-alkyne click reaction can provide a useful strategy for conjugation of various moieties onto the oligo ethyleneamine arms. The idea of conjugating chemotherapeutics or MRI active agents to the terminal ends of the oligoamines on the click cluster had spurred some work into identifying a synthetic strategy to accomplish this goal. Typically, the seven terminal primary amines of the click cluster are Boc protected along with the secondary amines after the click reaction. To this end a second protecting group is needed in order to selectively

Scheme 12.1. Synthesis of a terminal Cbz protected Boc$_4$N6 alkyne for click cluster synthesis
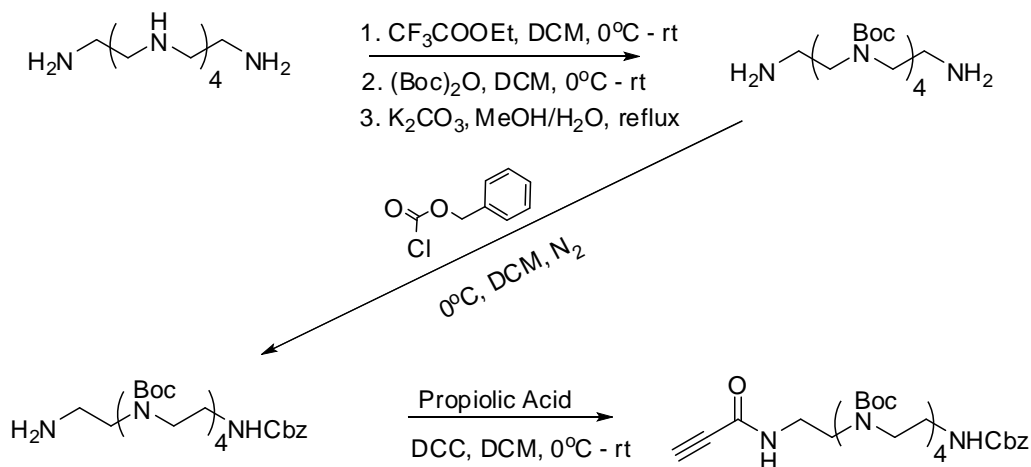

deprotect the primary amine of the click clusters. The initial investigation looked at the synthesis of a click cluster with a benzyl carbamate (Cbz) protected primary amine. Synthesis of the oligo ethylene alkyne with a Cbz protected amine was accomplished (Figure 12.1). The pure Cbz protected Boc$_4$N6 alkyne was obtained and analyzed with ^{1}H NMR and LC-MS. The initial azide-alkyne click reactions with the Cbz protected Boc$_4$N6 alkyne appeared very similar to

reactions with Boc$_5$N6 alkyne. Further studies will include the selective deprotection of the Cbz protected primary amine and also various chemistries to conjugate a variety of different groups into the end of the oligo ethyleneamine arms for chemotherapeutic and theranostic applications.

12.2 Active Targeting of Click Clusters with Peptide Targeting Ligands

The use of adamantyl terminated poly(2-deoxy-2-methacrylamido glucopyranose) (pMAG) and poly(ethylene glycol) (PEG) for *in vivo* passive targeting of cancer tumors is a future direction of these projects, but the ultimate goal was the *in vivo* active targeting of the click cluster nucleic acid delivery vehicles. The same non-covalent inclusion complexation strategy is envisioned for the active targeting of the click clusters. Initial work in this active targeting endeavor was synthesis of an Ad-PEG-peptide active targeting polymer. A cysteine temriated heptapeptide, which will actively target glioblastoma multiform cancer cells, was the targeting ligand of choice. The initial synthetic strategy for the active targeting polymer was

Scheme 12.2. Synthesis of Ad-PEG-peptide targeting polymers for inclusion complexation with click cluster delivery vehicles
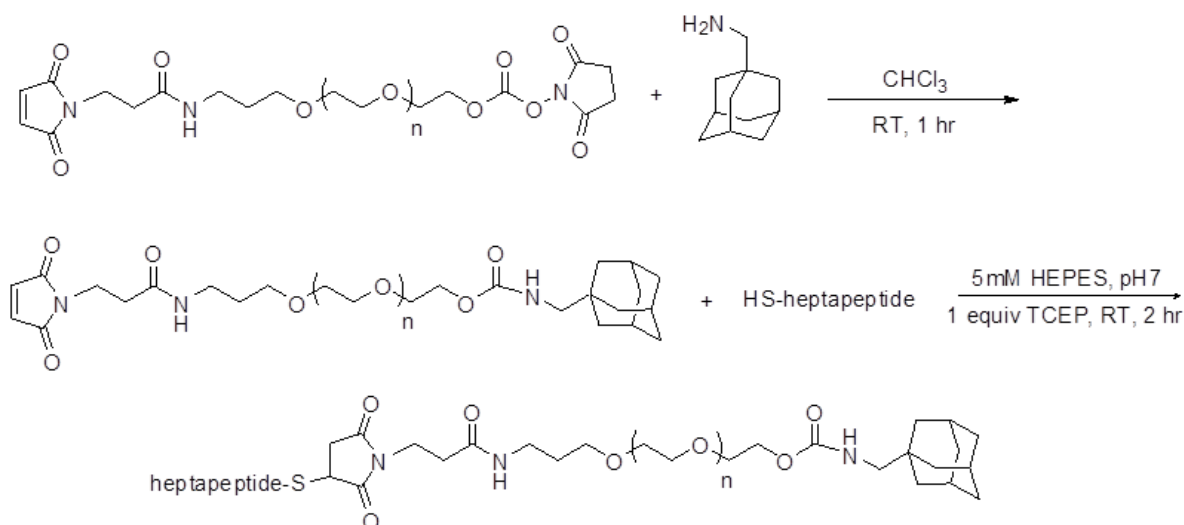
based on a difunctional PEG with a NHS activated ester and maleimide terminal functionality (Scheme 12.2). Initial results indicated low conversions to the peptide containing polymer and warranted an alternative strategy.

After many attempts to synthesize the Ad-PEG-peptide using the NHS and maleimide terminated PEG another route was developed. A commerically available difunctional PEG with terminal ortho-pyridine disulfide (OPSS) and NHS activated ester groups was utilized for the new synthetic strategy (Scheme 12.3). Initial results using the OPSS-PEG-NHS polymer appeared promising at yielding the desired Ad-PEG-peptide with the peptide linked to the polymer through a disulfide bond. MALDI-TOF analysis of each PEG polymer demonstrated the expected shift in the molecular weights of the polymer products after each step (Figure 12.1).

Scheme 12.3. Synthesis of Ad-PEG-peptide with an OPSS-PEG-NHS difunctional polymer

PEG MW: 5000
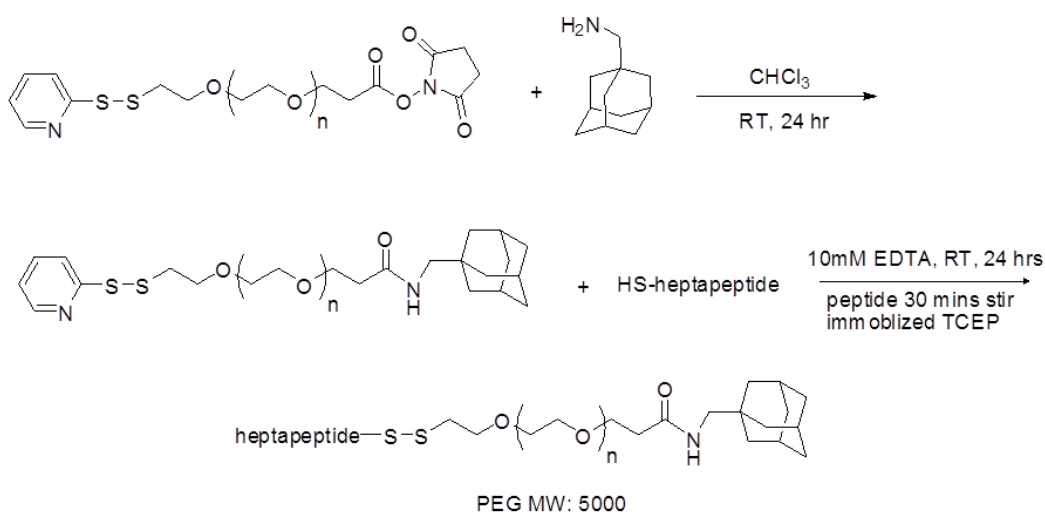
There is still a large amount of work needed to reach the goal of an active targeted click cluster complex with only the initial synthesis of the Ad-PEG-peptide worked out. Future studies include the optimization of the Ad-PEG-peptide synthesis with full characterization of the polymer and its complexation with the click cluster delivery vehicles. Optimization of the click

cluster-pDNA or siRNA polyplexes with Ad-PEG-peptide is the logical next step to investigate the colloidal stability and various polyplex properties. All the *in vitro* biological assays are then necessary to identify the potential for *in vivo* applications before taking the targeting strategy any further.
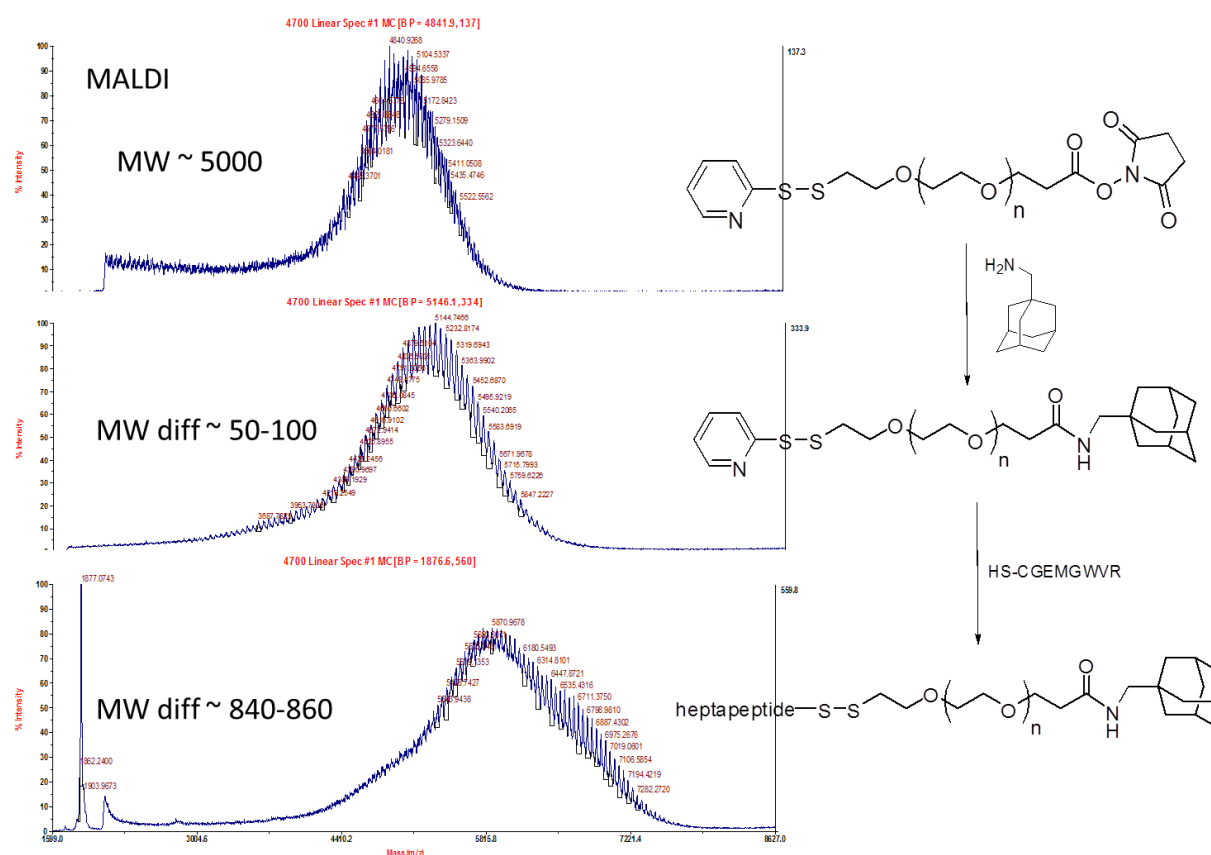

Figure 12.1. MALDI-TOF analysis of OPSS-PEG-NHS starting material, after Ad-NH$_2$ conjugation, and the final Ad-PEG-peptide

12.3 2,2'-bipyridine Based Fe^{+2} MRI Contrast Agents

The field of theranostic materials, which is a therapeutic material that also provides diagnostic capabilities, has grown in recent years. The idea of non-viral nucleic acid delivery vehicle that also included a MRI contrast agent is not a new concept. Examples of these materials are very limited and the need for new theranostics compounds is needed for various

medical applications. The initial idea is the development of a paramagnetic Fe(II) based

supramolecular structure which could be used as a drug carrier or even a non-viral gene delivery

vector. Initial studies for the synthesis of such materials was conducted and yielded a model 2,2'-

bipyridine with two primary amines to provide synthetic handles for other structural motifs

(Scheme 12.4). There are two initial routes envisioned for the formation of the Fe^{2+} complexes

Scheme 12.4. Synthesis of the 2,2'-bipyridine based model compound as a potential theranostic platform
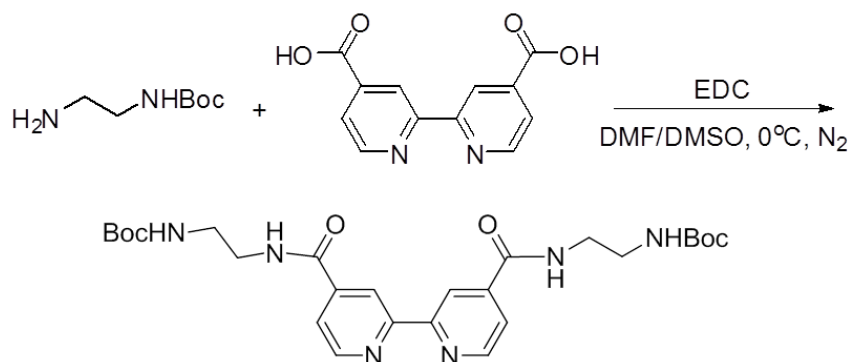
which should provide a useful paramagnetic center for MRI (Scheme 12.5). Future studies

include identification of a need in the medical field where this type of theranostic would prove

useful. After an application is identified then the synthesis and Fe^{2+} complexation work is

conducted to optimize the development of a useful and viable compound.

Scheme 12.5. Fe^{2+} complex with the model bi-pyridine compound